CALIFORNIA INSTITUTE OF TECHNOLOGY

SOIL MECHANICS LABORATORY

STATIC STRESS-DEFORMATION CHARACTERISTICS OF SAND

by

Hon-Yim Ko

A report on research conducted for the
National Science Foundation

Pasadena, California
1966

STATIC STRESS-DEFORMATION CHARACTERISTICS OF SAND

Thesis by

Hon-Yim Ko

In Partial Fulfillment of the Requirements

For the Degree of

Doctor of Philosophy

California Institute of Technology

Pasadena, California

1966

(Submitted January 25, 1966)

ACKNOWLEDGMENTS

The author wishes to thank his advisor, Dr. R. F. Scott, for his guidance during the course of this investigation. Thanks are also due to Dr. R. A. Westmann for his interest in this work.

The author is indebted to the California Institute of Technology for the tuition scholarships granted and to the National Science Foundation for the support of this work under Contracts GP657 and GK626.

ABSTRACT

A soil test box, capable of applying any combination of principal stresses to a cubical soil sample, was developed for the experimental investigation of the behavior of granular soils under static loading. A stress control device was also developed, enabling a continuous and proportionate change to be made in the stresses along a stress path and considerably simplifying the calculation of the stress state in the sample. The apparatus was used to investigate (a) the hydrostatic compression of an Ottawa sand, and (b) the behavior of the same soil under various deviatoric stress paths in both loading and unloading conditions.

A theoretical "holey" model was postulated for sand under hydrostatic stress and the results of the analysis of this model were found to correlate closely with the experimental data.

The qualitative behavior of sand under shear stresses was examined from a particulate point of view. Specially designed tests were performed on the Ottawa sand with loading and unloading along stress paths which involved different combinations of hydrostatic and deviatoric stresses, with the purpose of examining the proportions of recoverable and irrecoverable deformations. A failure envelope was obtained for a medium dense and a medium loose sand by monotonically increasing τ_{OCT} while keeping σ_{OCT} constant under various conditions of stress distribution, and it was found that the value of equivalent Coulomb φ increased from 42° in triaxial compression to 48° in triaxial extension for the medium dense sand and from 36° in triaxial compression to 44° in triaxial extension for the medium loose sand.

TABLE OF CONTENTS

LIST OF FIGURES

CHAPTER I

REFERENCE FRAMEWORK OF THEORY

(1) Principal Stress Space

It is desirable to set down a framework of reference at the beginning of this thesis, so that later discussions can continue without interruption by elaborate definitions.

The term "stress" is defined in the usual engineering sense as force per unit area [1].* It can be shown [1] that the stresses acting at a point of a material can be uniquely represented by three principal stresses whose directions of action are mutually perpendicular to each other. Hence, to describe the stresses in a material, it is necessary to specify only the three principal stresses and the directions in which they act. A homogeneous stress state in a body is one in which every point in the body has the same set of principal stresses acting in the same directions.

The state of principal stresses can be split into two additive systems of principal stresses [1]. The first, called the hyrostatic system, has all three principal stresses equal. The second, the deviatoric system, represents a state of pure shear.

It will be found convenient to represent the stress states of a body by plotting the three principal stresses in a system of rectangular coordinates in which the coordinates are made equal to the principal stresses σ_1, σ_2 and σ_3, of Fig. (I.1). It will be understood that, in

---

*Numbers in brackets refer to the references at the end of the thesis.

the content of this thesis all compressive stresses are positive and that, unless specified otherwise, the rule will be followed in which $\sigma_1 \geq \sigma_2 \geq \sigma_3 \geq 0$. Thus by plotting the stress state as a point in this principal stress space (or the Haigh-Westergaard space [2], [3]), one can easily trace how the stress state changes by following the stress point.

There are several features of the principal stress space which are relevant to the investigation described in this thesis. The first is the space diagonal or the hydrostatic axis [4], which is the line with equation $\sigma_1 = \sigma_2 = \sigma_3$, through the origin of the principal stress space, making equal angles of $\cos^{-1} 1/\sqrt{3}$ with each of the three coordinate axes, Fig. (I.1). A point of this line represents a hydrostatic stress state in which no shear stress exists and all normal stresses are equal. The second is that any plane perpendicular to the space diagonal is called an octahedral plane, with equation $\sigma_1 + \sigma_2 + \sigma_3 = C$, and all points on this plane have the same mean normal stress, the octahedral normal stress

$$\sigma_{OCT} = \frac{1}{3} (\sigma_1 + \sigma_2 + \sigma_3) = C/3 \qquad (I.1)$$

to which only the hydrostatic component of the principal stresses makes a contribution.

In particular, the plane perpendicular to the space diagonal containing the origin has the equation $\sigma_1 + \sigma_2 + \sigma_3 = 0$, so that only the deviatoric components of the principal stresses can affect the position of a point on this plane. This is called the deviatoric plane. An octahedral plane is any plane parallel to it. The resultant stresses

at a point such as P, Fig. (I.1), due to the hydrostatic and deviatoric components, can be determined by passing a plane through P perpendicular to the space diagonal which it will intersect at a point P' representing the hydrostatic stress at P. The line PP' in the plane then represents the deviatoric contribution to the stress state at P. The quantities σ_{OCT} and τ_{OCT}, as defined in [4], are then represented as shown in Fig. (I.1). A stress state can then be represented by σ_{OCT}, τ_{OCT} and an angle in the deviatoric plane in which τ_{OCT} acts.

The vertical plane which bisects the $\sigma_1\sigma_2$ and the $\sigma_1\sigma_3$ planes has its trace OA on the $\sigma_2\sigma_3$ plane, making equal angles of 45° with the axes $O\sigma_2$ and $O\sigma_3$. This plane is called the triaxial plane [4], because all points on it represent a triaxial stress state in which $\sigma_1 \gtrless \sigma_2 = \sigma_3$. (Here the rule $\sigma_1 \geq \sigma_2 \geq \sigma_3$ is not observed.) The triaxial plane OA is shown in Fig. (I.2), and has ordinates σ_1 and abscissae $\sqrt{2}\ \sigma_2 = \sqrt{2}\ \sigma_3$. A point on this plane above the space diagonal has $\sigma_1 > \sigma_2 = \sigma_3$ and therefore represents a triaxial compression state, whereas a point below it has $\sigma_1 < \sigma_2 = \sigma_3$ and represents a triaxial extension state. Here σ_3 is the major and σ_1 the minor principal stresses.

In the investigation of the failure condition of soils, the yield strength (the term "yield") will be discussed in detail in Chapter III) of the material is usually expressed in terms of an angle of internal friction, denoted by φ. For a triaxial stress state, φ is calculated from

$$\sin \varphi = \frac{\sigma_1/\sigma_3 - 1}{\sigma_1/\sigma_3 + 1} \qquad (I.2)$$

where σ_1 and σ_3 are the major and minor principal stresses at failure. Here the intermediate principal stress, σ_2, is either equal to the major or to the minor principal stress. The value of φ thus defined by Eq. (I.2) is usually called the Coulomb friction angle [5]. However, when the intermediate principal stress takes up a value other than the major or the minor principal stress, a friction angle as such, may have no physical meaning; however, we will continue to define a modified Coulomb friction angle, φ, by Eq. (I.2), irrespective of the value of the intermediate principal stress.

For terms such as the stress and strain invariant functions, the reader is referred to the book by Scott [4].

(2) General Behavior of Granular Soil under Stresses

It is also desirable at this point to briefly describe the general behavior of sand under stress, particularly as it has developed in connection with this research program.

Sand consists of a structural arrangement of grains, the pores of the structure being filled with fluids, normally air and water. Therefore sand is not a continuous medium and should be properly treated as a discrete system of particles. The mechanical properties of sand are then dictated by the interaction of the grains at their contacts, and are influenced also by the presence of the pore fluids under certain conditions.

When such a mass of grains is subjected to external stresses, these stresses will be resisted by the forces developed between grains at points of contact. The overall or macroscopic deformation of the

soil mass when the load (including both volumetric and shearing stresses) is applied and then removed after a certain time is shown in Fig. (I.3), after Scott [4]. The microscopic behavior will be examined in Chapter III. The deformation considered here can arise from both shearing strains and volume changes. When the load is first applied, there is an instantaneous deformation OA. If the load is immediately removed, the deformation would become OB, thus leaving a permanent set. The recoverable portion of the deformation is represented by AB. If the load is maintained on the soil for some time, the deformation will increase along the curve AC, which for sand will quickly flatten out to a horizontal line. Also, the deformations represented by A and C are almost equal, indicating that the deformations in sand under stresses are almost instantaneous.

When the load is removed at time represented by C, the deformation will suddenly return to the value represented by D and will then follow the curve DE until a steady value is reached. Again in the case of sand, elastic recovery takes place quickly, so that the deformations can be considered to be instantaneous both on loading and unloading. The total permanent set is represented by OF, which is not very different from the instantaneous permanent set OB.

When the results of tests with the conventional triaxial apparatus in the absence of vibrations [6], in which both σ_{OCT} and τ_{OCT} increase are examined by plotting axial stress versus axial strain, Fig. (I.4), it is found that a nonlinear stress-strain relationship is obtained between O and A. When the load is removed at A, the unloading curve is AB, with OB representing the permanent set due to the maximum

stress represented by A. Upon reloading, the portion BC of the curve is traced, which does not coincide with AB, thus forming a hysteresis loop. When the stress is increased beyond that represented by both A and C, the part CD of stress strain curve results, which is more of a continuation of OA than of BC. This qualitative behavior is true at all stress levels.

It can therefore be seen that sand is a non-linear, plastic-elastic material, which behaves differently from the ordinary linearly elastic material, such as steel. This is not surprising, because, as mentioned before, soil is a granular three-phase system, whereas steel is a continuum when examined at a scale of the grain size of the soil. Another important point of difference between the behavior of soil and that of a continuum is that under pure shear a soil dilates at small strains (positively or negatively) [7], whereas steel deforms without any volume change for small strains.

It is, therefore, not to be expected that the concepts of continuum mechanics can be applied without modification to soils, and it is important to examine the behavior of soil at the grain level.

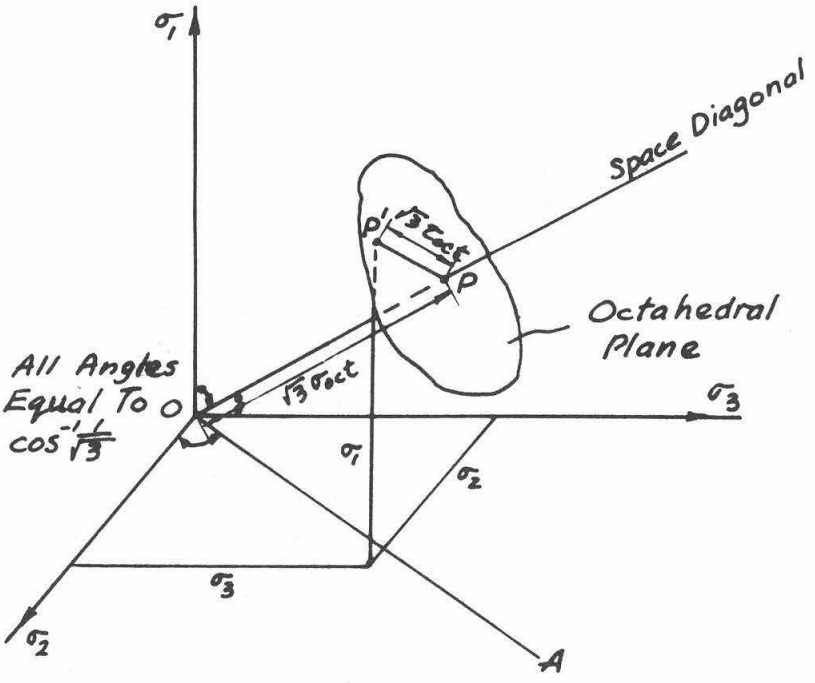

FIG. (I.1). PRINCIPAL STRESS SPACE

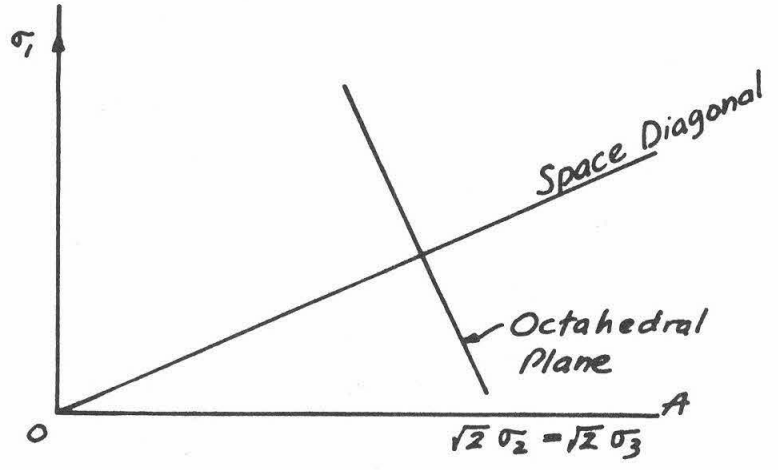

FIG. (I.2). TRIAXIAL PLANE

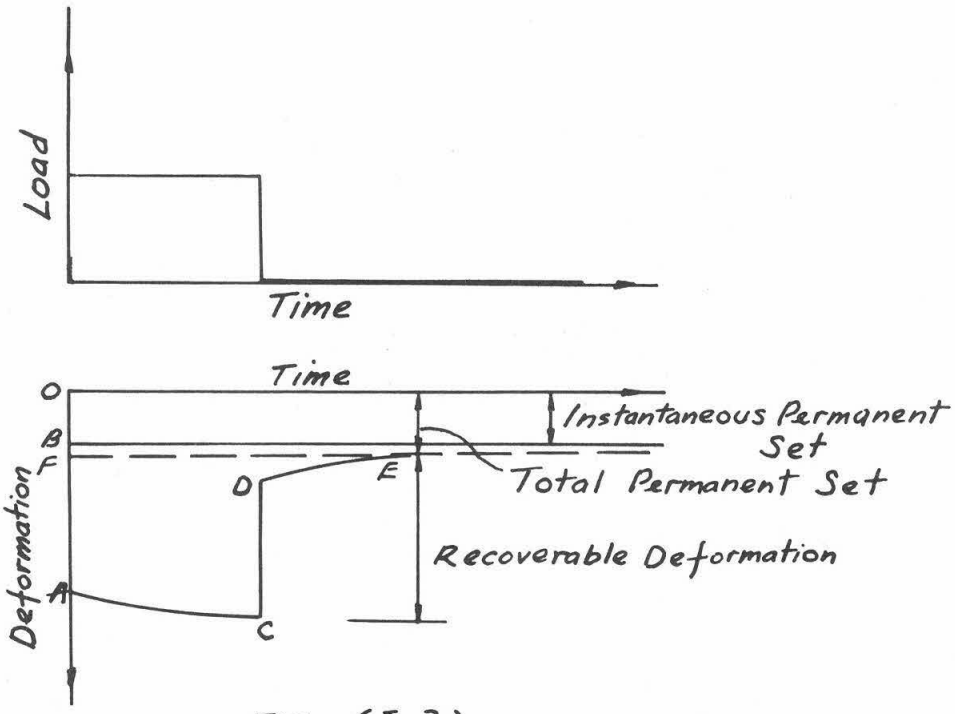

FIG. (I.3)
TIME - DEPENDENT SOIL BEHAVIOR

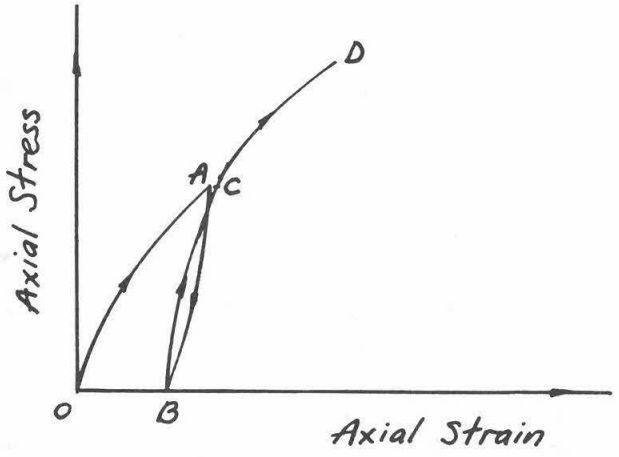

FIG. (I.4)
SOIL BEHAVIOR IN TRIAXIAL TEST

CHAPTER II

REVIEW OF OTHER INVESTIGATIONS AND SCOPE OF PRESENT WORK

(1) Review

A rather extensive survey of the literature on the mechanics of granular materials can be found in the book by Scott [4] and the thesis of Bell [8], and need only be summarized here.

Most of the research done in soil mechanics has been concerned with the failure state of the material, such as the work of Kjellman [9], Bishop and Eldin [10] and Kirkpatrick [11]. These investigators were interested in the failure envelope for soils. Only in a few cases was the pre-yield behavior the main object of the investigations. Chaplin [12] for example considered the compressibility of sand. He, and most other workers, used the triaxial apparatus for their experimental investigations and it is, therefore, necessary to discuss briefly the advantages and disadvantages of this apparatus.

In the triaxial apparatus, the sample is subjected to a stress system with radial symmetry. It is therefore not possible to study the sample under a general stress state with all three principal stresses different. The vertical load is applied through rigid caps on the top and bottom of the specimen. Due to the tendency of the soil to undergo radial deformations, shear stresses develop at the ends where the sample is restrained, thus producing a stress inhomogeneity in the sample. The actual stress state has been analyzed by Haythornthwaite [13] and Balla [14]. Attempts have been made to lubricate the end plates in the tri-

axial tests (Rowe and Barden [40], Lee and Seed [41], and Bishop and Green [42]), but it was found ([40], [41]) that the behavior of the soil was not appreciably affected by the removal of end restraints on samples of the standard size of 4 in. diameter and 8 in. height. The effect of the geometry of the sample was also investigated by testing shorter samples and it was then found that lubrication of the end plates produced results different from those obtained with standard end plates. The results of those investigations only show that, whereas the effect of end friction may be quite small, the dependence of the measured response of the soil sample on its geometry is an indication that the triaxial test is not a good one. This dependence can be explained by the presence of the rigid end plates. Any initial inhomogeneity in the soil sample favors the development of failure planes when the sample is sheared. Because of the presence of the rigid end plates, the stress conditions become inhomogeneous and the soil will deform more along the failure planes; whereas if a flexible boundary is present, it will deflect in such a way as to maintain the stress homogeneity and inhibit the propagation of these planes. Under an inhomogeneous stress system, different elements will contribute differently to the overall behavior or the sample. This argument is supported by the observation of failure planes and bulging in the soil sample, indicating a non-uniform deformation of the sample. This point will be taken up again in Chapter VII.

The measurements taken in a test using the triaxial apparatus are then not a true representation of the properties of soil but are influenced by the apparatus itself and the geometry of the sample.

Despite these handicaps, the apparatus is still widely used, mainly because a better test is generally not available. Although other pieces of soil testing equipment have been built, such as the simple shear box of Roscoe [15] and the hollow cylindrical sample of Kirkpatrick [11], they have not been developed as much as the triaxial apparatus. Bell [8] built a three-dimensional compression apparatus which is capable of applying any combination of principal stresses to a rectangular plate sample. Since Bell's work is very close to what will be described in this thesis, it is worthwhile to examine his apparatus and discuss his findings.

First of all, his test specimen was contained in a rubber bag which had the shape of a rectangular plate, and was placed in a test frame. A rubber bag (pressure cell) was laid on each of the four sides of the sample bag and touching it, and another flat rubber bag was put under the sample bag. These bags were filled with water which could be subjected to pressure. On the top of the sample bag was placed a rigid lucite plate. Each pair of the pressure cells could apply a principal stress to the sample, while the base cell applied the third principal stress. By varying the pressures in these cells, the sample could be studied under different stress conditions. The stress increments in the three principal stresses were applied in succession and the deformations in the sample were measured by the amount of water coming out or going into the pressure cells. Bell claimed that a homogeneous stress state was attained in the test specimen; however, it is the author's opinion that, since the base cell only covered about 60% of the bottom area of the sample bag, the stress state inside the sample was not homogeneous.

The base cell was made smaller because a 10% strain was anticipated, with the hope of achieving an average homogeneous stress state, whereas only a maximum strain of 2% occurred.

The sample was completely sealed in the sample bag except for a hole at each of the corners. Prior to testing, through one of these holes, the bag was filled with sand with the bag turned into an upright position and rotated through 45° in its own plane. Bell only tested dense samples of standard Ottawa sand (e = 0.53), because he could prepare samples only at the dense state by his method in which the sample was vibrated during preparation.

Although he could carry out hydrostatic compression tests in this apparatus, for that purpose he also built a spherical compression apparatus, consisting of a cylindrical sample bag provided with drainage lines at the ends. The hydrostatic pressure was applied through water in a chamber akin to that of the conventional triaxial apparatus. Evidently this is much easier to operate than the three-dimensional compression apparatus.

In these hydrostatic tests, Ottawa sand was used and it was prepared at different densities. To obtain the true volumetric changes in the sample, Bell had to apply a correction for the penetration of the rubber membrane into the spaces between the sand grains on the surface of the sample. The piece of rubber membrane used in obtaining this correction was thicker (0.051 in.) than the sample bag (0.032 in.), and he argued that, since an average grain diameter was 0.024 in., this discrepancy was not important. He observed that with suitable experimental precautions, the deformation of sand under hydrostatic stress was

almost completely elastic, but non-linear. The fact of elasticity being observed might not be affected by the discrepancy in membrane thickness noted above, but in the opinion of the author the magnitudes of the actual corrected deformations may have been affected, since the magnitude of the corrections was the same as that of the actual deformations.

There were two main kinds of shearing tests performed apart from the hydrostatic tests; the first was one in which the stress point was confined to the octahedral plane and moved radially outward from the hydrostatic axis, Fig. (II.1). This was called a radial compression test. The second was one in which the stress point, also confined to the octahedral plane, moved in a circular path with center at the hydrostatic axis, and this test was called a circular compression test. In some of the radial compression tests, the sample was not stressed to yield (failure). Yield was defined by Bell to be the condition that at least one of the material coefficients relating stress increments and strain increments becomes zero. Upon unloading in these tests, elastic recovery in the principal strains was found to be between 15-20%, and the volumetric strain due to shearing was 40% elastic. With the dense samples tested, an initial contraction in sample volume and then an expansion were observed on the sample when being sheared under radial compression, as in the conventional triaxial tests on dense sand.

In the circular compression tests, starting from a deviatoric stress state below yield midway between the triaxial compression stress state and the triaxial extension stress state, Bell found that a movement of the stress point toward the triaxial extension stress state led toward yield (associated with volume expansion and increasing shear

strain), whereas a movement of the stress point toward the triaxial compression stress state led toward increased "stability" (volume contraction and decreasing shear strain).

He also performed experiments in which the sample was carried to yield in radial compression. For a dense sample under different radial paths, yield was reached at an axial strain of 2-3%, radial strain of $1\frac{1}{2}$-$2\frac{1}{2}$% and volumetric strain of $\frac{1}{2}$-1%, with the equivalent Coulomb friction angle $\varphi = 38°$ for triaxial compression and $\varphi = 52°$ for triaxial extension. The yield (failure) envelope obtained by Bell is shown plotted on the octahedral plane in Fig. (II.2), where the Mohr-Coulomb envelope was also shown. On the basis of standard triaxial compression tests on the same soil ($\sigma_3 = 8$ psi), the peak point friction angle was 37.5° at 4% axial strain and 2% volumetric strain.

Bell also formulated stress-strain relationships in terms of the modified stress and strain invariant functions that he developed. He expressed them in incremental forms and gave numerical values to the coefficients. However it is the opinion of the author that, although the functional forms of these relationships may be correct, the numerical values are not necessarily correct for the following reasons:

(i) The apparatus defects mentioned earlier.

(ii) Stratification in the sample produced by the method of preparation could affect the results of the tests.

(iii) Since it was found that stress-strain behavior of sand was non-linear and largely plastic, the fact that stress increments were applied sequentially meant that if these increments had been applied in a different order, the

results might have been different. However if we consider that the increments are small enough so that a fairly smooth stress path is traced in the principal stress space, this point might not be very important.

(iv) Since only one type of soil at one density was tested, it is not known whether results were general for other soils, and if they were, whether the coefficients in the expressions would vary from soil to soil.

In short, Bell's approach to the problem of mechanics of granular materials was an empirical one, as is the author's, dictated by the necessity of obtaining information on the qualitative soil behavior, and without attempting an explanation of the behavior of the particles at the grain level. His method of curve fitting made it necessary to perform a series of tests on each type of soil in order to extract the necessary coefficients to completely describe the soil behavior. Although he had an adequate apparatus at his disposal, except for the base cell which can be redesigned, the difficulty of sample preparation and the amount of time required for a single test precluded his obtaining a general qualitative view of soil behavior under various conditions of loading.

In spite of the above comments on Bell's work, it must be pointed out that his idea of testing samples three-dimensionally using rubber bags was a good one, and some of his tests (e.g., the circular compression tests) were new. It is felt that, with some improvements, his apparatus could be used more conveniently. In this investigation, Bell's idea of testing soil is pursued further by developing a new soil

test box which operates on the same principle as Bell's apparatus.

(2) Scope of Present Work

The author feels that the stress-deformation characteristics of granular soils have not been systematically investigated. Although in some cases stress-strain relationships have been proposed, ([12], [16], [17]) they were mostly formulated for mathematical convenience and do not necessarily represent the true behavior of soils.

It is desirable to examine the interaction of particles at the grain level and if, from such considerations, stress-deformation relationships can be formulated, to compare them with experimental observations. However, since little work has been done with this object in mind, there is a scarcity of information on which to base our intuition. It is the purpose of this research to study the behavior of a granular medium, sand in particular, by specially designed experiments and then, after extracting the characteristics of its behavior, to explain them from a particulate point of view. In order to obtain meaningful experimental results, it was found necessary to design a new apparatus and this has been found to be useful in studying soil behavior. The design and construction of such an apparatus constitutes a substantial part of the research described in this thesis.

It is pertinent at this point to indicate how the work described in this thesis will fit into the general picture of the mechanics of materials. The ultimate aim in research of this kind is the formulation of valid constitutive relations that describe the behavior of granular matters in general, which can be used to solve practical prob-

lems. The first step towards the formulation of these relations is to understand the qualitative behaviors of one material under simple loadings. Then a different granular material should be studied to see what influence different factors (such as density, grain size distribution and shape of grains) may have in the qualitative behaviors. After determining such influence, we may proceed to propose a continuum that behaves in a similar manner as a granular material, incorporation into it the various factors described above. These factors will appear in the coefficients in the constitutive equations, the formulation of which may require results from tests involving complicated stress paths. Since we are dealing with a non-linear elastic-plastic material, it can be easily seen that such methods as indicated above are really necessary. The work described in this thesis is just the first step towards the systematic study of the mechanics of granular materials.

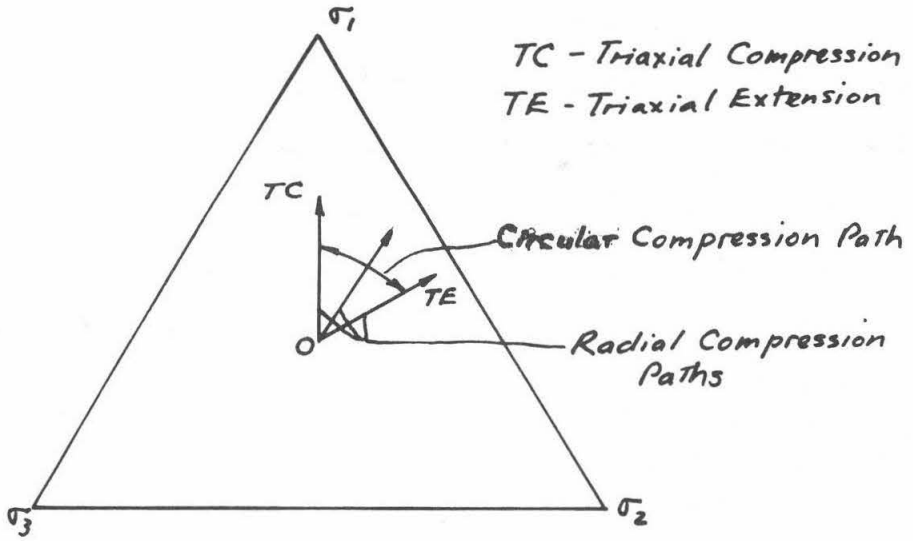

FIG. (II.1)
BELL'S SHEAR STESS PATHS

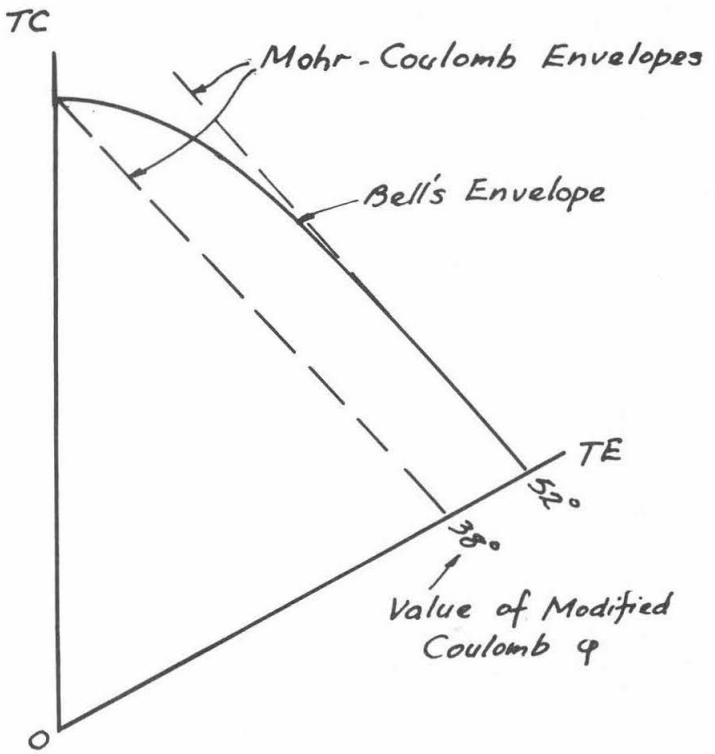

FIG. (II.2). BELL'S YIELD ENVELOPE AND MOHR-COULOMB ENVELOPES.

CHAPTER III

THEORETICAL CONSIDERATIONS

(1) Introduction

It has been mentioned that most work in soil mechanics is empirical, and that very seldom explanation of the soil's behavior from a particulate point of view has been attempted. Some consideration has been devoted to the analysis of regular packings of spheres and rods as models of sand; a review of these works which are mainly concerned with the elastic behavior of the packings is given by Deresiewicz [18]. The results of these analyses were sometimes checked by experiments with the triaxial apparatus [19,20], and, because of the limitations of the apparatus, it is not apparent that the analytical results were actually borne out by experiments. The yield or sliding behavior of regular packings was studied by Dantu [21], Rennie [22], Scott [4], and Parkin [23]. Rowe [24,25] analyzed a few regular packings of rods and spheres under shear stress and from the results drew conclusions about the behavior of a random assembly of granular material. His work has been critically examined [26,27].

A statistical approach to the problem of surface subsidence due to an underground excavation was used by Litwiniszyn [28] and Sweet and Bogdanoff [29]. This statistical approach to the study of a stress-strain relationship of sand is more realistic than one based on the consideration of regular packings, since sand is a random assemblage of granular particles.

In this research, it is proposed to study the behavior of sand under two types of stress state. One is the hydrostatic stress state and the other is a deviatoric stress state. By separating the actual stress state into these two systems, as is usually done in classical linear elasticity, we hope to investigate the degree of coupling between the deformations caused by these stress systems.

In considering the compression of sand by a hydrostatic stress, we can base our analysis on the results of Bell and also on some preliminary tests which were carried out to check on Bell's conclusion about the elasticity of sand under hydrostatic stress. These also showed that the deformation was almost completely elastic. However, when we come to consider the deviatoric stress effects, it is felt that, since this situation is very complicated, Bell's findings regarding the qualitative behavior cannot give sufficient information to help our intuition, and that it is necessary to first carry out some experiments especially designed to extract the characteristic behavior of the material.

(2) Model for Sand under Hydrostatic Compression

Based on Bell's findings [8] that sand under hydrostatic stress undergoes a volumetric strain which is largely reversible, an idealized stress-strain relationship for sand under hydrostatic stress is developed in the following, in which individual grains deform and rebound without permanent deformation and without slippage and rotation. The behavior is assumed to be perfectly elastic.

Let us, first of all, analyze the behavior of regular arrays of equal spheres. It has been found [18] that such spheres can be arranged in the face-centered cubic array or in the tetrahedral array to give the densest possible packing. On the other hand, to give the least dense and yet stable packing, the spheres must be arranged in the simple cubic array. Both the densest (e.g., the face-centered cubic array) and the least dense packing will be examined.

A unit element of a regular array is such that when unit elements are put together they will form the regular array without addition or subtraction of spheres or parts of them, and without rotation of the elements. A unit element of the simple cubic array and one of the face-centered cubic array are shown in Fig. (III.1).

Under hydrostatic stress, the forces developed between the spheres in these regular packings are purely normal forces. (A stress history involving shear forces is excluded). It is assumed that, in any random assembly of particles of more or less spherical shape with non-uniform particle sizes, the intergranular forces developed under hydrostatic stress are also purely normal. (If the grains are angular, the following development has to be modified. This will be discussed in Chapter VII.) This may be essentially true after the granular medium has been subject to a few cycles of loading and unloading with a hydrostatic stress, since this gives the potentially slipping grains a chance to slip and attain more stable positions. Then, based on Bell's experimental results, which show that the volumetric strains are largely reversible, we can assume that the tangential forces acting between grains are small, because tangential forces would produce irreversible deformations [30].

Turning our attention to sand as one particular kind of granular medium, it is observed [31] that the void ratio of a natural deposit of sand lies between 0.43 and 0.85 and is within the limits of those values representing the densest and the least dense regular packings, as given in Fig. (III.1). According to Smith, Foote and Busang [32], an assembly of randomly packed spherical particles may be regarded as an arrangement of separate clusters of face-centered cubic and simple cubic arrays, each present in a proportion to yield the observed porosity of the assembly. Thus if x is the volumetric fraction of face-centered cubic grains, and (1 - x) that of simple cubic grains, then

$$n_{obs.} = x n_{F.C.C.} + (1 - x)\, n_{S.C.} \qquad \text{(III.1)}$$

where n = porosity.

This assumption may be an oversimplification, but has the merit of leading to a statistical estimate which is otherwise impossible.

Some investigators [19,20] have tried to predict the compressibility of a porous granular medium by using Hertz's contact theory [1], which gives the volumetric strain as a two-thirds power function of the hydrostatic stress. However, Bell's results show that for sand such a relationship did not hold. The soil becomes stiffer more rapidly than predicted by a two-thirds power law.

If we postulate that, in addition to the Hertzian compression at existing contact points, successively more contacts are made during a gradual increase in external hydrostatic stress, a model for the behavior of sand can be developed. In this model initially gaps exist

between some grains. These gaps represent potential contacts with are made as the gaps are closed by increasing pressures. The distribution of gap sizes will be discussed later. The compressional characteristics of this "holey" model will be obtained first by considering the two regular arrays discussed above and then approximating the behavior of the sand by the same reasoning as that behind Eq. (III.1).

The Hertz contact theory will be considered to apply at each contact. According to Hertz [1], the centers of two perfect spheres in contact under a normal force N will approach one another by an amount α given by

$$\alpha = 2\left[\frac{\omega N}{R^{\frac{1}{2}}}\right]^{2/3}, \qquad \text{(III.2)}$$

where R = radius of spheres,

$$\omega = \frac{3}{4}\frac{(1-\nu^2)}{E},$$

ν = Poisson's ratio of the material,

and E = Young's modulus of elasticity of the material.

When N increases to N + dN, the relative approach becomes

$$\alpha + d\alpha = 2\left[\frac{\omega(N+dN)}{R^{\frac{1}{2}}}\right]^{2/3}. \qquad \text{(III.3)}$$

$$d\alpha = 2\left(\frac{\omega}{R^{\frac{1}{2}}}\right)^{2/3}\left[(N+dN)^{2/3} - N^{2/3}\right]$$

$$= 2\left[\frac{\omega N}{R^{\frac{1}{2}}}\right]^{2/3}\left[\left(1 + \frac{dN}{N}\right)^{2/3} - 1\right].$$

The last equation is not valid when N is initially zero. In that case

$$d\alpha = 2\left[\frac{\omega dN}{R^{\frac{1}{2}}}\right]^{2/3} . \qquad \text{(III.5)}$$

To represent the holey model in the case of the simple cubic array, we make some of the spheres of the unit element a little smaller than the rest, so that at zero external stress these smaller spheres are not touching each other or the larger spheres. The gaps between these two sets of spheres will be closed under an arbitrary pressure p_i. However, if we take the simple cubic element in Fig. (III.1) and make some of the spheres smaller than the rest, an unstable unit will result and it is therefore necessary to consider a larger element, such as the one shown in Fig. (III.2a).

In Fig. (III.2a), the unshaded spheres are smaller and they do not carry any force at an external pressure $p \leq p_i$. The force-carrying structure in the element is then composed of the shaded spheres. Note that although the smaller spheres are not a part of the force-carrying structure, they do contribute to the measurement of the void ratio. Let the forces between the shaded spheres be N_1 for $p \leq p_i$. As the external stress increases beyond p_i, all spheres including the unshaded (smaller) spheres will carry force. Let N_2 be the force between a shaded and an unshaded sphere, which is the same as the force between two unshaded spheres.

Corresponding to an increase dp in the external pressure p, these forces, N_1 and N_2, change by an amount dN_1 and dN_2 respectively. Equilibrium requires

$$dN_1 + 3\,dN_2 = 16\,R^2\,dp\ . \qquad \text{(III.6)}$$

The compressibility of the holey model is given by

$$\frac{\Delta V}{V} = \frac{3\,\Delta L}{L} = 3\,\frac{\alpha}{2R} = \frac{3}{R}\left[\frac{\omega\,N_1}{R^{\frac{1}{2}}}\right]^{2/3}\ .$$

For $p \leq p_i$,

$$N_1 = 16\,R^2 p.$$

$$\therefore\ \frac{\Delta V}{V} = 3(16\,\omega p)^{2/3}\ .$$

Assuming that the sand grains are the same material as silicon glass, then materials properties can be assumed to be [33]

$$E = 10 \times 10^6 \text{ psi},$$

and $\nu = 0.17$.

From these values we can calculate ω as

$$\omega = \frac{3}{4}\,\frac{(1 - 0.17^2)}{10^7} = 0.0729 \times 10^{-6},$$

and

$$\omega^{2/3} = 0.174 \times 10^{-4}\ .$$

For $p < p_i$,

$$\frac{\Delta V}{V} = 3 \times 16^{2/3} \times 0.174 \times 10^{-4}\ p^{2/3}$$

$$= 3.32 \times 10^{-4}\ p^{2/3}. \qquad \text{(III.7)}$$

When the gaps in a unit element are closed by p_i, we require each unit cube to remain a cube as the pressure increases, so that they can still be put together to form an assembly. This means that $d\alpha_1$ and $d\alpha_2$, the relative approaches caused by the incremental forces dN_1 and dN_2 respectively, must be equal.

Initially, $N_2 = 0$.

$$\therefore\ d\alpha_1 = \frac{4}{3}\left[\frac{\omega N_1}{R^{\frac{1}{2}}}\right]^{2/3} \frac{dN_1}{N_1}\left[1 - \frac{1}{6}\frac{dN_1}{N_1}\right], \qquad \text{(III.8)}$$

(to first approximation)

$$\text{and } d\alpha_2 = 2\left[\frac{\omega dN_2}{R^{\frac{1}{2}}}\right]^{2/3}. \qquad \text{(III.9)}$$

$d\alpha_1 = d\alpha_2$ then gives

$$dN_2 = \left[\frac{2}{3}\frac{dN_1}{N_1}\left(1 - \frac{1}{6}\frac{dN_1}{N_1}\right)\right]^{3/2}. \qquad \text{(III.10)}$$

For $N_2 \neq 0$, instead of Eq. (III.9) we have

$$d\alpha_2 = \frac{4}{3}\left[\frac{\omega N_2}{R^{\frac{1}{2}}}\right]^{2/3} \frac{dN_2}{N_2}\left[1 - \frac{1}{6}\frac{dN_2}{N_2}\right]. \qquad \text{(III.11)}$$

For $d\alpha_1 = d\alpha_2 = d\alpha$, we can solve Eqs. (III.8) and (III.11) for dN_1 and dN_2.

$$\frac{dN_1}{N_1} = 3\left[1 - \sqrt{1 - \frac{d\alpha R^{1/3}}{2(\omega N_1)^{2/3}}}\right]. \qquad \text{(III.12)}$$

$$\frac{dN_2}{N_2} = 3\left[1 - \sqrt{1 - \frac{d\alpha R^{1/3}}{2(\omega N_2)^{2/3}}}\right]. \qquad \text{(III.13)}$$

For the numerical calculations, in the first step an increment dN_1 is made and $d\alpha_1$ calculated from Eq. (III.8). Then dp is obtained from Eq. (III.6) with $dN_2 = 0$. After the first step, an increment $d\alpha$ is made and dN_1 and dN_2 are calculated from Eqs. (III.12) and (III.13), and dp obtained from Eq. (III.6); knowing α, the volumetric strain $\frac{\Delta V}{V}$ can be calculated as a function of p.

Hence, given a simple cubic holey element with a certain given gap width with the corresponding closing pressure p_i, a $\frac{\Delta V}{V} \sim p$ curve can be obtained for all values of p.

For the face-centered cubic array, the holey structure is shown in Fig. (III.2b). The governing equations are essentially the same, except that Eq. (III.6) becomes

$$\frac{4\ dN_1}{\sqrt{2}} + \frac{4\ dN_2}{\sqrt{2}} = 8R^2 dp\ ,$$

$$\text{or,} \quad dN_1 + dN_2 = 2\sqrt{2}\ R^2 dp\ . \qquad \text{(III.6a)}$$

Also for the holey model before closure of the gaps,

$$N_1 = 2\sqrt{2}\ R^2\ p\ ,$$

$$\text{and } \frac{\Delta V}{V} = \frac{3\alpha}{2R} = \frac{3}{2} \cdot 2(2\sqrt{2}\ \omega p)^{2/3} = 1.045 \times 10^{-4} p^{2/3}\ . \qquad \text{(III.7a)}$$

A $\frac{\Delta V}{V} \sim p$ curve can be worked out as for the simple cubic holey element for any p_i.

A Fortran program has been written to solve this problem numerically on the IBM 7090 electronic computer. Curves of $\frac{\Delta V}{V} \sim p$ have been

obtained for both types of regular packings for p_i = 2, 4, 8, 12, 20, 30, 45 and 60 psi are shown in Figs. (III.3) and (III.4).

In Eq. (III.2), R is the radius of curvature at the point of contact. Actual sand grains are not perfect spheres and on their surfaces they have small bulges which have a smaller radius of curvature r, although the overall diameter of the grain is 2R. By sprinkling Ottawa sand (-20 + 40 sieve sizes), which is the same soil as used in later experiments in this investigation, on a flat surface and observing through a microscope their radii of curvature of the grains at the points of contact, it was found that the average value of a = r/R was about 1/3. This will change Eq. (III.2) to

$$\alpha = 2\left(\frac{\omega N}{r^{\frac{1}{2}}}\right)^{2/3} = 2\left(\frac{\omega N}{R^{\frac{1}{2}}}\right)^{2/3} \cdot \left(\frac{1}{a}\right)^{1/3} = 2(3)^{1/3}\left(\frac{\omega N}{R^{\frac{1}{2}}}\right)^{2/3} . \qquad \text{(III.2a)}$$

Hence all the subsequent equations for α and for $\frac{\Delta V}{V}$ should have an extra factor of $(3)^{1/3}$ in them. The curves in Figs. (III.3) and (III.4) all have this factor incorporated. This value of a would be different for another soil.

It is now necessary to consider the distribution of gap widths in a real granular assembly. It must be remembered that the gaps considered are only those which will close at hydrostatic stresses up to a certain maximum pressure (e.g., 100 psi). There may be gaps between adjacent grains which will not be closed under laboratory pressures, because the compressional deformations are very small and deformations due to slippage of grains are supposed to be non-existent. The maximum pressure is chosen as being a reasonable practical value low enough for

no grain fracturing to occur during an experiment.

We expect that these gaps which are potential contacts decrease in number as the pressure under which they may close increases. Another way of looking at this is to consider a succession of models beginning with one in which all the spheres are originally of equal sizes. Any deviation in the sizes of some spheres from this uniform size will give rise to a certain gap distribution. By the same reason also, we expect the peak of the gap size distribution at a very low pressure to be at zero gap width (i.e., contact).

Since a gap width and the pressure to close it are related by Eq. (III.2), we can speak of the distribution of number of gaps, N_α, with respect to pressure, p, or rather to $p^{2/3}$. Let us consider a normal distribution with respect to $p^{2/3}$, Fig. (III.5a). At $p^{2/3} = 3s$, where s = standard deviation of the normal curve, the ordinate of the curve is only 1% of its peak, and the area enclosed between $p^{2/3} = \pm 3s$ is 99.74% of the total area. Let us therefore assume that at $p^{2/3} = 3s$ all the potential gaps have been closed and normalize the area under the curve from $p^{2/3} = 0$ to $p^{2/3} = 3s$ to be unity. An arbitrary pressure p_m is assigned to 3s, and we can then mark off abscissae along the $p^{2/3}$ scale at each 10% increment, say, of the total area under the curve, Fig. (III.5b). Assuming that the gaps of all sizes are uniformly distributed throughout the mass of sand, then each 10% of the sand will have its gap closing pressure p_i at the value of p where 5%, 15% etc. of the total area occurs. Hence by summing up the behavior of all 10 portions, we will have the total overall behavior of an assembly of unit elements having different gap-closing pressures.

Such summation procedures have been carried out for both the face-centered cubic and the simple cubic packings, using a normal distribution of gap width as well as a triangular one, Fig. (III.5c, 5d). The resulting $\frac{\Delta V}{V} \sim p$ curves are shown in Figs. (III.6) and (III.7). It is seen that the two types of distribution employed do not give widely different curves for $\frac{\Delta V}{V} \sim p$, indicating that the compressional behavior of such an assemblage is not very sensitive to the gap distribution. It is also seen that for $p_m = 60$ psi and for $p_m = 100$ psi, the curves lie fairly close to one another.

To obtain the compressional behavior of a granular medium with a porosity n, we again apply the approximation suggested by Smith, et al., [27], thus obtaining

$$\left(\frac{\Delta V}{V}\right)_{assembly} = x\left(\frac{\Delta V}{V}\right)_{F.C.C.} + (1 - x)\left(\frac{\Delta V}{V}\right)_{S.C.}, \qquad (III.14)$$

where x has the same meaning as in Fig. (III.1).

In the laboratory, it was found necessary to base volumetric readings on the volume at a certain non-zero datum pressure, because of the uncertainty involved in obtaining the correction curves for membrane penetration and wall bulging effects. (These will be discussed in Chapter V.) An arbitrary value of 4 psi has been chosen. The theoretical curves shown in Figs. (III.6) and (III.7) are reduced to the same zero volumetric change value at 4 psi and are shown in Fig. (III.8), where the compressibility curve for a random assembly with e = 0.53 as calculated from Eq. (III.14), is also shown. This value of void ratio is that of a medium dense sand tested in the experimental investigation to be described later.

(3) Behavior of Sand under Shear

Mindlin [30] showed that, for two equal spheres compressed by a normal force N and a non-zero tangential force T, there was an elliptical annulus on the area of contact which would undergo "slipping," while no slipping occurred between the two spheres in the area within this annulus. This annulus increased in area as T increased until $T/N = \mu$ = coefficient of solid friction, when the two spheres "slid" past each other. When a force $T < \mu N$ was decreased, slipping in the opposite direction occurred until at zero external force T there was a residual self-equilibrating system of tangential stress on the region of contact. The shear force-shear displacement ($T \sim \delta$) relationship can be represented as in Fig. (III.9). A hysteresis loop resulted from the loading and unloading of the tangential force. Here, "slip" and "slide" have special meanings; slipping can occur on a small scale on only part of the area of contact of the two spheres, while if sliding takes place between them the whole area of contact slips.

The amount of work supplied by shear force T is represented by the area under the curve OA_1. Part of this work is dissipated by the friction force over the annulus where slipping occur and the rest is stored as elastic shear strain energy in the grains. When T is removed, the elastic shear strain energy is recovered and is represented by the area under the curve A_1B_1. Hence the portion of work input which is dissipated is represented by the loop $O\ A_1B_1$. Since the $T - \delta$ relation is non-linear, the ratio of work dissipated by friction to work stored as shear strain energy increases with the maximum value of T reached.

Duffy and Mindlin [34] showed that the stress-strain relations of a regular array of spheres must be expressed in incremental forms to account for the non-linear and inelastic effects of the tangential forces and twisting moments acting at the contacts of spheres when the array is subject to a shear stress. These relations comprise a system of simultaneous, non-linear, integro-differential equations. A solution of this system was obtained by Thurston and Deresiewicz [35], for a stress path in which the tangential and normal forces at the contacts increased proportionately. The same problem for a simple cubic array was analyzed by Deresiewicz [36], and he suggested that the approximation proposed by Smith, Foote and Busang [32] might be applied to a real random granular medium. Although such an approximation may be applicable for the case where the material is under a purely hydrostatic stress, as discussed in Section (2) of this chapter, the situation under a deviatoric stress is much more complicated, because here, if we still use the approximation of Smith, et al., the orientation of the packings with respect to the principal axes of the applied stress is also important [26]. This means that the system of non-linear differential equations has to be solved for each orientation of the packing, and how this orientation is distributed spatially is not known. The mathematics would become exceedingly complicated and look almost impossible. For this reason, the analysis of regular packings has not produced results that describe the behavior of real soils satisfactorily.

In a random assembly of grains of all sizes, as in sand, the factors which affect the shearing behavior of the assembly are, among others, the distribution of contacts and of angles of inclination of

these contacts. Beginning from a state of hydrostatic stress represented by the stress point on the hydrostatic axis, and following the stress path that moves radially outwards from the centroid of the octahedral plane, we can visualize tangential forces being developed at the grain contacts, as in the case of a regular packing. These tangential forces produce first slipping and later sliding and hence largely irreversible displacements, whenever the ratio of tangential force, T, to normal force, N, is equal to the coefficient of friction, μ, of the material of which the grains are made of; i.e., when the condition

$$T/N = \mu \qquad \text{(III.15)}$$

is reached.

For the assembly under a given shear stress, which contact will slide depends partly on its contact angle. However, although two grains have their contact force at an inclination to the normal plane through the contact greater than the angle of friction, $\varphi_\mu = \tan^{-1}\mu$, they are surrounded by other grains and are hence prevented from undergoing any major movement, except a slight slide which brings about a force redistribution in the neighborhood of this contact. This may stabilize the contact but may bring another one into the critical condition, Eq. (III.15), which will in turn slide and cause another force distribution whereby the first contact may become unstable again. This process goes on until equilibrium is attained everywhere and the condition $T/N \leq \mu$ is satisfied at each contact. The disturbance at the grain level is propagated to the boundaries of the mass and we notice irreversible (not elastic) deformations on the boundaries. It is readily seen that this force

redistribution and propagation process is time-dependent and hence the deformations at the boundaries are also time-dependent, even when real diffusion or relaxation effects are absent.

In general, the work done on the boundaries by an increment of applied shear stress can be decomposed into three parts. The first part is stored as elastic strain energy in the grains, causing elastic deformations. The second part is dissipated by slipping of the grains; this occurs at all the grain contacts. The third part is dissipated by the grains sliding at contacts where $T = \mu N$; this occurs at certain contacts. The deformations observed on the boundaries are combinations of the elastic deformation and deformation due to slipping and sliding of the grains. When the shear stress on the mass is removed, the stored elastic strain energy is released, causing elastic rebounds at the boundaries. Counter-slip also occurs on all the contacts, which also contributes to the deformations observed on the boundaries during unloading. Presumably, the unloading may also cause another grain rearrangement by sliding, with a consequent force redistribution.

Should the load be applied again along the same stress path as before and up to the same stress level, another series of grain rearrangements and force redistributions may occur, while at the same time elastic strain energy is being stored in the grains. Both the plastic deformations due to grain slipping and sliding and the elastic strain energy stored may be different from those occurring on first loading. Hence, when the shear stress is taken beyond the level attained at the first loading, the deformations (plastic and elastic) may be different

from those obtained if there has not been an unloading cycle at a lower stress level. In other words, the stress history is important in the stress-deformation behavior of the soil.

For a second increment of shear stress in the first cycle of loading equal in magnitude to the first one, the grains undergo some more elastic deformation and therefore store up elastic energy as before. More contacts are brought into the critical condition and slide. It must be noted that for each increment of the octahedral shear stress, there is a plastic deformation. Hence the material as a whole can be considered to "yield" from the initiation of shearing stresses, where the term "yield" has the usual meaning of classical plasticity theory. By this reasoning there is no point distinguishable on the shear stress-deformation curve of sand, above which the material is said to have "yielded." Yielding occurs at all shear stress levels.

However, if we consider the amount of elastic strain energy stored in the grains, we see that this will increase as the shear stress increases, while the plastic deformation also increases. For a stress path, Fig. (III.10a) in which the shear stress is always increasing, we can plot the stress, τ_{OCT}, against one of the principal deformations, u_1, Fig. (III.10b). Here u_1 is the total deformation corresponding to the major principal stress σ_1, after the grain rearrangement and force redistribution process has stopped. This relationship between stress and deformation is non-linear with the deformation increasing more rapidly than the stress. There is a point, F, on this curve, where the total elastic strain energy stored in the mass reaches a maximum. Any additional energy input at the boundaries caused by another increment of

shear stress has then to be dissipated completely by sliding of the grains. The subsequent grain rearrangement releases some of the previously stored energy which is dissipated by further grain sliding. Hence on the stress-deformation curve, we may notice an increase in the rate of deformation with respect to stress. However, the point F at which this increase occurs may be difficult to distinguish in an experiment in which the stresses are varied continuously. But when the stresses are varied step-wise, a discontinuity may be noticeable depending upon the size of the stress increment.

The amount of elastic strain energy stored in the grains depends, for the same stress level, on the state of packing of the medium, whether dense or loose. A densely packed medium can store a larger amount of maximum strain energy than one which is loosely packed. Hence when the stress is increased after the energy has reached a maximum at F, more energy will be released in a dense medium than in a loose one. We expect to find a larger deformation due to this release and the accompanying slipping for a dense medium, and, therefore, the discontinuity of the stress-deformation curve is pronounced. For a very loose soil, it may not be noticeable at all on the experimental curve.

We have therefore seen that "yield" actually occurs in the medium at all levels of shear stress, whereas at a certain point along the stress path, there is a change in the rate of displacement due to the release of strain energy. This point represented by F in Fig. (III.10) is here called the "failure" point. There is considerable grain movement at failure, and the grain structure may undergo a major adjustment. Since the stress-deformation relation is influenced directly by the grain

structure, we expect it to be different after failure. After failure, most of the energy input as well as some of the released energy is dissipated by grains sliding and the medium can be considered to be completely plastic.

The initial yielding at small stresses produces a preferred direction for the grains to orient themselves. Even if we start with an isotropic material, it will become anisotropic when sheared, as observed by Bell [8]. However, the degree of anisotropy is related to the stress history. Hence, if we only study the behavior of initially isotropic material being sheared from a hydrostatic state of stress, we need only keep track of the stress history.

Dilation (positive or negative) in soil when sheared is a well-known phenomenon. It has been observed on soils tested in all kinds of apparatus. Although in the conventional triaxial compression test the mean stress increases, which always causes initial volumetric compression of the soil, it is felt that eventual dilation is not caused by characteristics of the apparatus and would occur even if the soil is sheared under constant hydrostatic stress.

This intrinsic property of soil can be explained from the particulate point of view. When a granular medium is subjected to pure shear, tangential forces develop at the contacts of the grains which will slip over one another, and there will be observed a net volume change in the medium. While the grains slide in such a way as to make more contacts in one direction than the other (producing subsequent anisotropy), we can imagine that more contacts will now have their tangential planes perpendicular to the major principal stress and less

contacts with tangential planes perpendicular to the minor principal stress. This is, in general, necessary to provide equilibrium although the presence of tangential forces at the contacts produces complications. Further shearing is produced by an increase in the major principal stress and a decrease by the same amount in the minor principal stress (in a two dimensional situation). Assuming, for the sake of argument, that external stresses are resisted by normal forces, the change (an increase) in these forces at the contacts perpendicular to the major principal stress will be smaller than that (a decrease) in those forces at the contacts perpendicular to the minor principal stress, because the former contacts are greater in number. However, the forces at the latter contacts are decreasing, and since the normal force ~ normal displacement relation is a non-linear one (Eq. (III.2)), the compression due to increase in the former forces is therefore less than the expansion due to the decrease in the latter forces, and as a result the net volume change of the medium will be an expansion.

Hence it is seen that the volume change in soil under pure shear is due to two factors. While the non-linearity in the force-displacement relation at a single contact gives rise to an expansion, the effect of the grains slipping over one another can be either an expansion or a contraction, depending upon the initial density of medium. Which factor will dominate the dilational behavior depends on the density as well as the state of shear. Initially for a dense soil, both factors may produce an expansion, while for a loose soil, the grain sliding effect may dominate, thus producing a compression. When the failure state is approached, a large proportion of the grains will have been oriented in the preferred

direction, and it may be conceivable that in such an arrangement they are able to slide past one another without contributing noticeable volumetric effects. Therefore, at this state the dilation results only from the contribution of the non-linear effect, indicating that an expansion should always accompany the shearing near failure. This is in agreement with the mathematical analysis of Drucker and Prager [39], who found that a granular material has to expand while yielding. Presumably, when the deformations become very large (20% or more) the soil may reach a constant void ratio irrespective of the initial void ratio. This constant void ratio is called the critical void ratio of the soil.

We have therefore seen that the shearing behavior of a granular medium is very complicated. It has been suggested by Scott that, to study such behavior, we can generate a random assembly of spherical particles by the method suggested by Vold [32]. We can next treat the structure of the grains subject to external loading as an indeterminate structure with a certain elastic properties attached to the grains. It is immediately seen that, in order to reduce the effects of the boundaries, we require a large number of grains and the degree of indeterminacy of the structure goes up quickly. Although electronic digital computers have been used to solve plane stress problems by means of one-dimensional elements with node points on a regular grid work, [38], the present problem is a three-dimensional one with random node points, which is very difficult to program for the computer. If this difficulty could be overcome, this approach is attractive in that it is applicable under all loading conditions.

However we would like to examine various aspects of the qualita-

tive behavior described. Therefore it is here proposed to obtain more experimental results with the purpose of helping our intuition in formulating stress-strain relationships for sand. The theory and purpose of the tests carried out in this investigation is now described.

(4) Theory and Purpose of Experiments

We separate a stress state into two components, the hydrostatic and the deviatoric states, and we propose to study the relations between the deformations caused by them.

(i) Hydrostatic Compression Test

In this test, the three principal stresses are kept equal to each other. The stress path is represented in the principal stress space as shown in Fig. (III.11). The hydrostatic stress, denoted by p (or σ_{OCT}), is equal to $1/\sqrt{3}$ times the distance of the stress point along the hydrostatic axis. In this test, the value of p is increased from zero at O to a maximum p_m at B, and then decreased to a datum pressure p_o at A. As many cycles of hydrostatic stress are applied as desired between p_o and p_m.

The purpose of this test is to find out what proportion of the volumetric strain is elastic and the effects of repeated cycles of loading and unloading, and to compare the compressibility curve with the theory in Section (2) of this chapter.

(ii) Shear Tests in the Triaxial Plane

The stress path here is either the triaxial extension ($\sigma_1 = \sigma_2 \geq \sigma_3$) or the triaxial compression ($\sigma_1 \geq \sigma_2 = \sigma_3$) stress path. It can be readily represented in the triaxial plane. There are five tests in this

category. In all tests, stresses are applied, removed and reapplied to examine the proportion of the soil's behavior which is elastic.

(a) The stress path in this test, designated TCa for triaxial compression and TEa for triaxial extension, is shown in Fig. (III.12). Starting at any initially hydrostatic stress state at A, the stresses are varied so that the stress point remains on the octahedral plane through A. The hydrostatic, or the mean, stress is therefore kept constant. As the stress point moves away from A, the value of τ_{OCT} increases from zero.

The purpose of this test is to determine the shear deformation when only the shear stress is varied while starting from an initially isotropic state and the only stress history consists of hydrostatic stresses. It is also used to determine the point at which the soil fails under the stress conditions stated.

(b) This test has the stress path shown in Fig. (III.13). The shear stress, τ_{OCT}, is increased from zero at A to a certain value at B_1, and is then returned to zero. The next step is from A to B_1 again, and then increased further to B_2, after which it is returned to zero and so on. These cycles of loading, unloading, reloading to the previous maximum value, and then loading to another new maximum value, are carried out until the soil is believed to have passed the failure point as found in (a). (The TE stress path is shown only in Fig. (III.12) and not shown in subsequent figures.)

This test, designated as TCb (TEb), is for determining what proportion of the shearing deformation is elastic, and, by comparing the total deformation obtained when the shear stress reaches a new maxi-

mum to that obtained in (a), to find out the effect of stress history on the stress-deformation relation of the soil.

(c) The stress path for this test, shown in Fig. (III.14), is the same as that in (b), except that each time when the shear stress is returned to zero value at A, a cycle of hydrostatic stress is applied along the hydrostatic axis from A to C and back to A. After this, the shear cycle begins again.

This test, TCc (TEc), is to find out what is the effect of stress history on the hydrostatic compression of the soil. The compressional behavior of the soil under hydrostatic stress is determined by tests (i).

(d) The stress path for this test, shown in Fig. (III.15), consists of shearing with constant hydrostatic stress from A to B_1, an increase in both τ_{OCT} and σ_{OCT} from B_1 to C_1, a return from C_1 to B_1, and then further shearing from B_1 to B_2. The portions of the path, B_1C_1, B_2C_2, etc., pass through the origin O when produced. That means the stress ratios, $\frac{\sigma_1}{\sigma_3}$ or $\frac{\tau_{OCT}}{\sigma_{OCT}}$, do not change along these portions of the stress path, but between B_1 and B_2, or B_2 and B_3, these ratios do change. From B_1 to C_1, B_2 to C_2, etc., the magnitude of τ_{OCT} changes in proportion to σ_{OCT}. These cycles of loading and unloading with constant stress ratios are carried out at each value of the stress ratios at B_1, B_2, etc., until the soil is believed to have failed.

The deformation in the soil when the stresses are changed from B_1 to C_1 consists of two portions, one due to the change in the mean stress, $\Delta \sigma_{OCT}$, and the other due to the change in the shear stress, $\Delta \tau_{OCT}$, whereas there is no effect due to the stress ratios which are kept constant. If we could provide measurement for the volumetric strain

alone, we may determine how these two components are related. The unloading cycle from C_1 to B_1 is important in that it tells us whether the deformation due to $\Delta\,\sigma_{OCT}$ is elastic or not.

(e) The stress path employed in this test is shown in Fig. (III.16). It consists of shearing at constant hydrostatic stress from A to B_1, applying a hydrostatic stress on top of the existing shear stress from B_1 to C_1, removing this hydrostatic stress from C_1 to B_1, and then applying a further increment of shear from B_1 to B_2.

The portions of the path B_1C_1, B_2C_2, etc. are parallel to the hydrostatic axis, and hence the value of the shear stress, τ_{OCT}, does not change along these portions. But the hydrostatic stress, σ_{OCT}, is increasing, therefore, $\frac{\tau_{OCT}}{\sigma_{OCT}}$ decreases. The deformation in the soil then comprises of two portions, one due to $\Delta\,\sigma_{OCT}$ and the other due to $\Delta\left(\frac{\tau_{OCT}}{\sigma_{OCT}}\right)$. Therefore, this test shows us the effect of a hydrostatic stress state superimposed on a shear stress state. The unloading portions, C_1B_1, C_2B_2, etc., determine what portions of the deformations are elastic.

Along a general shear stress path, shown for convenience on the triaxial plane in Fig. (III.17), the difference in the stress states at A and B can be represented by the change in the hydrostatic stress σ_{OCT}, the change in the shear stress τ_{OCT}, and the change in the stress ratio $\frac{\tau_{OCT}}{\sigma_{OCT}}$. These are the factors which affect the deformations in the given soil. By the shear tests (a) - (e) described above, we can differentiate among these effects and determine to what extent they are superposable upon each other. These tests need not be confined to the triaxial plane,

but for convenience of presentation and, since we want to extract the qualitative characteristics only, they are assumed to reflect the behavior of the general case in which the stress path is not confined to the triaxial plane.

(iii) Radial Shear Tests

For the purpose of investigating the stress-deformation relations of the soil under general three-dimensional stress states, these tests are carried out by keeping the mean stress constant. The stress paths, therefore, lie on an octahedral plane, whose position is determined by the value of the mean stress. One such plane is shown in Fig. (III.18), where stress paths are chosen radially from the hydrostatic axis O. Three such paths, OA_1, OA_2 and OA_3, are chosen, which divide the 60°-sector bounded by the triaxial compression and the triaxial extension stress paths into four equal segments. They are termed RS-45°, RS-60° and RS-75° respectively. The middle one, RS-60°, is especially interesting in that σ_2 is constant along it. The plane strain stress condition lies somewhere among these three stress paths, although it is not necessarily represented by a straight stress path.

These radial tests are part of the investigation of the failure envelope. They, when combined with tests TCa and TEa, carried out for various values of the hydrostatic stress, will define a failure envelope in the principal stress space for soil loaded once directly to failure. The other tests, TCb, c, d, and e, will determine how the position of the envelope is affected by the stress history in those tests.

(iv) Tests for Anisotropy of the Sample

Naturally occurring soils are inherently anisotropic due to the conditions prevailing during deposition of the soils. We want to determine the degree of anisotropy in the samples that are prepared for use in the tests outlined above. One way of doing this is to prepare two samples to the same density by the same procedure, testing one sample by applying a certain combination of principal stresses, and testing the other sample by applying the same combination of principal stresses but with a rotation of the directions of the stresses, as demonstrated in Fig. (III.19). The strains measured in the two tests may then be compared. If they differ, we can conclude that anisotropy exists in the sample.

This method of testing for anisotropy is a more sensitive one than just measuring and comparing the three principal strains in a hydrostatic compression test, because the shearing deformations in the present method are much greater than the volumetric strain in the hydrostatic test.

SIMPLE CUBIC ARRAY
UNIT ELEMENT

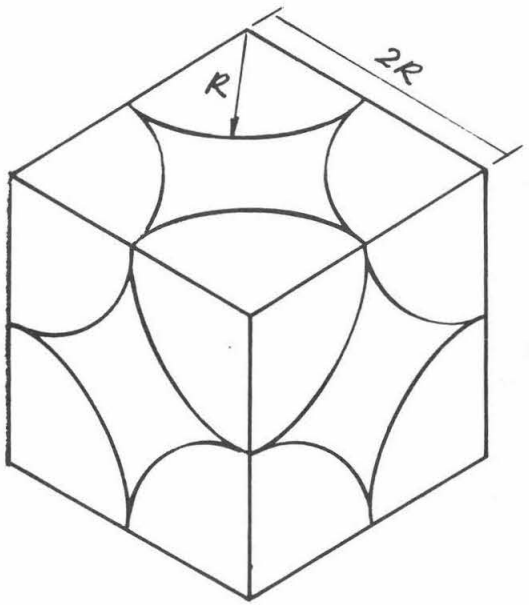

$e = 0.910$; $n = 0.476$

FACE-CENTERED CUBIC ARRAY
UNIT ELEMENT

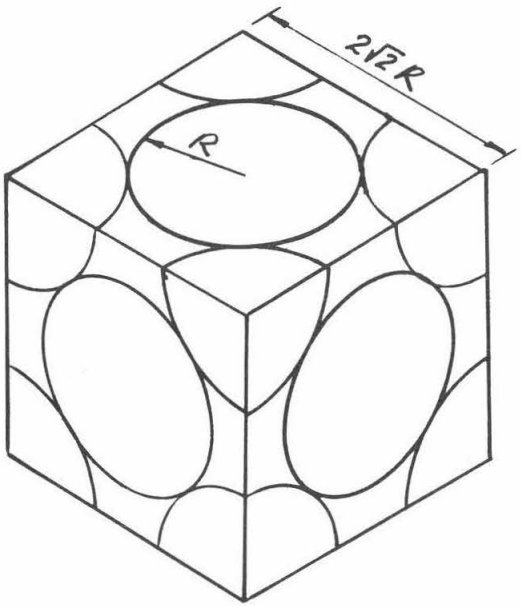

$e = 0.351$; $n = 0.260$

(e – Void Ratio ; n – porosity ; $e = \frac{n}{1-n}$)

FIG. (III.1)

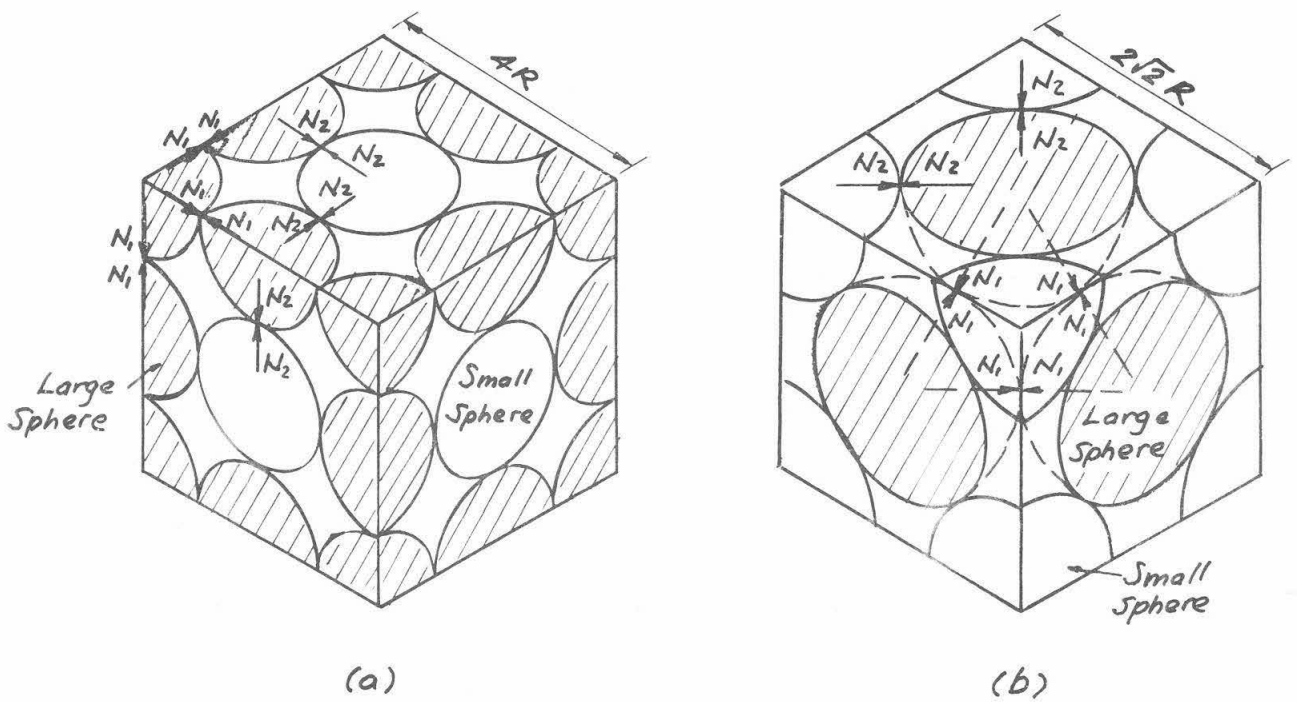
HOLEY ELEMENT, S.C.
HOLEY ELEMENT, F.C.C.
4R
2√2 R
N1
N2
Large Sphere
Small Sphere
(a)
(b)

FIG. (III.2)

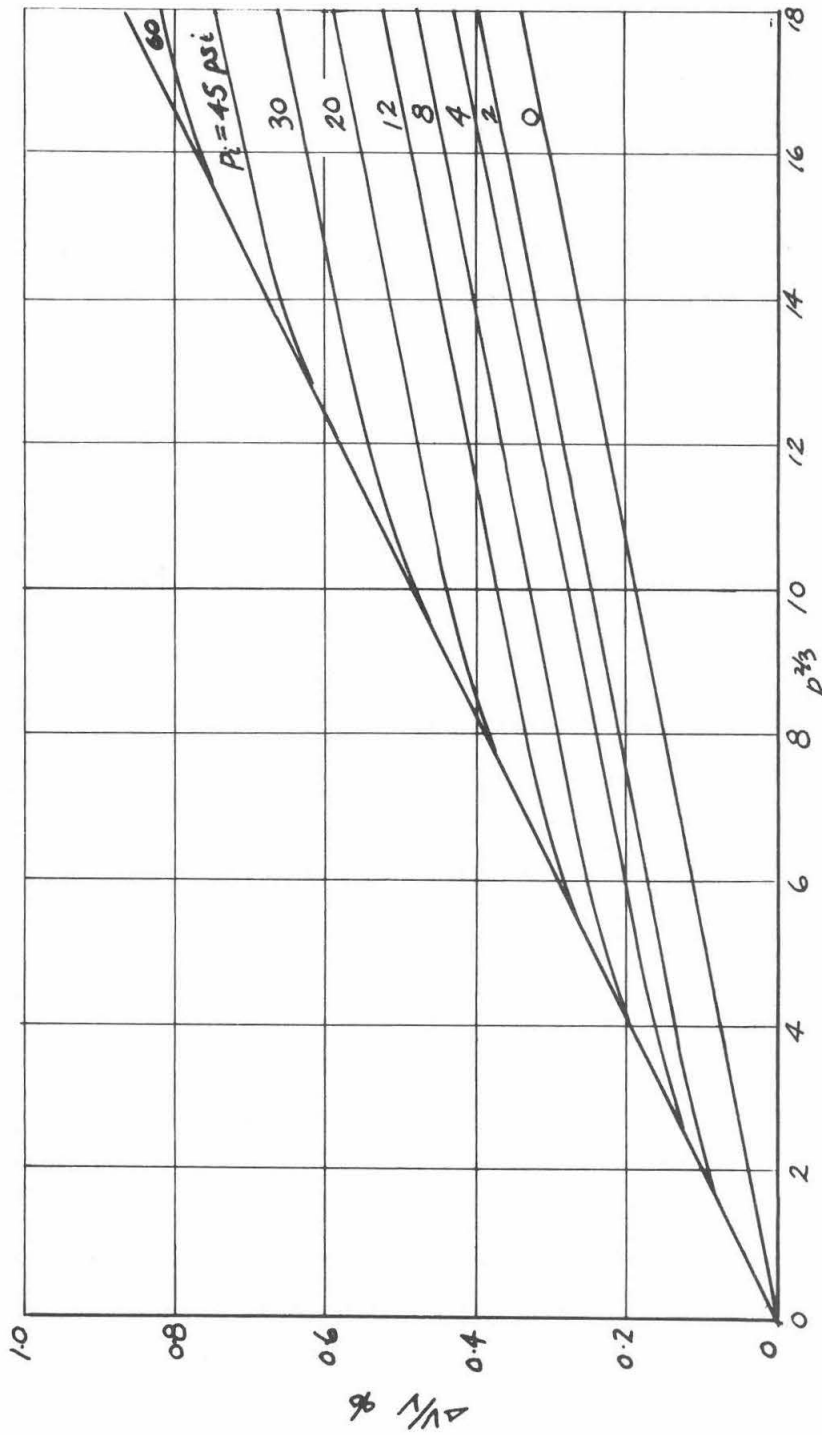

FIG. (III.3). COMPRESSIBILITY OF S.C. HOLEY MODEL

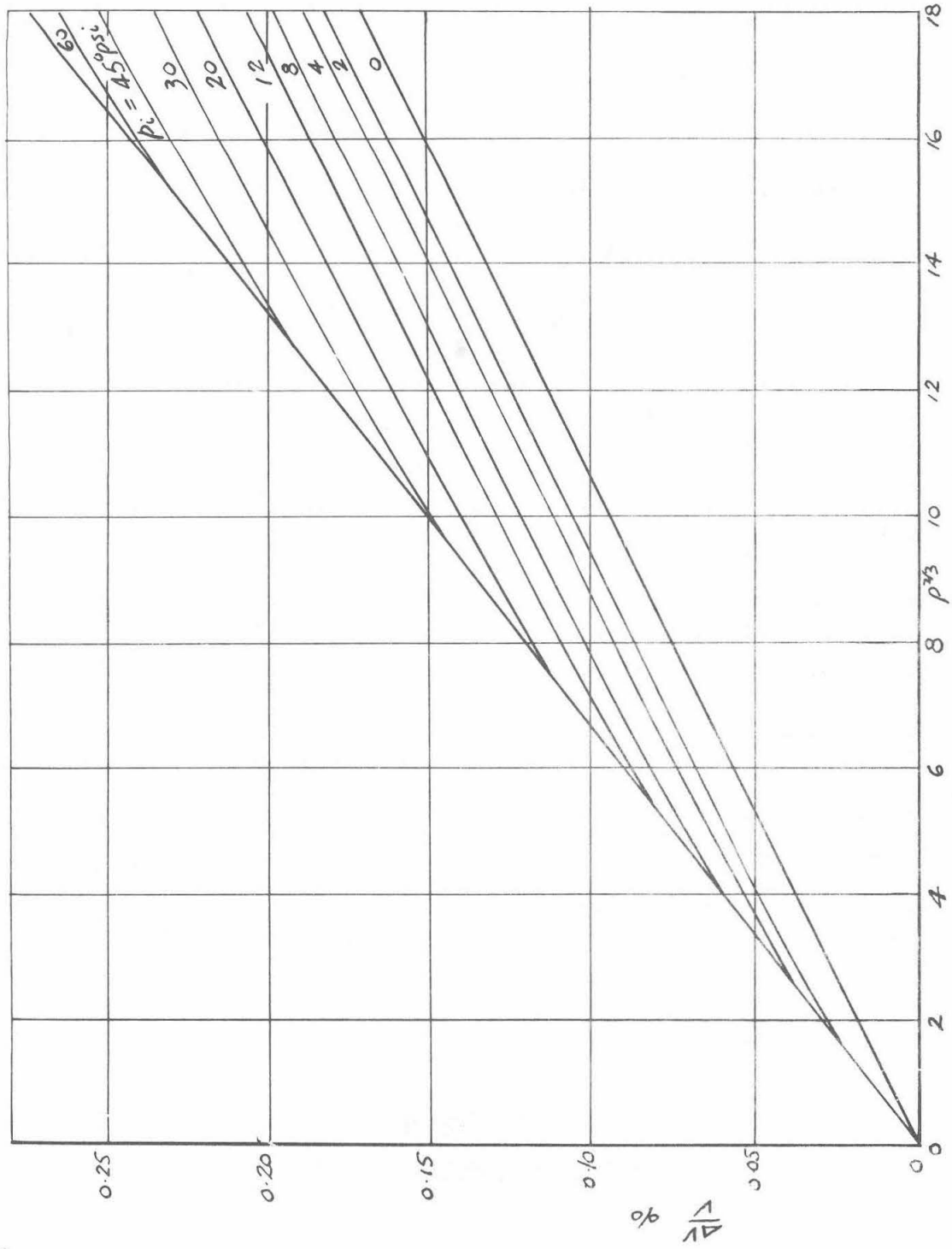

FIG. (III. 4). COMPRESSIBILITY OF F.C.C. HOLEY MODEL.

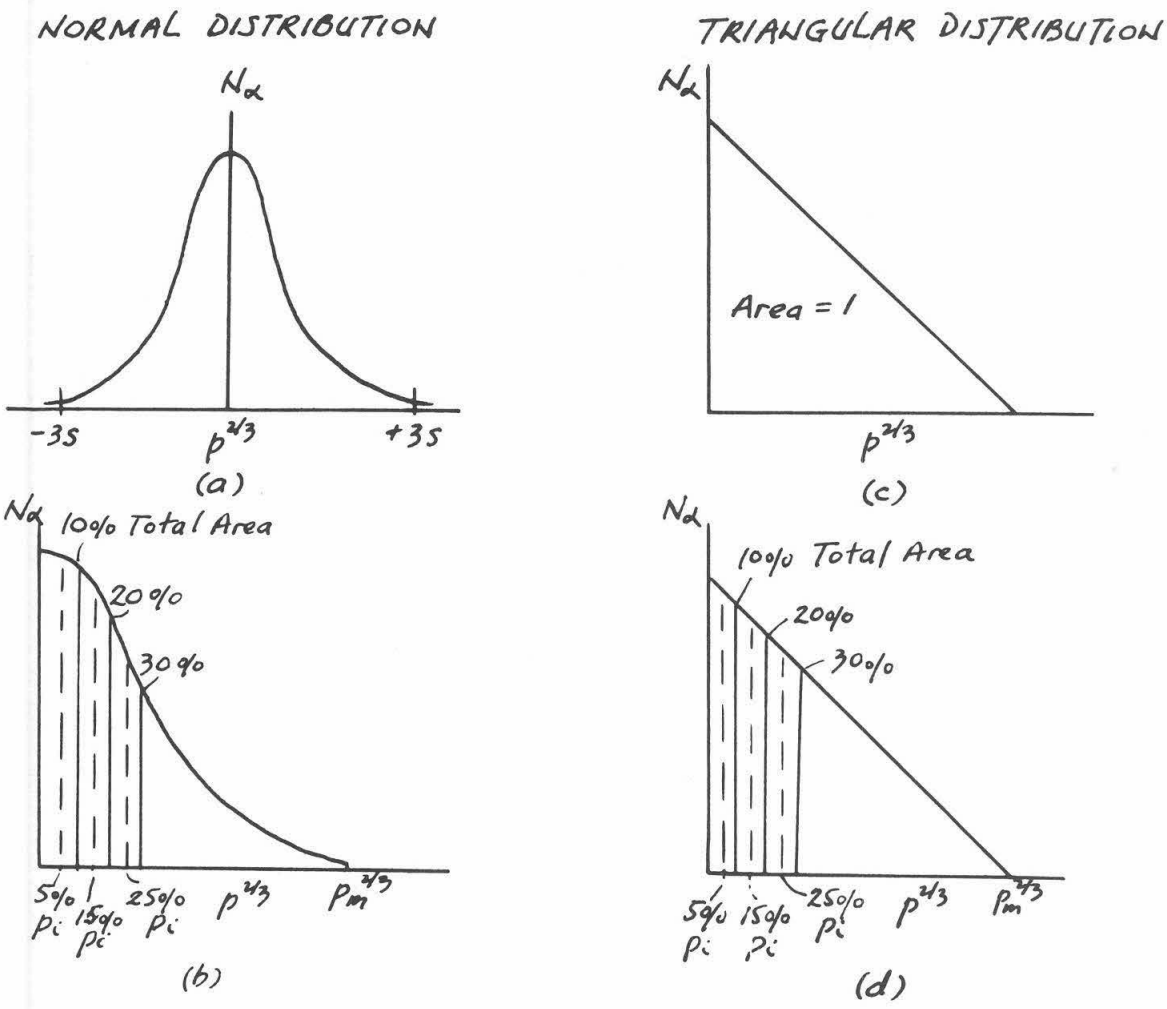

FIG. (III. 5)
GAP DISTRIBUTIONS

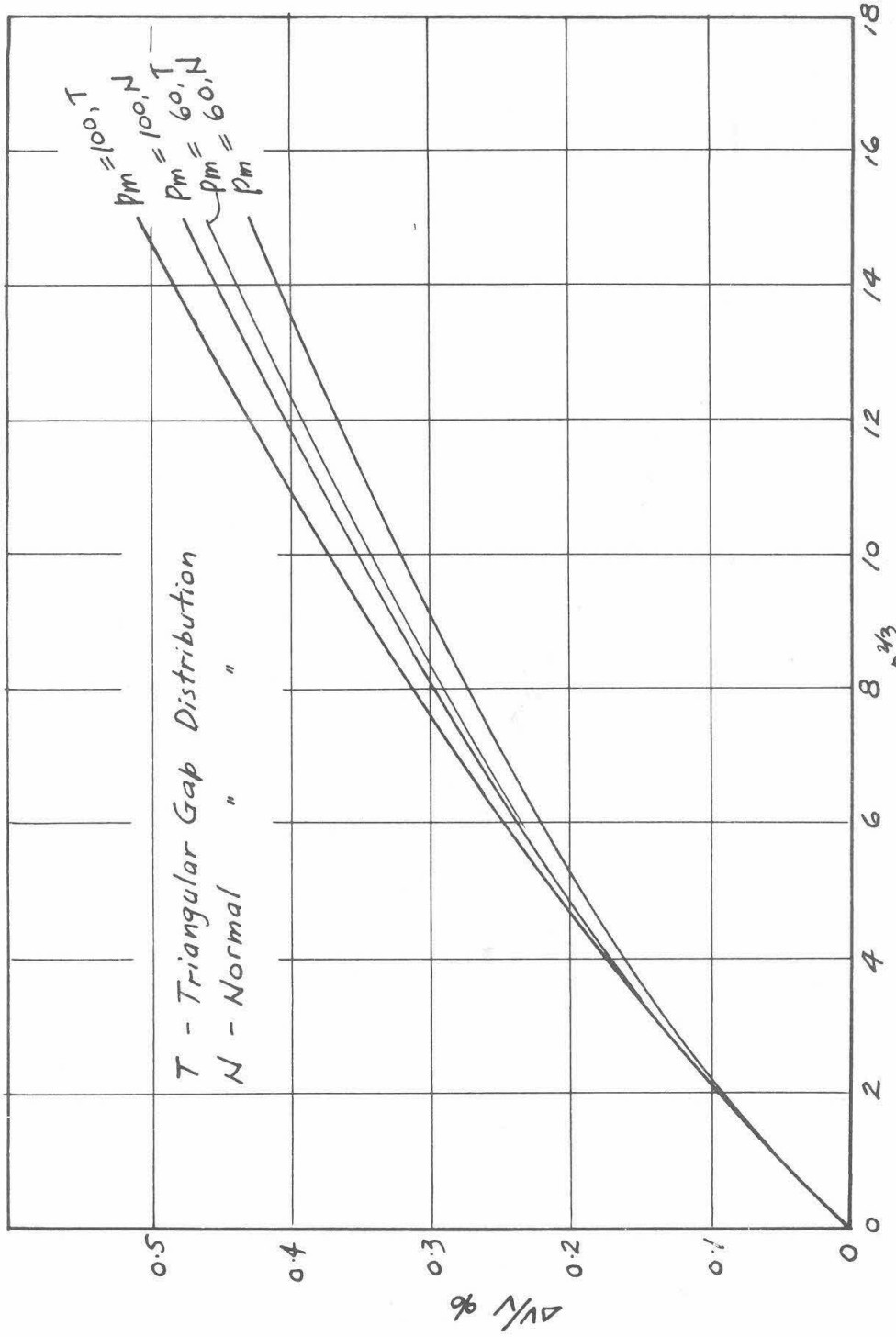

FIG. (III.6). COMPRESSIBILITY OF S.C. HOLEY MODEL FOR DIFFERENT P_m AND GAP DISTRIBUTIONS

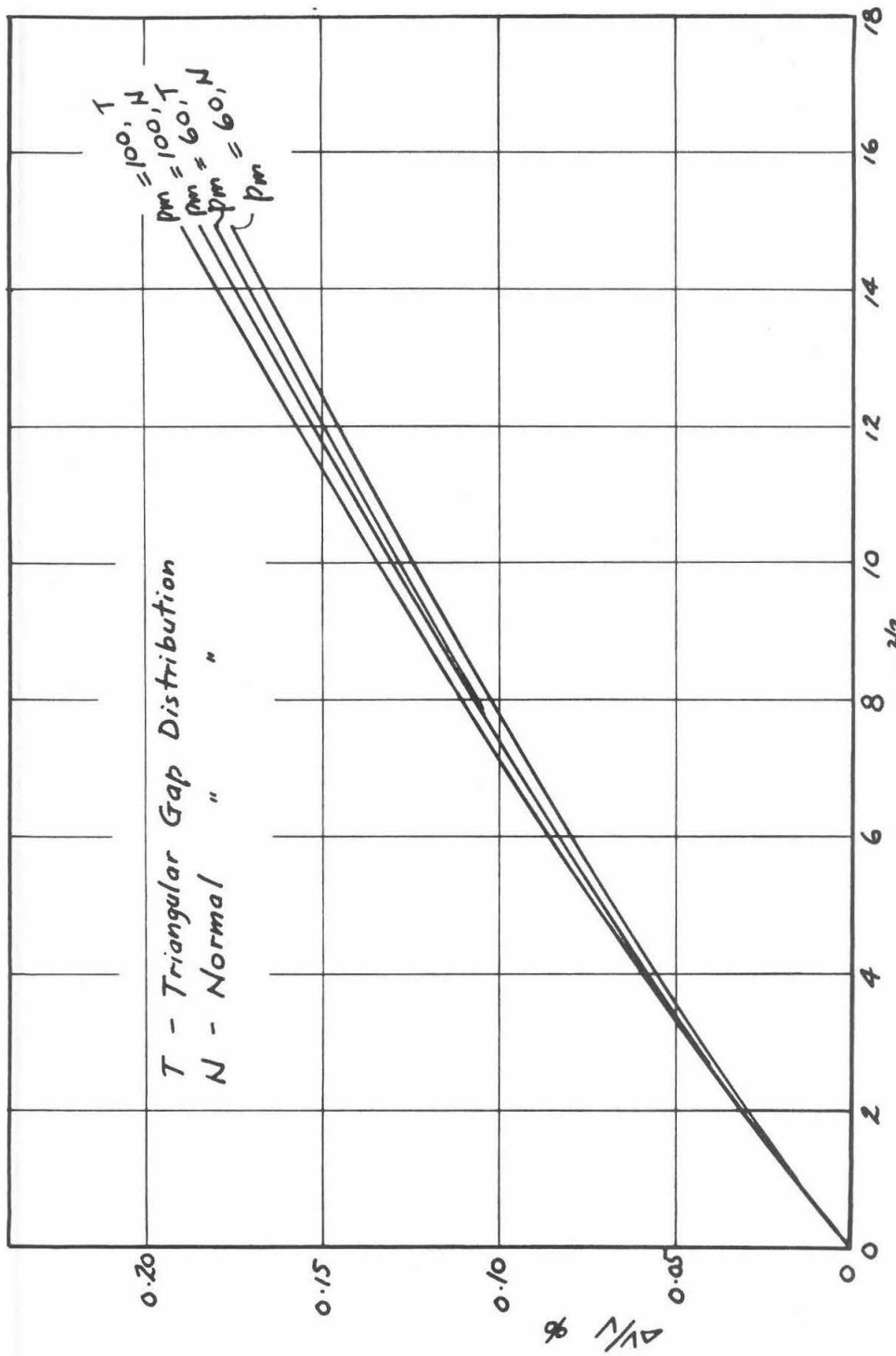

FIG. (III. 7). COMPRESSIBILITY OF F.C.C. HOLEY MODEL FOR DIFFERENT p_m AND GAP DISTRIBUTIONS.

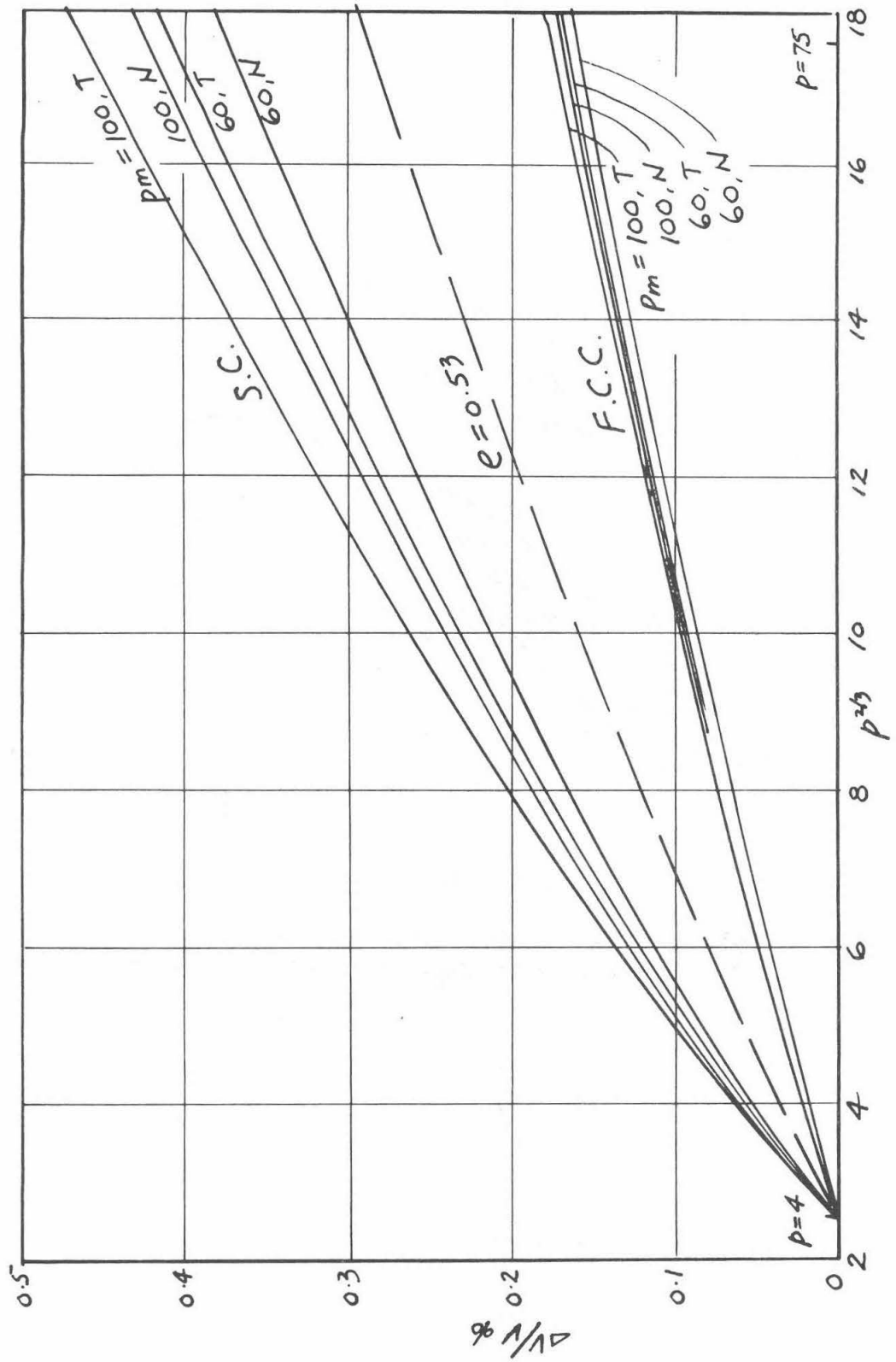

FIG. (III.8). COMPRESSIBILITY OF HOLEY MODELS REDUCED TO A DATUM PRESSURE

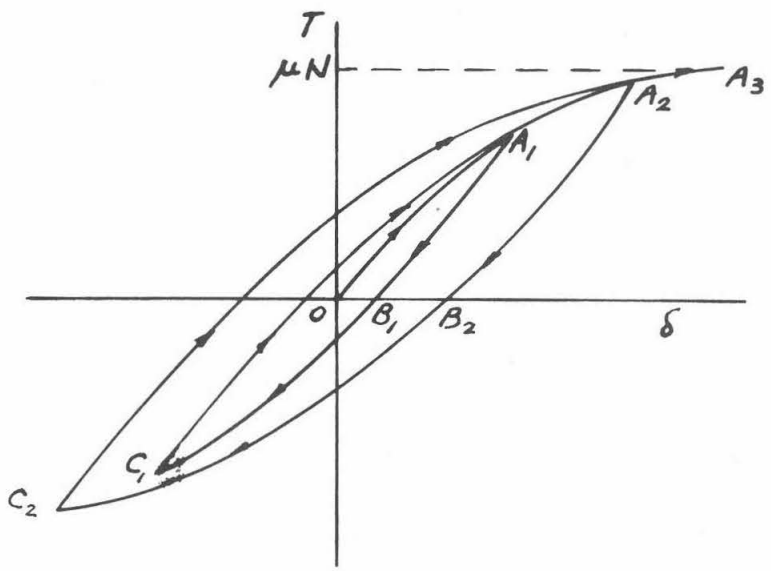

FIG. (III.9)

TANGENTIAL FORCE - DISPLACEMENT
RELATIONSHIP FOR TWO SPHERES IN CONTACT

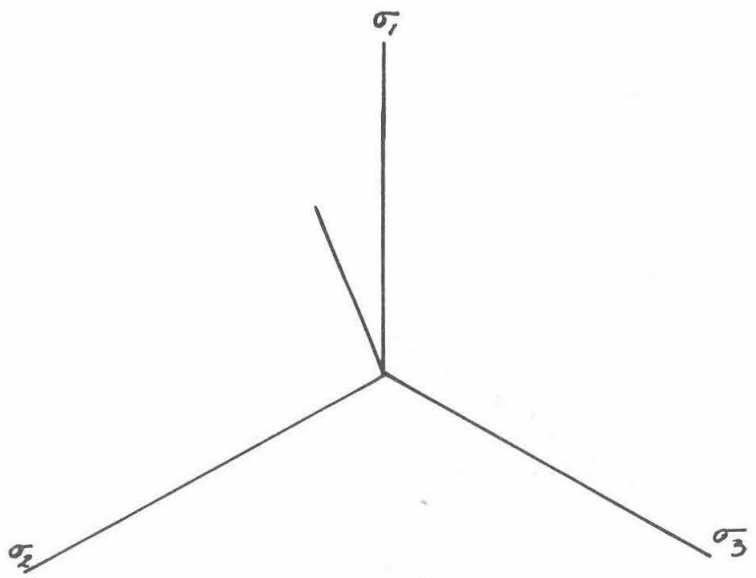

(a) Stress Path on Octahedral Plane

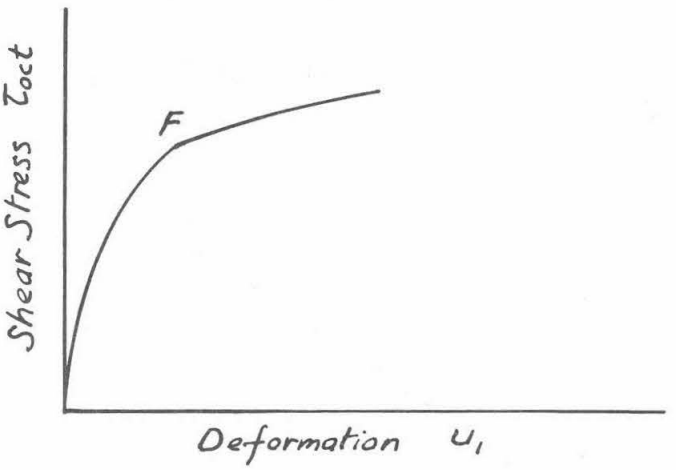

(b) Stress Deformation Curve

FIG. (III.10)

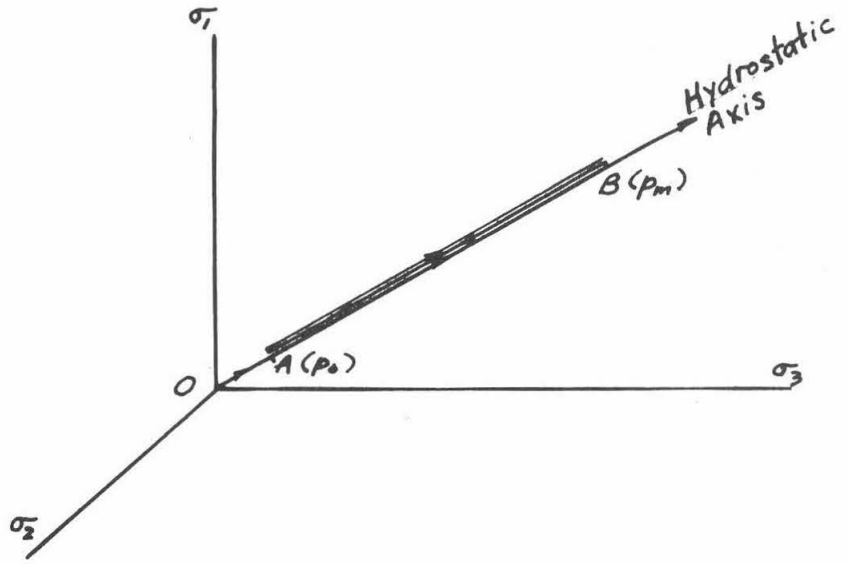

FIG. (III. 11). STRESS PATH FOR HYDROSTATIC COMPRESSION TEST

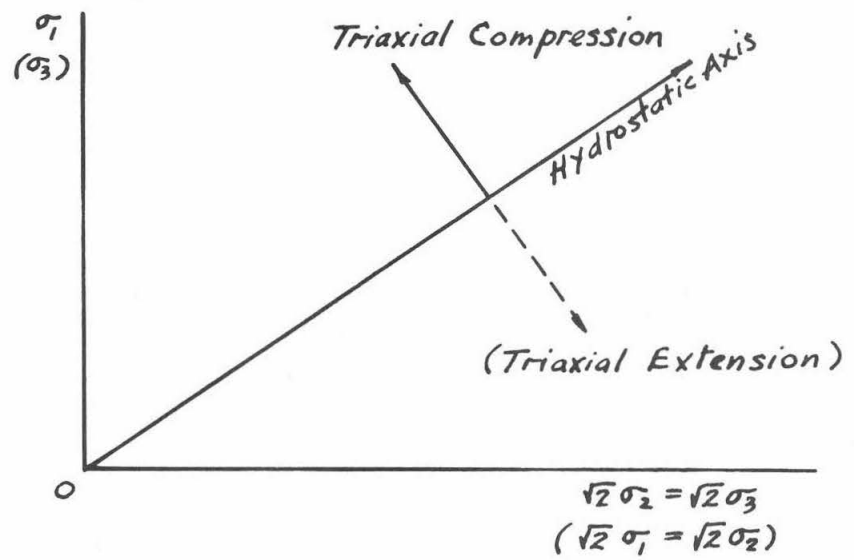

FIG. (III.12) STRESS PATHS FOR SHEAR TESTS TC a (TEa)

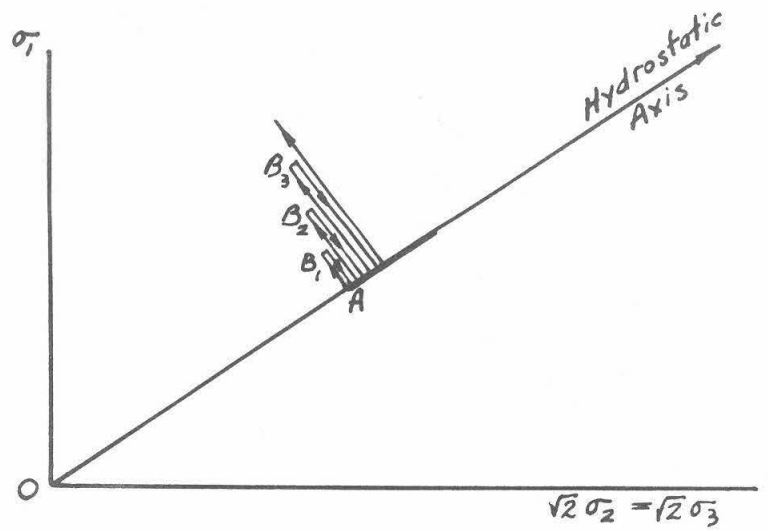

FIG. (III.13). STRESS PATH FOR SHEAR TEST TC 6 (TE6)

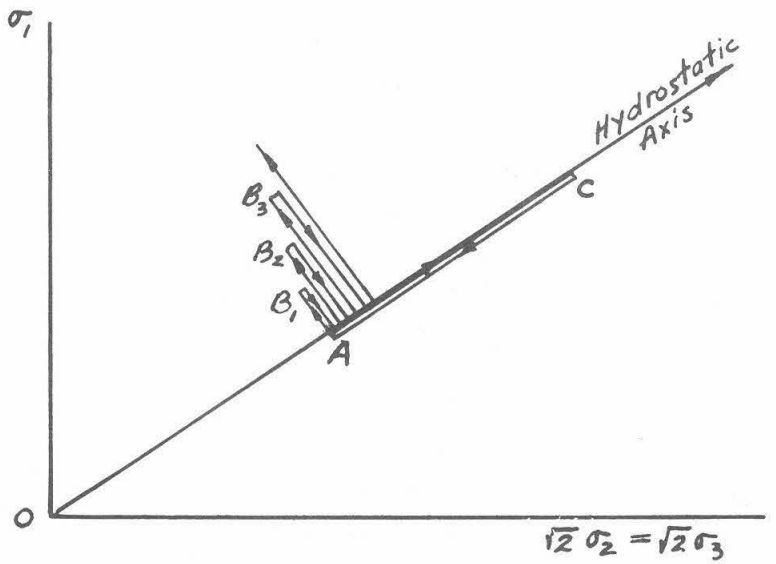

FIG. (III.14). STRESS PATH FOR SHEAR TEST TCc (TEc).

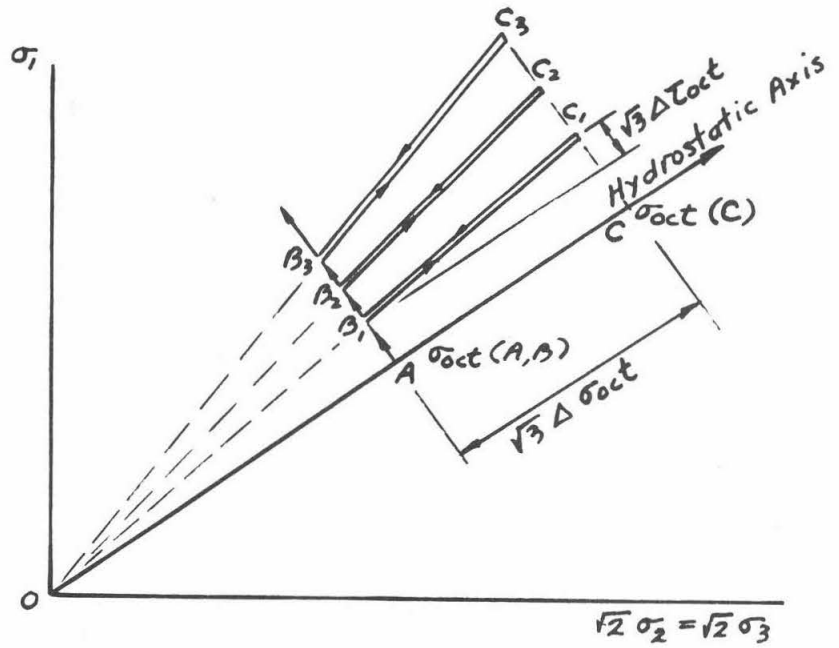

FIG. (III.15). STRSS PATH FOR SHEAR TEST TCd (TEd)

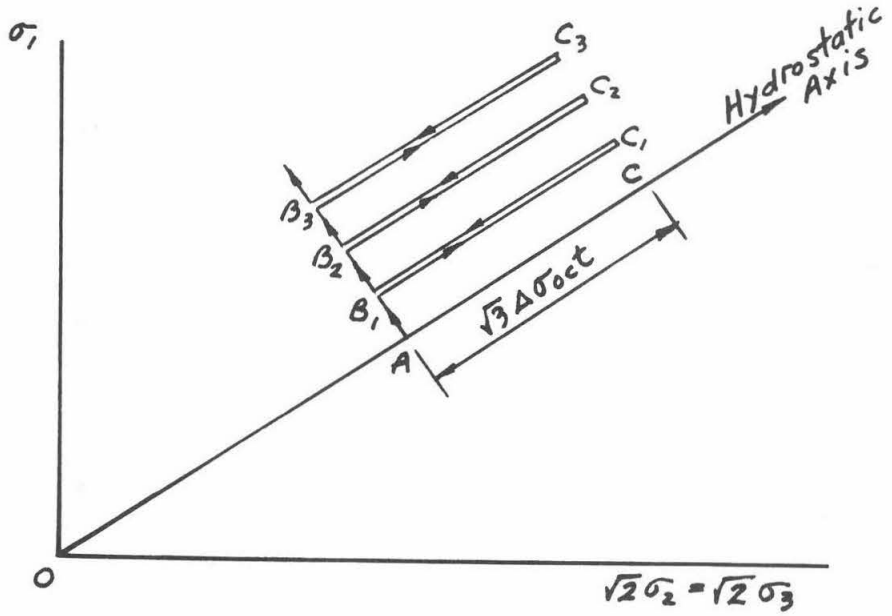

FIG. (III.16). STRESS PATH FOR SHEAR TEST TCe (TEe)

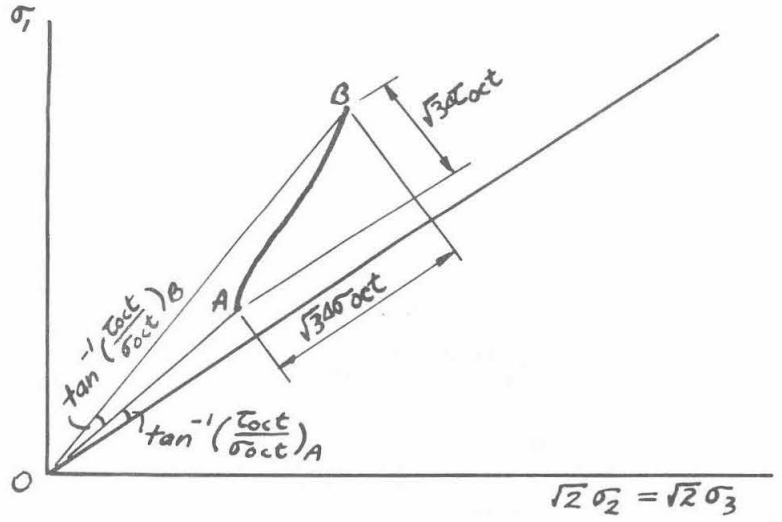

FIG. (III.17). GENERAL STRESS PATH

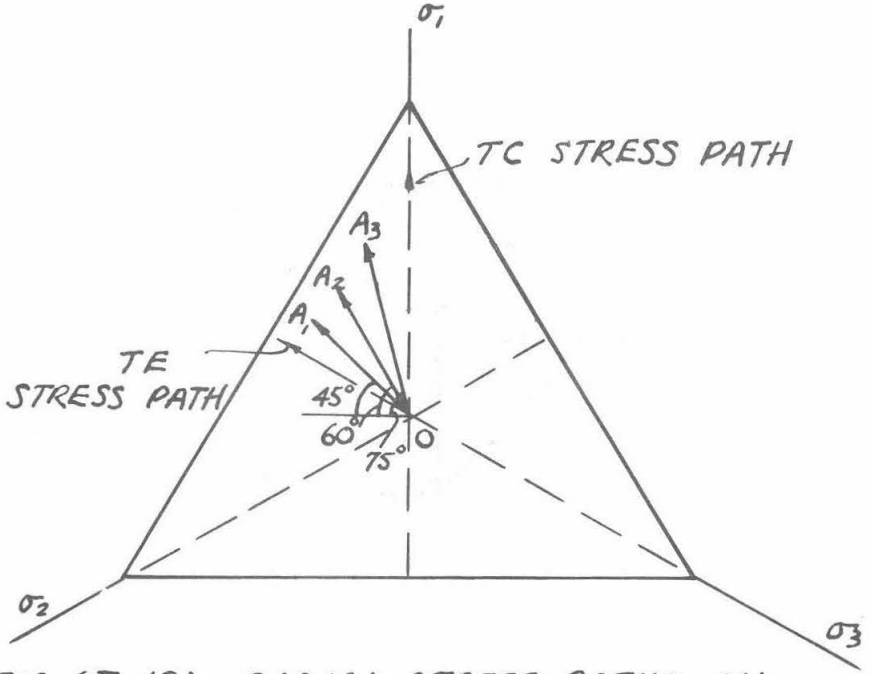

FIG. (III.18). RADIAL STRESS PATHS ON AN OCTAHEDRAL PLANE

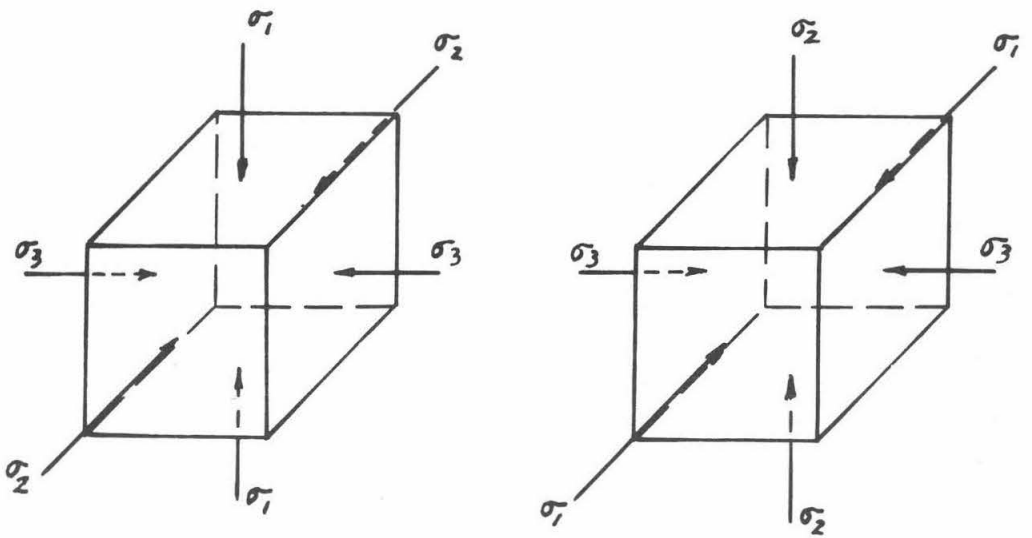

FIG. (III.19). TEST FOR ANISOTROPY OF SAMPLE : ROTATION OF DIRECTION OF PRINCIPAL STRESSES

CHAPTER IV

DESCRIPTION OF APPARATUS

(1) Introduction

The inadequacy of the triaxial apparatus as a piece of research equipment was noted in Chapter II. Other devices, such as the one using a hollow cylindrical sample [11], use samples whose geometric shape is not simple, and what is more important is that they are strain-controlled devices, i.e., they deform the sample in a definite manner and then the resistance of the sample is measured, and they often impose mixed boundary conditions on the sample so that inhomogeneous stress states are produced. Also different stress paths in the principal stress space require different apparatuses.

In order to investigate the three-dimensional stress-deformation characteristics of soils, it is necessary to have an apparatus which is capable of applying any homogeneous stress state to a sample with a simple shape, such as a cube. It is also necessary that the time to prepare a sample for use in this apparatus be a minimum. Preferably, it should be stress-controlled, because we want to perform loading and unloading tests in which we vary the stresses along a chosen stress path and measure the deformations.

To the present Bell's apparatus seems to come closest to these requirements, and the disadvantages of this equipment have been discussed earlier. In the present investigation, improvements over Bell's three-dimensional compressional apparatus were sought. A soil test box and a stress control device have been built and they are described in the

following sections. A U.S. patent is being applied for each of these two pieces of equipment.*

(2) Soil Test Box

This is a cubical box whose walls are built of aluminum and are 5/8" thick. Each wall is machined separately, and the drawings giving dimensions for their construction are shown in Fig. (IV.1). The vertical walls are identical, so the box has two perpendicular vertical planes of symmetry. The top and the bottom of the box are slightly smaller than, but are otherwise identical to, the vertical walls. The top is shown in Fig. (IV.2).

Each wall has 45° bevelled edges, and along these edges there is a continuous rectangular groove which is slightly shallower at the corners of the wall, as shown in Fig. (IV.1). Special preformed latex rubber membranes, prepared by a dipping process from aluminum molds which are the same sizes as the walls, are fitted on top of each wall. These membranes also have rectangular grooves in the position corresponding to that on the wall, Fig. (IV.2). The thickness of the membrane is 0.010-0.012 in. on the flat portion, and 0.015-0.020 in. along the grooves. The size of the rectangular grooves on the walls is such that, when a rubber membrane is fitted on the top of the wall, a 0.139" diameter O-ring can just run in the grooves around the wall, Fig. (IV.3).

Each wall has a 1/4" drilled and tapped hole on its back for attaching a Poly-flo tubing connection, except the top wall which has

---

*For the soil test box, the identification number in the California Institute of Technology Patent Office is CIT Docket No. 1152, and for the stress control device, it is CIT Docket No. 1173.

two holes for such purpose. Each wall has three holes along each of the edges and there are three holes in the rubber membrane in the corresponding positions, Fig. (IV.2), to accommodate 10-24 machine screws.

The box is assembled by putting the four vertical walls together first. This is done by putting 10-24 Allen screws through the holes and Allen nuts on the other end of the screws, and then tightening the nuts. It is important not to turn the screws themselves because they may tear up the rubber membrane. When the screws are tightened, the O-rings will press against one another along the common edges, thus giving a sealing action to the space between each membrane and its walls, and to the inside of the box.

In order that the top or the bottom of the box can be removed without disturbing the vertical walls, a retaining aluminum frame is used on the top and another on the bottom. This frame is shown in Fig. (IV.4). It has the same shape as the bevelled rim of the rectangular cylinder made from the vertical walls. For the purpose of attaching these retaining frames onto the vertical walls, another set of holes, two on each edge, are made on the top and bottom edges of the vertical walls, Fig. (IV.1), as well as on the retaining frames, to accommodate 4-40 machine screws. The retaining frames, of course, have the 10-24 screws in the appropriate positions, Fig. (IV.4).

With the vertical walls loosely assembled, the aluminum retaining frames are put in place and the 4-40 Allen screws are inserted and Allen nuts put on their ends. The whole thing is then assembled by tightening both sets of screws a little bit one at a time, to avoid unsymmetrical distortions of the set up, until all the screws are completely tightened.

After this, the top and the bottom walls can be put on after they have been fitted with the membrane and the O-ring. In Fig. (IV.5), the box is shown assembled but with the top removed, and the walls are connected to Poly-flo tubings.

The space between each wall and its membrane is filled with water which can be pressurized. Each pair of opposite walls is interconnected and applies the same pressure to the sample which is placed in the box. As the membranes deflect under pressure, the sample is compressed. The deformation in the three perpendicular directions can then be measured by recording the volumes of water coming out or going into each pair of membranes. These then represent the principal "strains" arising from the principal stresses applied through the membranes.

On one side of the top aluminum retaining frame, a small hole is drilled through, Fig. (IV.5), enabling a hypodermic needle to be inserted for independent measurement of the internal volume changes of the sample.

When the membranes carry equal pressures, the whole sample is under a hydrostatic stress state, except the small fractions next to the aluminum retaining frame. Even though the membranes are curved and bulge inwards, we can take the sample as under a homogeneous hydrostatic stress state. However, when there exists a shear stress in the system, the curved boundaries of the sample, as defined by the rubber membranes, produce complications. If we can keep the membranes fairly straight and not greatly inflated while the sample is being prepared in an unstressed state (sample preparation will be described in Chapter V), and since in all the tests the maximum strains encountered are only 1-1.5%, represent-

ing about 1 mm. movement of each membrane, it is quite safe to assume that in the bulk of the sample a homogeneous stress state exists, whereas the small volumes of the sample at the corners and along the edges of the box may be under a slightly different stress system. This is not considered important.

It was observed in tests after the box had been built that, since the side membranes actually touched one another at the common edges, they tended to interfere with one another whenever they were under different pressures. A stainless steel spacing frame was therefore constructed, by silver-soldering 1/2" × 3/16" metal strips together, to fit closely into the box so that its strips would act as separators between each pair of adjacent membranes, Fig. (IV.5).

Fig. (IV.6) shows the box completely assembled, and connected with the needle for internal volume measurement.

(3) Stress Control Device

Bell [8] found that shear stresses produced irreversible deformations in sand. Hence the stress history of a soil has an important bearing on its behavior. Yet in his tests the stress state on the sample was changed by successively adding or subtracting an increment to each of the three principal stresses in order to reach a new stress state. Because of the irreversible behavior we would expect to obtain different results from the tests if the increments were applied in a different order. It was, therefore, thought desirable to eliminate this factor by changing all the stresses simultaneously and proportionately along a controlled selected stress path.

The conventional triaxial test is carried out by keeping $\sigma_2 = \sigma_3$ = constant and changing σ_1. The hydrostatic stress therefore changes in a test. But it is customary to show the results by plotting them on one octahedral plane, as Kirkpatrick did [11]. This then assumes that the behavior of the soil tested does not depend on the hydrostatic stress. In order to separate the effects of the hydrostatic stress from those of the deviatoric stress, it is necessary to keep the hydrostatic stress constant by confining the stress path to an octahedral plane.

A stress control device which satisfies these requirements has been designed and built. This device is shown diagrammatically in Fig. (IV.7), and a photograph of the actual set up is shown in Fig. (IV.8). (In the following, when items are referred to, such as cylinder A, plate E, etc., without specification of the figure, it is to be understood that they refer to Fig. (IV.7).) It is a mechanical-hydraulic analog of the octahedral plane, consisting of a 1/4" equilateral triangular steel plate E, supported from underneath at the corners by three hydraulic cylinders A filled with Mobil D.T.E. oil. The weight of the plate is counter-balanced at the corners by weights H. Acting vertically downwards on the plate is a fourth inverted hydraulic cylinder B, which is connected to an air supply whose pressure is controlled by a regulator. The ends of the piston rods of all the cylinders are capped with a ball bearing, and the ball bearing of each of the cylinders A fits into a spherical dent on the underside of plate E. All four cylinders are identical and have a cross sectional area of 2.26 sq. in. and a stroke of 1.03 in. The pressures in cylinders A correspond to the three principal

stresses. The force exerted by the top cylinder B is distributed among the cylinders A. By keeping the pressure in cylinder B constant, the sum of the pressures (and therefore the mean pressure) in cylinders A is also constant. The ratio of the three principal stresses generated in A is dependent on the position of B. If the piston rod of B acts on the centroid of plate E, the three principal stresses are equal; by varying the position of B, various stress ratios can be obtained.

It can be shown (see Appendix A) that there exists an exact analogy between the location of the point of action of the top cylinder B on the triangular plate and the position of the stress point, defined by the principal stresses generated in cylinders A, on the octahedral plane, whose position in the principal stress space is determined by the mean stress. This analogy applies when the displacements in cylinders A are small. Hence, much of the tedium involved in calculating the stresses required and/or the stress invariants from a desired position of the stress point along a given path is eliminated by using this analog. Any stress path on the octahedral plane can be easily marked in the triangular plate and the top cylinder is then moved to follow this path. The pressures in cylinders A automatically give the combination of principal stresses desired. For example, if we want to carry out a triaxial compression test with a constant mean stress, starting from a hydrostatic stress state, all we need to do is to move the top cylinder from its centroidal position along a straight line towards the σ_1-cylinder. A triaxial extension test is carried out by moving the cylinder away from the σ_3-cylinder.

Another attachment is shown in Figs. (IV.7) and (IV.8). It is a fifth hydraulic cylinder C identical to A and B, suspended symmetrically about the centroid of plate E. It rests centroidally on a 3/16" equilateral triangular steel plate J, which is suspended symmetrically by the rods I from plate E. The piston rod of C, therefore, points through the centroid of plate E. When the cylinder C is pressurized, it increases the pressures in cylinders A by equal amounts, and the stress point in the principal stress space then moves along a straight line parallel to the hydrostatic axis. This attachment doubles the capacity of the system as far as the magnitude of the hydrostatic stress available is concerned, and proved to be very useful in investigating the effects of a hydrostatic stress superimposed on a deviatoric stress.

Along a chosen straight stress path on plate E, the ball bearing on the piston rod of the cylinder B is guided by two metal strips with slots made on them at $\frac{1}{2}$" spacing as shown in Fig. (IV.9). The cylinder can be moved in $\frac{1}{2}$" steps, or, if finer steps are required, it is moved to let the ball bearing bear against two adjustable screws (Fig. (IV.8)), so that, theoretically speaking, any small stress increment can be obtained. The $\frac{1}{2}$" spacings are numbered, j = 0,1,2, ··· etc., with the zero value corresponding to the centroidal position of cylinder B. Other methods of control of the movement of cylinder B are possible.

The system in which the pressures generated in the cylinders A are transmitted to the soil test box as principal stresses is shown schematically in Fig. (IV.10), and a photograph of the whole setup is shown in Fig. (IV.11).

The hydraulic oil in a cylinder A is connected to a graduated

glass stand pipe (3/8" I.D. and 1/2" O.D.), the bottom part of which is filled with water communicating with a pair of opposite walls of the soil test box. The pressure in the hydraulic cylinder is thus transmitted through the water to the sample. The oil and the water are immiscible, thus the elevation of their interface, Fig. (IV.12), gives an indication of the deformation taking place in the sample in the direction of this principal stress. This deformation includes that of the sample and those due to the tubing and membrane penetration and wall effects, and has to be corrected, as will be discussed in Chapter V. The volume change in each pair of membranes can be read to 0.1 c.c. on the glass tubes.

In order that this system may work satisfactorily, it is necessary that the friction in the hydraulic cylinders be kept very low. An ordinary hydraulic cylinder with O-rings around the piston is not suitable from this point of view, and it was found that a special kind of cylinder using rolling diaphragms practically provides no frictional resistance to the movement of the piston (see Appendix B). All the cylinders used in the stress control device are the demonstration model 10-100 actuator made by the Bellofram Corporation, Mass., and can be subjected to maximum pressure of 100 psi. They perform very satisfactorily for the present purpose. Such an actuator is shown in Fig. (IV.13). To adapt this to a hydraulic cylinder used in the stress control device, a hardened steel extension rod is attached to the piston rod of the actuator and passes through a linear ball bearing embedded in a lucite plate which is part of the framework of the cylinder shown in Figs. (IV.9) and (IV.14). When fixed this way, the piston rod of the

cylinder is constrained to move linearly. The linear ball bearing offers very little resistance to the movement of the extension rod.

Figs. (IV.9) and (IV.14) show the top cylinder B. The base of the cylinder is supported on three ball bearings, for the purpose of allowing free movement of the cylinder on the underside of plate G, Fig. (IV.7). When plate E tilts as cylinders A change in their oil contents due to deformations in the soil test box, the cylinder B would tend to slide out of position. It is therefore necessary to embed an electromagnet, L, on the base of cylinder B, Figs. (IV.7) and (IV.9), which when energized will attach itself to the bottom of plate G, thus preventing any lateral movement of B. When cylinder B is required to move to a new position, the electromagnet is de-energized, the cylinder moved and the electromagnet energized again.

It can thus be seen that the stress control device is easy to operate and has merits in that it enables the stresses, as represented by the pressures in cylinders A, to be varied simultaneously and continuously (as smoothly as we care to move the top cylinder), while the hydrostatic stress can be kept constant if desired, and in that a great simplification is introduced with respect to the calculation of the stresses required to give a desired stress path and quantities related to them. The attachment of the hanging cylinder C makes it possible to obtain any desired stress path in the principal stress space. For calibration of the stress control device, see Appendix B.

When we want to compress the sample hydrostatically, it is, of course, not necessary to employ the stress control device. Since the three principal stresses are equal during a hydrostatic stress cycle,

each pair of membrances can be connected to a column of water subject to a common air pressure, as shown in Fig. (IV.10). By changing one pressure only and recording the changes in levels of the water columns, we can study the behavior of the sample under hydrostatic stress.

The oil reservoirs shown in Figs. (IV.10) and (IV.12) provide the possibility of oil transfer from the reservoir to the cylinders A and vice versa.

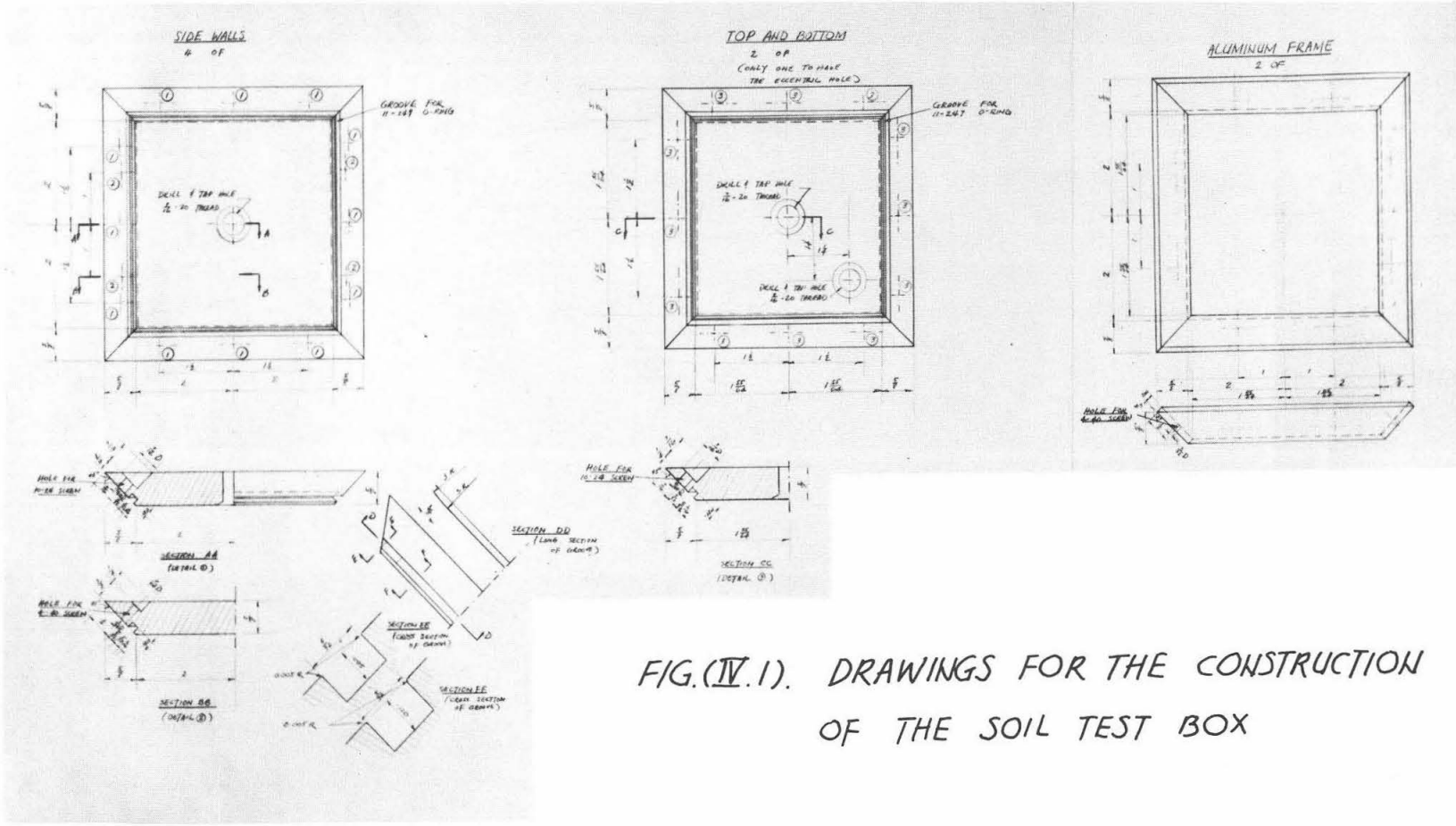

FIG.(IV.1). DRAWINGS FOR THE CONSTRUCTION OF THE SOIL TEST BOX

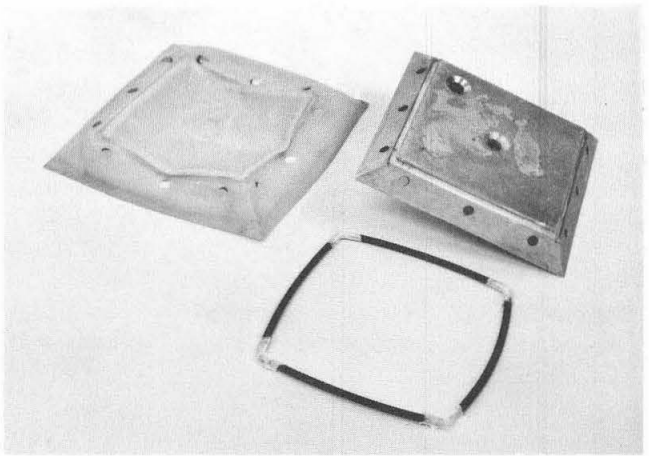

FIG. (IV.2). TOP WALL, RUBBER MEMBRANE AND O-RING

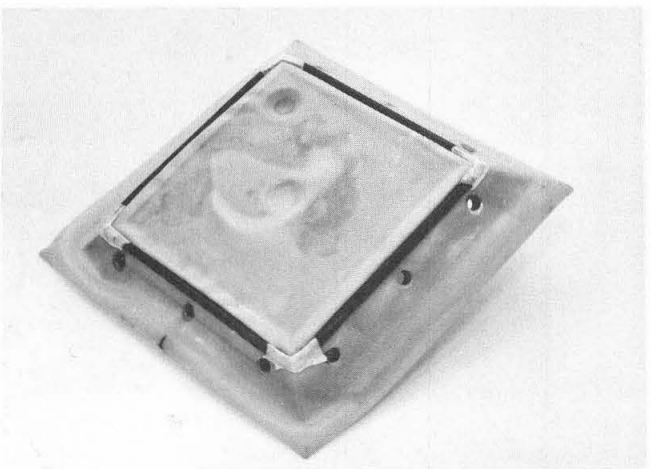

FIG. (IV.3). TOP WALL WITH RUBBER MEMBRANE FITTED

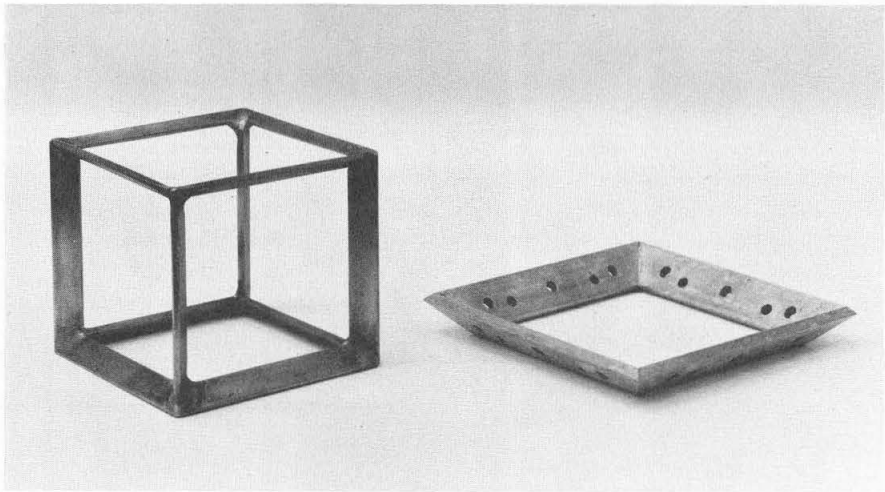

FIG.(Ⅳ.4). SPACING AND RETAINING FRAMES

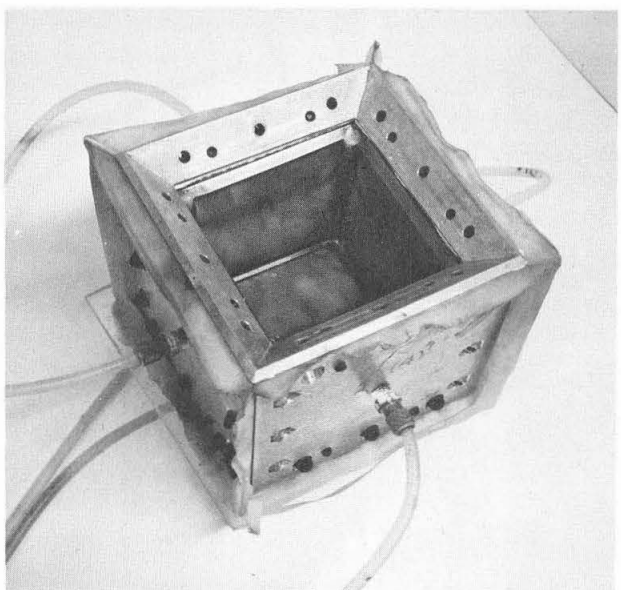

FIG.(Ⅳ.5). OPEN BOX SHOWING SPACING FRAME

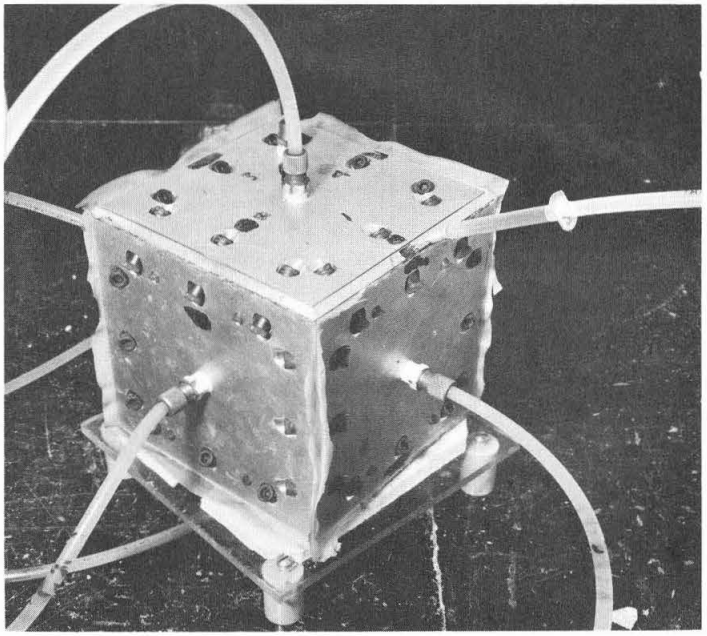

FIG. (IV.6). BOX COMPLETELY ASSEMBLED, SHOWING HYPODERMIC NEEDLE

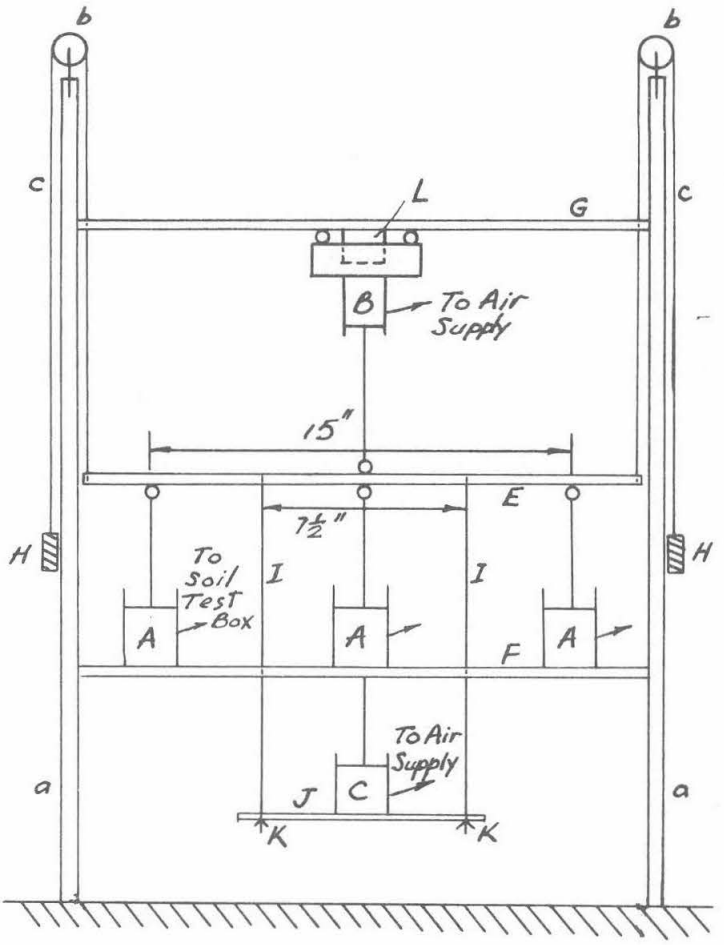

A	Middle Cylinders	J	$\frac{3}{16}$" Triangular Steel Plate
B	Top Cylinder	K	Adjusting Wing Nuts
C	Bottom Cylinder	L	Electromagnet
E, F, G	$\frac{1}{4}$" Triangular Steel Plate	a	Slotted Angle Columns
H	Counterbalancing Weights	b	Pulleys
I	Threaded Suspension Rods	c	Nylon Thread.

FIG. (IV. 7)

SCHEMATIC SKETCH OF STRESS CONTROL DEVICE

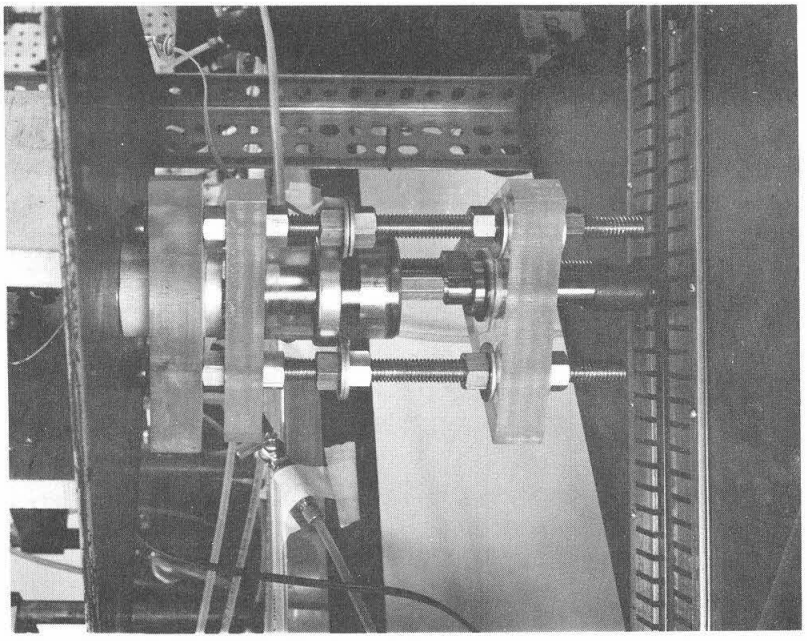

FIG. (IV.9). TOP CYLINDER AND GUIDING STRIPS

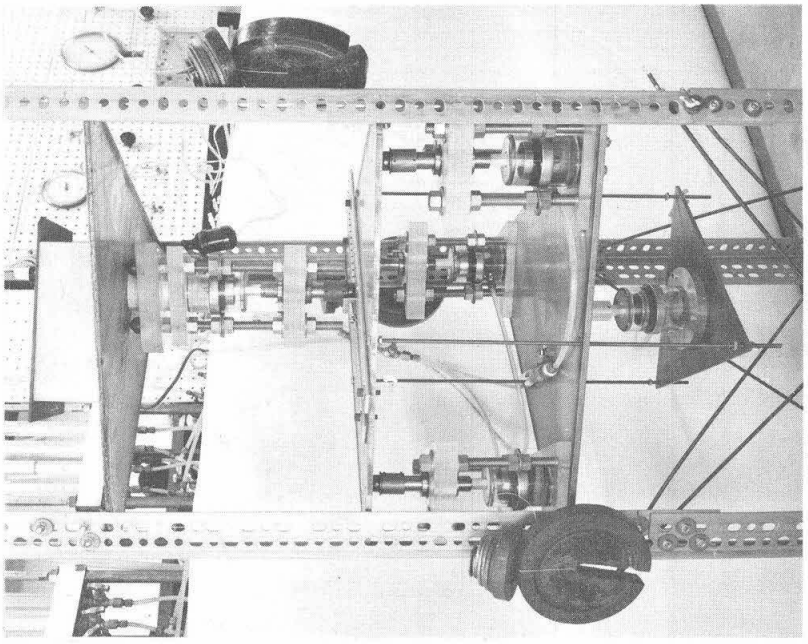

FIG. (IV.8). STRESS CONTROL DEVICE

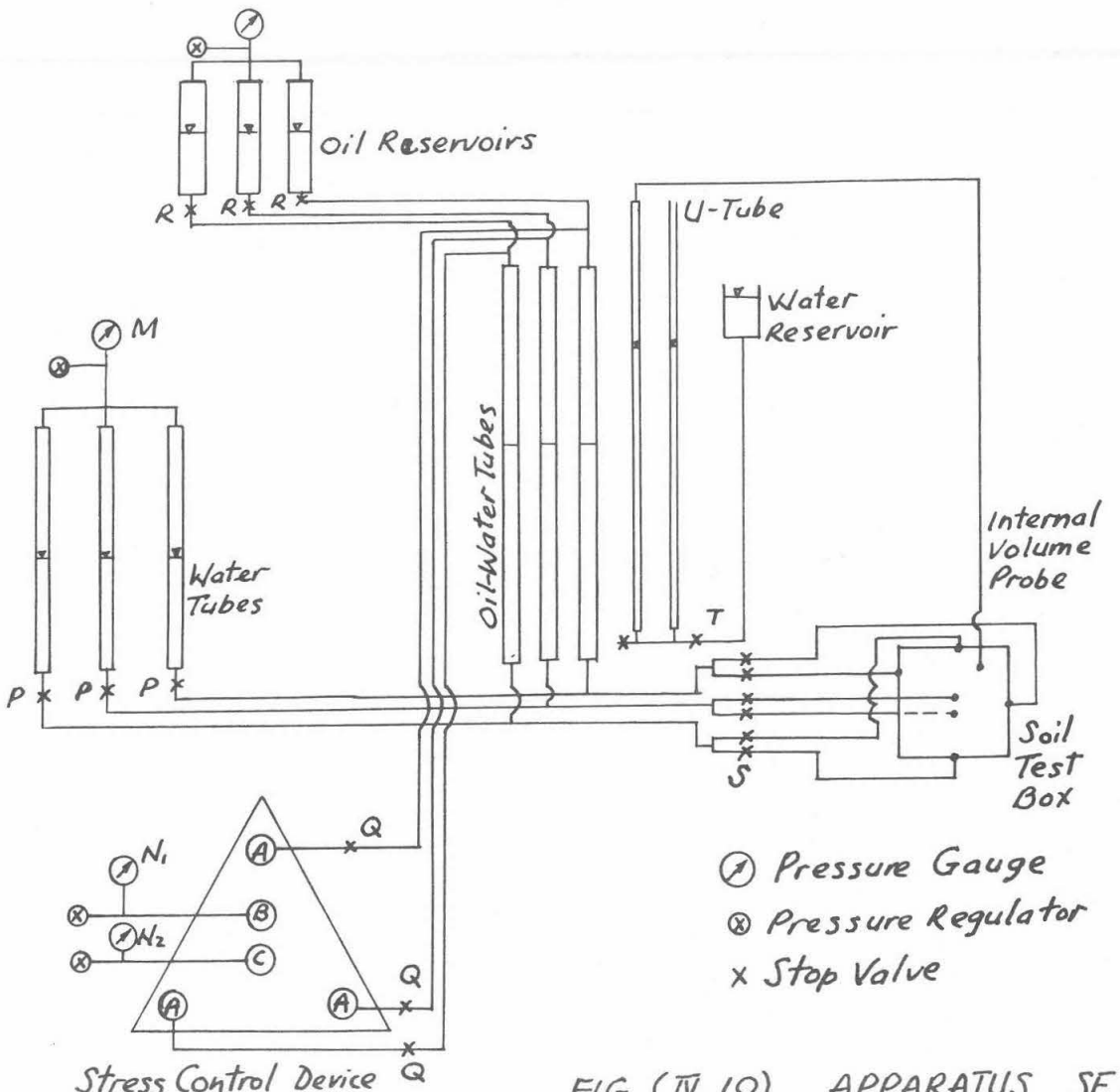

FIG. (IV.10). APPARATUS SET-UP

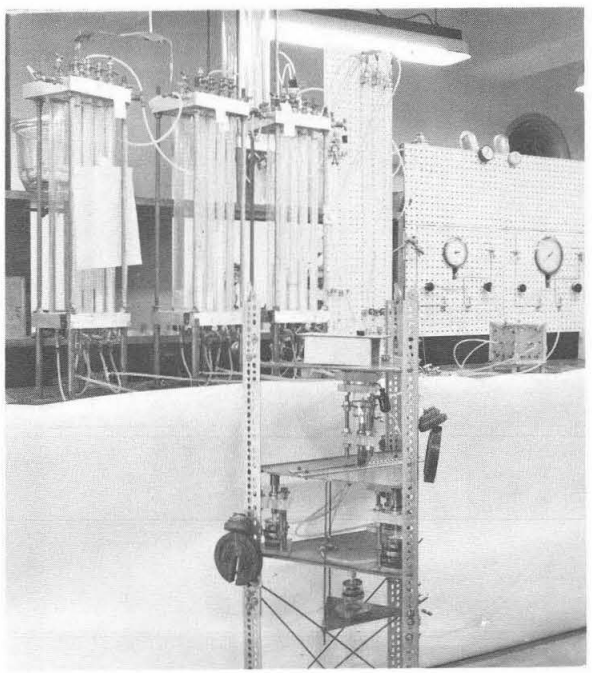

FIG. (IV. 11). COMPLETE APPARATUS SET-UP

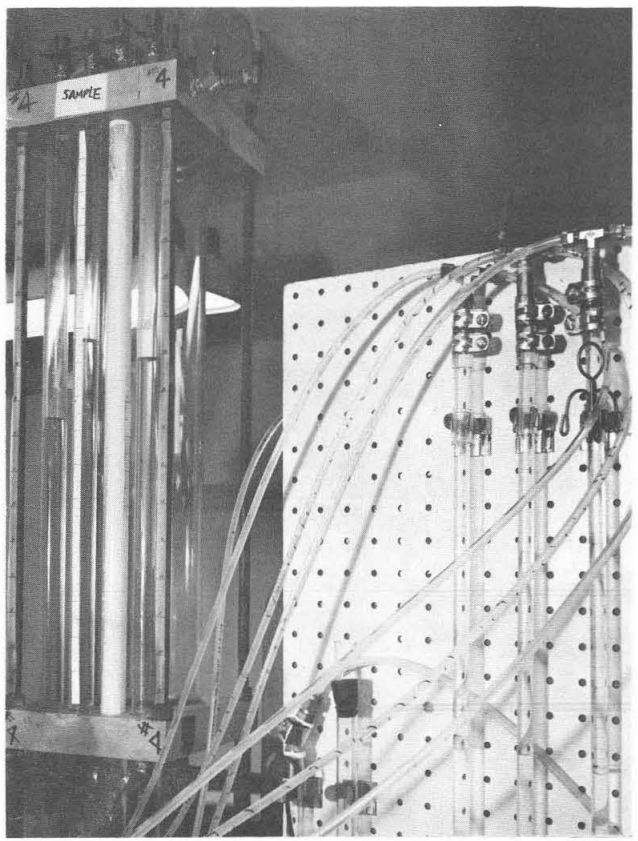

FIG. (IV. 12). OIL RESERVOIRS AND MEASURING TUBES

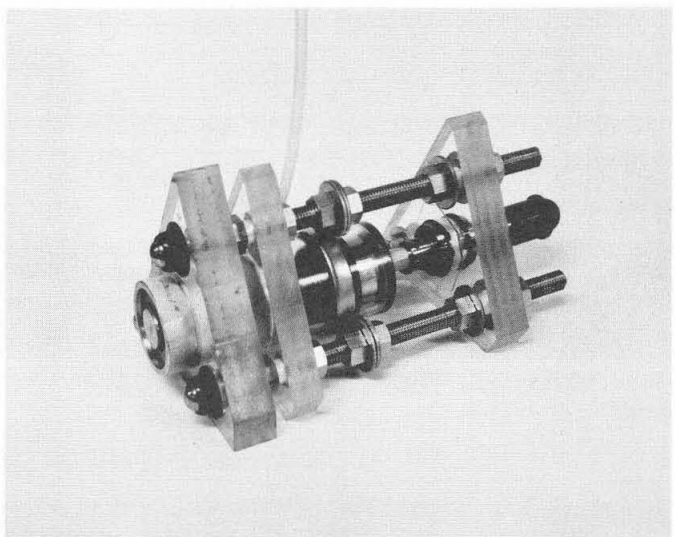

FIG. (IV. 14). TOP CYLINDER

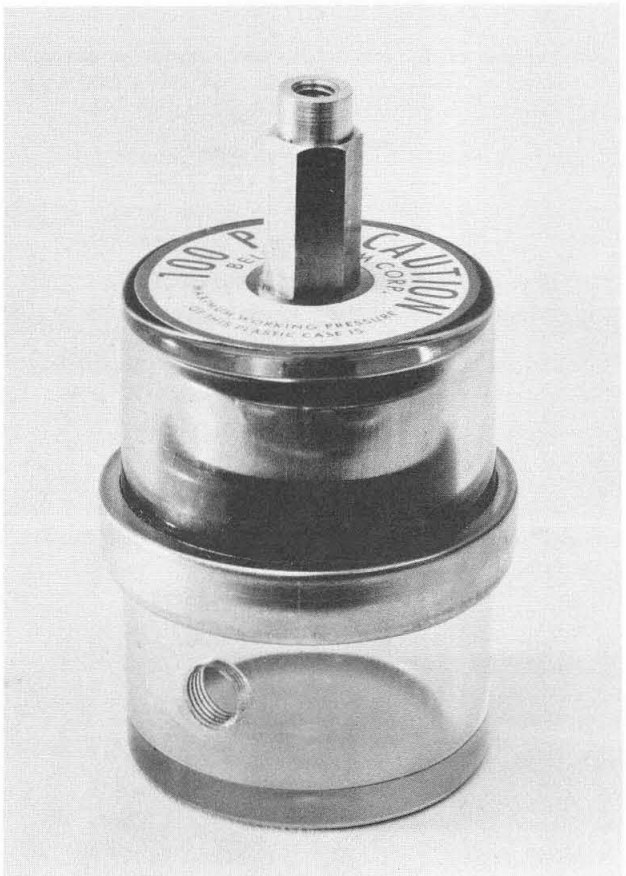

FIG. (IV. 13). BELLOFRAM PRESSURE ACTUATOR

CHAPTER V

EXPERIMENTAL PROCEDURES

(1) Introduction

The reasons why simple load tests, including unloading, are required to extract the characteristic behavior of the soil were given in Chapter III, and the purpose of each test was also discussed there. In this chapter, the experimental procedures required in carrying out these tests are described.

(2) Preparation of Sample

The soil tested in this investigation was standard Ottawa sand, whose grain size distribution is shown in Fig. (V.1). It can be seen that most of the grains lie between U.S. Sieve Nos. 20 and 40. Only dry samples of this soil were tested and a description of their preparation to different densities is given below. This applies to samples for all the tests to be described in later sections of this chapter.

Prior to testing, a small amount of water, which was tap water kept in a flask in the laboratory for a few days, was introduced into the space behind each membrane of the box with the lid removed, care being taken to remove any air bubbles from the water. The valves S, Fig. (IV.10), were shut off and water was poured into the box to a level determined by the bottom of the plastic scraper which was resting on the rim of the box, Fig. (V.2). The volume of water thus introduced was recorded. The box was then emptied by siphoning out the water, and the inside of the box was dried with tissue paper. The box was then ready to be filled with sand.

To obtain a loose sample of the soil, a glass funnel was filled with sand with its tip touching the bottom of the box. By moving the funnel around inside the box and gradually raising it while its tip was kept just above the surface of the sand accumulating in the box, a loose sample was obtained. To get denser samples, the sand was allowed to drop through the funnel at a constant height above the surface of sand accumulated on the bottom, Fig. (V.4). The density of the sample obtained increased with the height through which the grains had fallen, within the test limits of 0 to 42 inches, and it is believed that, if the rate at which the grains dropped was kept fairly uniform, a homogeneous sample was obtained. The question of the measurement of possible anisotropy in the sample will be discussed later in this chapter.

It was not advisable to introduce too much water into the side membranes initially, because the membranes would bulge too much, causing the shape of the sample to be far from cubic, as illustrated in Fig. (V.5a). However if the membranes were not filled, water would rest in the bottom leaving practically no water in the top position to accommodate expansion of the sample, Fig. (V.5b). Since a couple of millimeters of lateral movement of each membrane was all that was required to accommodate the total deformation of the sample during a test, it was found best to load the box in three or four stages. In each stage, enough water was introduced to inflate the side membrane about 5 mm. for a height of about 1 in. (Fig. V.5b). Then sand was dropped into the box as described above, until a little bit less than one inch of sand had accumulated, Figs. (V.5c) and (V.6). Next, a lucite stamp was placed on top of the sand accumulated (Fig. V.7), and valves P and S were opened

to let measured amounts of water flow into the spaces behind the membranes, until the membranes were inflated about 5 mm. for another inch or so above the sand surface, Figs. (V.5d) and (V.8). The lucite stamp was removed and the process of pouring sand into the box resumed until another inch of sand had accumulated. This procedure was repeated until the whole box was filled to the level as determined by the bottom of the lucite scraper (which was the same level as the water before), Figs. (V.5e) and (V.9). Although the sides of the sample might not be made plane by the technique, its overall shape was roughly cubic.

When the box was filled with sand in this way to the same level as the water before, the density of sample could be calculated from the weight of sand put in and the volume it occupied, which was equal to the volume of water required to fill the box initially minus the total volume of water introduced into the membranes during preparation. The void ratio, e, of the sample was calculated from

$$e = \frac{\text{vol. of void}}{\text{vol. of grains}}$$

$$= \frac{V - \dfrac{1000\ W}{2.204 \times 2.65}}{\dfrac{1000\ W}{2.204 \times 2.65}} \qquad \text{(V.1)}$$

$$= \frac{V}{171\ W} - 1$$

where W = weight of sample, in lb.,

V = volume of sample, in c.c.

and the specific gravity of the grains was taken to be 2.65 [8].

The void ratio thus determined was rather sensitive to both the weight and the volume of the sample and was usually determinable only to $\pm$ 0.005.

After preparing the sample in the manner described, the top of the box was put on. We could not inspect the top membrane to see whether it was air free or not, because the O-ring was effective in sealing the spacing behind the membrane only after the top was screwed down tight. Hence we had to circulate water through this membrane through the two connections on the top plate of the box with the box slightly tilted, as illustrated in Fig. (V.5f).

The hypodermic needle was inserted into the holes in the top aluminum retaining frame, as shown in Fig. (IV.6), and connected to one arm of a U-tube while the other arm was under atmospheric pressure, Fig. (IV.10).

The sample was then ready to be tested.

(3) Corrections

Since the deformations of the soil were measured by the amount of water that went into or came out of the spaces behind the membranes, it is necessary to consider how these measurements were related to the actual deformations and to determine the necessary corrections. Three of these corrections may be distinguished:

(i) The rubber membranes under pressure penetrate into the spaces between the soil grains, Fig. (V.10), and make the volumetric readings too large by an amount which depends nonlinearly upon the pressure.

(ii) The screws holding the walls of the box together lengthen and the walls themselves bulge outward under the pressure applied to the water behind the walls.

(iii) The connecting Poly-flo tubings expand under pressure.

The first two corrections were obtained together empirically by the following method. Two aluminum blocks were made of respective sizes 3 5/8" × 3 5/8" × 3 15/16" and 3 15/32" × 3 15/32" × 3 21/32". One block was inserted into the box and the voids between it and the membranes were filled with sand. The volume changes in the membranes were then recorded for different hydrostatic pressures. The same procedure was repeated for the other block. The two tests differed only in the thickness of the sand layer existing between the block and the membranes under the test pressures, while the aluminum blocks themselves were considered relatively incompressible at the pressures employed. The results are shown in Fig. (V.11), in which an extrapolation was made to give the volume changes in the case where the amount of sand present in the box is zero, so that there is no contribution from the compression of the sand. Then the changes in this case represent the corrections to be made for both wall-bulging and membrane penetration effects.

To measure the effect of the expansion of the tubings, a piece of about 10 ft. length was filled with water and pressure applied to the water, as illustrated in Fig. (V.12). The amount of water going into the tubing was found to be proportional to the pressure, as shown in Fig. (V.13), where the values had been adjusted to those for the length of tubing (about 17 ft.) used in the setup shown in Fig. (IV.11)

and illustrated in Fig. (IV.10).

Combining these corrections, a single correction curve was obtained for each pair of walls, as shown in Fig. (V.13). An arbitrary datum pressure was chosen at 4 psi, because at smaller pressures, an uncertainty exists as to the state of the sample at the boundaries next to the membranes, and as to whether or not the membranes were touching the sample completely at the edges and corners of the box.

(4) Hydrostatic Compression Tests

Hydrostatic compression tests, described in Section 4(i) of Chapter III, were performed on samples of different densities. In each test, the pressure was applied through the water tubes with the valves Q and R (Fig. (IV.10)) closed and valves P and S open, and was adjusted by the regulator M. Hence the stress control device was not needed and the three principal deformations were read on the graduated water tubes. The test pressure range (4-60 psi) was divided into intervals, smaller in the lower pressure range. Each increment was left on for two minutes, during which time the deformations would normally reach steady values. At the end of each increment, the levels of the three water columns were read to 0.1 c.c. and recorded. The water in the U-tube for the measurement of the internal volume change was balanced and the level read. After reaching the maximum pressure, the unloading cycle began and the decrements of pressure were the same as the increments during loading. The water columns and the U-tubes were read after each decrement had been left on for two minutes.

A few cycles of hydrostatic stress were applied, depending on the density of the sample. A larger number of cycles was applied to a loose sample, because a loose sample was expected to undergo more irreversible volumetric strain for each cycle of hydrostatic stress. The results of these and subsequent tests will be shown in Chapter VI.

(5) Shear Tests in the Triaxial Plane

The guiding strips were adjusted on the triangular plate of the stress control device to give a triaxial compression or extension stress path. A sample was prepared and subjected to a few cycles of hydrostatic stress (4-60 psi), to enable some of the unstable grains to attain more stable positions. These cycles were applied through the water columns as in Section (4), and then control was transferred to the stress control device. This was done by placing the top cylinder B (here, the reference figures are (IV.7) and (IV.10)) at the centroid of the triangular plate and loading it to generate a hydrostatic stress of 4 psi in each of the lower cylinders A. The valves P were closed and valves Q opened. One to two cycles of hydrostatic stress were applied using this device, the results of which were compared with those obtained by means of the water columns.

The capacity of each cylinder was 100 psi, but the laboratory supply to the top cylinder B could not be maintained steady by the regulator N_1 at 75 psi. Consequently, if the top cylinder alone was used, a maximum hydrostatic stress of only 25 psi on the sample could be generated. It was therefore necessary to employ the hanging cylinder C to obtain higher hydrostatic pressures. It was important to see that the

hanging cylinder had its piston upright before applying pressure to it by means of the regulator N_2, and that the hanging rods I did not touch the holes through which they passed. This sometimes involved leveling the small triangular plate J on which this cylinder sat, by adjusting the screws K on the lower ends of the hanging rods.

After these cycles of hydrostatic stress, the pressure in the top cylinder was adjusted to give the value of σ_{OCT} desired, with the bottom hanging cylinder exerting no pressure. Next began the shear test which was one of the five types outlined in Section 4(ii) of Chapter III. The experimental manipulations were described in the following:

Test (a). To produce the stress path for this test, as shown in Fig. (III.11), the top cylinder B was moved along the path defined by the guiding strips, in steps which were larger in the beginning and smaller as the test went on, while the air pressure in the cylinder was kept constant. The deformations after each step were measured by the changes in elevations of the oil-water interfaces in the columns. The readings were taken at frequent intervals (1 minute or so) and recorded on standard forms as shown in Appendix C, until they reached a stationary value. This usually took 3 to 4 minutes. The internal volume change obtained through the hypodermic needle was also recorded.

During the test, or any other tests involving the stress control device, it was necessary to watch the level of pistons in all cylinders (A, B and C), and care was taken not to let the capacity of any cylinders run out. (The total capacity of any one cylinder is about 35 c.c., which corresponds to about 3% strain. However, the piston of any one cylinder was not necessarily set initially at an extreme position.) This might

necessitate transferring oil to and from an oil reservoir into the cylinder, via valves R, so as to adjust the level of the piston. When this had to be done, valves S were closed to shut off the box, and pressure was applied to the reservoir at a value slightly higher or lower (depending which way we wanted the oil to flow) than that in the cylinder whose capacity was nearly exhausted. Then valve R was opened to allow a slow transfer to take place. After this, the reservoir was disconnected by closing valve R and the box connected by opening valves S. When the deformations were large, such transfers might be necessary in more than one cylinder and more than once in one cylinder during the test, especially when the plate began to tilt too steeply. The plate should be kept fairly level, otherwise the analogy between the plate and the octahedral plane (see Appendix A) would not hold. When the soil was believed to have failed (see Section 3 of Chapter III), the top cylinder was moved back to the centroid of the plate in steps. The deformations and the internal volume change were recorded at the end of each step. The test ended after the cylinder had been returned to the centroidal position.

This test was carried out in both triaxial compression and extension on samples of four different densities (dense, medium dense, medium loose and loose) at values of σ_{OCT} equal to 15 psi and 20 psi.

Test (b). To produce the stress path shown in Fig. (III.12), the top cylinder was moved one step out and, after a steady state was reached, the deformations were recorded. The cylinder was then brought back to the centroid, and the deformations recorded. Next it was moved to re-

trace its previous steps, readings taken, and it was moved one further step out, then returned and so on. The test was stopped after the cylinder had been taken beyond the failure position found in test (a) and brought back to the centroid.

This test was carried out in both triaxial compression and extension on samples of two different densities (medium dense and medium loose) at a value of σ_{OCT} equal to 20 psi.

Test (c). To produce the stress path shown in Fig. (III.13), the same procedures as in (b) were taken, except that following each return of the cylinder to the centroid, the pressure in the bottom hanging cylinder was increased from zero to 75 psi by three increments and decreased back to zero by the same increments. At the end of each increment the deformations were recorded.

The value of σ_{OCT} used at the beginning was 15 psi and therefore increased from 15 psi to 40 psi during the hydrostatic cycle between A and C. The test was performed in triaxial compression and extension and at two densities (medium dense and medium loose).

Test (d). The stress path for this test was shown in Fig. (III.14). To produce this, the top cylinder B was moved along the selected path and, at each new position, after the deformations were recorded, the pressure in the top cylinder was increased from the initial value of 45 psi to 75 psi in two equal steps. Since the stress ratio $\frac{\tau_{OCT}}{\sigma_{OCT}}$ depends solely on the position of the top cylinder (see Appendix A), the increase in pressure in this cylinder had the effect of producing the stress path B_1C_1. The pressure was next returned to its former value,

and the cylinder moved another step outward until it had passed the failure point found in (a).

The two values of σ_{OCT} in this test were 15 and 25 psi, and the test was carried out in triaxial compression and extension and at two different densities (medium dense and medium loose).

Test (e). The stress path for this test was shown in Fig. (III.15). To achieve this, the top cylinder B was moved out one step, the plate which supported the bottom cylinder C was leveled and pressure in this cylinder was increased from zero to 75 psi in 3 steps. Equal incremental pressures were generated in the middle cylinders A, thus producing the stress path B_1C_1. The pressure in the hanging cylinder was then released and the top cylinder moved one more step out, until it had passed the failure point determined in (a).

The value of σ_{OCT} used in this test was 15 psi and was increased to 40 psi along B_1C_1. The test was carried in both triaxial compression and extension on samples of two different densities (medium dense and medium loose).

(6) Radial Shear Tests

There were three different tests in this category. The experimental procedures were the same for each and they only differed in their stress paths, as shown in Fig. (III.17).

The guiding strips on the triangular plate of the stress control device were adjusted to give the stress path desired. From then on, the procedures were the same as those for tests 5(a) (or TCa and TEa).

These tests were carried out on samples of two different densities (medium dense and medium loose) at a value of σ_{OCT} equal to 20 psi.

(7) Tests for Anisotropy of Sample

Normally, the directions of the major, intermediate and minor principal stresses with respect to the soil test box was as shown in Fig. (V.14a), but two tests were carried out by rotating these directions as shown in Fig. (V.14b and c). All that was involved was interchanging some of the connecting tubing between the stress control device and the soil test box.

The first one had a triaxial compression stress path and was performed on a medium dense sample at a value of σ_{OCT} equal to 20 psi.

The second had a RS-60° stress path and was performed on a medium loose sample at a value of σ_{OCT} equal to 20 psi.

The results of these tests could be compared to those obtained in the test without a rotation of the axis of the principal stresses.

The results of all the tests described in this chapter will be shown in Chapter VI.

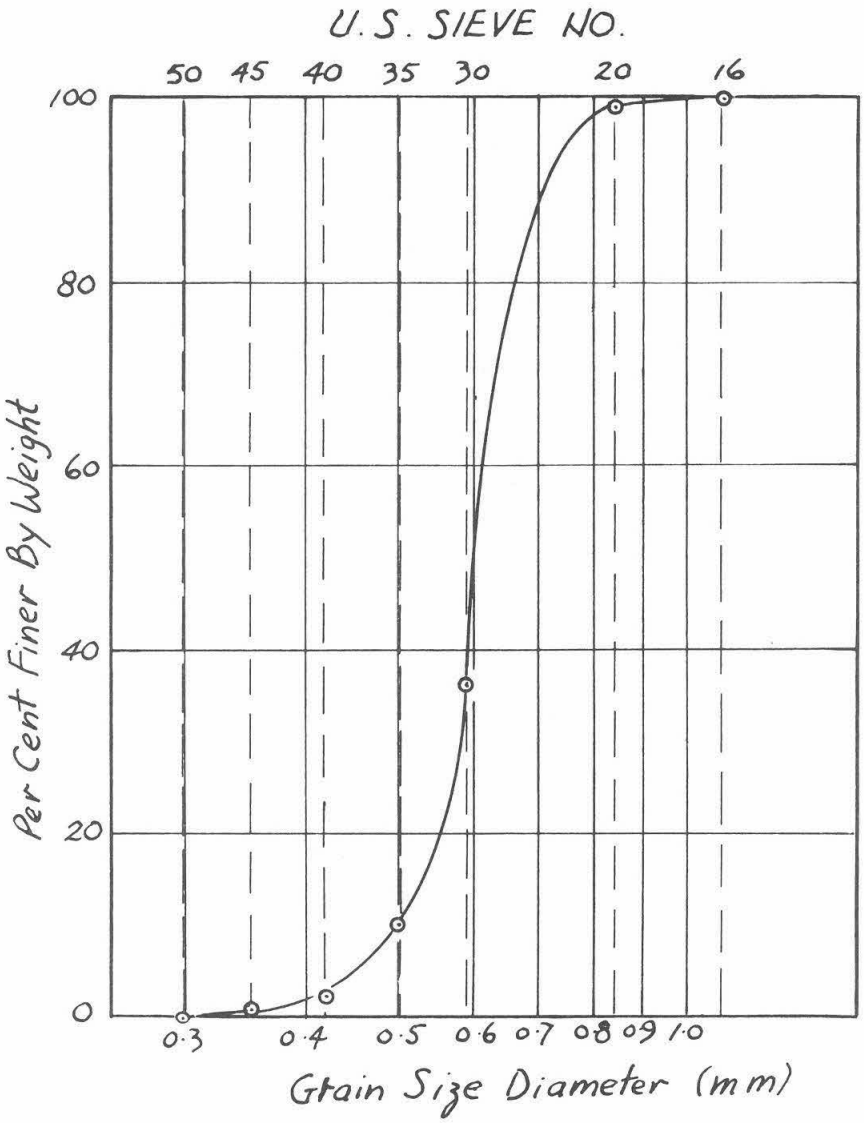

FIG. (V. 1)
GRAIN SIZE DISTRIBUTION CURVE OF OTTAWA SAND

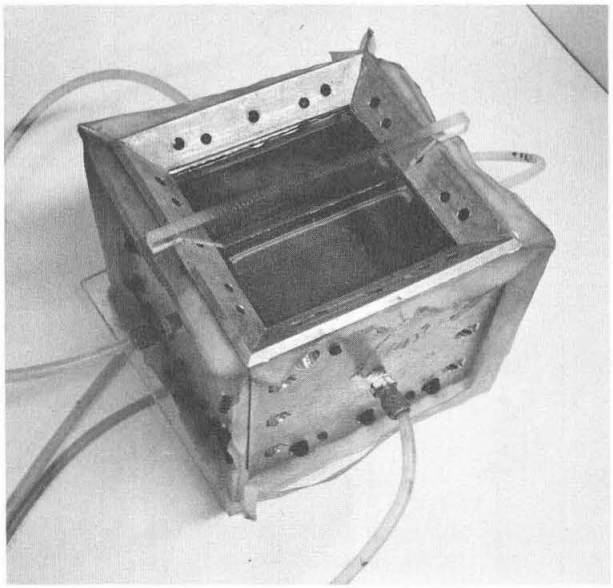

FIG. (V.2). OPEN BOX FILLED WITH WATER AND SCRAPER

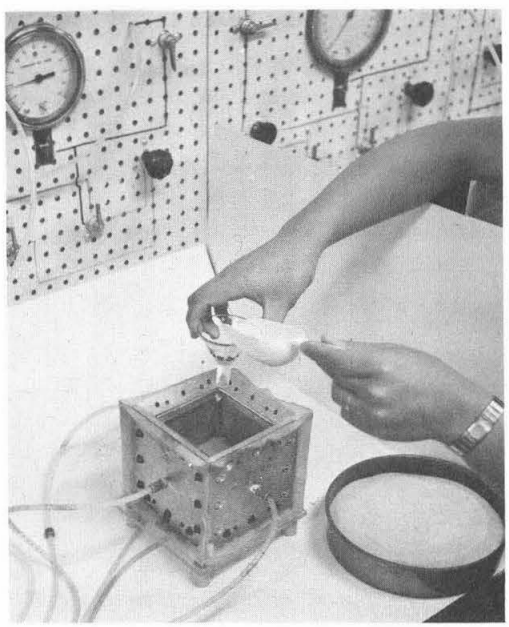

FIG. (V.4). FILLING THE BOX WITH SAND

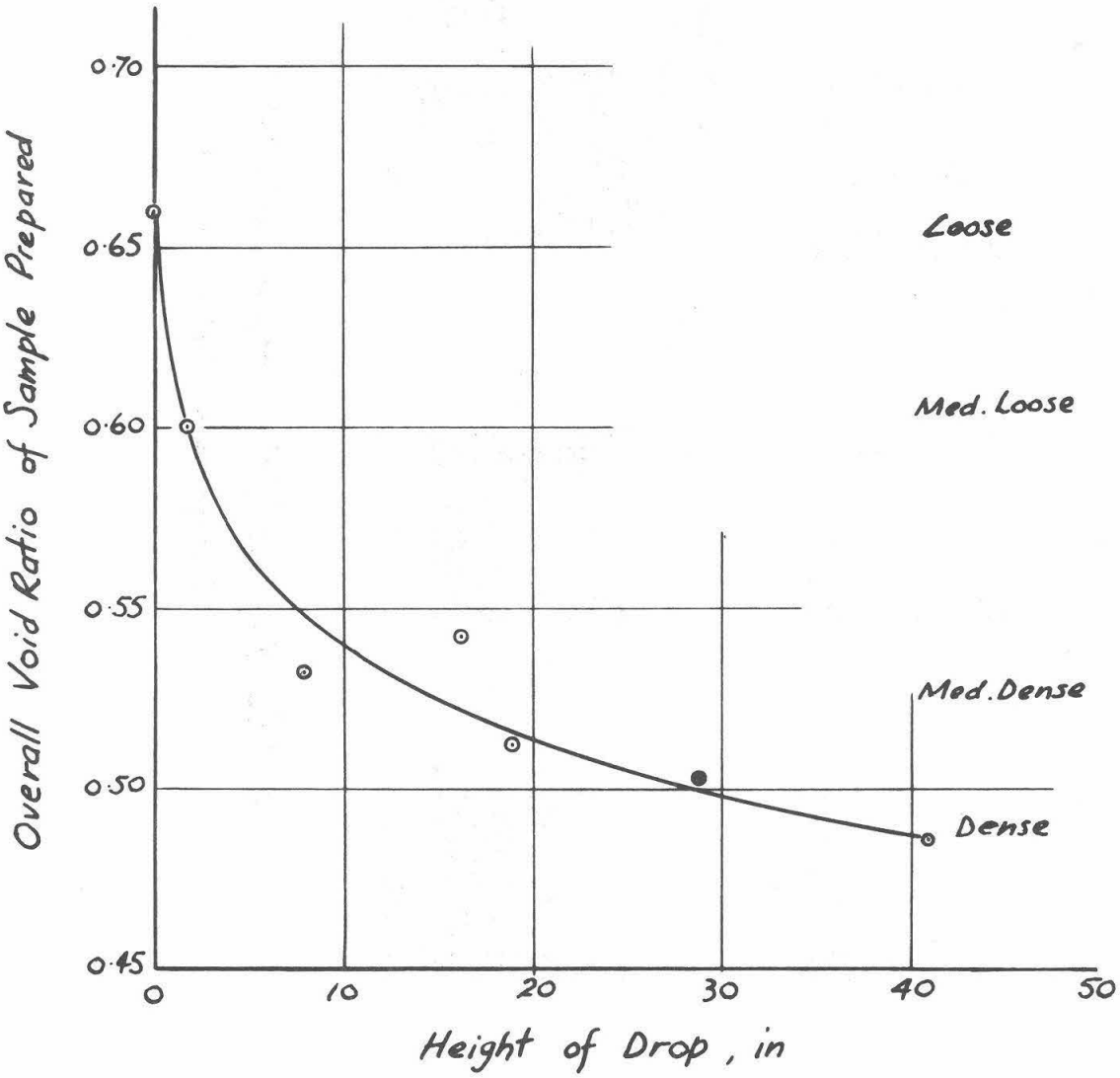

FIG. (V. 3)
VOID RATIOS OF SAMPLES PREPARED

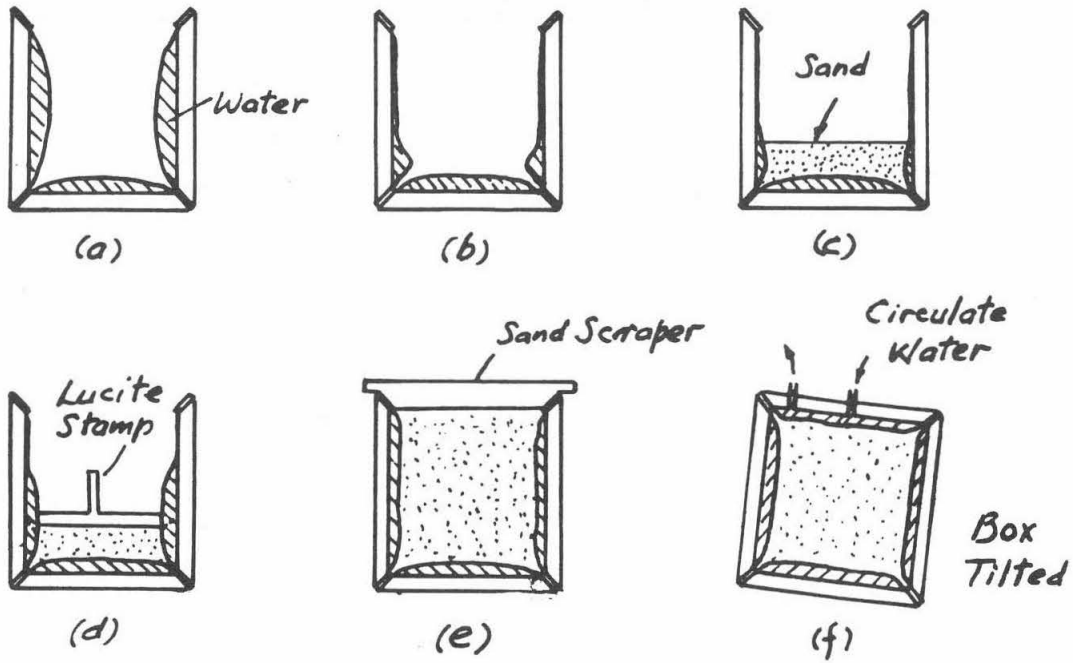

FIG. (II.5). SAMPLE PREPARATION

(Spacing Frame Not Shown)

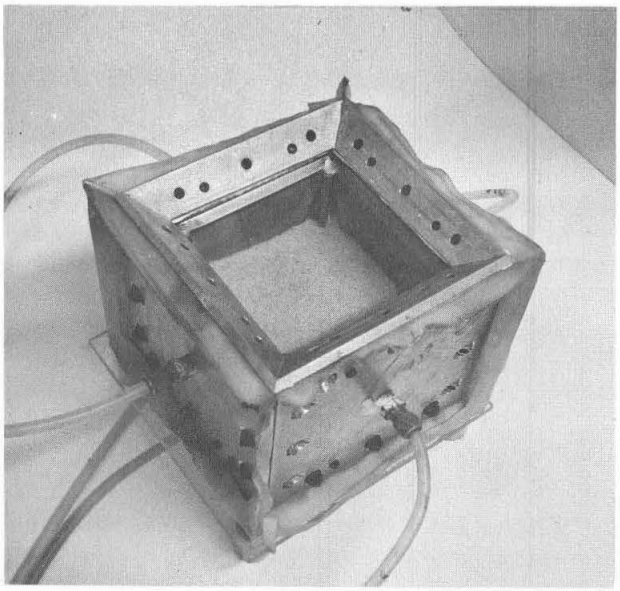

FIG. (V.6). BOX HALF FILLED WITH SAND

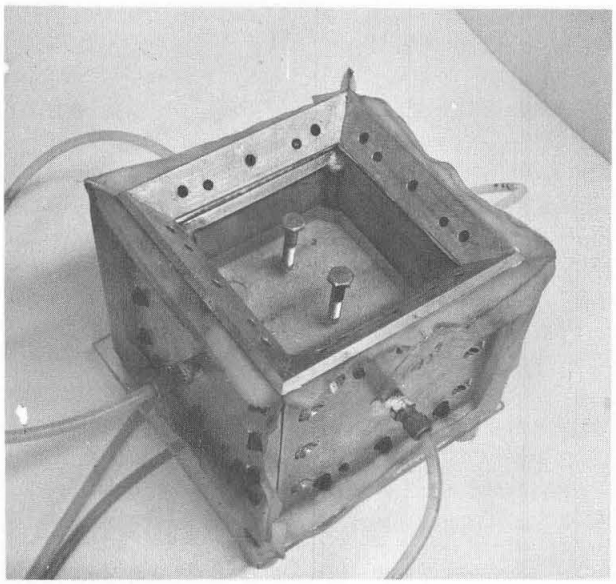

FIG. (V. 7). BOX HALF FILLED WITH SAND AND LUCITE STAMP ON TOP

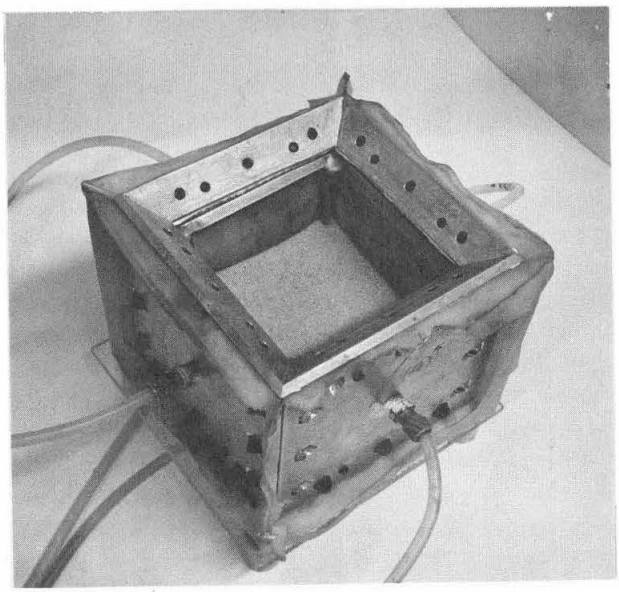

FIG.(V.8). MEMBRANS ABOVE SAND SURFACE INFLATED

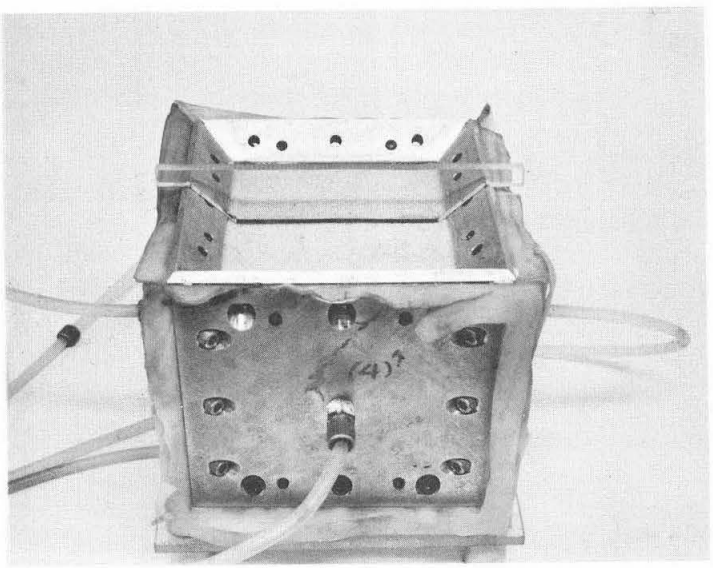

FIG.(V.9). BOX FILLED WITH SAND TO THE LEVEL OF SCRAPER

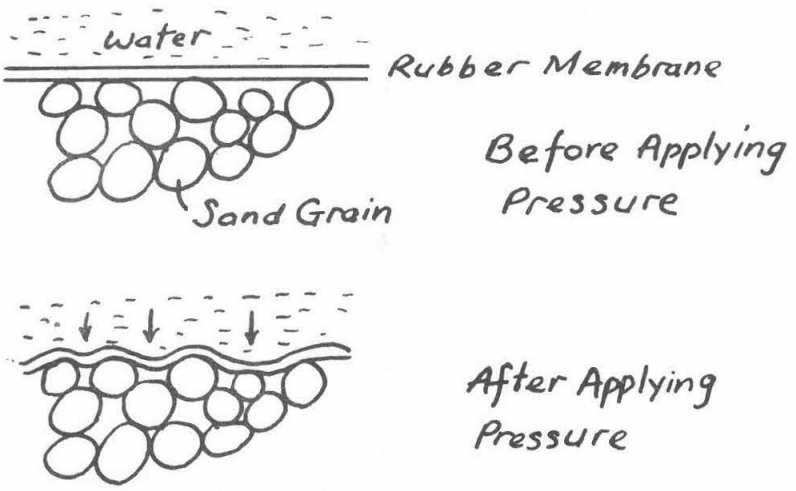

FIG (Ⅴ.10)
MEMBRANE PENETRATION

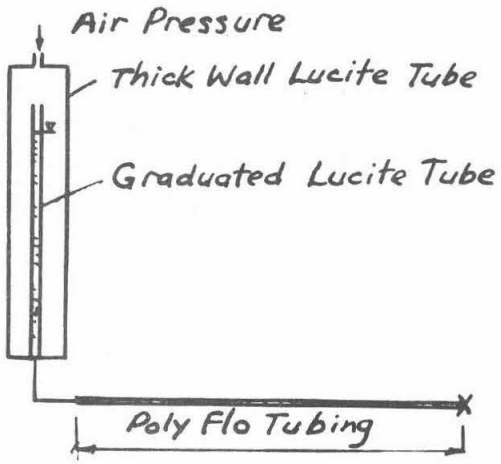

FIG. (Ⅴ.12)
MEASUREMENT OF TUBING CORRECTION

FIG. (II.11). CORRECTION CURVE FOR WALL AND MEMBRANE EFFECTS

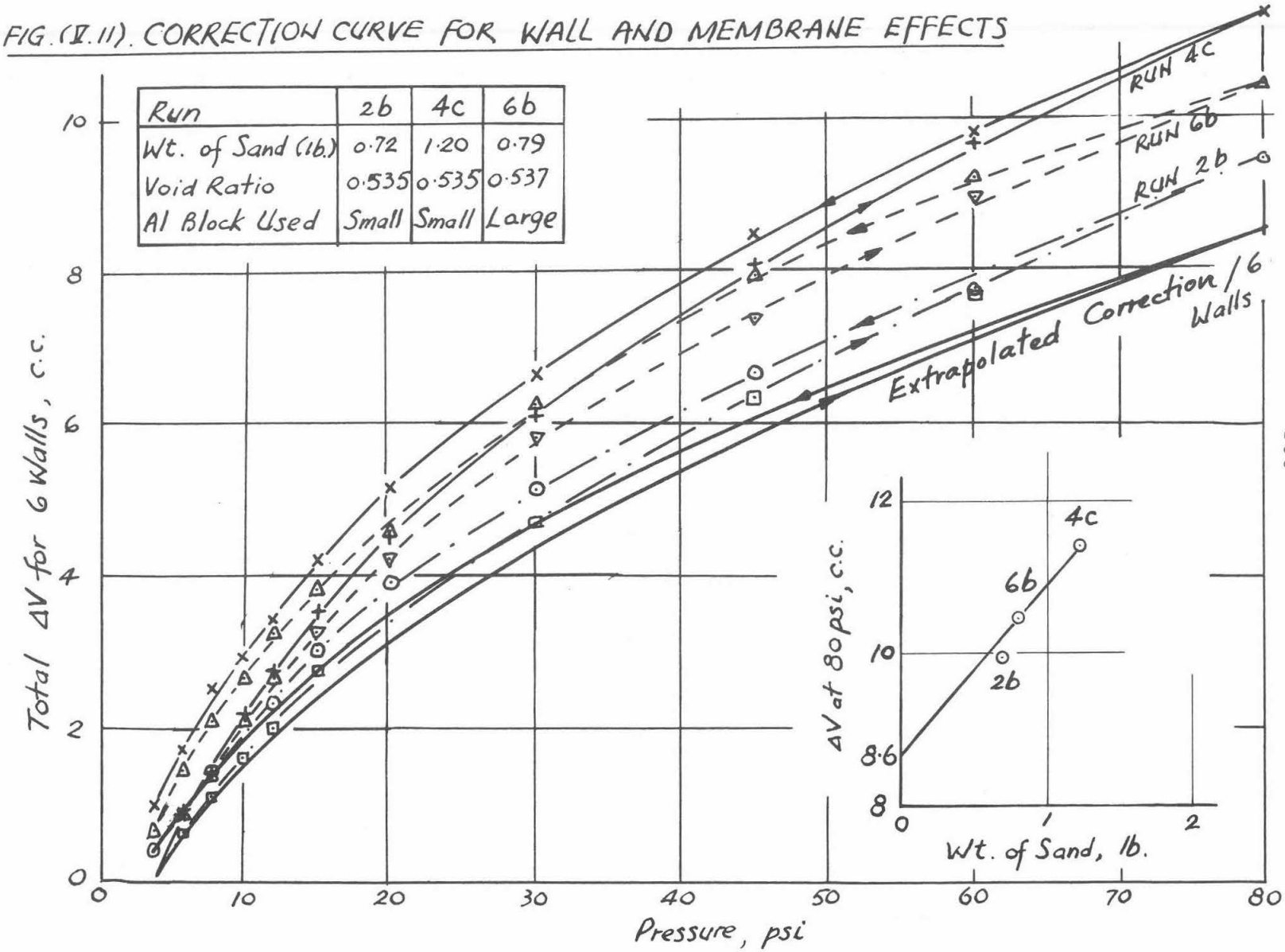

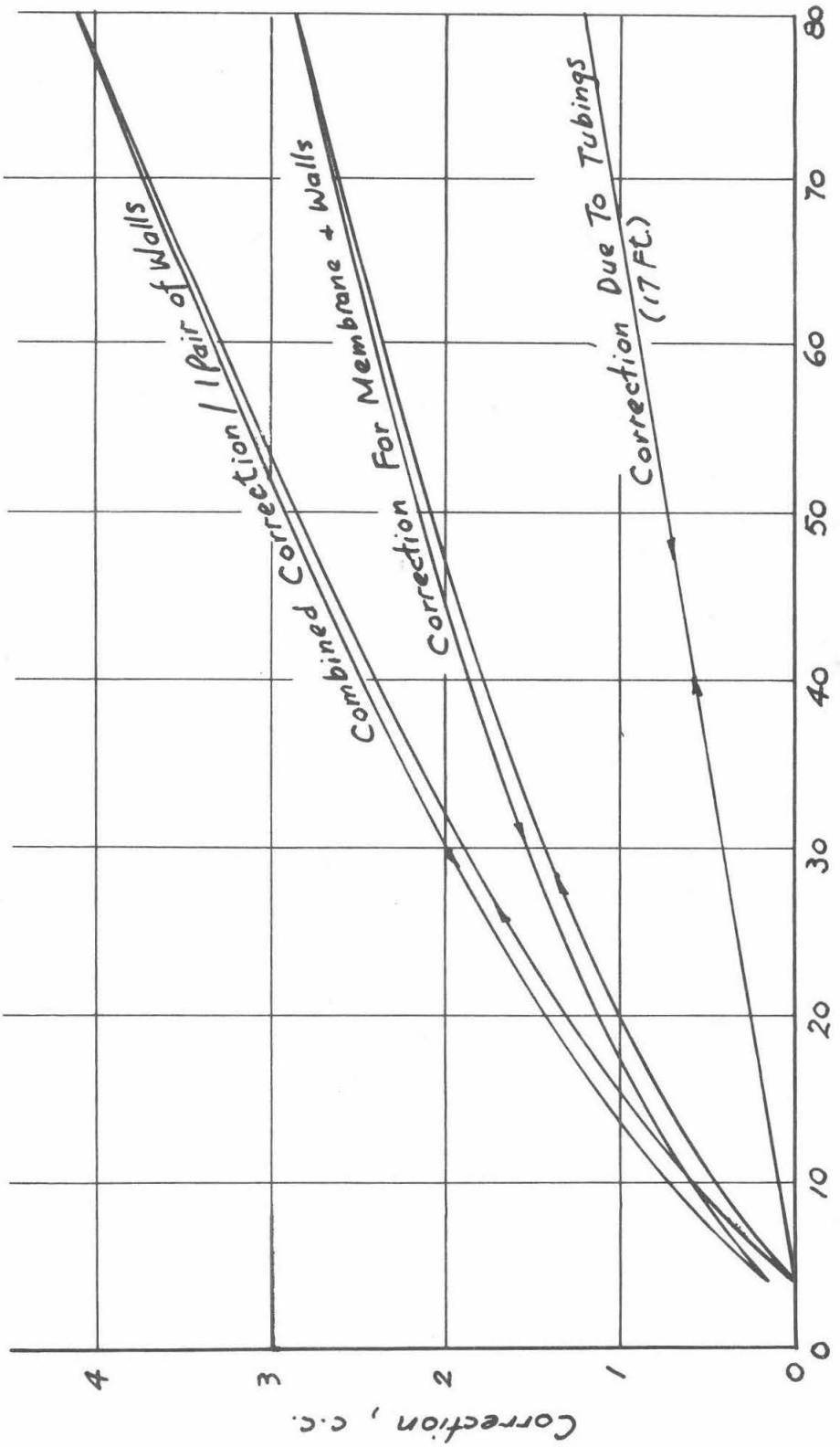

FIG. (II.13). TOTAL CORRECTION CURVE

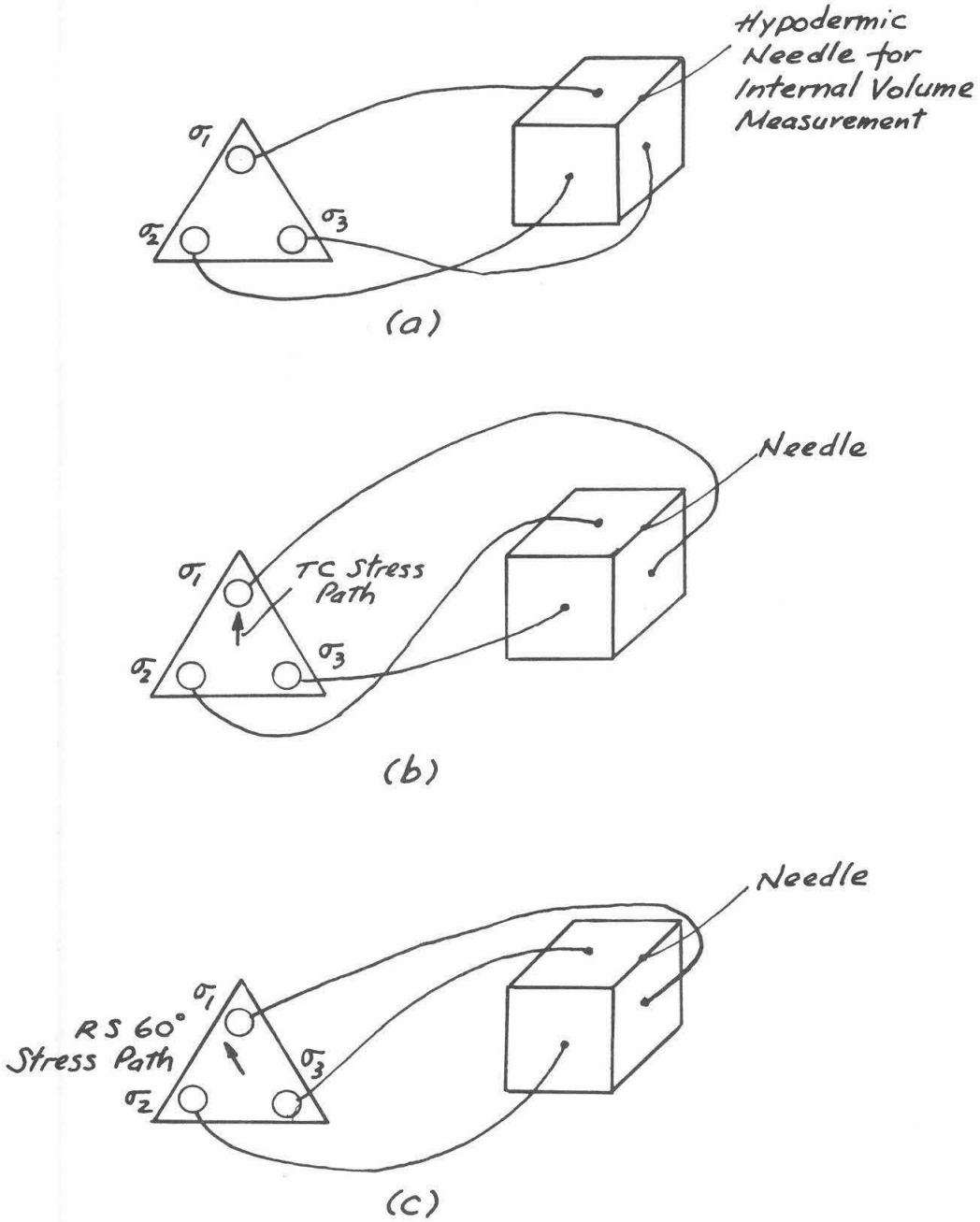

FIG. (V.14). ROTATION OF DIRECTIONS OF PRINCIPAL STRESSES

CHAPTER VI

EXPERIMENTAL RESULTS

(1) Summary of Tests

The theory of tests performed in this research was given in Chapter III, where the stress paths for various tests were also given. In Table (VI.1) is given a summary of these tests.

(2) Results of Hydrostatic Compression Tests

The results of hydrostatic compression tests of a dense, medium dense and loose sand are shown in Figs. (VI.1), (VI.2) and (VI.3) respectively. In each figure, the total volume compression, ΔV, of the sample, after applying the correction shown in Fig. (V.13), is plotted versus the hydrostatic pressure, p. The volume compression ΔV was calculated on the basis that the volume change was taken to be zero at the datum pressure of 4 psi.

Assuming that the sample was isotropic during the hydrostatic compression test, and that its shape was roughly cubic, the principal deformations, ΔV_i, in the three perpendicular directions should be equal. However it was sometimes observed that the vertical deformations ΔV_1 was greater than the two horizontal deformations ΔV_2 and ΔV_3 which are always equal, while at other times, the three were nearly equal. This discrepancy could be due to the fact that the box has only two planes of symmetry, both vertical, and we had not taken this into account when we applied the correction to the deformation readings. Or it could be due to the sample being anisotropic, but this effect was considered not important, as supported by the results of anisotropy

Table (VI.1)

Test	Stress Path Shown in Fig.	Void Ratio of Sample	Volume of Sample, c.c.	Value of σ_{OCT} Used, psi	Results Shown in Fig.
HC-1	III.11	0.486	810	4-60	VI.1
HC-2	"	0.537	837	4-60	VI.2
HC-3	"	0.692	820	4-60	VI.3
TCa-1	III.12	0.510	816	20	VI.4
TCa-2	"	0.540	783	20	VI.5
TCa-3	"	0.610	798	20	VI.6
TCa-4	"	0.637	812	20	VI.7
TCa-5	"	0.670	817	20	VI.8
TCa-6	"	0.535	779	15	VI.9
TEa-1	"	0.502	812	20	VI.10
TEa-2	"	0.538	790	20	VI.11
TEa-3	"	0.640	808	20	VI.12
TEa-4	"	0.670	808	20	VI.13
TEa-5	"	0.531	801	15	VI.14
TCb-1	III.13	0.535	809	15	VI.15
TCb-2	"	0.620	826	15	VI.16
TEb-1	"	0.526	793	15	VI.17
TCc-1	III.14	0.540	783	15-40	VI.18
TCc-2	"	0.604	807	15-40	VI.19
TEc-1	"	0.528	791	15-40	VI.20
TCd-1	III.15	0.534	772	15-25	VI.21
TCd-2	"	0.590	829	15-25	VI.22
TEd-1	"	0.530	767	15-25	VI.23
TCe-1	III.16	0.534	764	15-40	VI.24
TCe-2	"	0.605	825	15-40	VI.25
TEe-1	"	0.530	788	15-40	VI.26
RS45°-1	III.18	0.526	814	20	VI.27
RS45°-2	"	0.610	823	20	VI.28
RS60°-1	III.18	0.518	836	20	VI.29
RS60°-2	"	0.614	837	20	VI.30
RS75°-1	III.18	0.532	834	20	VI.31
RS75°-2	"	0.606	827	20	VI.32
A-1	V.14(b)	0.520	802	20	VI.33
A-2	V.14(c)	0.614	836	20	VI.34

tests given later in this chapter. The probable reason for the measured vertical deformation being greater than the horizontal ones is the trapping of air in the water behind the rubber membrane of the top wall. This was possibly due to the fact that, whereas we could inspect the side wall and the bottom membranes to make sure that there was no air in the water behind these membranes, we could not do the same with the top one, and the circulation of water behind this membrane through the two connections on the top (see Fig. (V.5f)) did not completely remove all the trapped air. Since the pressure range in the hydrostatic compression test was nearly four atmospheres, the compressibility of any amount of air trapped in the top membrane was rather significant, especially when the compressibility of the sample itself was so small.

In order to better represent the true compressibility of the sample, the assumption was made that the three principal deformations were equal. The total volume change ΔV was then calculated by $\Delta V = 3/2 (\Delta V_2 + \Delta V_3)$. It is estimated that the error thus involved is no greater than the uncertainty due to membrane correction. The values of ΔV shown in Figs. (VI.1), (VI.2) and (VI.3) were calculated in this way.

A word must be said about the internal volume change measured by the hypodermic needle. This reading included the volume change of the sample itself and also the volume of membrane penetration. Since we had not determined the membrane penetration factor independently, it was not possible to isolate these two components in the internal volume change as measured by the needle. However, this reading afforded a check on the possible presence of a leak in the membrane into the box in

which case this reading would increase with time, as this was different from a leak outside of the box in which the hypodermic needle reading would be stationary. A leak outside would be indicated by the increasing volume of water going into the spaces behind the membranes.

In each of the three hydrostatic compression tests, the results of two cycles (loading and unloading) or hydrostatic stress were shown. In each cycle, the datum for ΔV was taken at that value of volume reading at 4 psi. The compressibility was not shown in terms of the void ratio, since the changes in e were very small.

(3) Results of Shear Tests in the Triaxial Plane

Tests TCa and TEa. The results of these tests are shown in Figs. (VI.4) to (VI.14), by plotting j versus ΔV_i. The parameter j is the number of steps through which the top cylinder of the stress control device is moved and is a measure of the shear stress. For the relation between j and the stresses, see Figs. (A-3) and (A-4) (Appendix A). We use the convention that ΔV_i is positive for compression.

In these tests, in which the intermediate principal stress was equal either to the major or to the minor principal stress, it was observed that the two principal displacements corresponding to the two stresses which were equal were always nearly the same (maximum difference less than 10%). Hence for the sake of clarity, only the major and the minor principal displacements are shown in Figs. (VI.4) to (VI.14) except in Fig. (VI.4b) where the three displacements are shown for a typical test. These displacements were also plotted on a semi-logarithmic graph.

In these figures are also shown the total volume changes ΔV ($= \sum_i \Delta V_i$). The internal volume change $\Delta V_{int.}$ measured by the hypodermic needle is not shown, because it was found to be nearly equal to ΔV (maximum difference less than 0.2 c.c.). That this was so could be explained by the fact that the mean stress was held constant in these tests. Had the membrane penetration correction function been a linear one, there would be no contribution from this factor to $\Delta V_{int.}$. Although this correction function was not linear, over the pressure range of these tests (say from 8 to 36 psi in triaxial compression) the deviation from linearity only contributed a little to $\Delta V_{int.}$. Therefore ΔV_{int} essentially measured the actual total volume change of the sample, which was ΔV and it was observed that ΔV and ΔV_{int} were indeed always nearly equal.

To obtain the strains from displacements, we need only to divide the deformations (ΔV_i and ΔV) by the volume of the sample, assuming that the sample was initially a cube and the displacements were small.

Tests TCb and TEb. The stress-deformation curves for these tests are shown in Figs. (VI.15) - (VI.17). The same remarks for tests TCa and TEa are applicable here, except that on the semi-logarithmic plots only the displacements when a new maximum shear stress ($\sim$ j) was reached are shown.

Tests TCc and TEc. The stress-deformation curves for these tests are shown in Figs. (VI.18) - (VI.20). The compressibility of the sample during the hydrostatic stress cycle when each time the sample was unloaded to the hydrostatic stress is shown in Figs. (VI.18c), (VI.19c)

and (VI.20b). Here ΔV was calculated by directly summing ΔV_i.

Here again, the semi-logarithmic plots only show the displacements corresponding to a new maximum shear stress.

Tests TCd and TEd. The stress-deformation relations for these tests are shown in Figs. (VI.21) - (VI.23). When the pressure in the top cylinder was increased from 45 to 75 psi and then reduced back to 45 psi with the cylinder in an eccentric position, the value of j remained unchanged. For such cycles of stress in which σ_{OCT} changed from 15 psi to 25 psi and back to 15 psi, the displacements induced are shown in Figs. (VI.21a) - (VI.23a). In Figs. (VI.21b) - (VI.23b), the total volume changes ΔV $(= \sum_i \Delta V_i)$ for one cycle of stress of each value of j are plotted versus σ_{OCT}.

Tests TCe and TEe. The stress-deformation relations for these tests are shown in Figs. (VI.24) - (VI.26). Strictly speaking, when the pressure in the hanging cylinder was increased from zero to 75 psi and then reduced back to zero with the top cylinder in an eccentric position, the value of j decreased and then increased to its former value. The actual value of j at each increment of the pressure in the hanging cylinder could be calculated from τ_{OCT} and σ_{OCT}; this was not attempted and, for the sake of clarity of presentation, the deformations in this cycle of stress were plotted as if j were constant, as in Figs. (VI.24a) - (VI.26a).

The value of σ_{OCT} changed from 15 psi to 40 psi and back to 15 psi; the corresponding total volume changes ΔV $(= \sum_i \Delta V_i)$ were plotted versus σ_{OCT} in Fig. (VI.24b) - (VI.26b), for different values of j.

(4) Results of Radial Shear Tests

The results of these tests are shown in Figs. (VI.27) to (VI.32). The three principal displacements ΔV_i and the total volume change ΔV ($= \sum_i \Delta V_i$) are plotted versus j. ΔV_i are also plotted on a semi-logarithmic graph.

(5) Results of Tests for Anisotropy

The results of these tests, A-1 and A-2, are shown in Figs. (VI.33) and (VI.34).

In A-1, the stress path was triaxial compression, and it was observed that ΔV_2 and ΔV_3 were nearly equal (maximum difference less than 0.5 c.c.). Hence only ΔV_1 and ΔV_2 are plotted in Fig. (VI.33), both arithmetically and semi-logarithmically.

In A-2, the stress path was RS60°. All the three principal displacements are plotted in Fig. (VI.34), both arithmetically and semi-logarithmically.

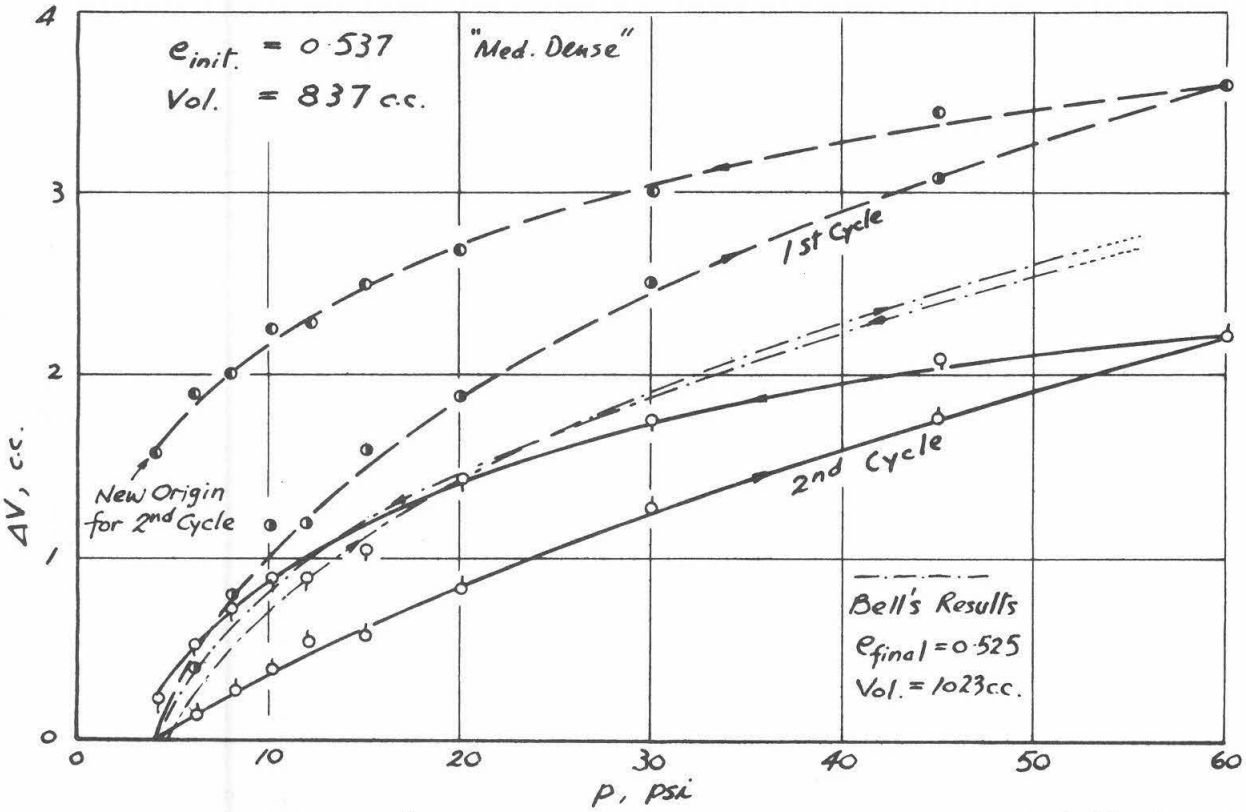

FIG. (VI.2) RESULTS OF HYDROSTATIC COMPRESSION TEST HC-2

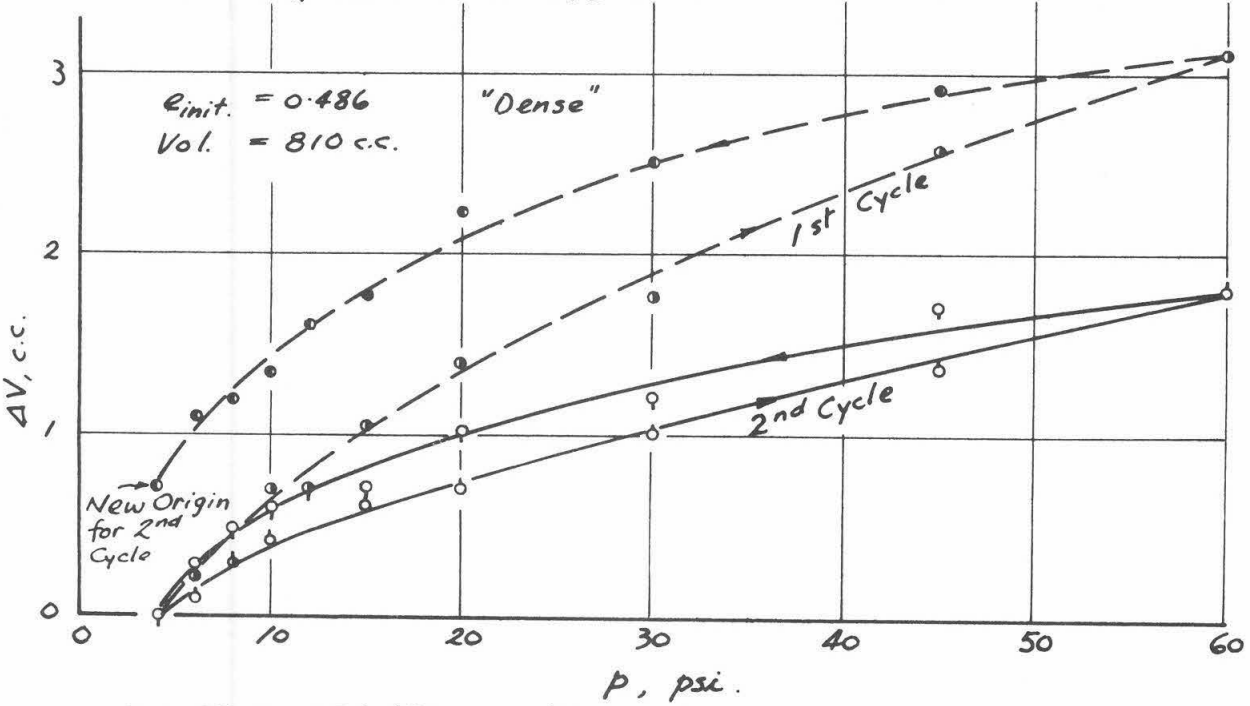

FIG. (VI.1). RESULTS OF HYDROSTATIC COMPRESSION TEST HC-1

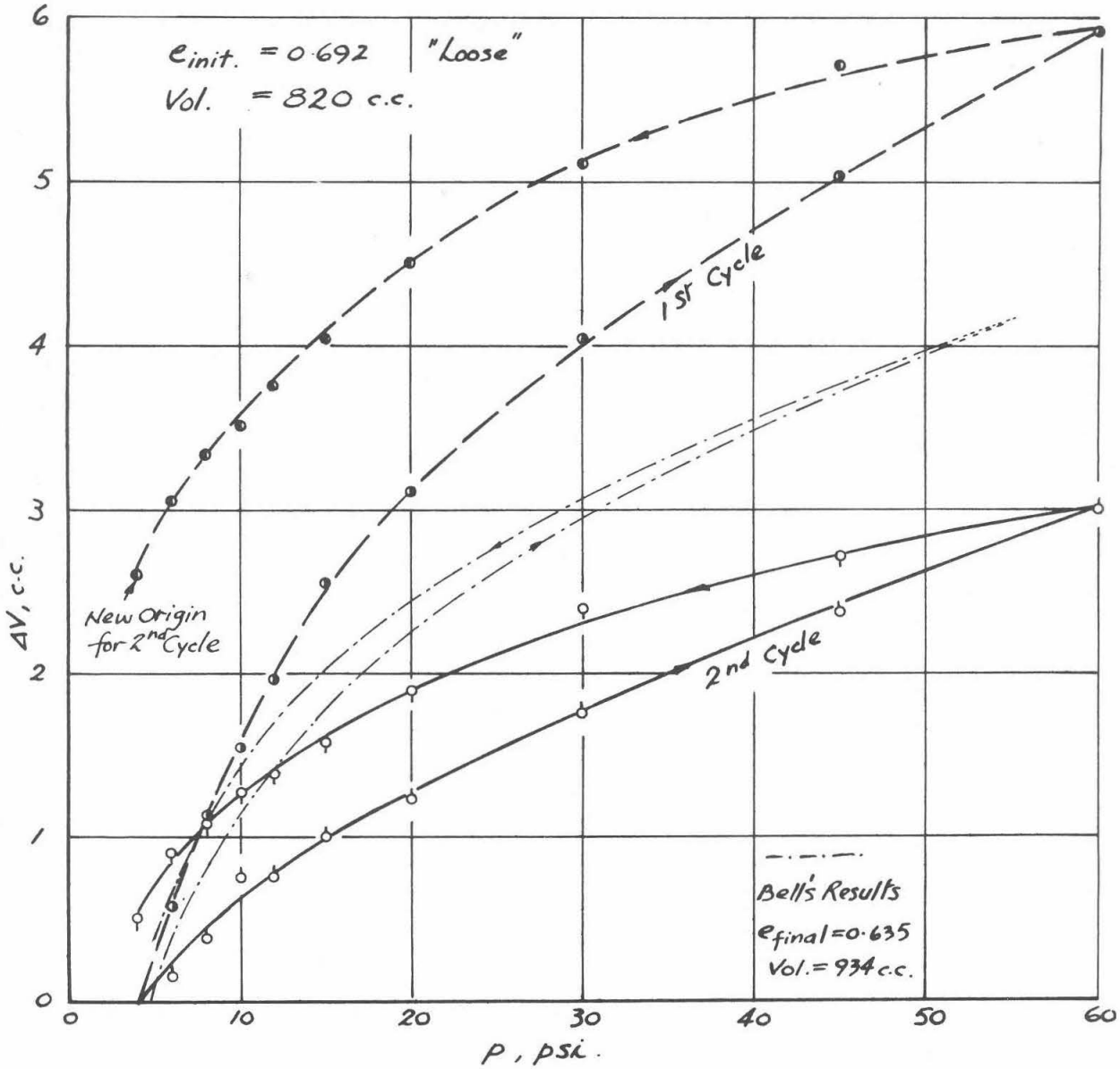

FIG. (VI.3). RESULTS OF HYDROSTATIC COMPRESSION TEST HC-3

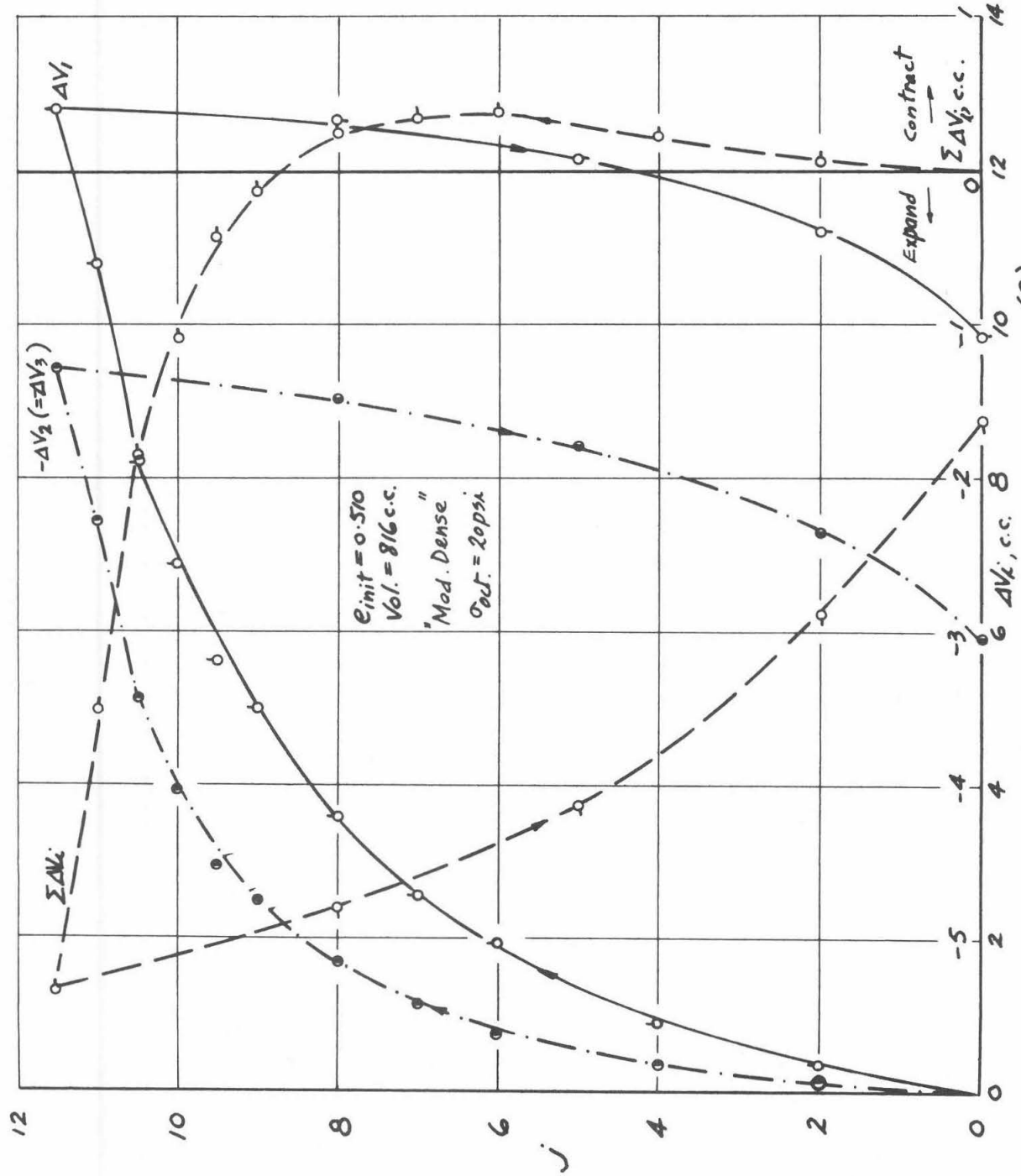

FIG. (VI.4). RESULTS OF TEST TCa-1

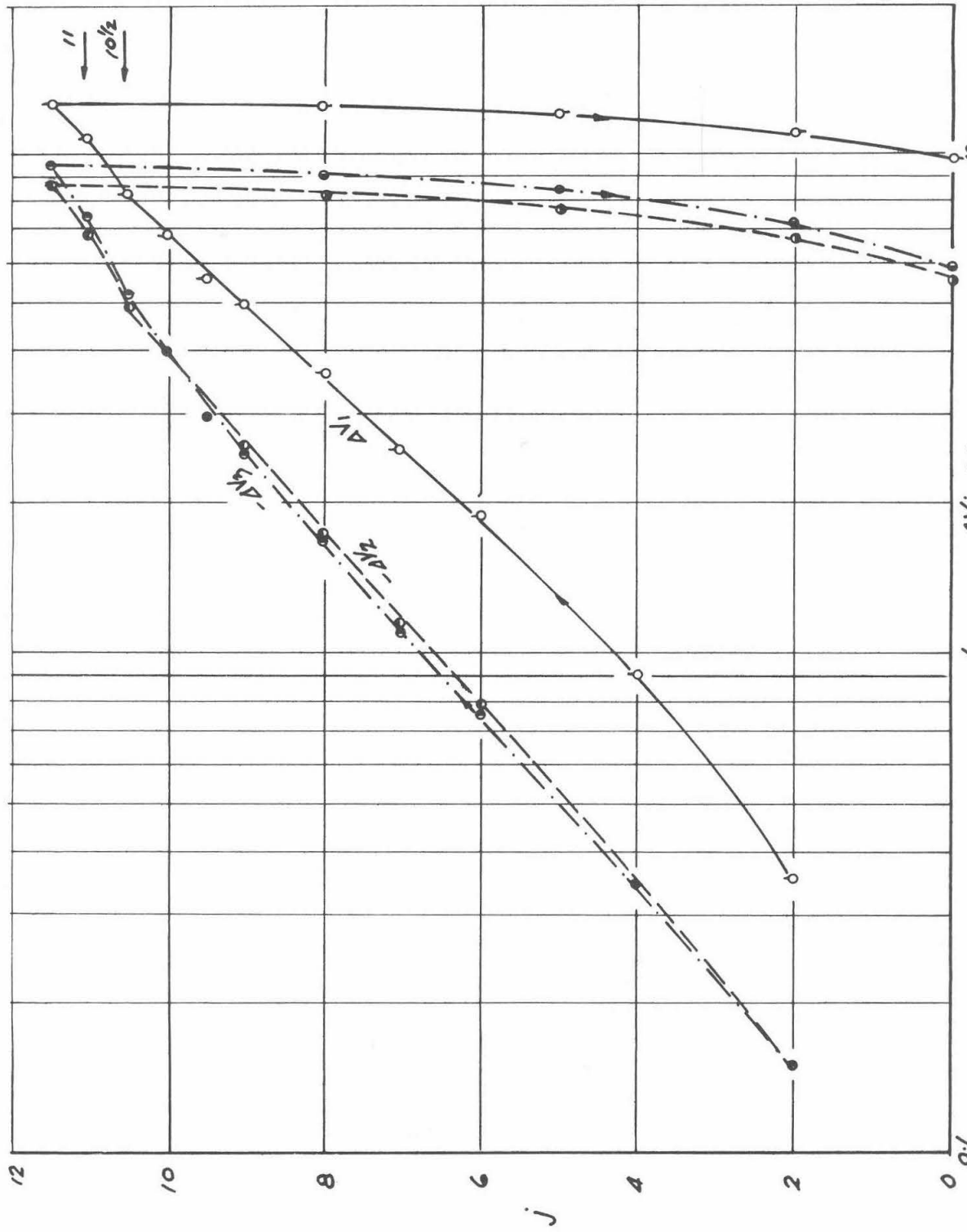

FIG. (III. 4). (b)

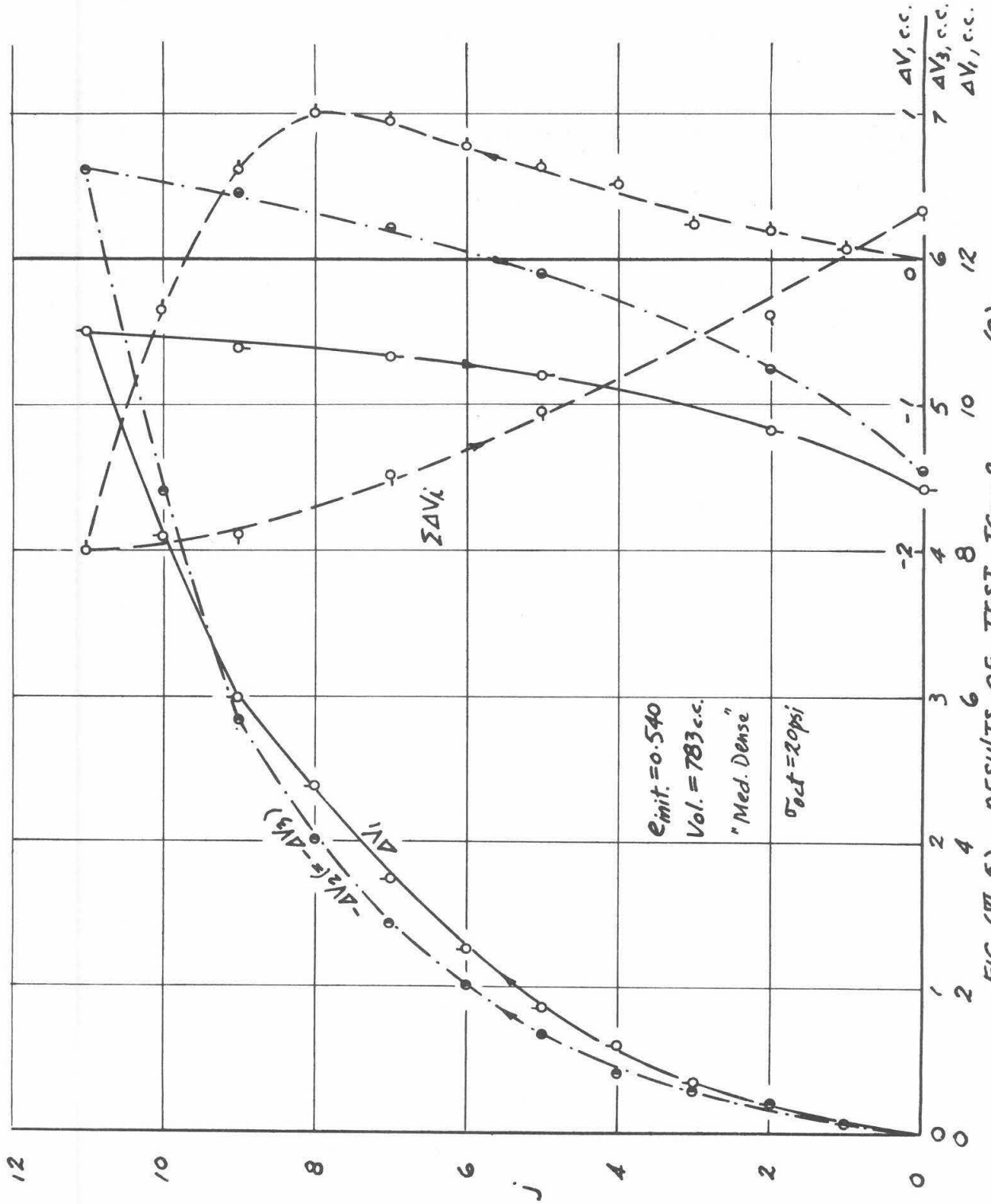

FIG. (III.5) RESULTS OF TEST TCa-2

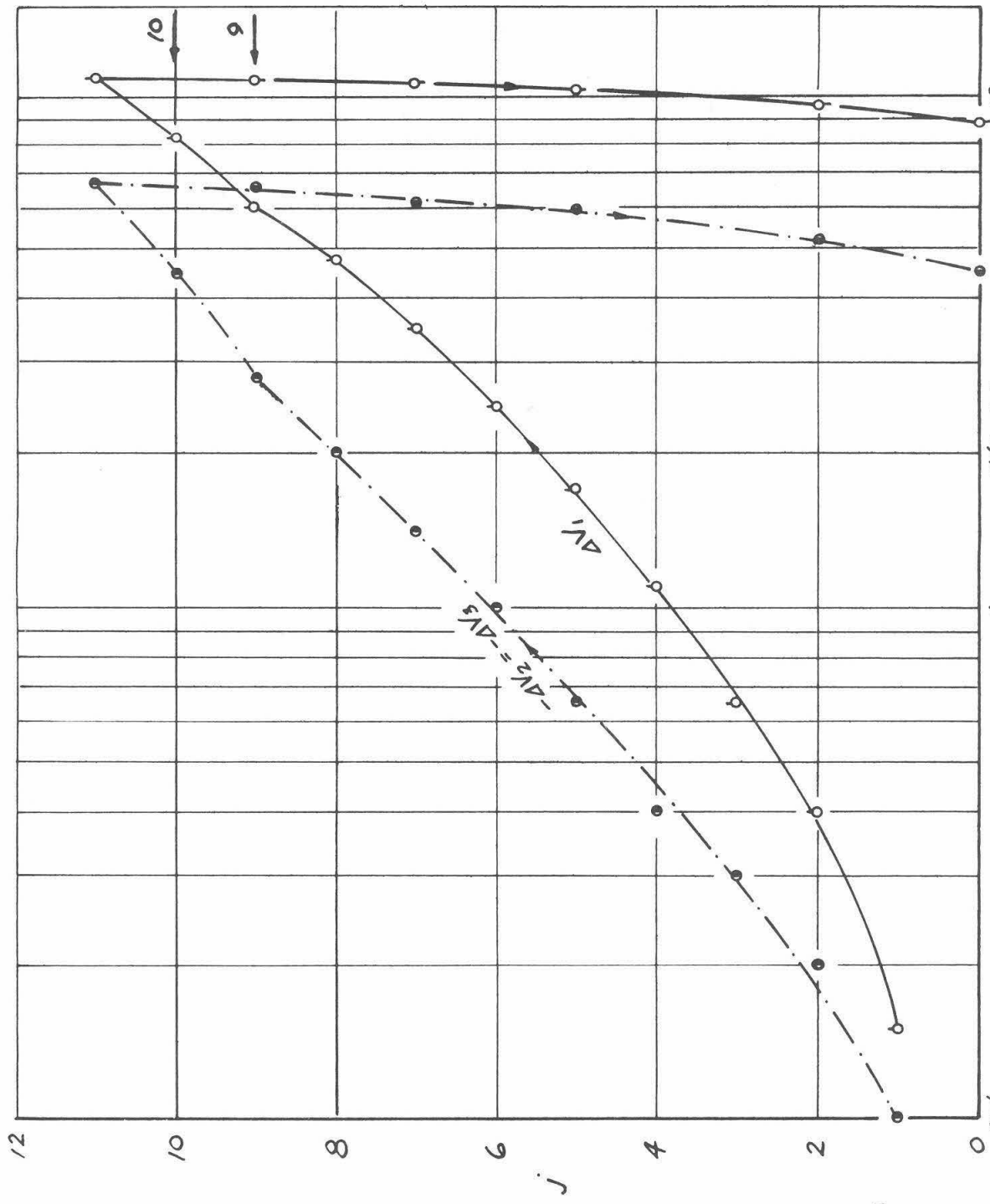

FIG. (III. 5). (6)

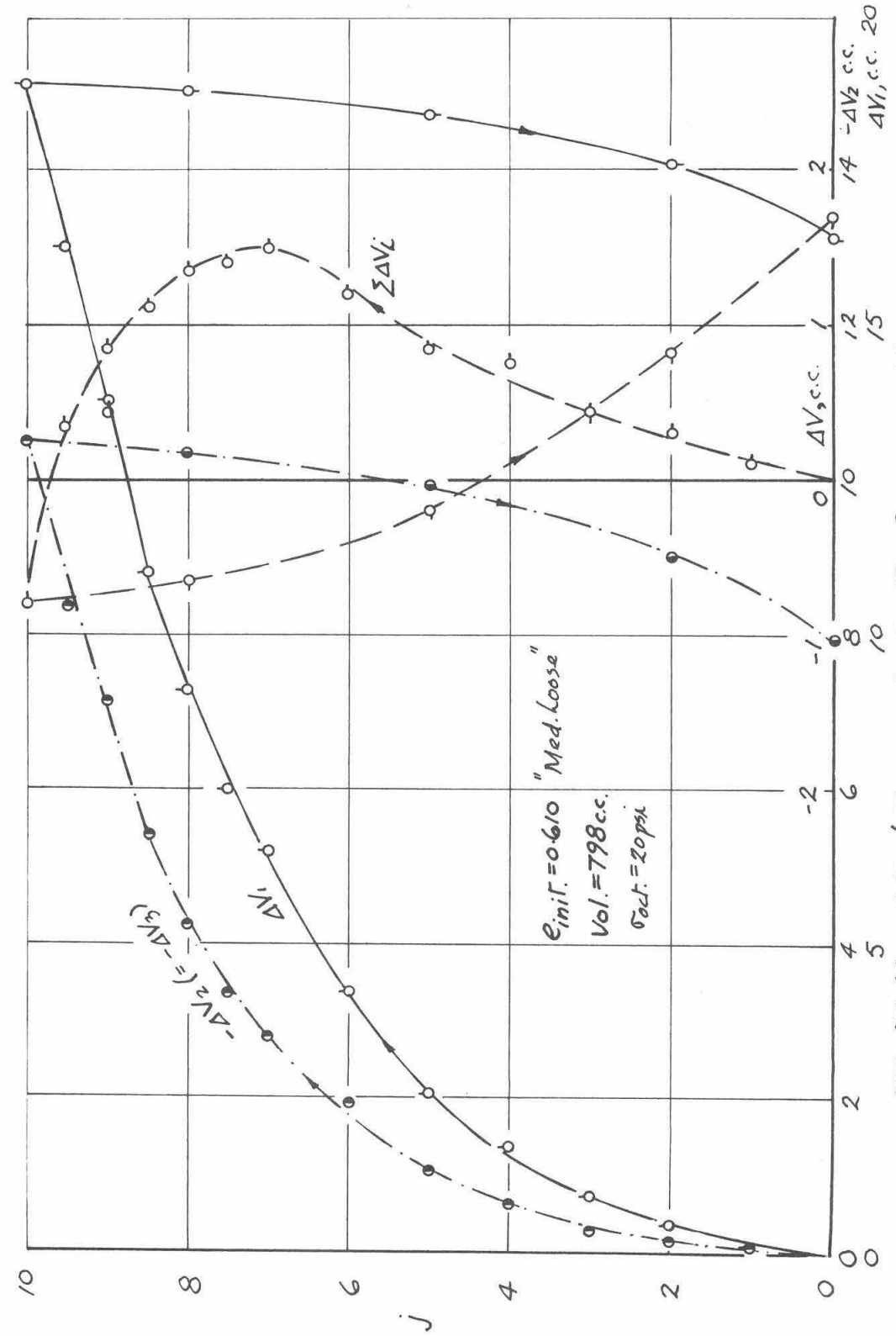

FIG. (III.6). RESULTS OF TEST TCa-3

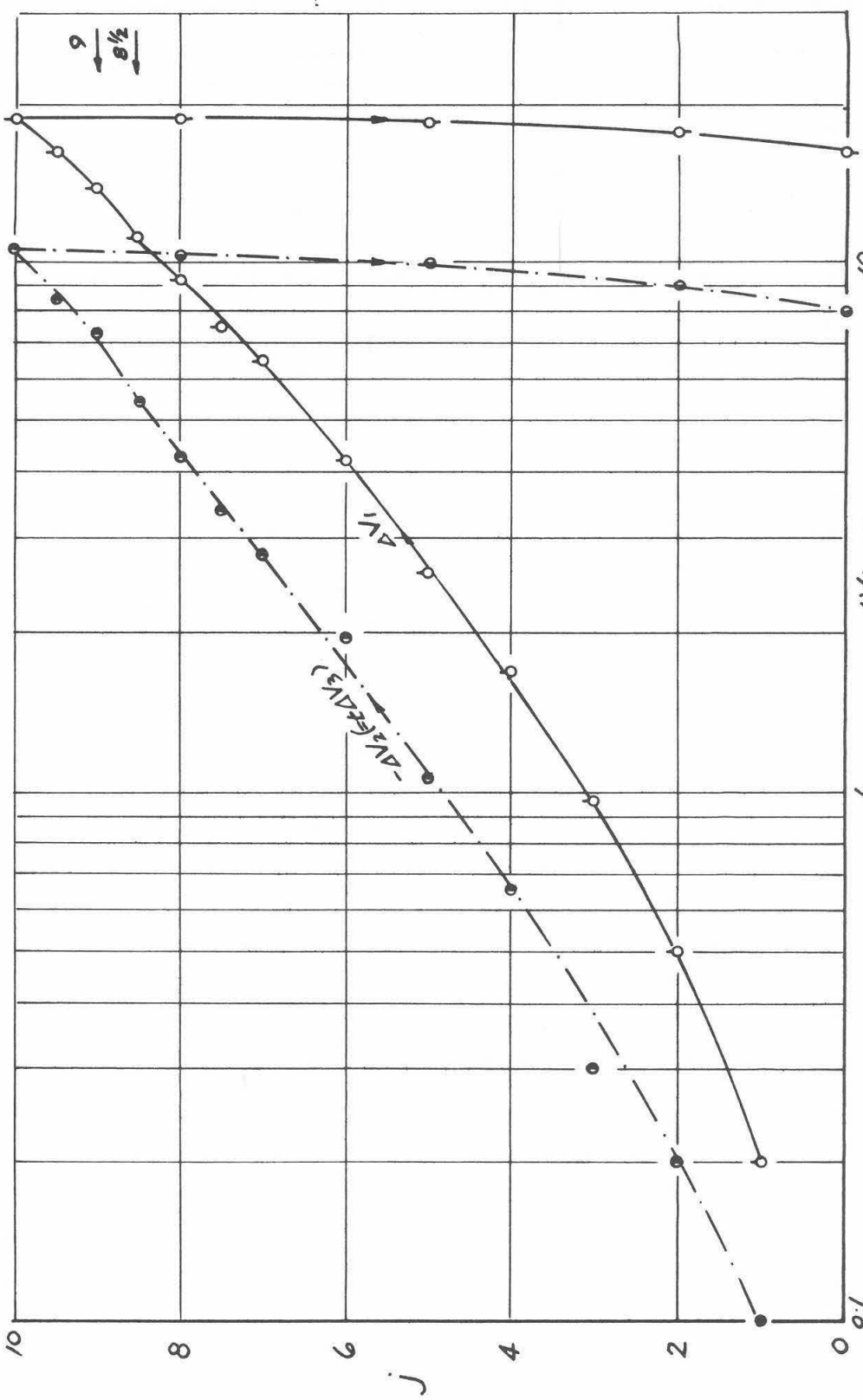

FIG. (III. 6). (b)

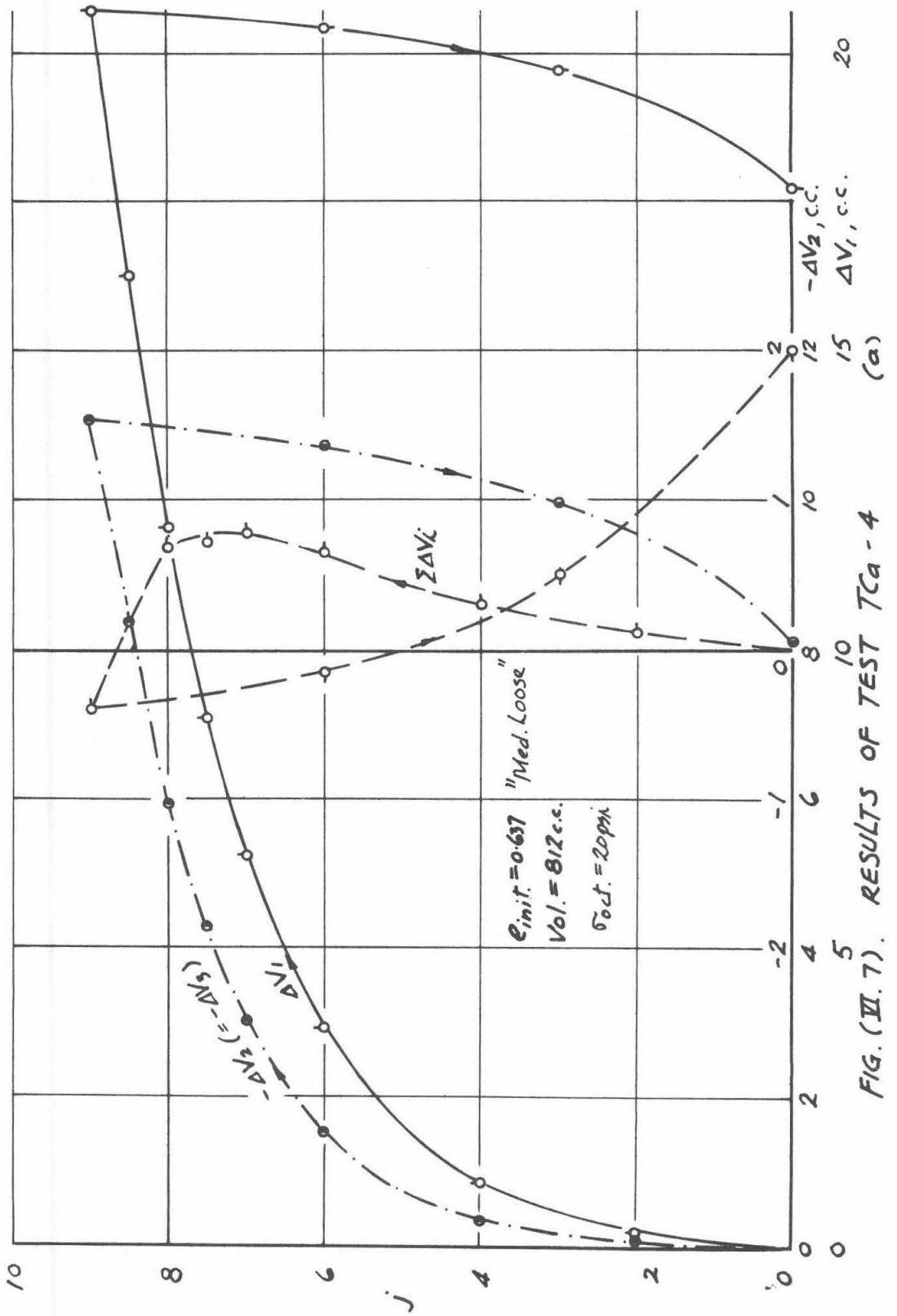

FIG. (III. 7). RESULTS OF TEST TCa - 4

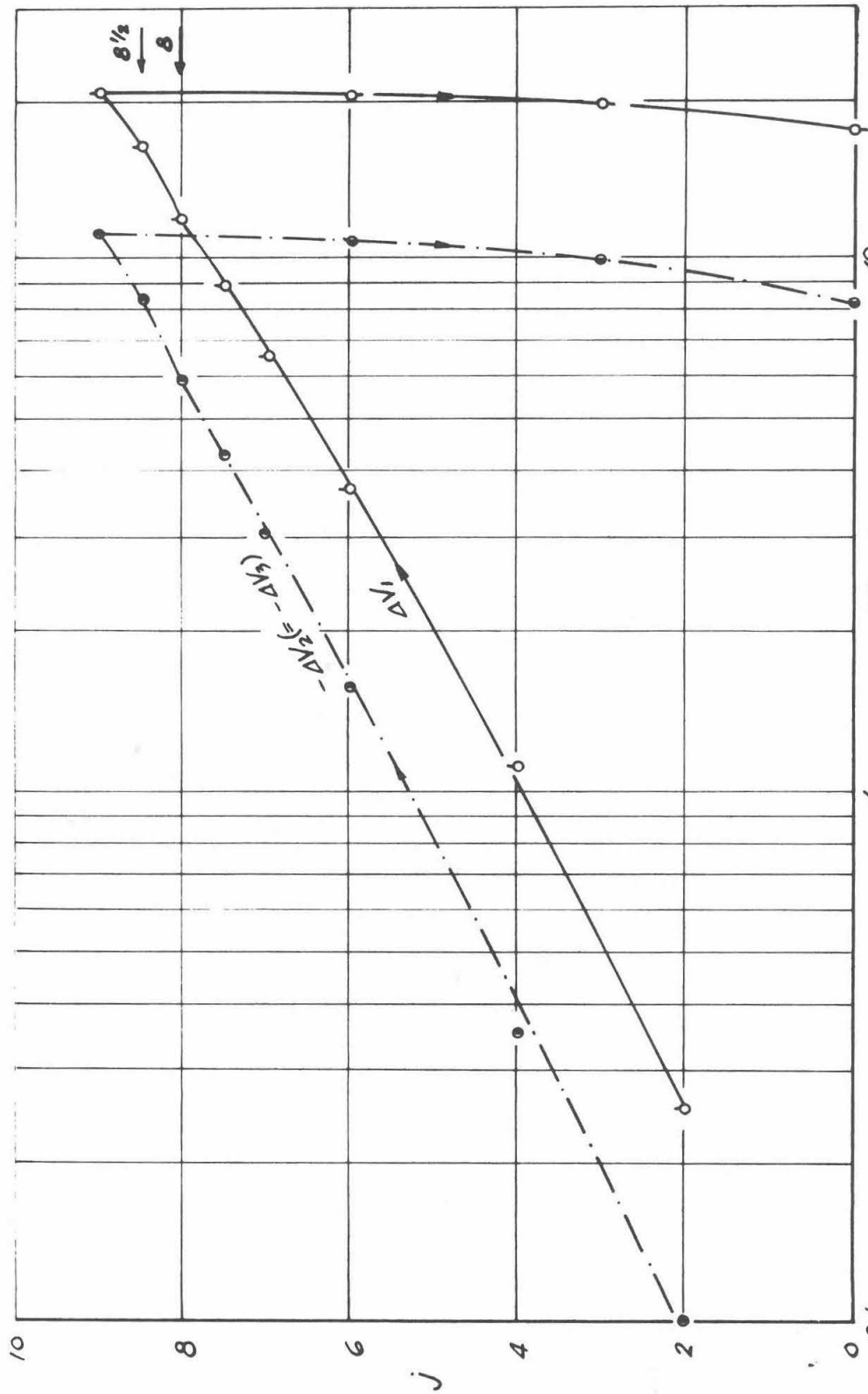

FIG. (VII.7). (b)

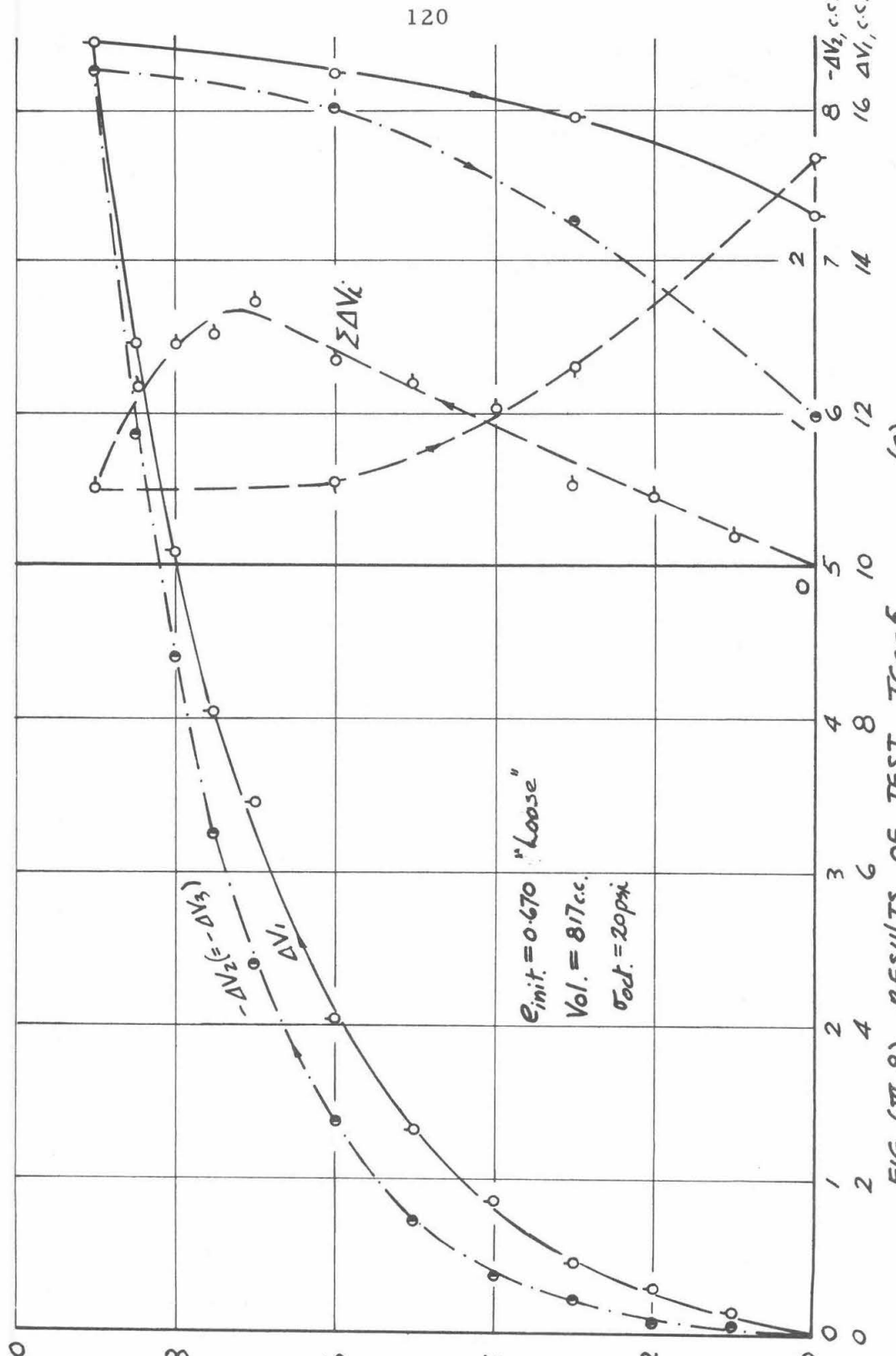

FIG. (III.8). RESULTS OF TEST Tca-5

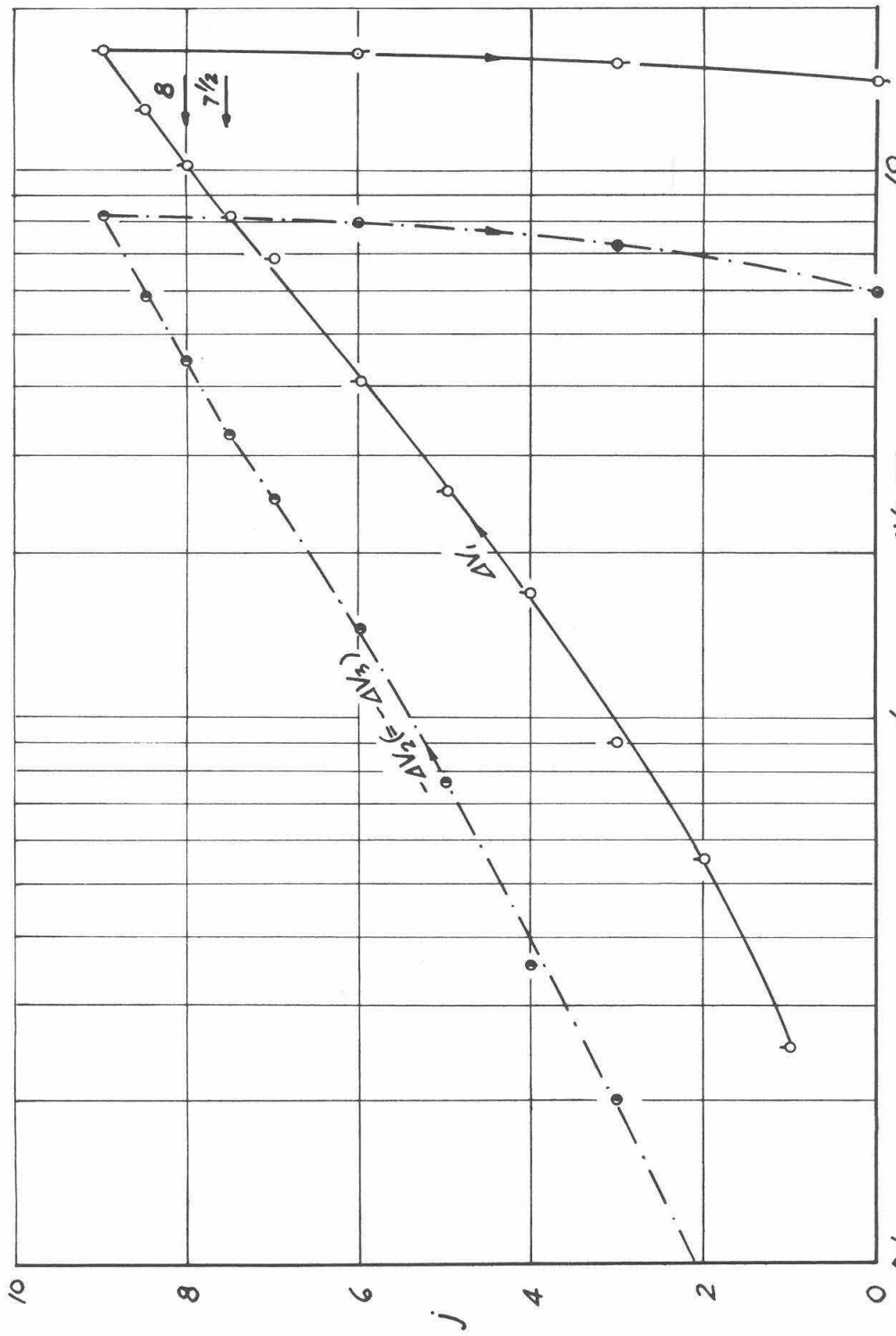

FIG. (VII.8). (b)

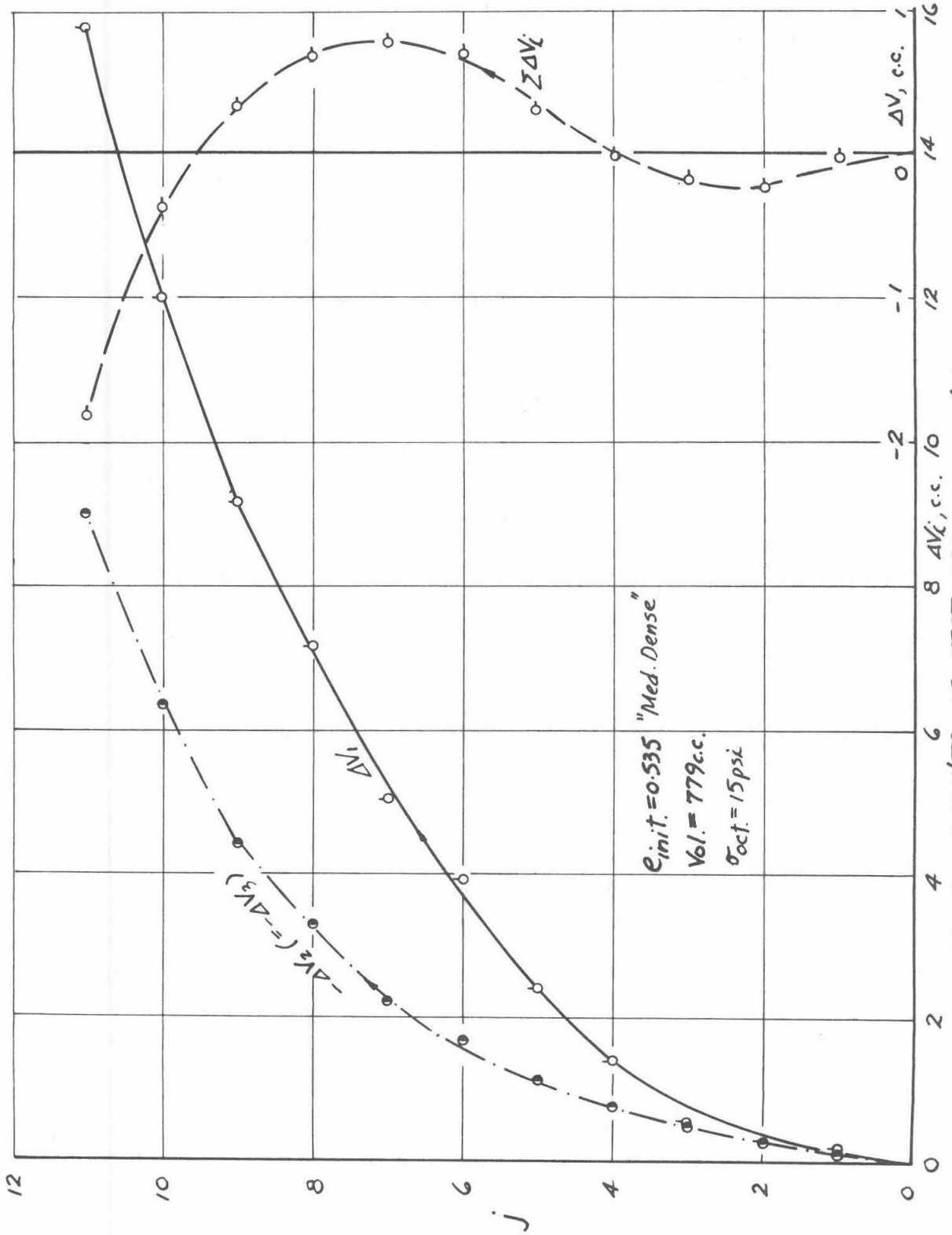

FIG. (III. 9). RESULTS OF TEST TCa-6 (a)

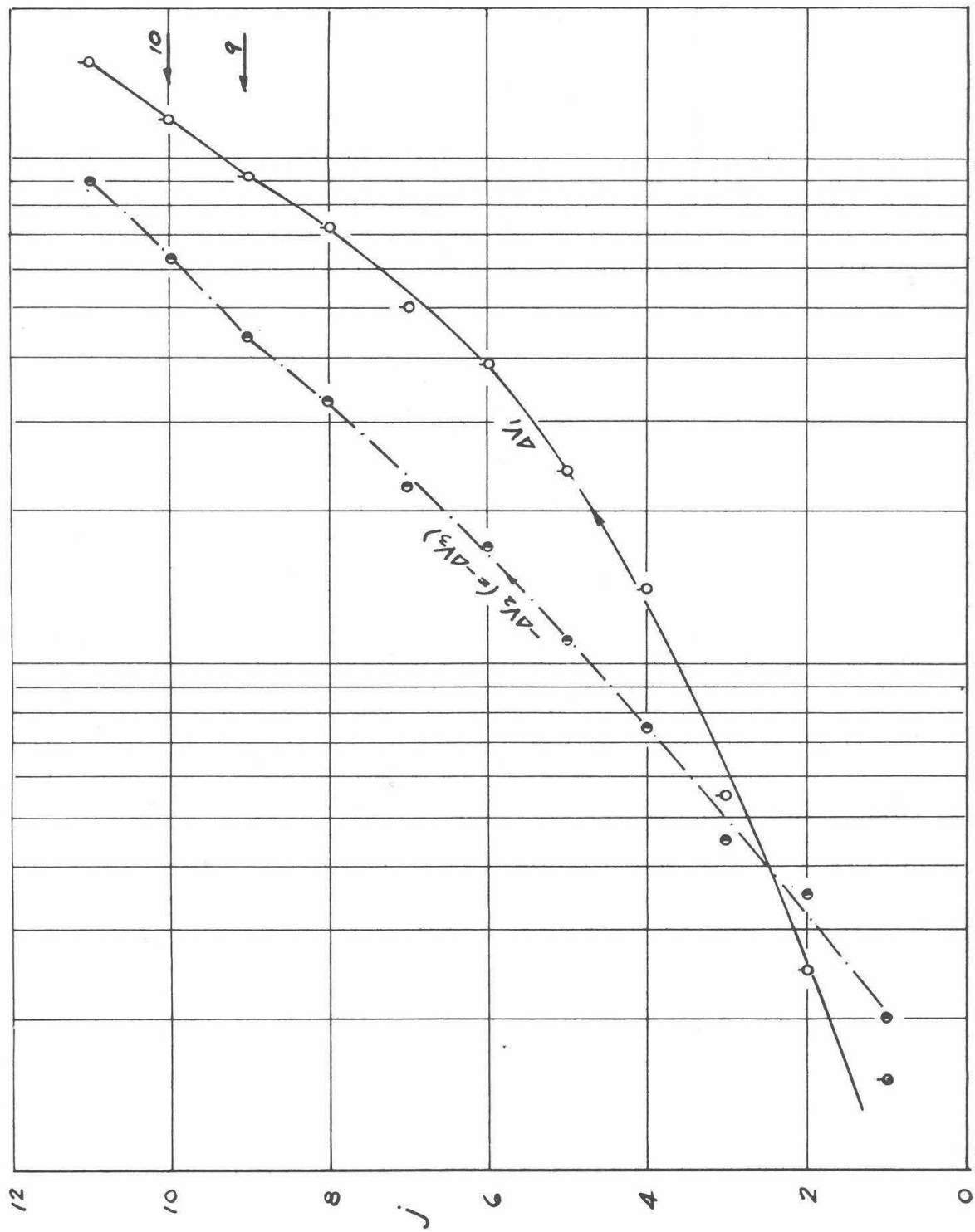

FIG. (III. 9). (b)

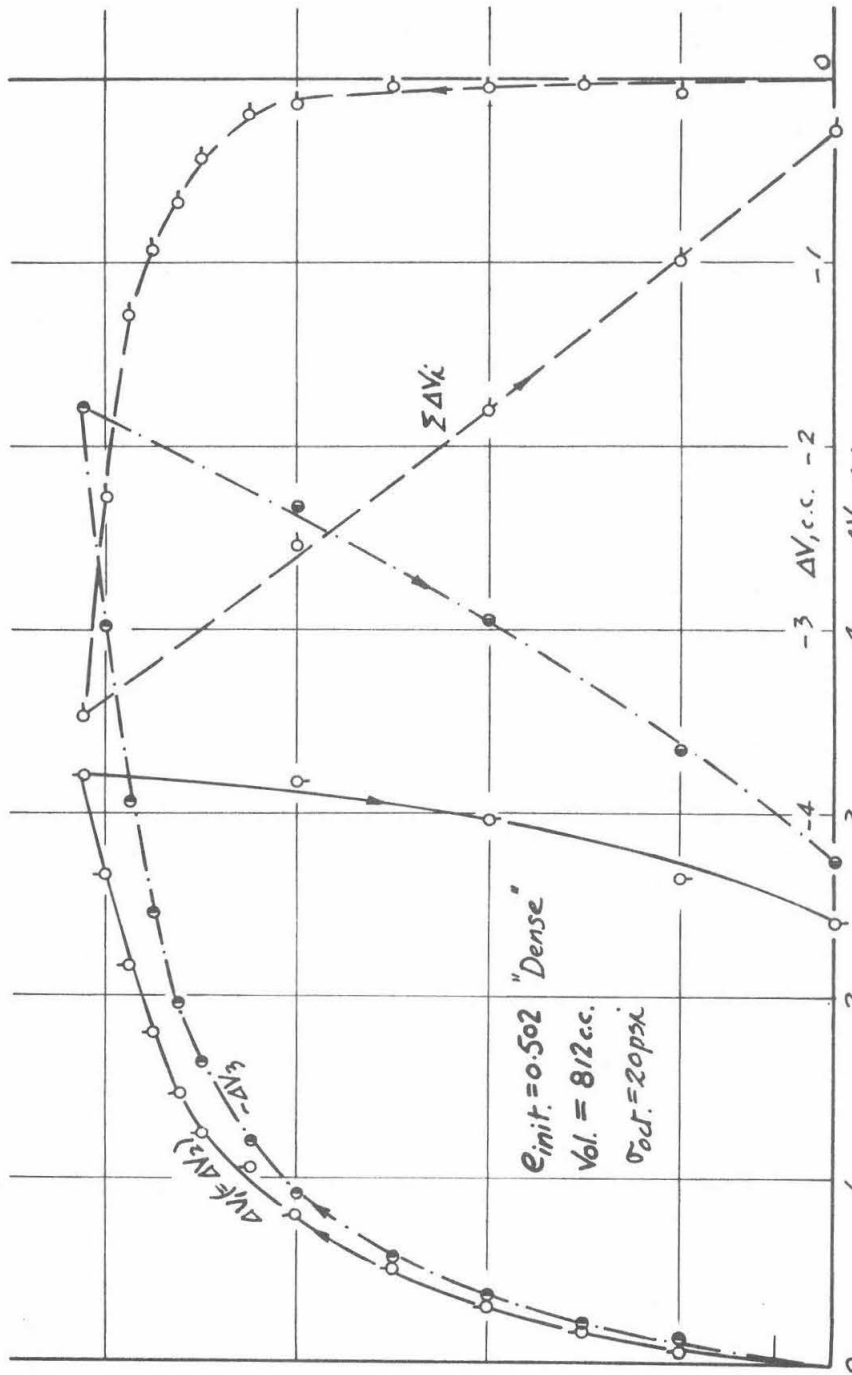

FIG. (VI.10) RESULTS OF TEST TEa-1 (a)

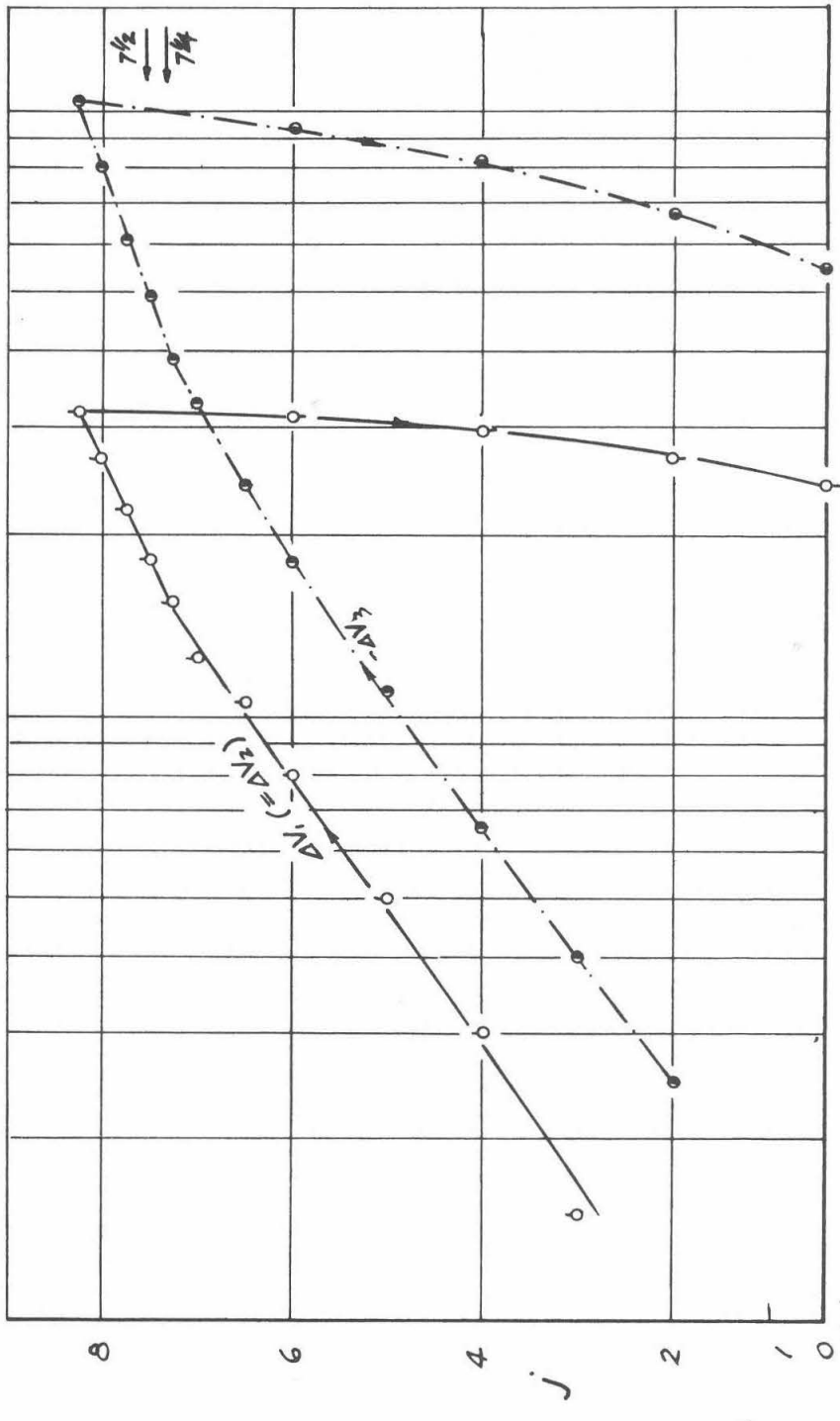

FIG. (VII.10). (b)

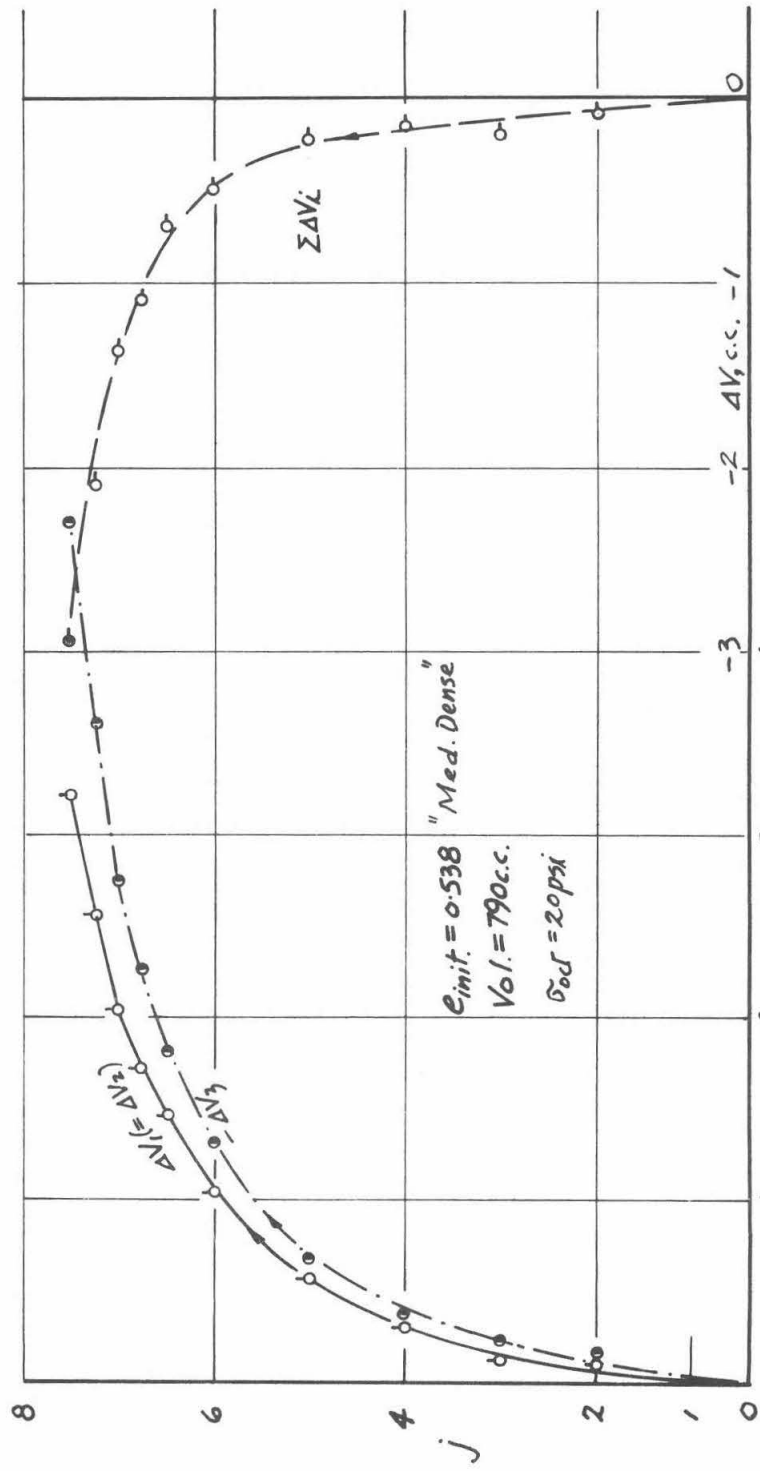

FIG. (VI.11). RESULTS OF TEST TEa-2

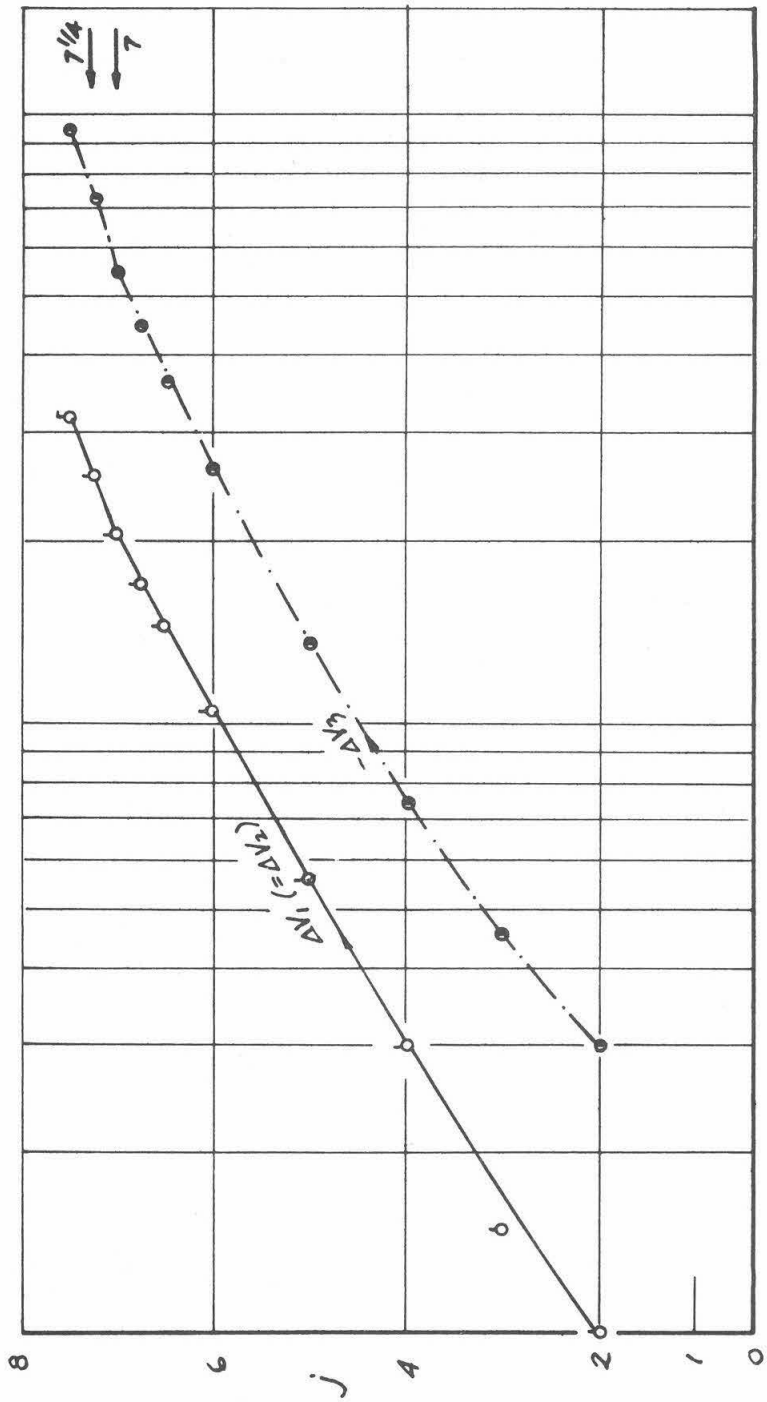

FIG. (VI.11). (b)

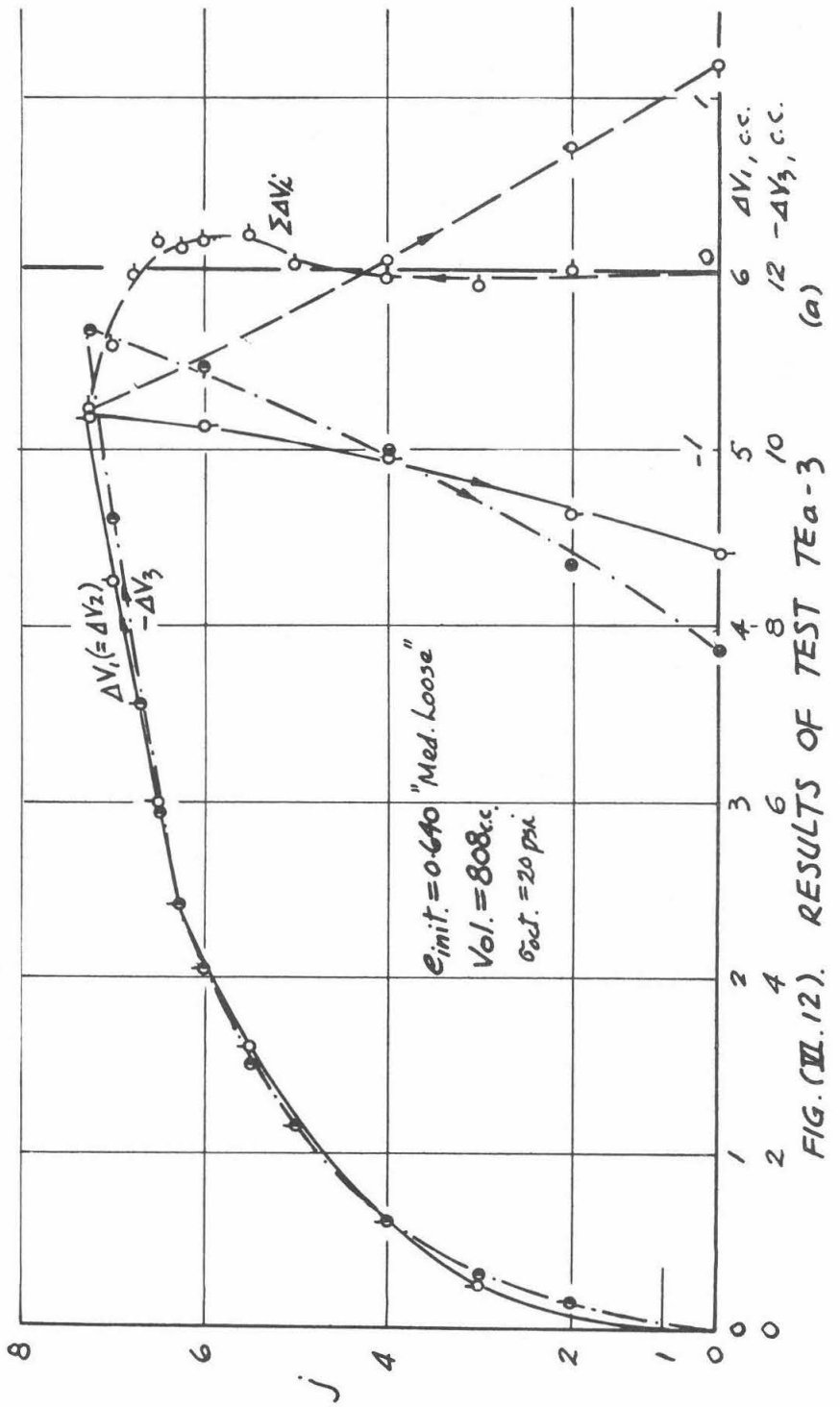

FIG. (III.12). RESULTS OF TEST TEa-3

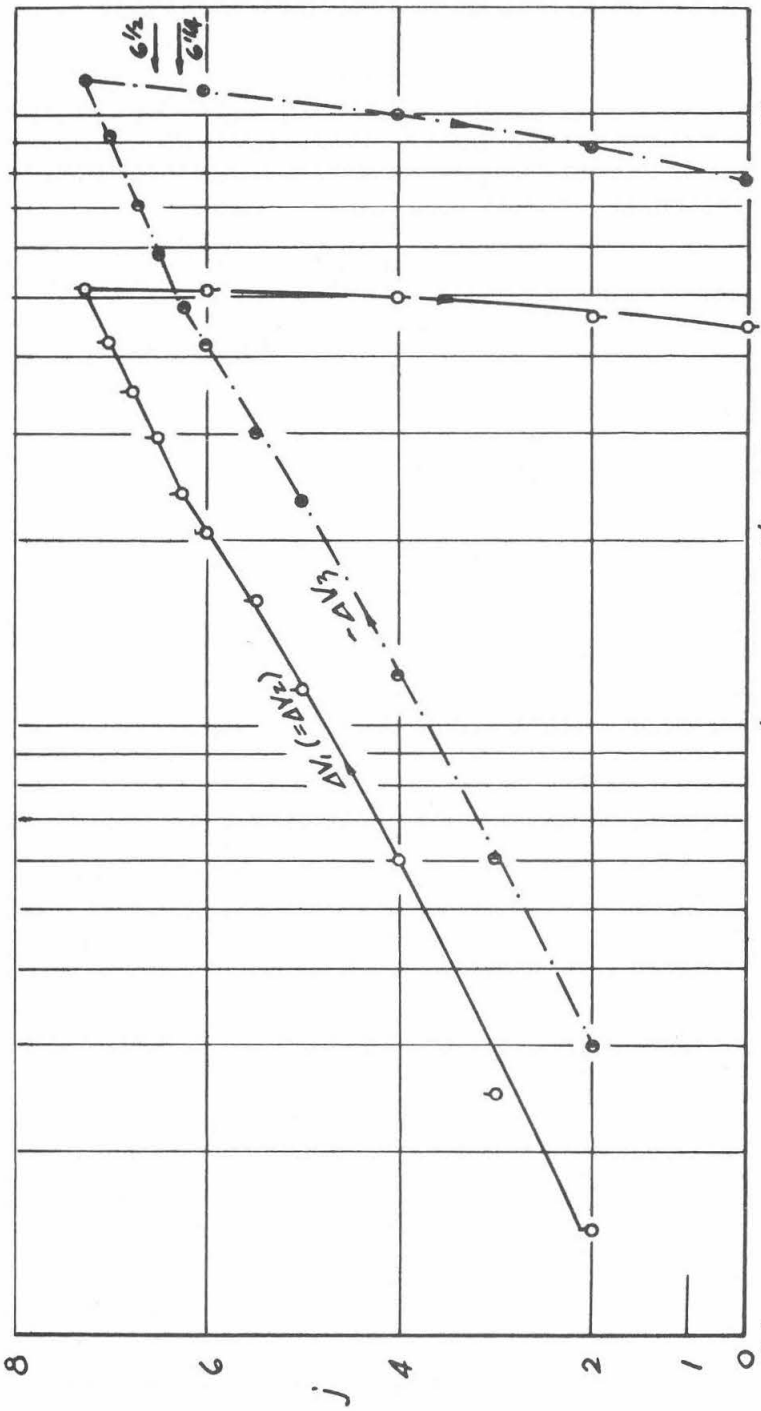
$\frac{\sigma_2}{\sigma_4}$
$\Delta V_1 (=\Delta V_2)$
$\Delta V_2 (=\Delta V_1)$
j
8
6
4
2
1
0
0.1
1
10
ΔV_2, c.c.

FIG. (III.12). (6)

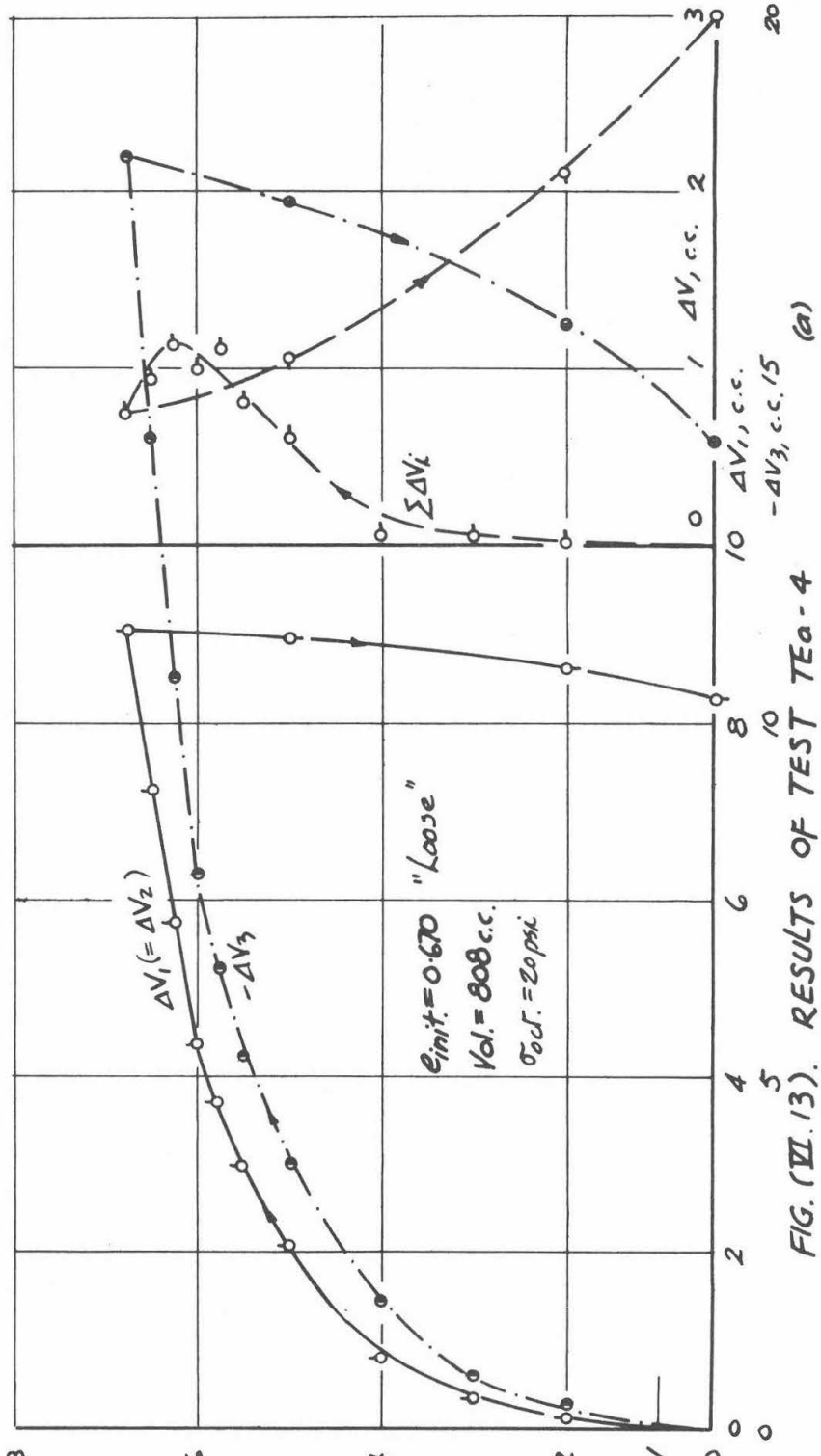

FIG. (VI. 13). RESULTS OF TEST TEa - 4

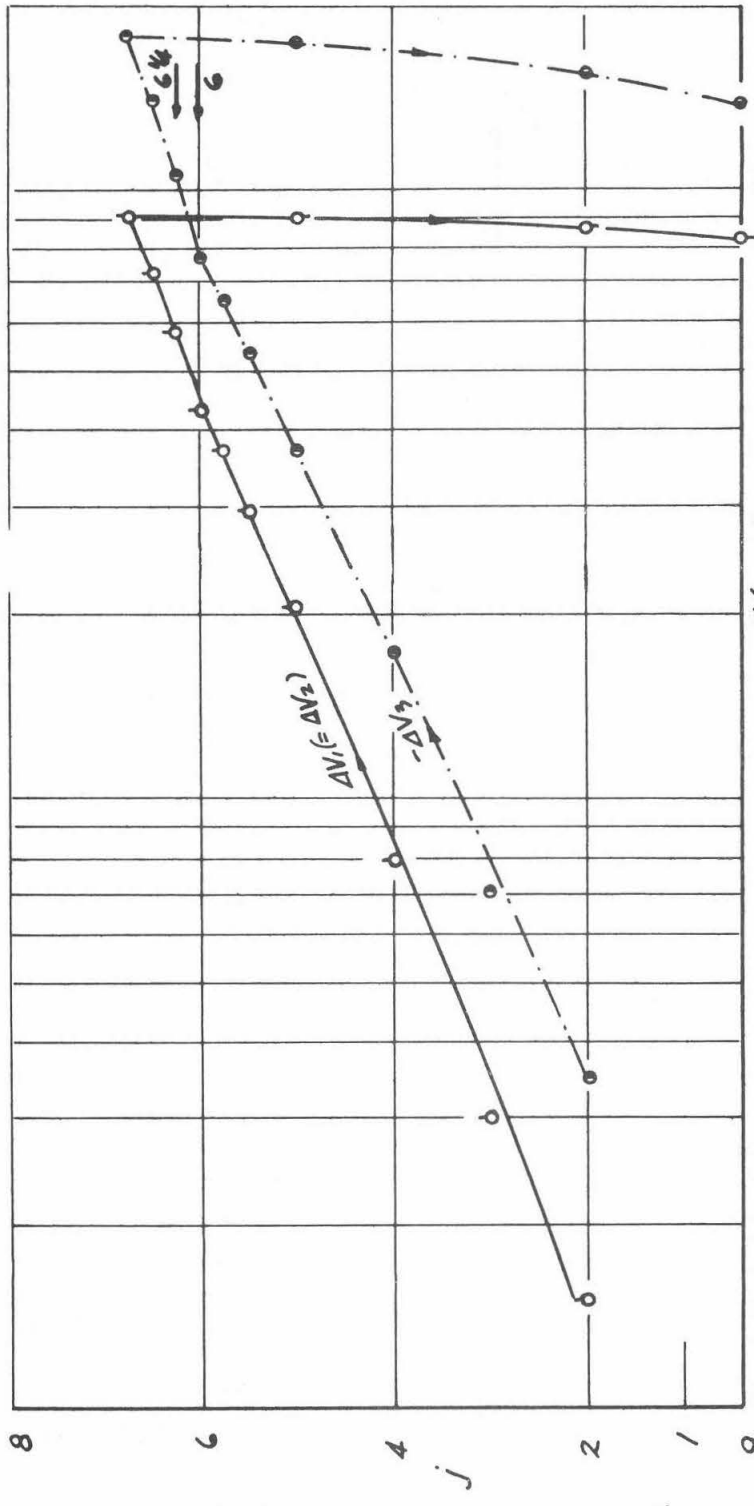

FIG. (XI. 13). (b).

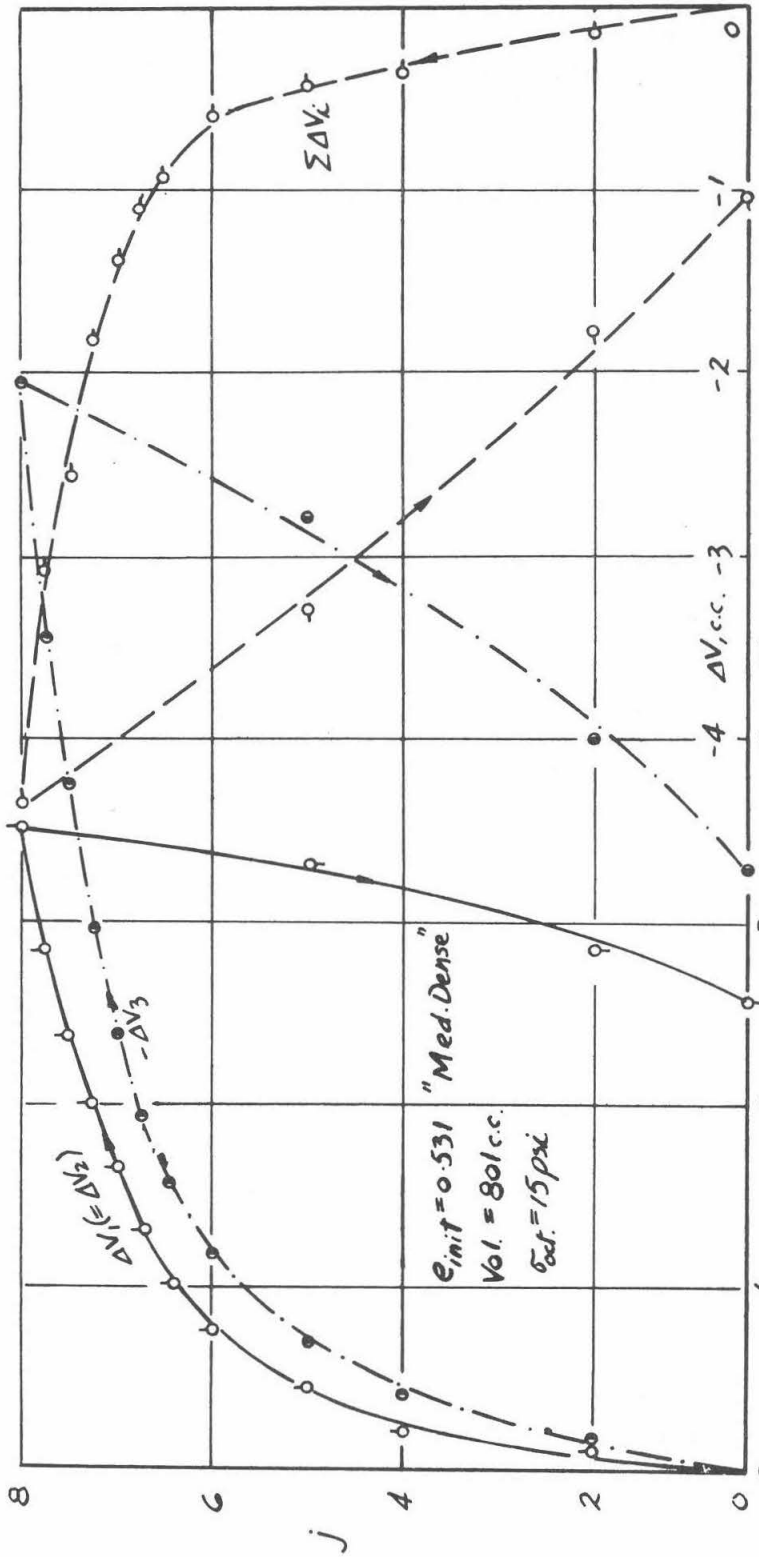

FIG. (VI.14). RESULTS OF TEST TEa-5 (a)

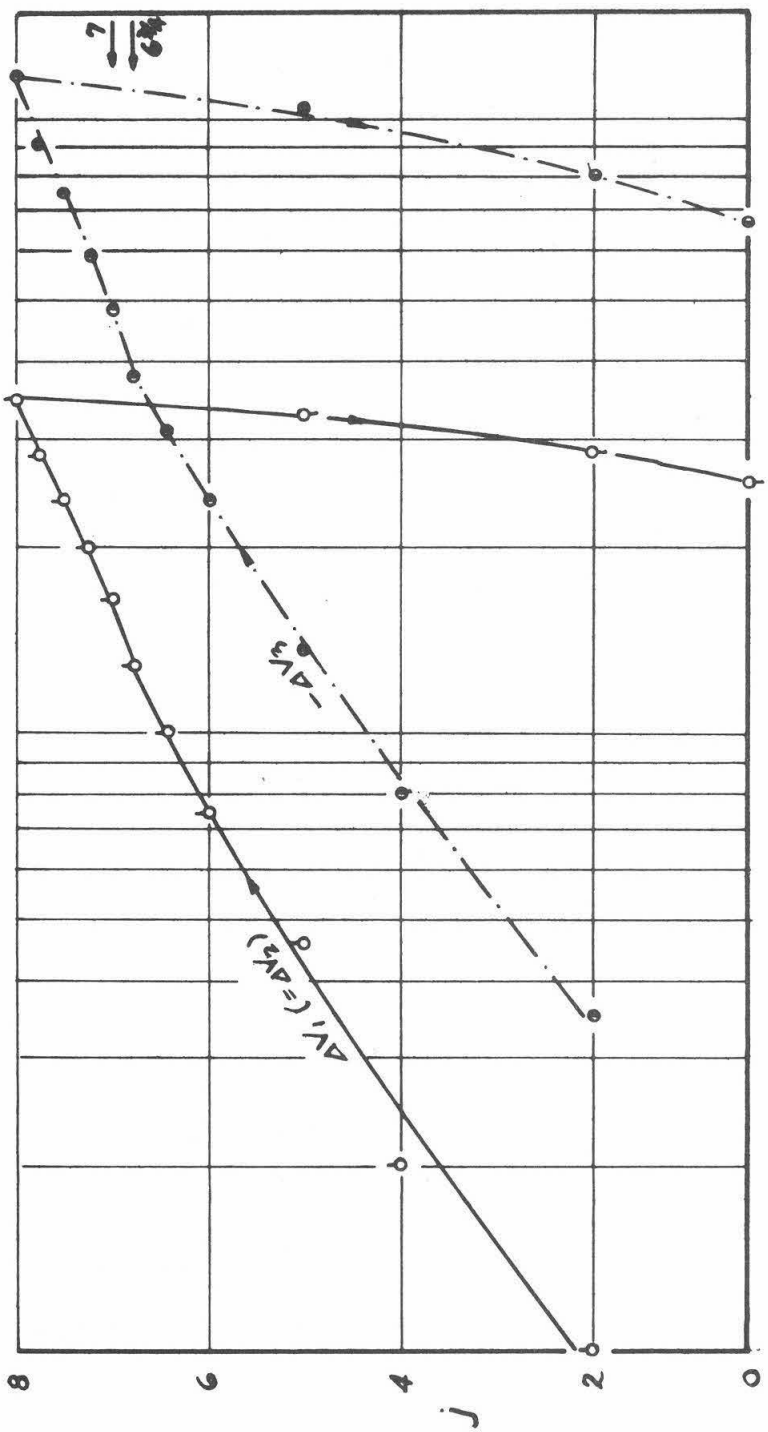

FIG. (VI. 14). (b)

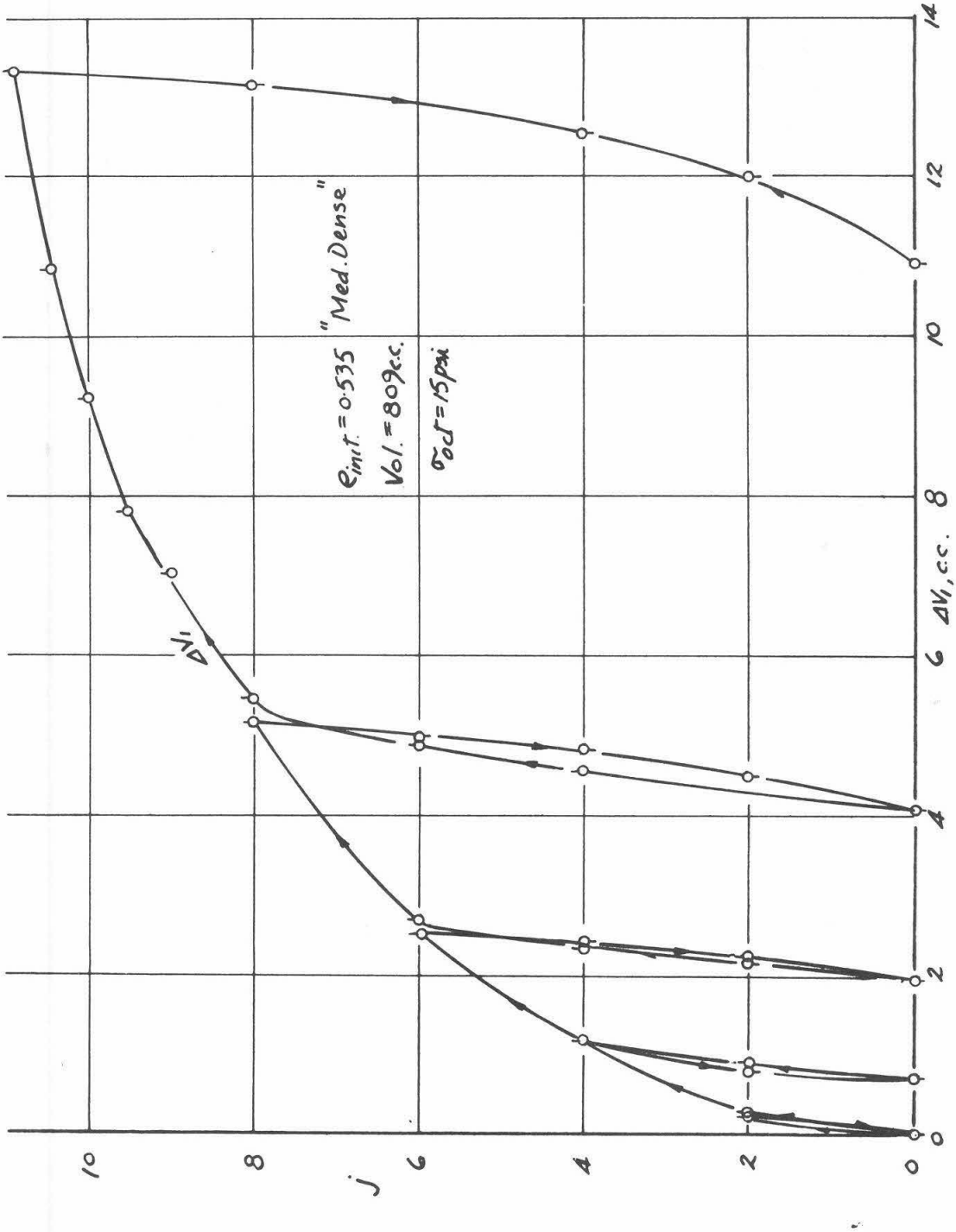

FIG. (VI.15). RESULTS OF TEST TC6-1 (a)

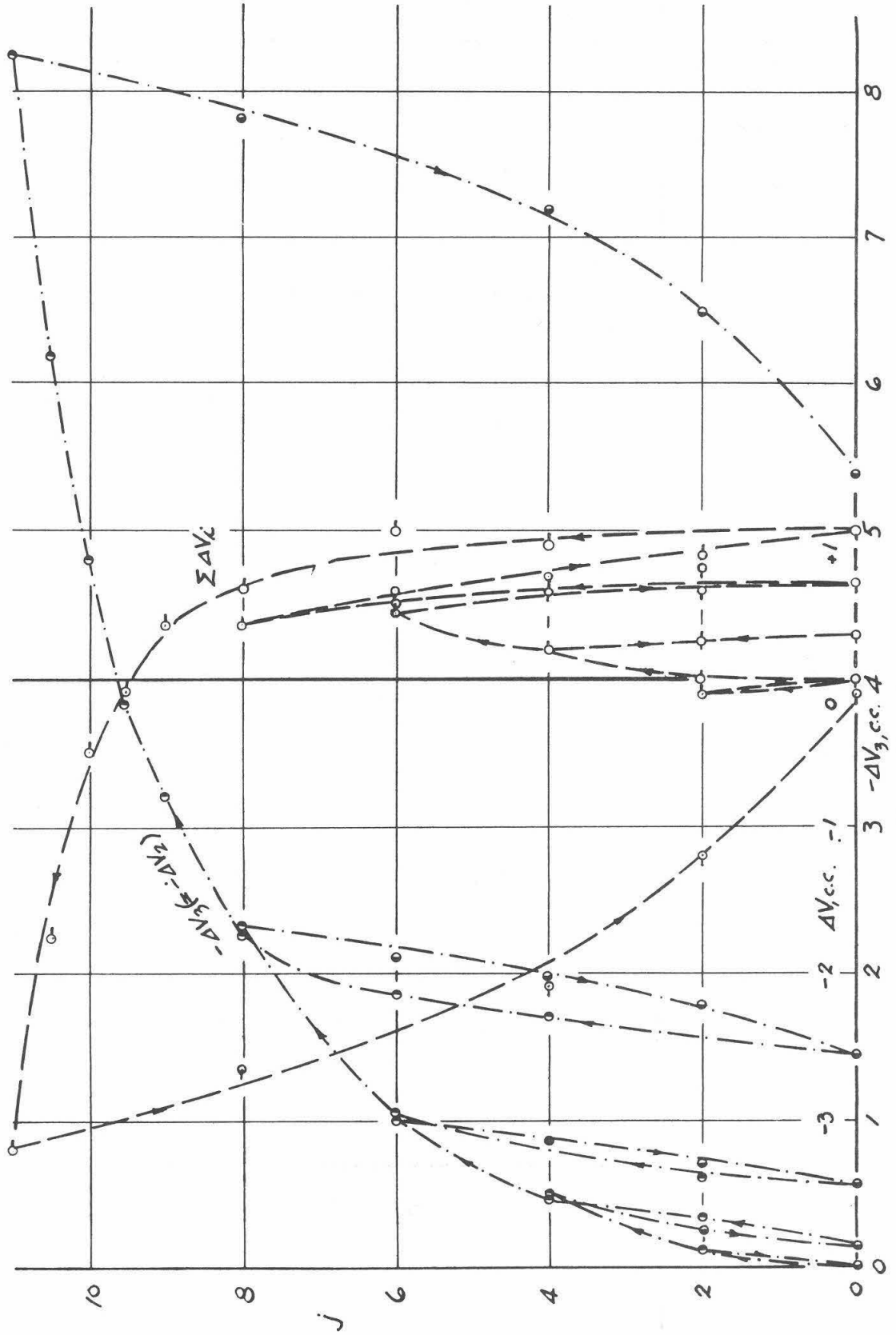
j
10
8
6
4
2
0
$\Sigma\Delta V_c$
$-\Delta V_3(\neq -\Delta V_2)$
$\Delta V_{c.c.}$
+1
0
-1
-2
-3
$-\Delta V_{3,c.c.}$
0
1
2
3
4
5
6
7
8

FIG. (VII.15). (b)

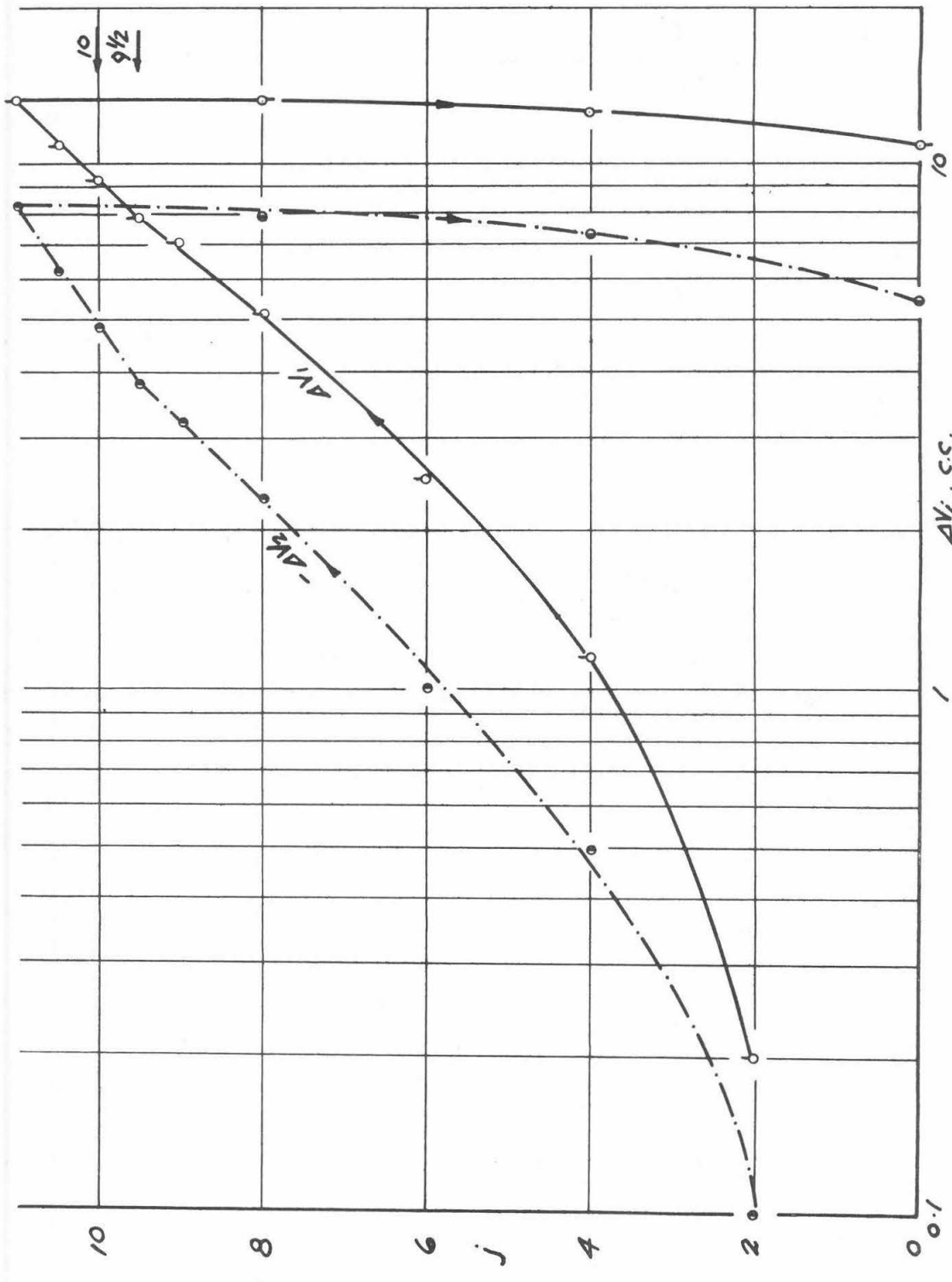

FIG. (III. 15). (c)

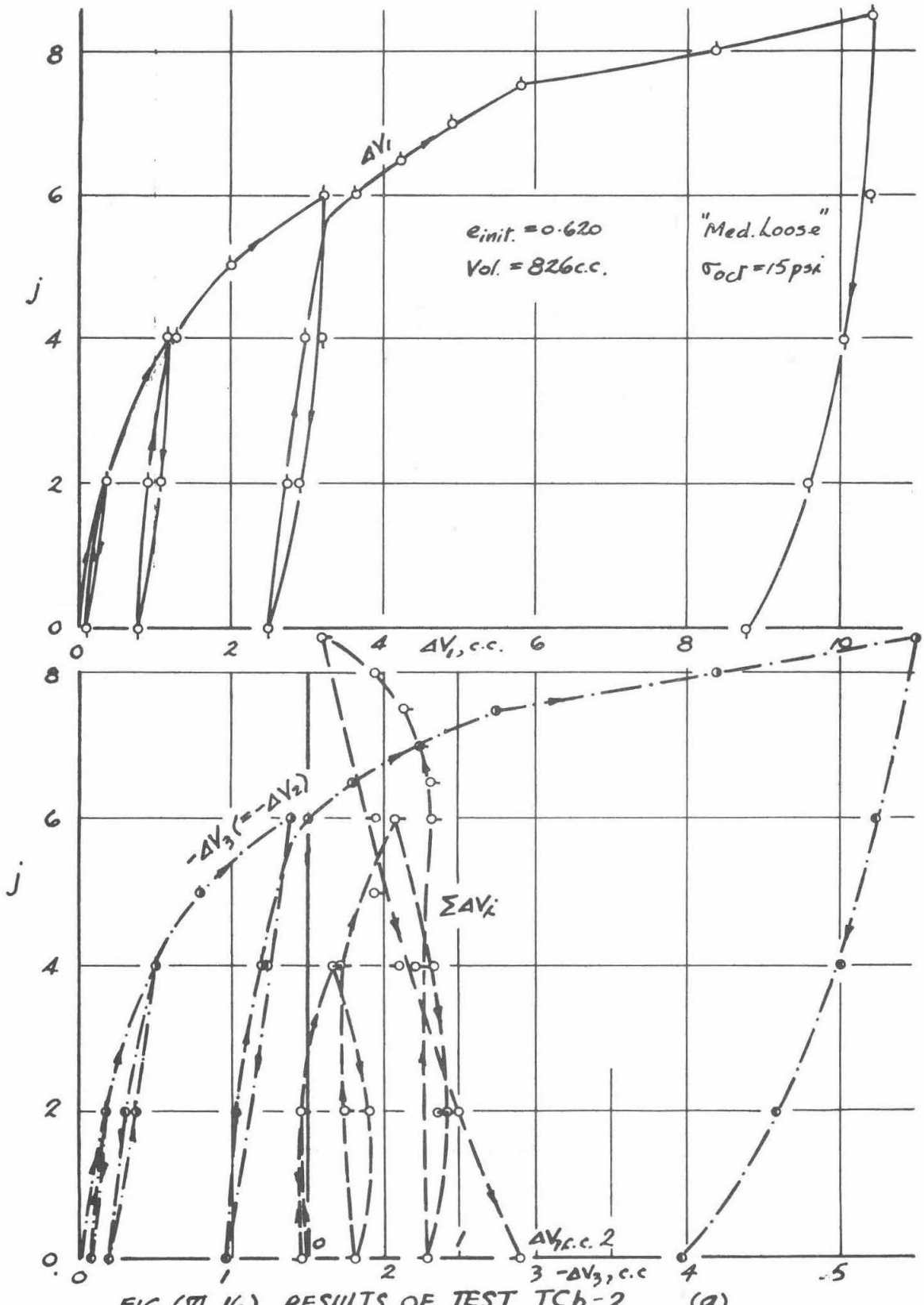

FIG. (VI. 16). RESULTS OF TEST TCb-2 (a)

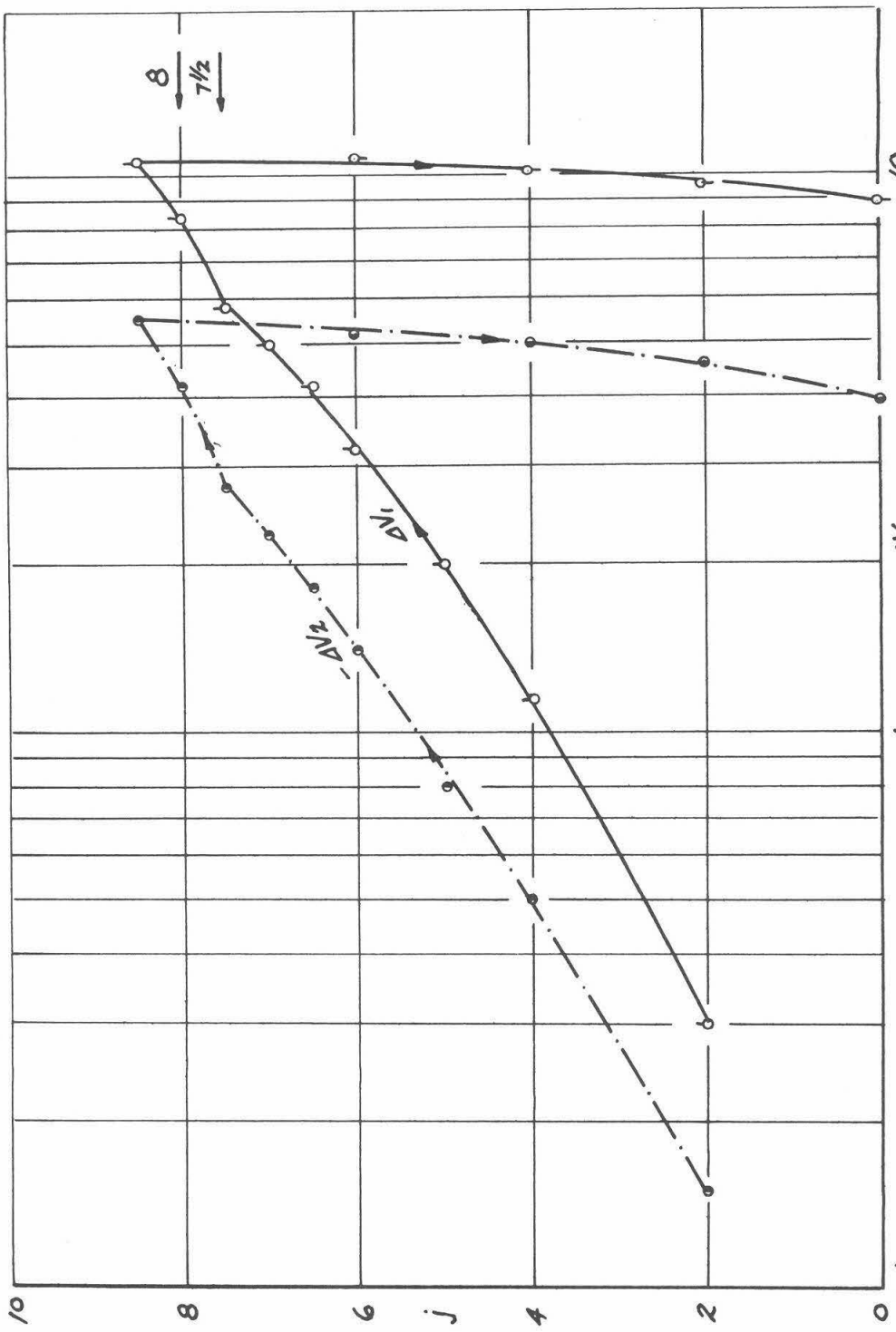

FIG. (VII. 16). (b)

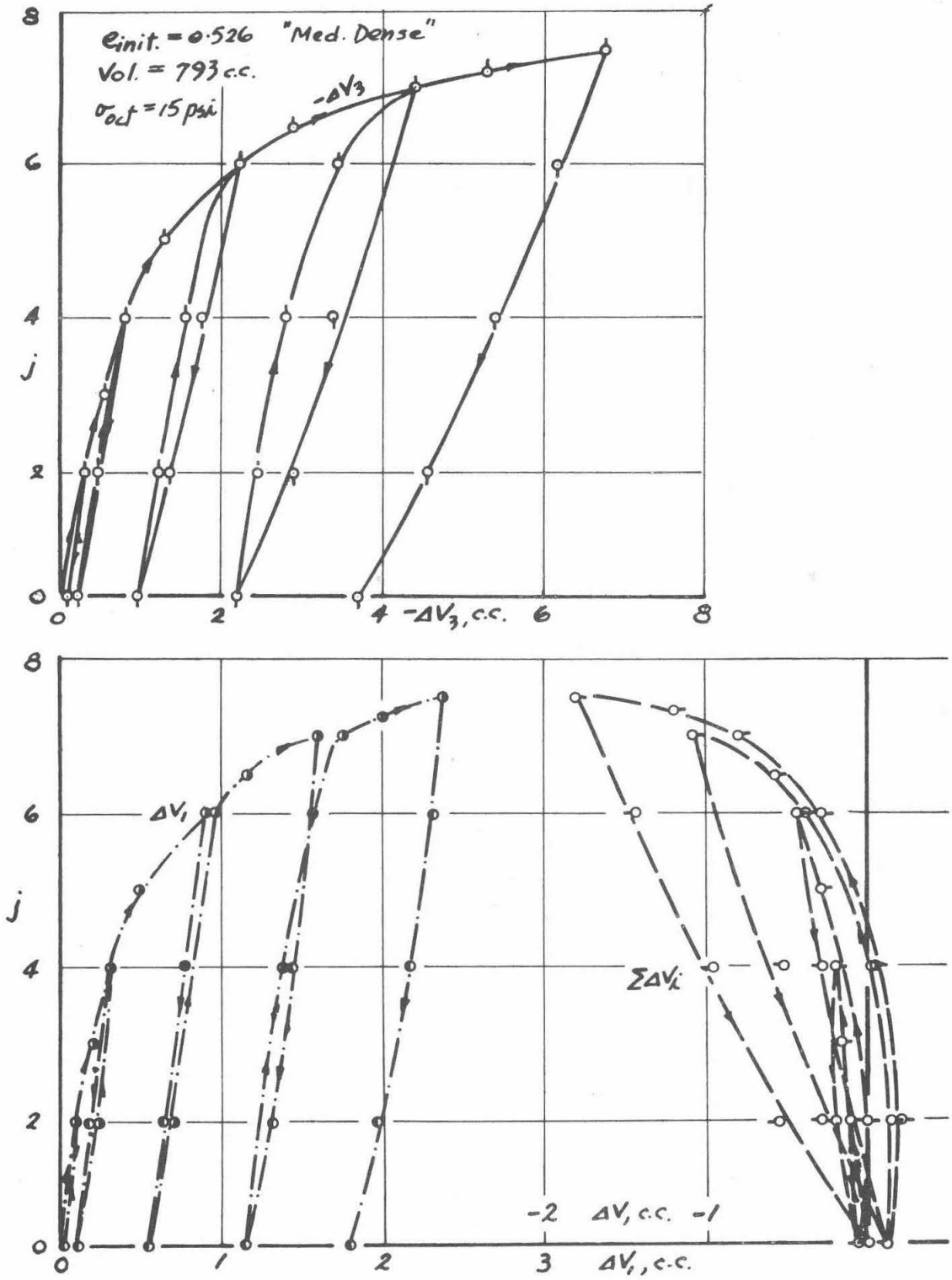

FIG. (VI.17). RESULTS OF TEST TEb-1 (a)

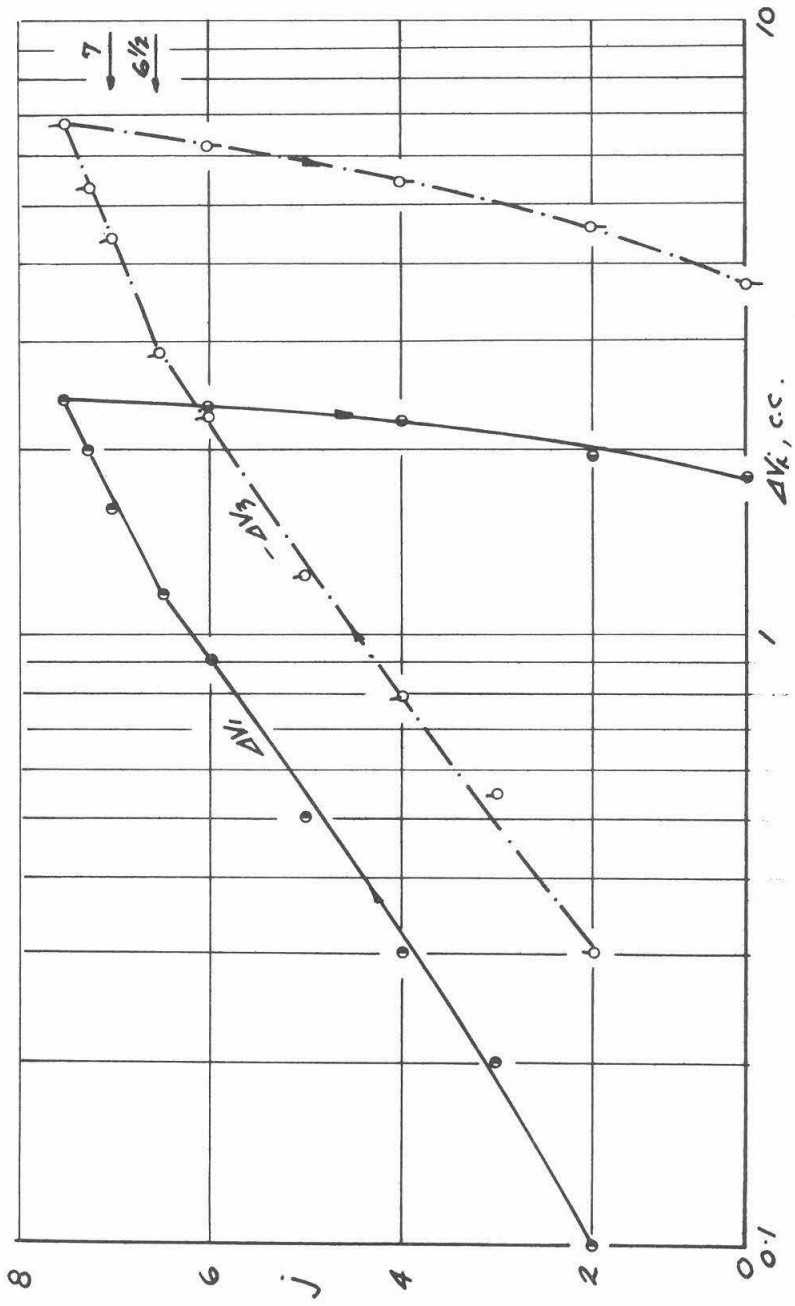

FIG. (XII.17). (b)

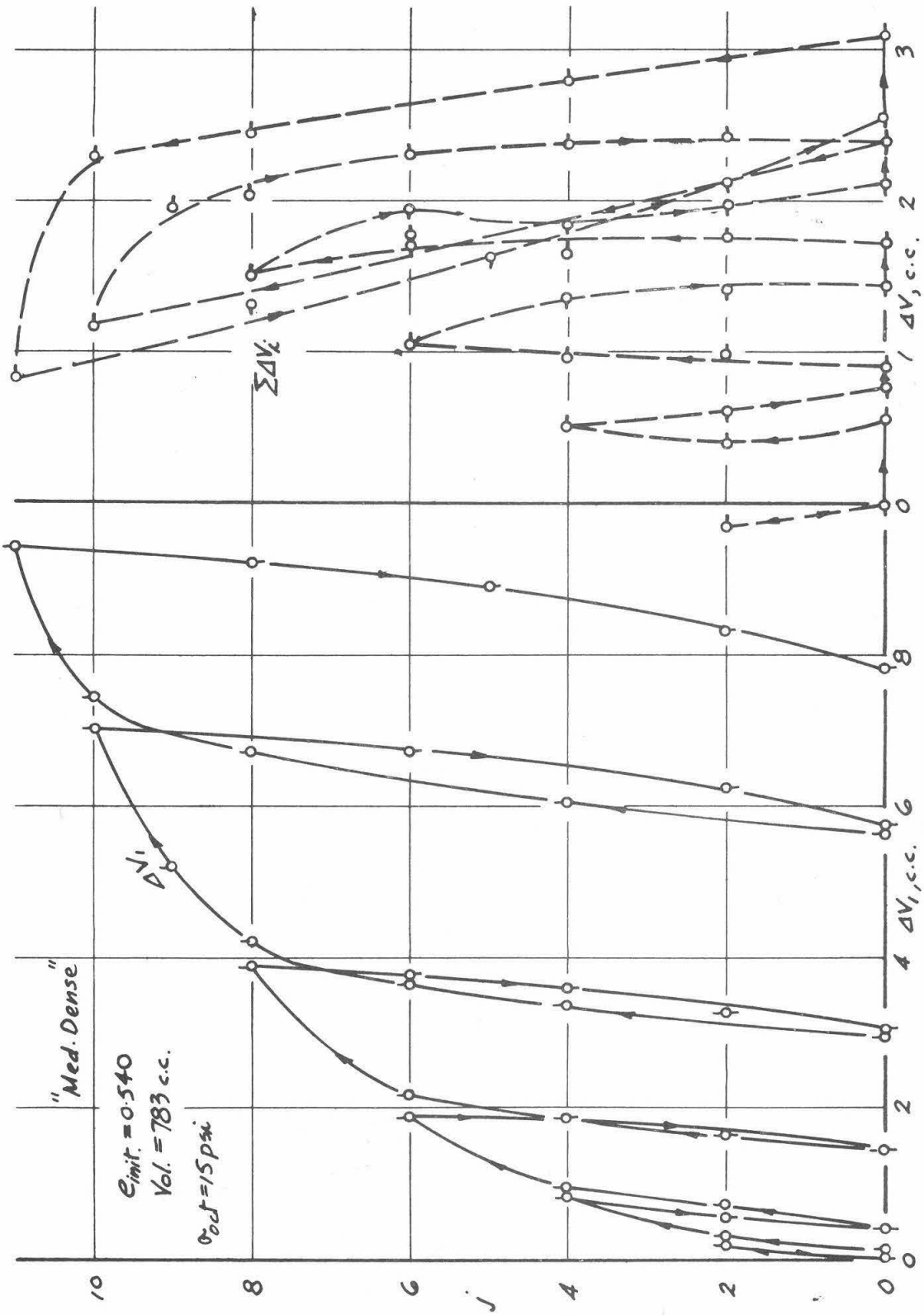

FIG. (III. 18). RESULTS OF TEST TCc - 1. (a).

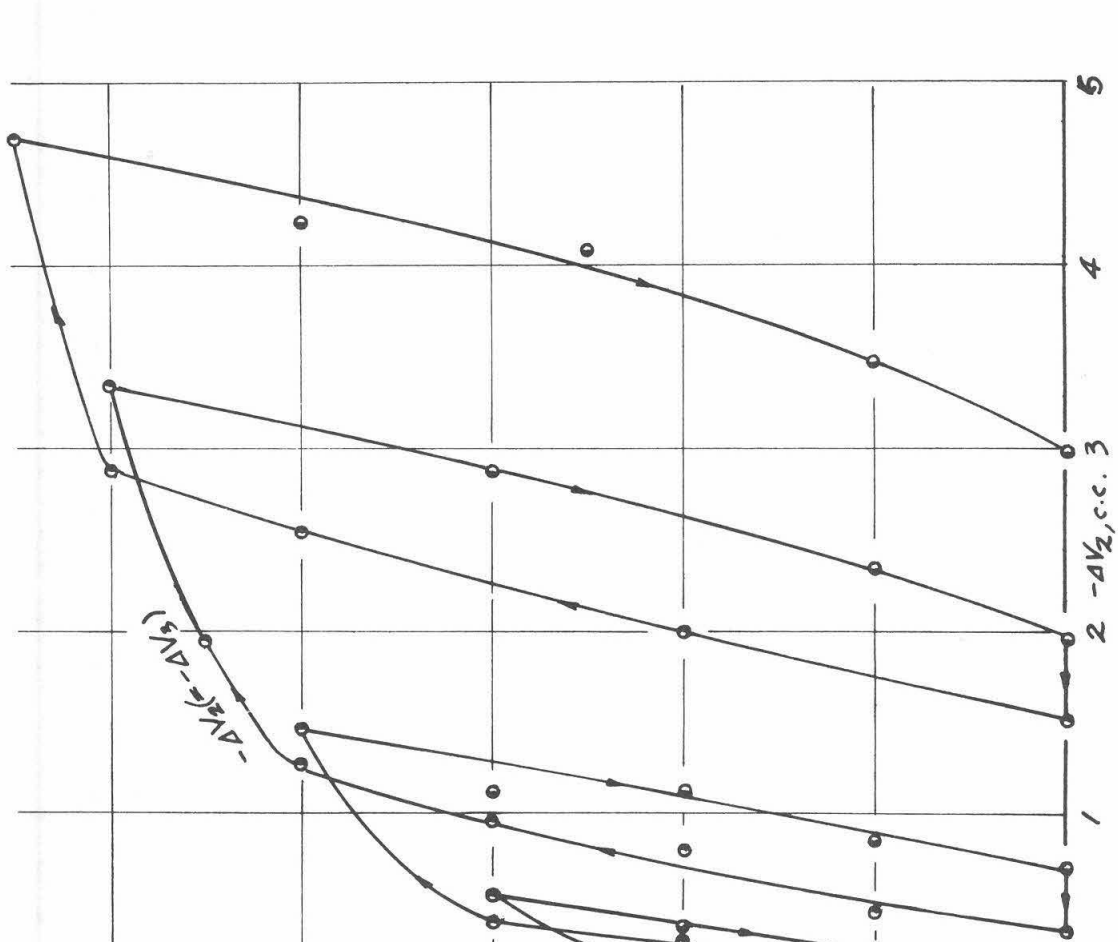

FIG. (VII. 18.) (b)

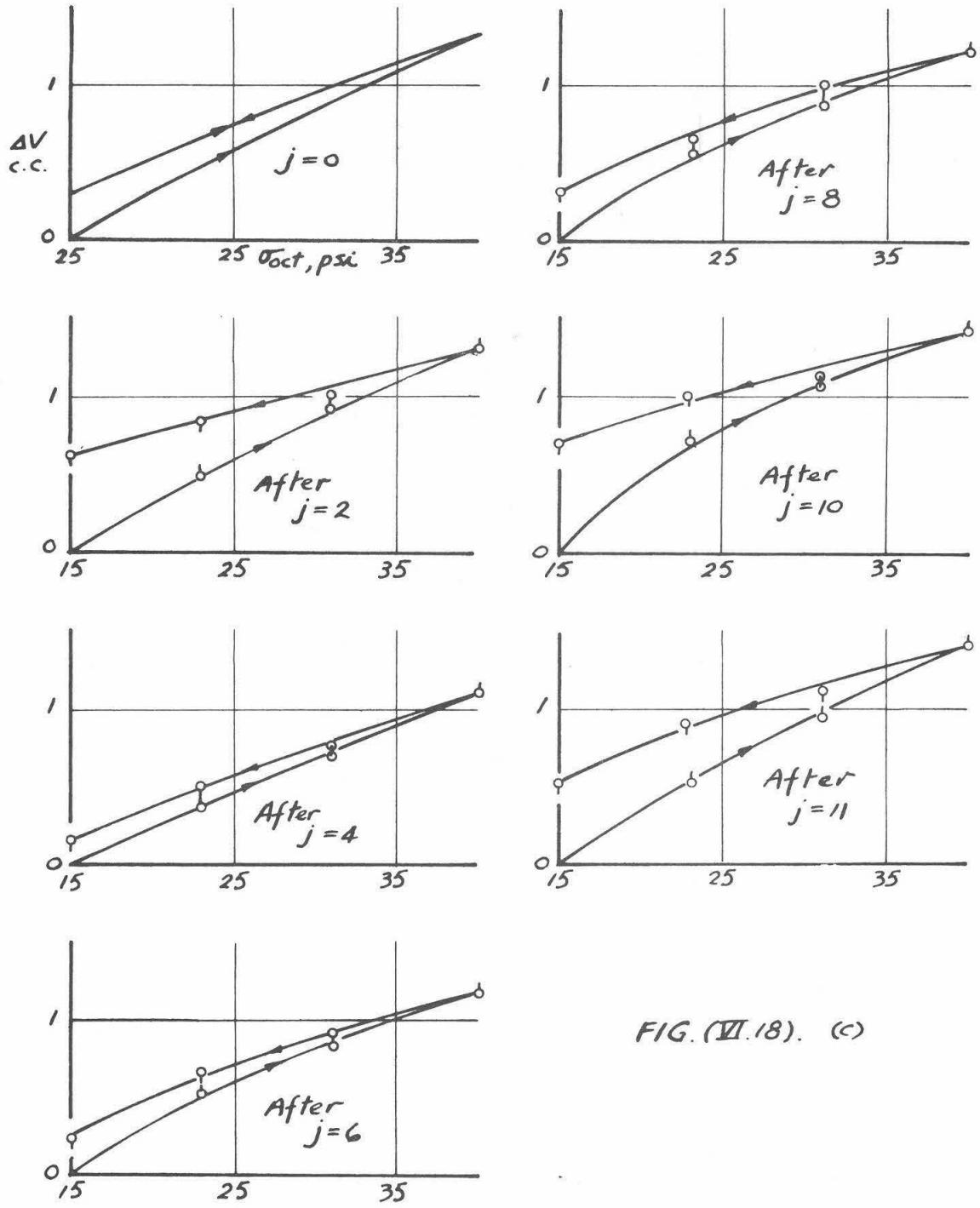
ΔV
c.c.
1
0
25
25
σoct, psi
35
j = 0
After
j = 8
15
After
j = 2
After
j = 10
After
j = 4
After
j = 11
After
j = 6

FIG. (VI.18). (c)

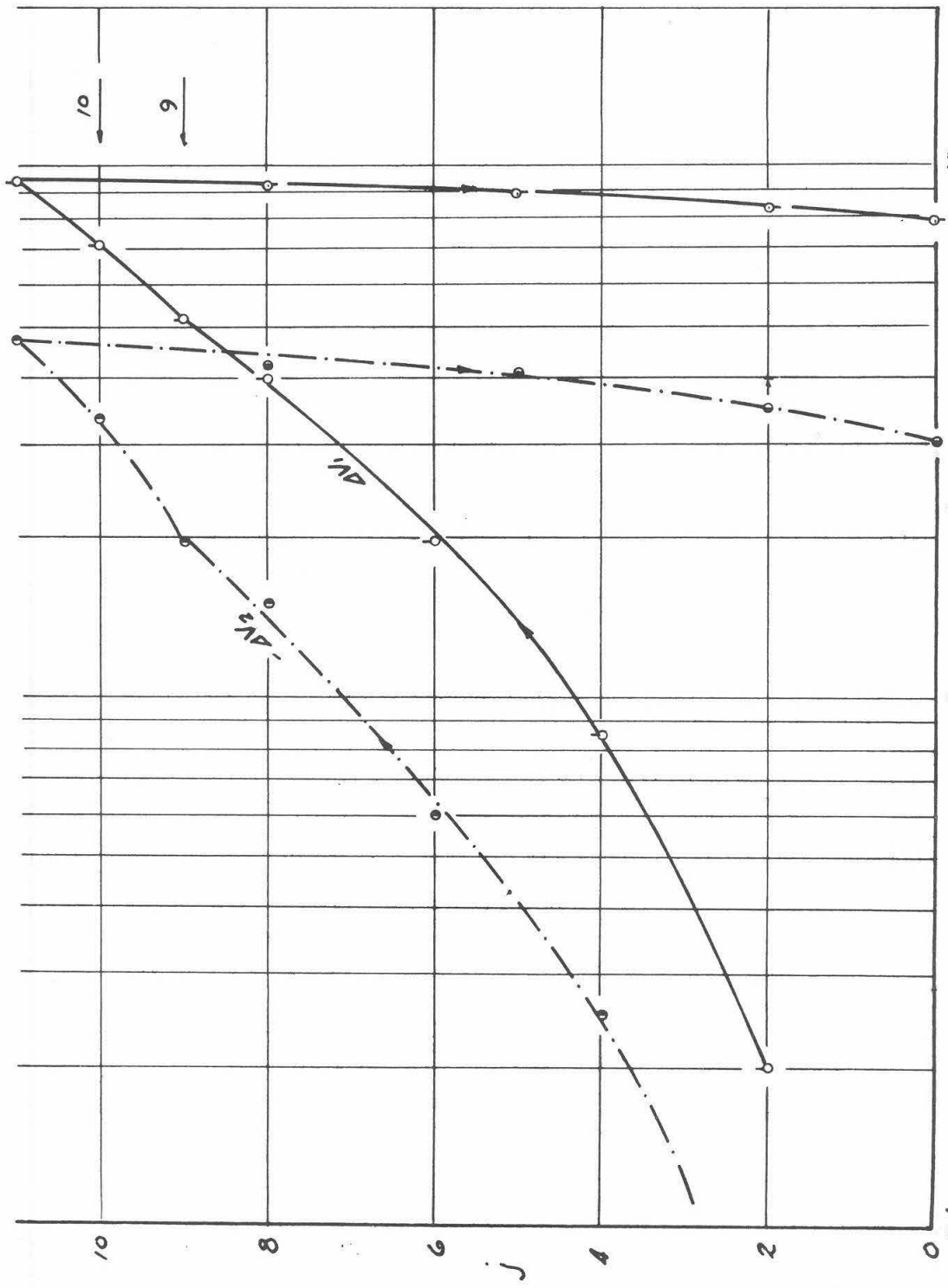

FIG. (XII. 18). (d)

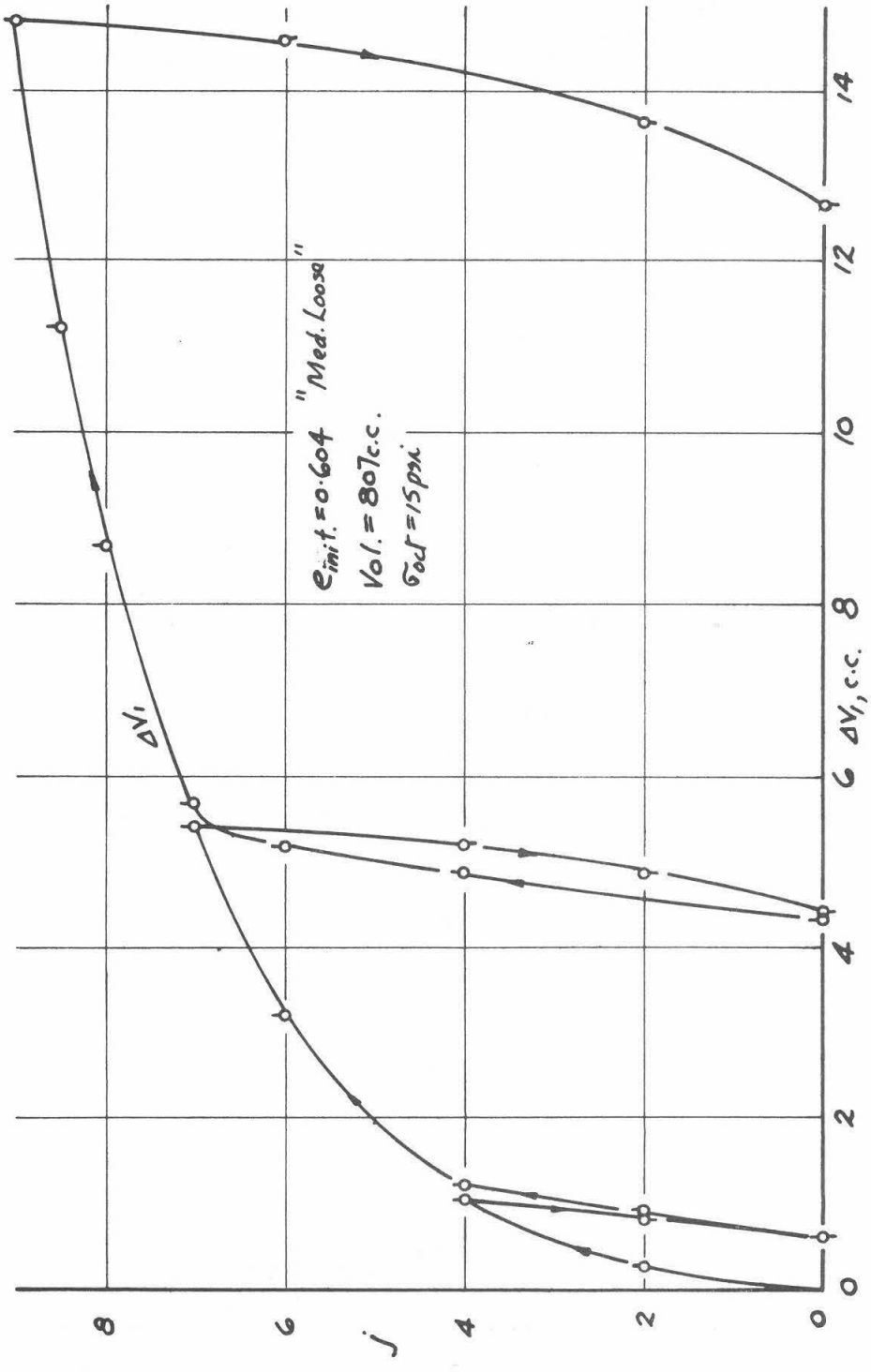

FIG. (VI.19). RESULTS OF TEST TCc-2. (a)

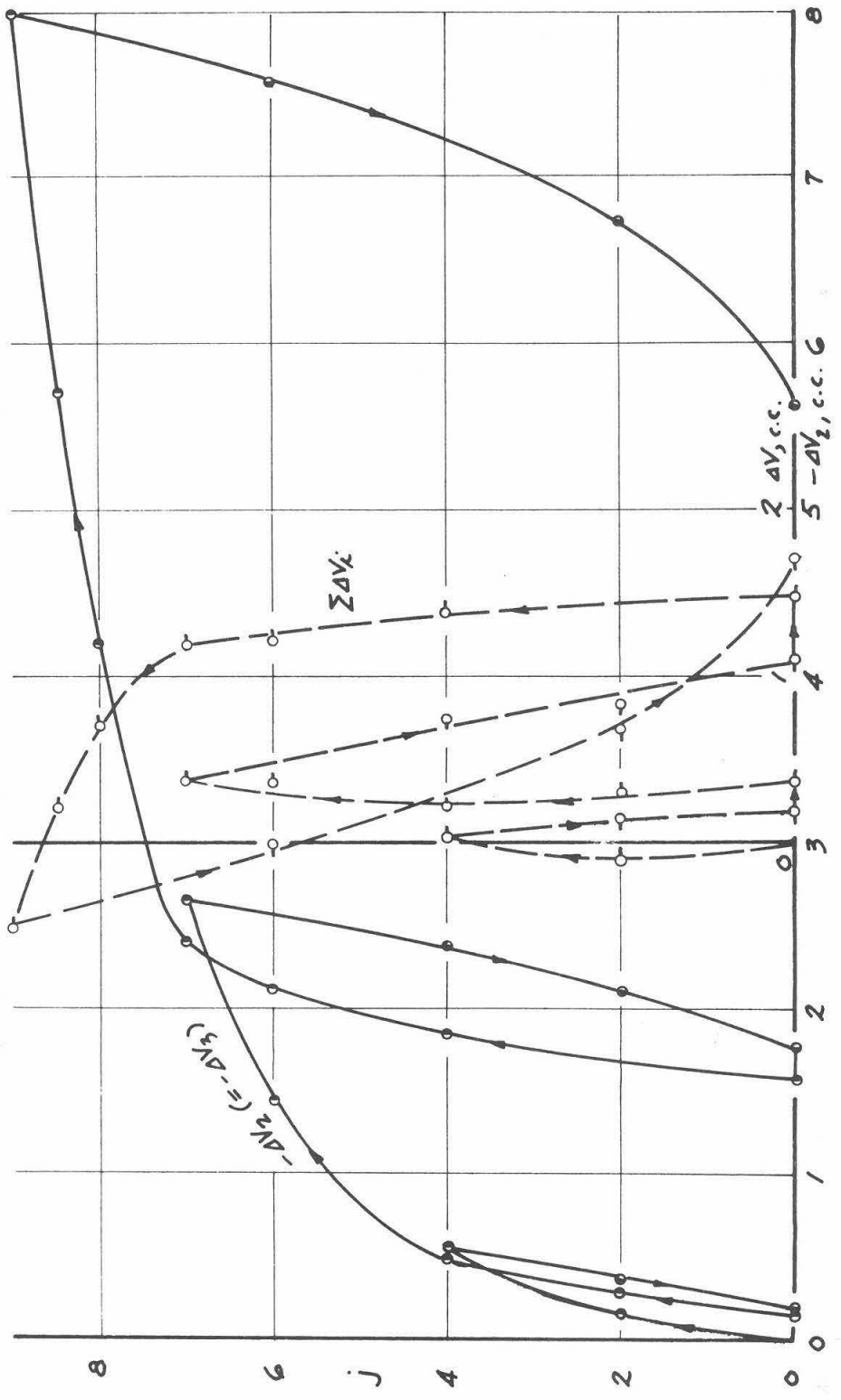
$\Sigma \Delta V_i$
$-\Delta V_2$ (= $-\Delta V_3$)
$2\ \Delta V_3$, c.c.
$5\ -\Delta V_2$, c.c.
j
0
2
4
6
8
0
1
2
3
4
5
6
7
8

FIG. (XI.19). (b)

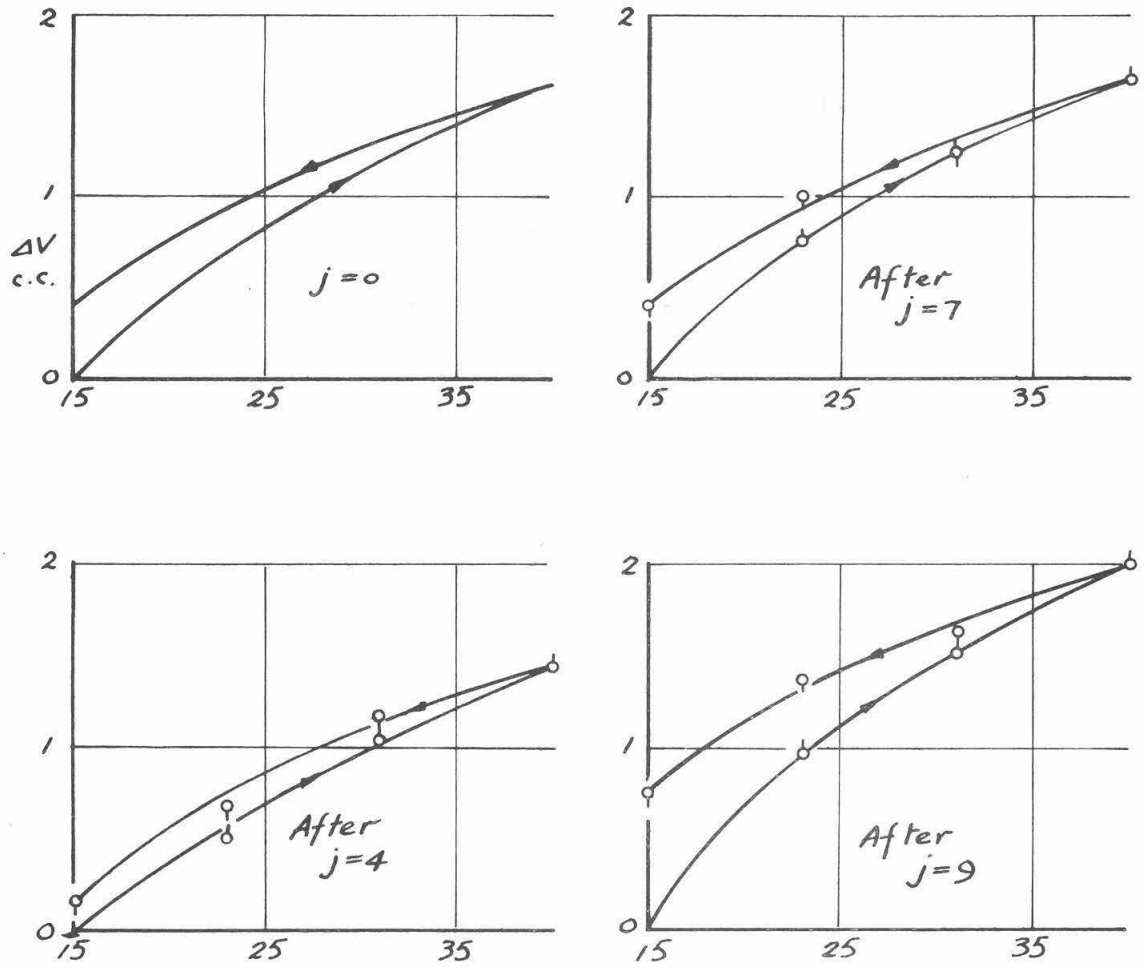

FIG. (VI. 19). (c)

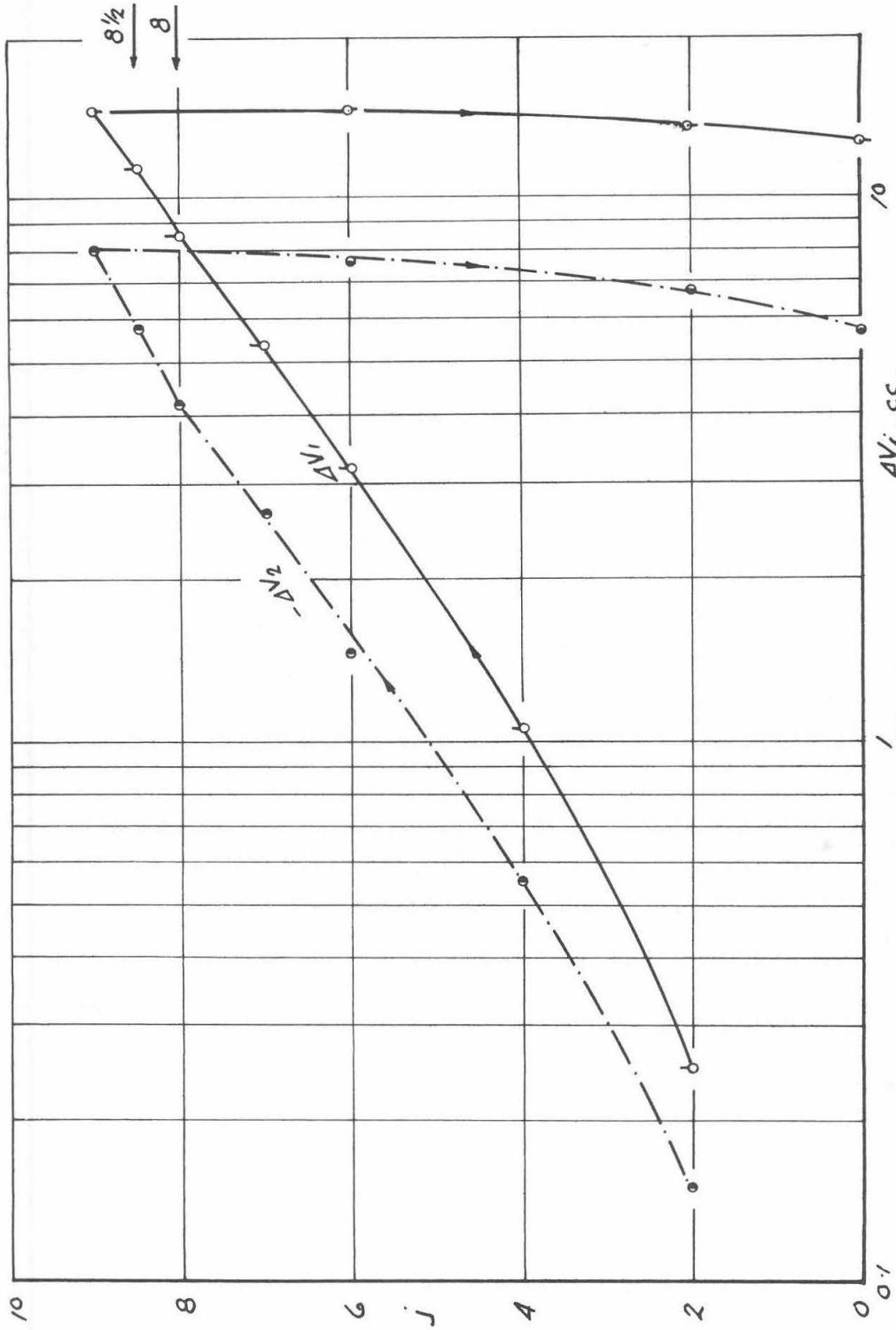

FIG. (III.19). (d)

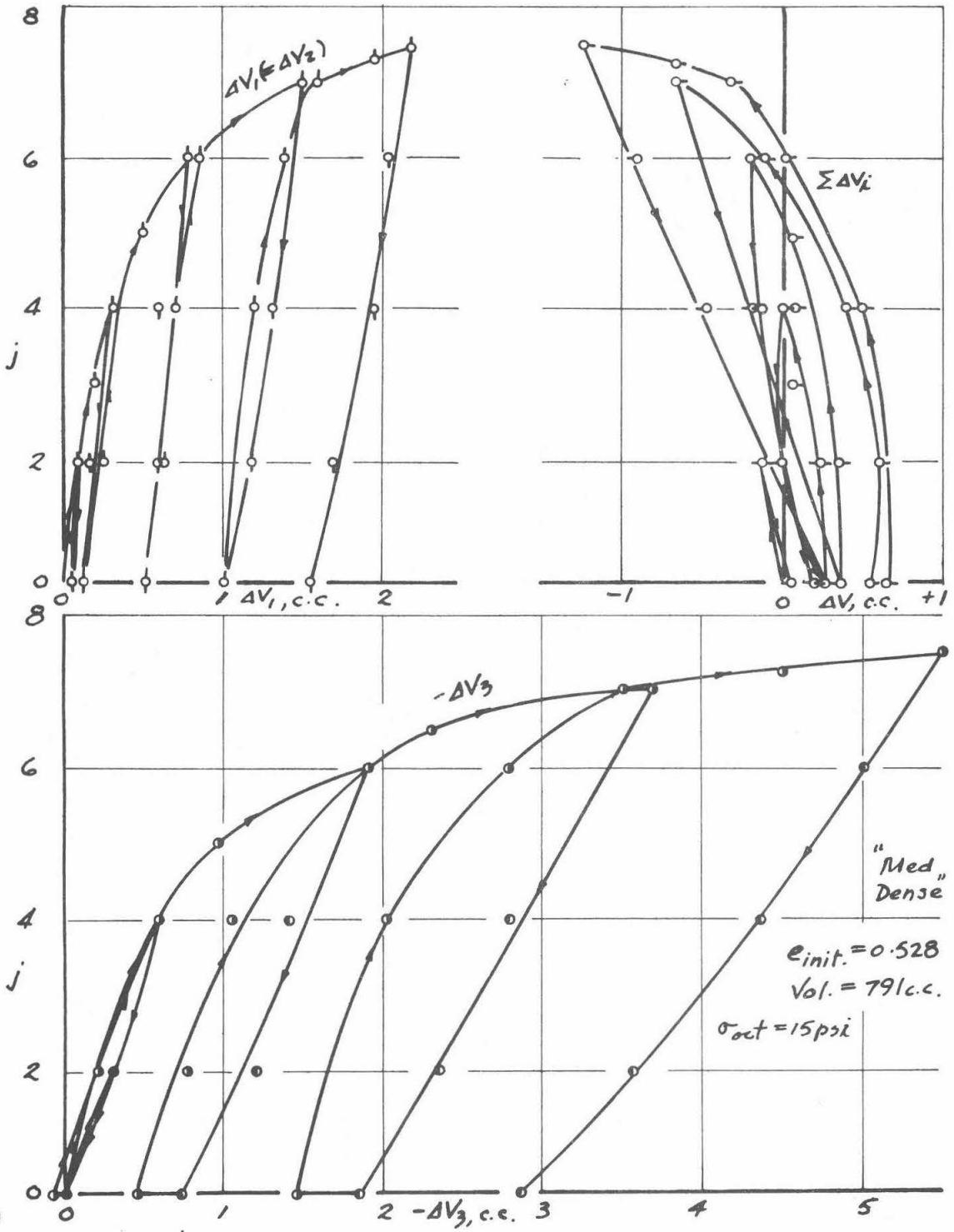

FIG. (VI.20). RESULTS OF TEST TEc-1 (a).

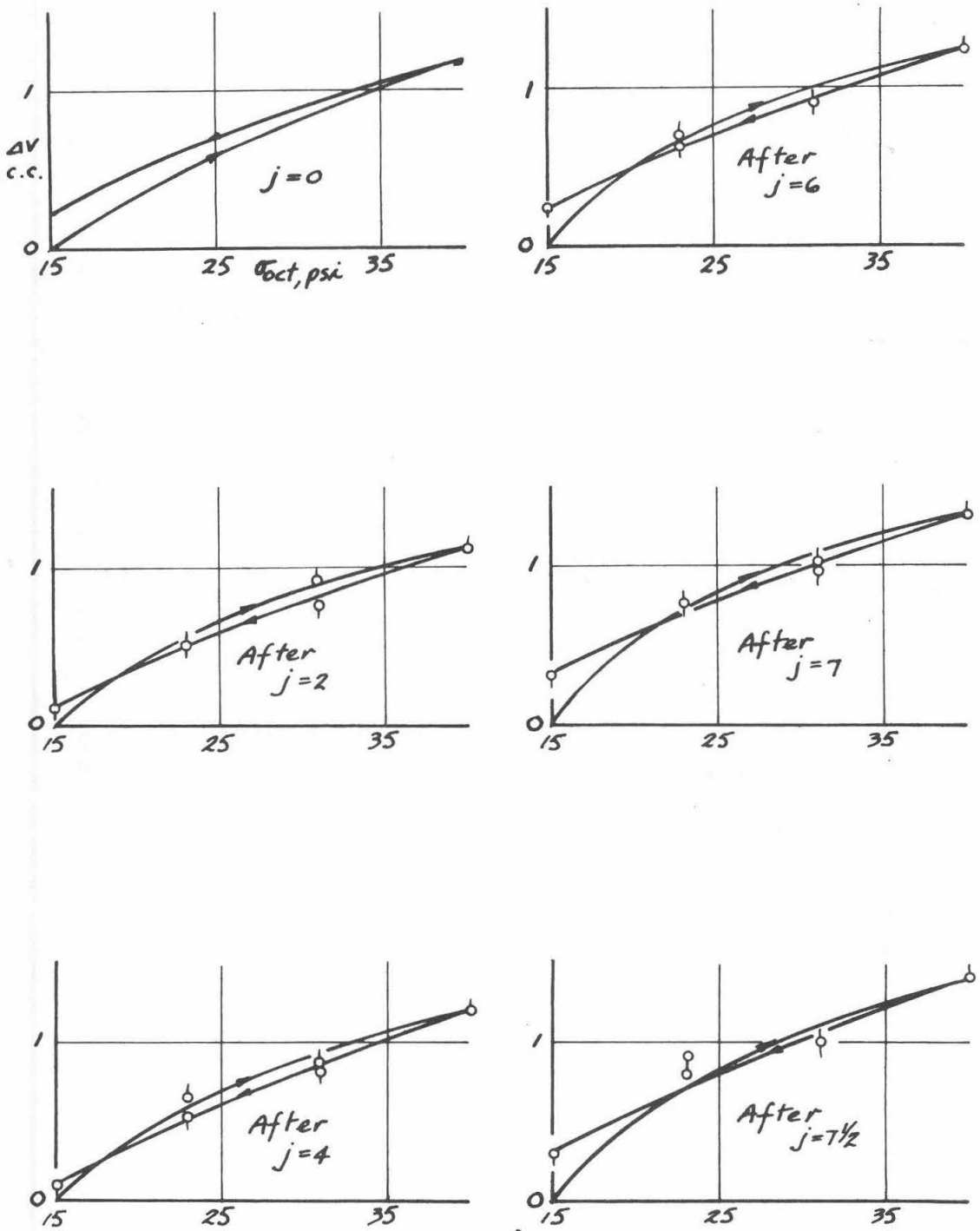
1
ΔV
c.c.
0
15
25
σoct, psi
35
j=0
After
j=6
After
j=2
After
j=7
After
j=4
After
j=7½

FIG. (VI.20). (b)

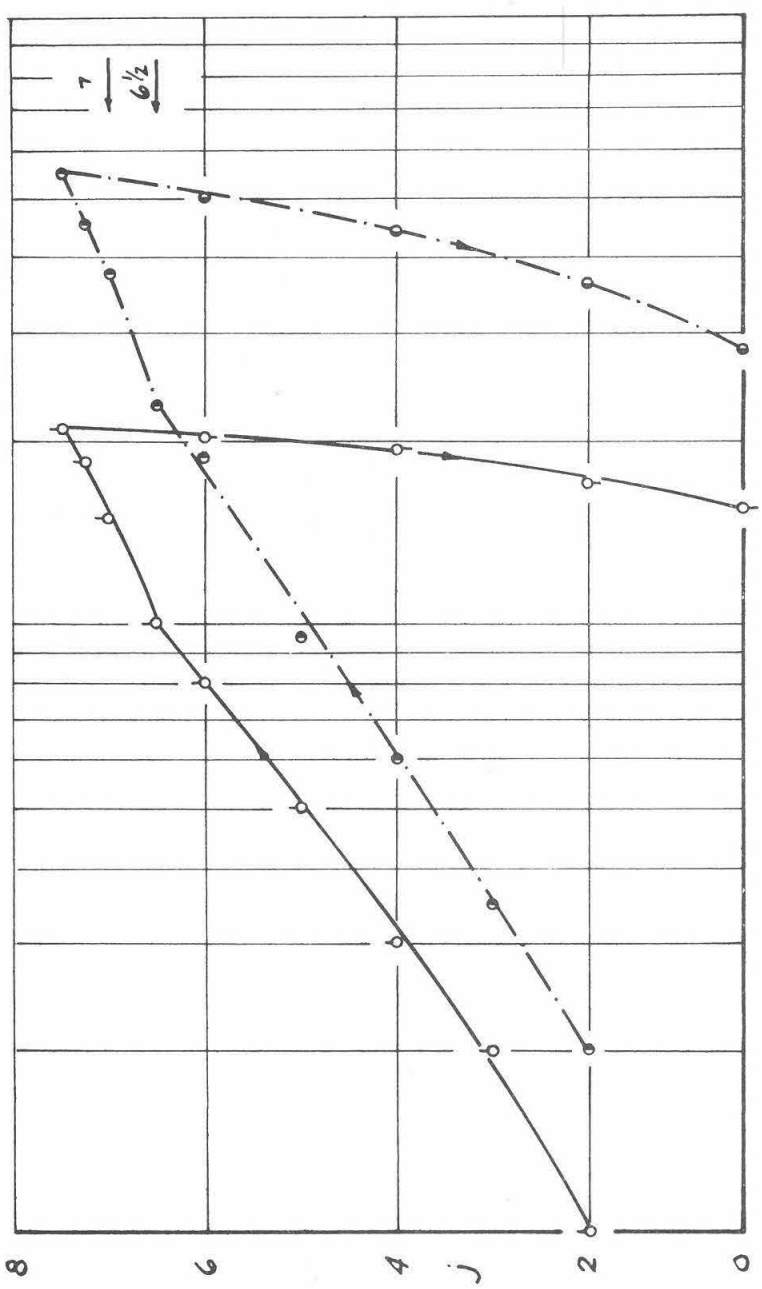

FIG. (VI. 20). (c)

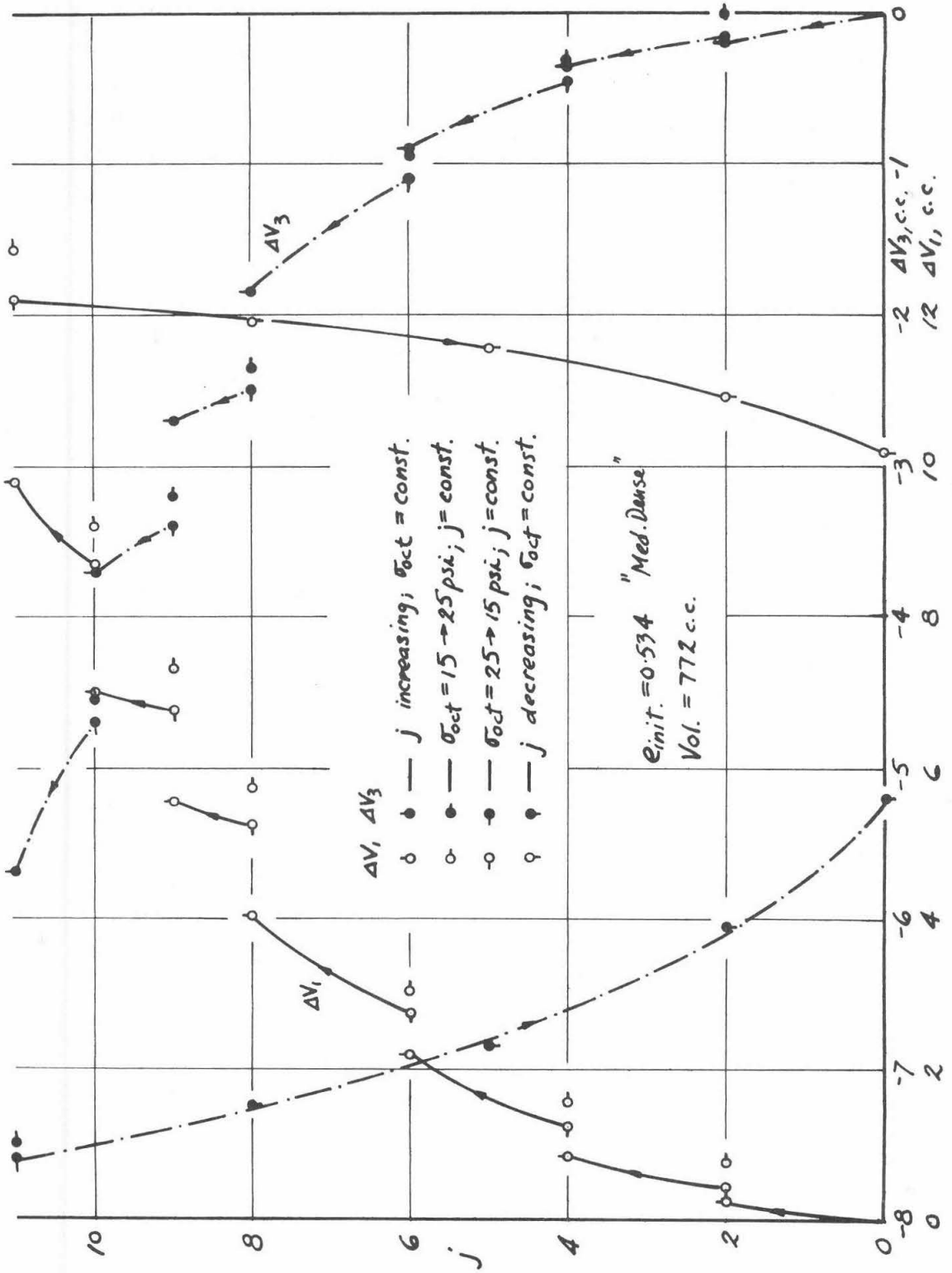

FIG. (VI. 21). RESULTS OF TEST TCd-1

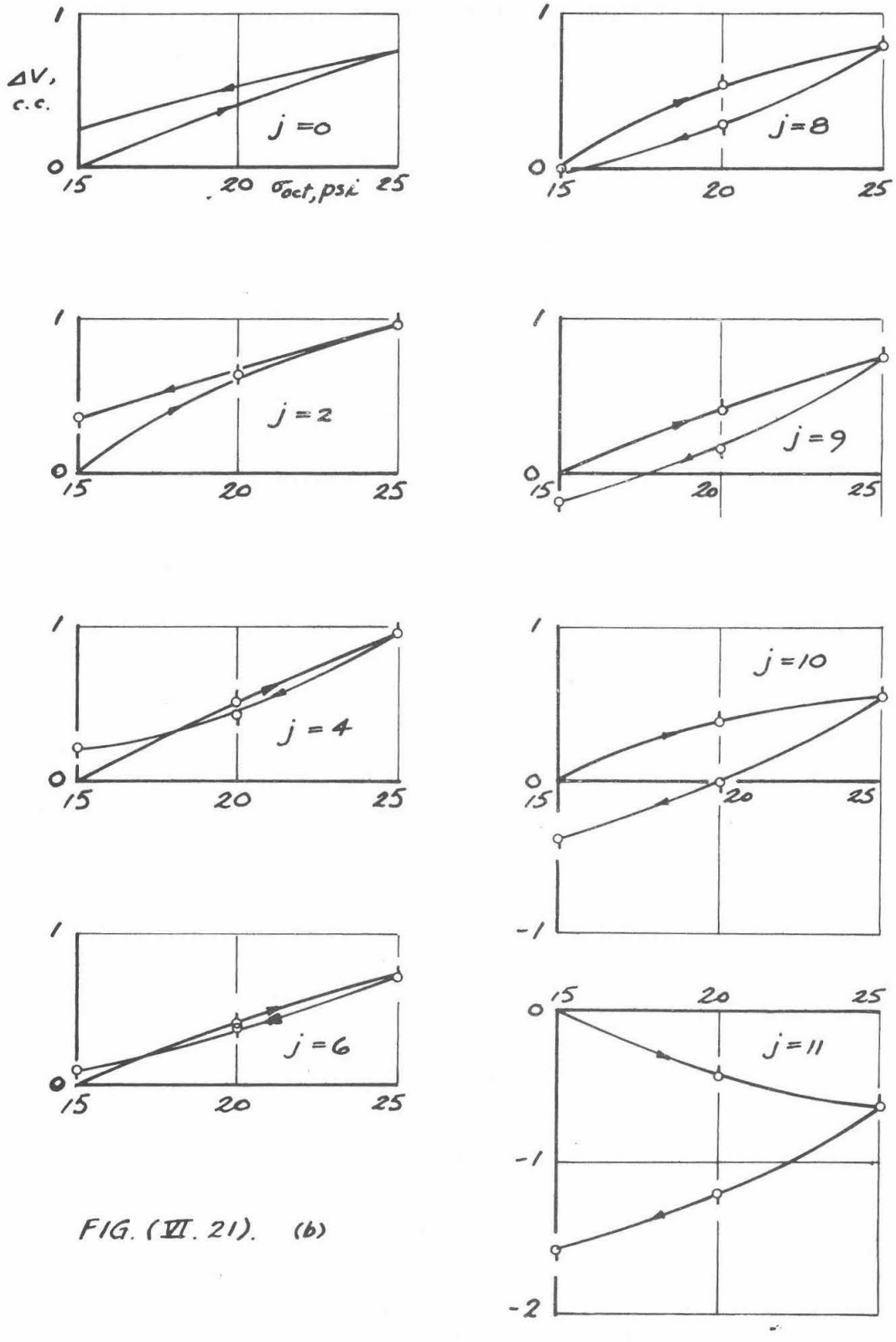

FIG. (VI. 21). (b)

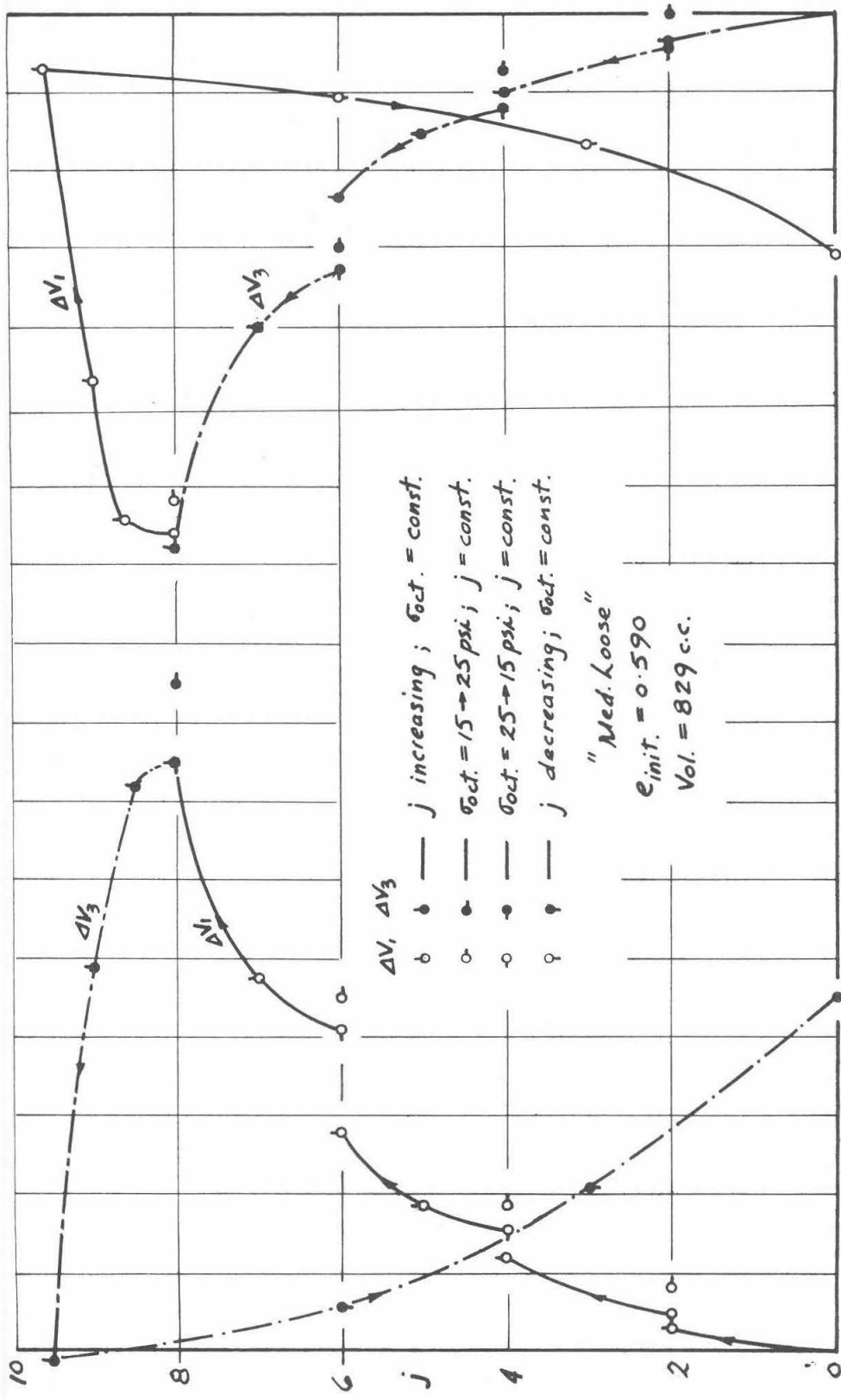

FIG. (VI. 22). RESULTS OF TEST TCd-2 (a)

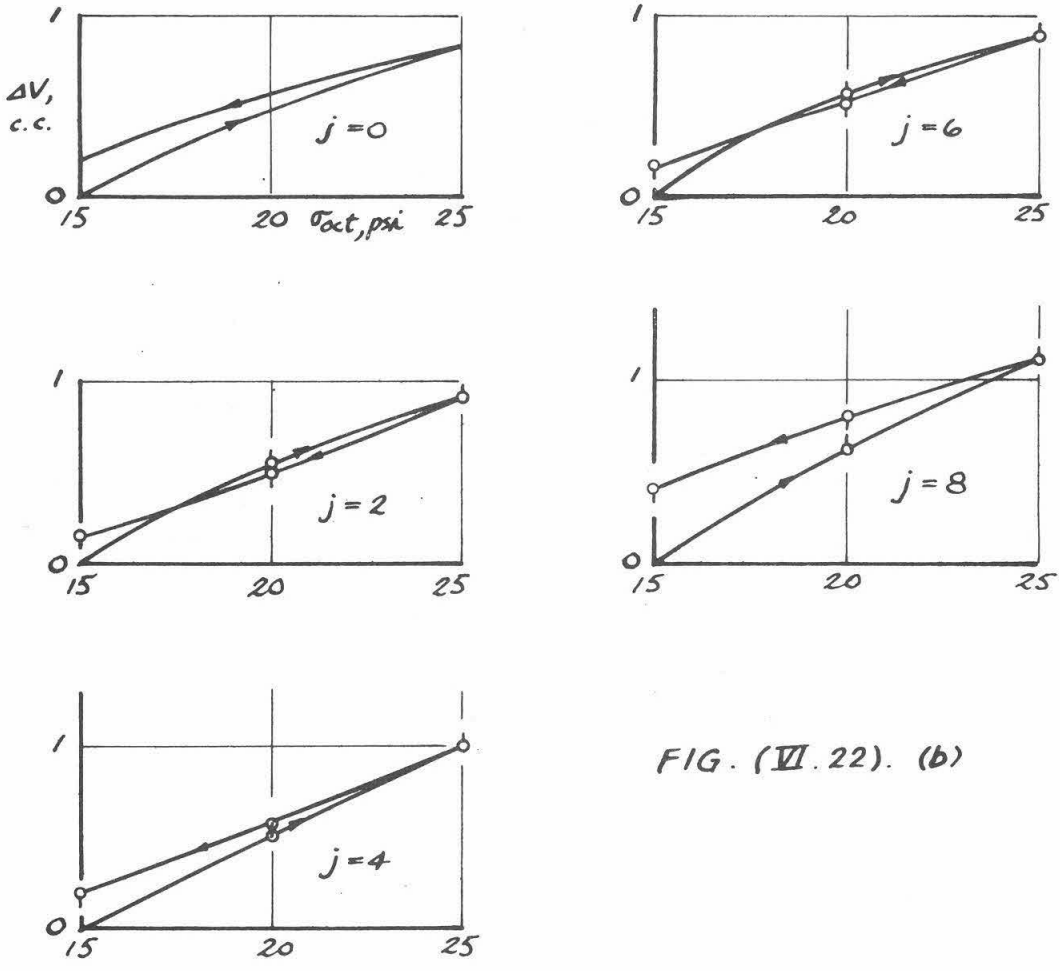

FIG. (VI.22). (b)

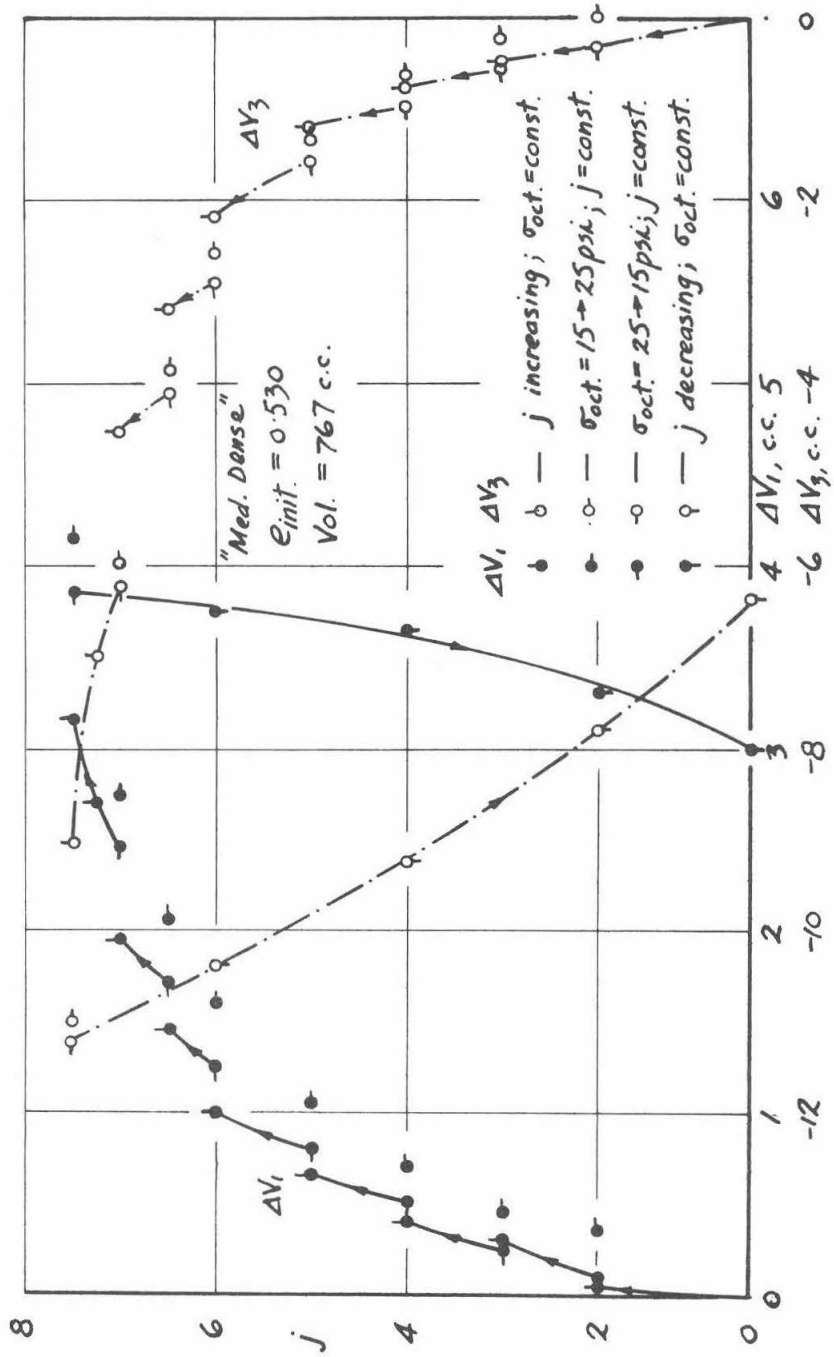

FIG. (VII.23). RESULTS OF TEST TEd-1 (a)

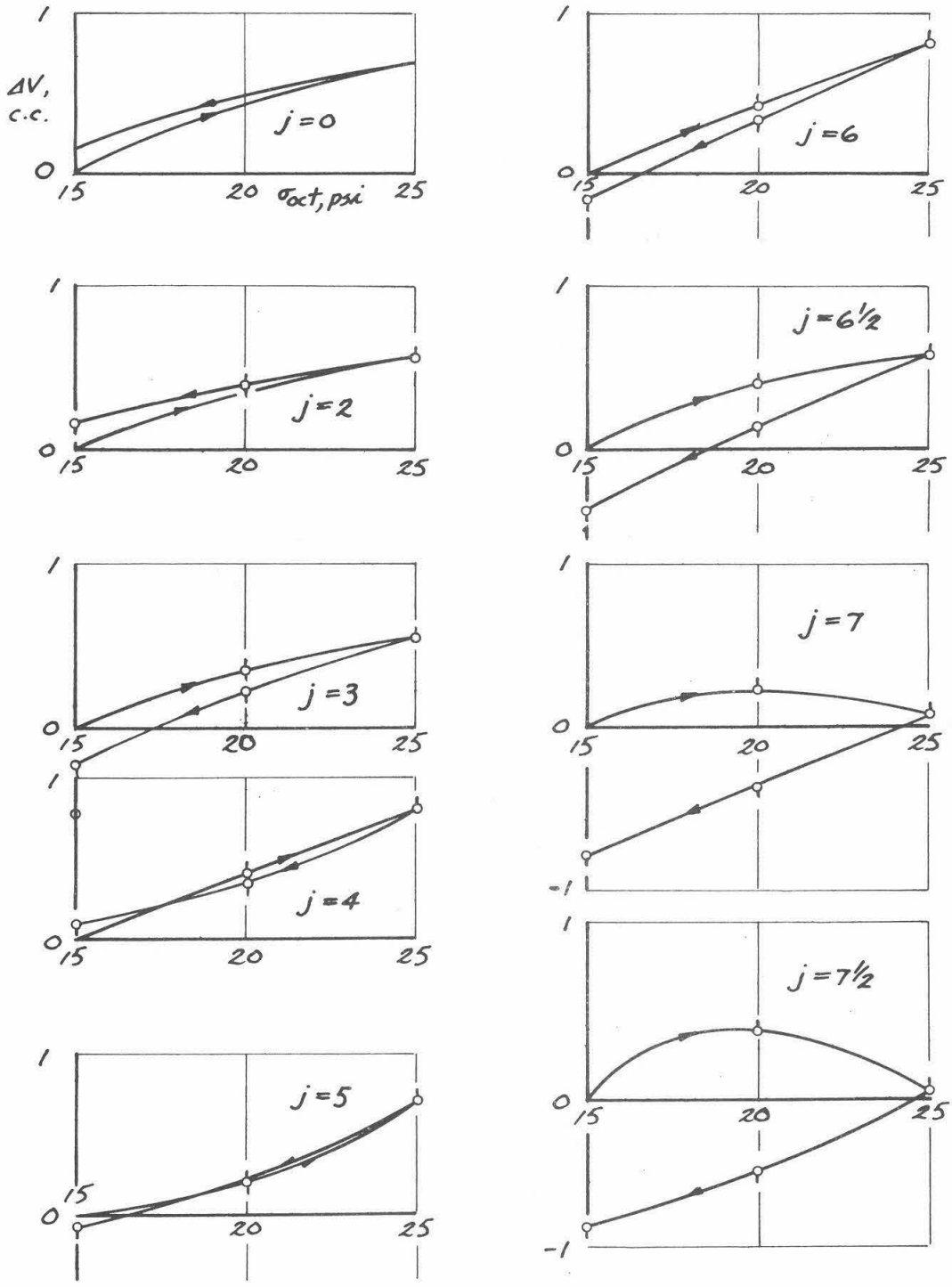

FIG. (VI.23). (b)

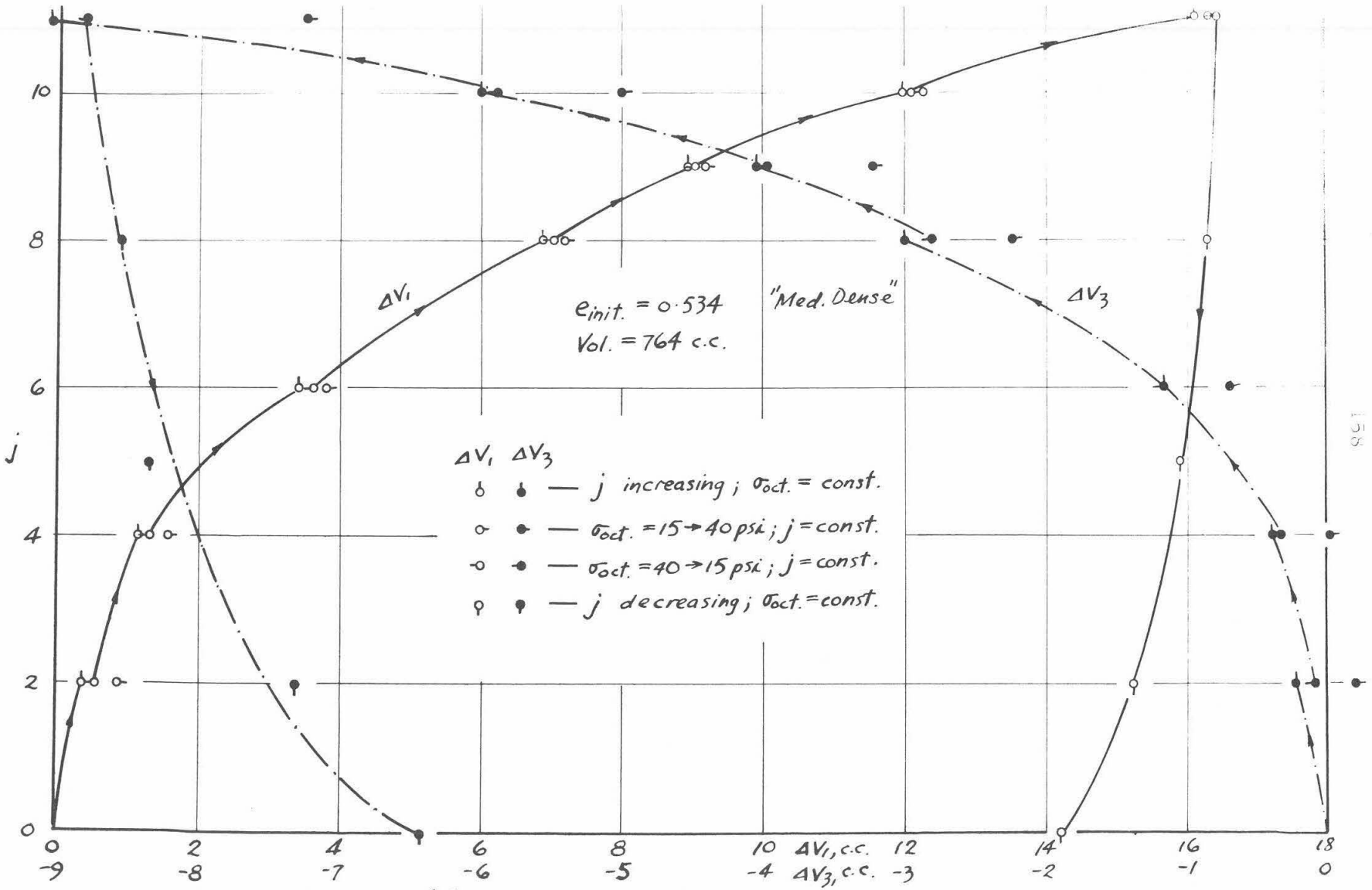

FIG. (VI.24). RESULTS OF TEST TCe-1 (a)

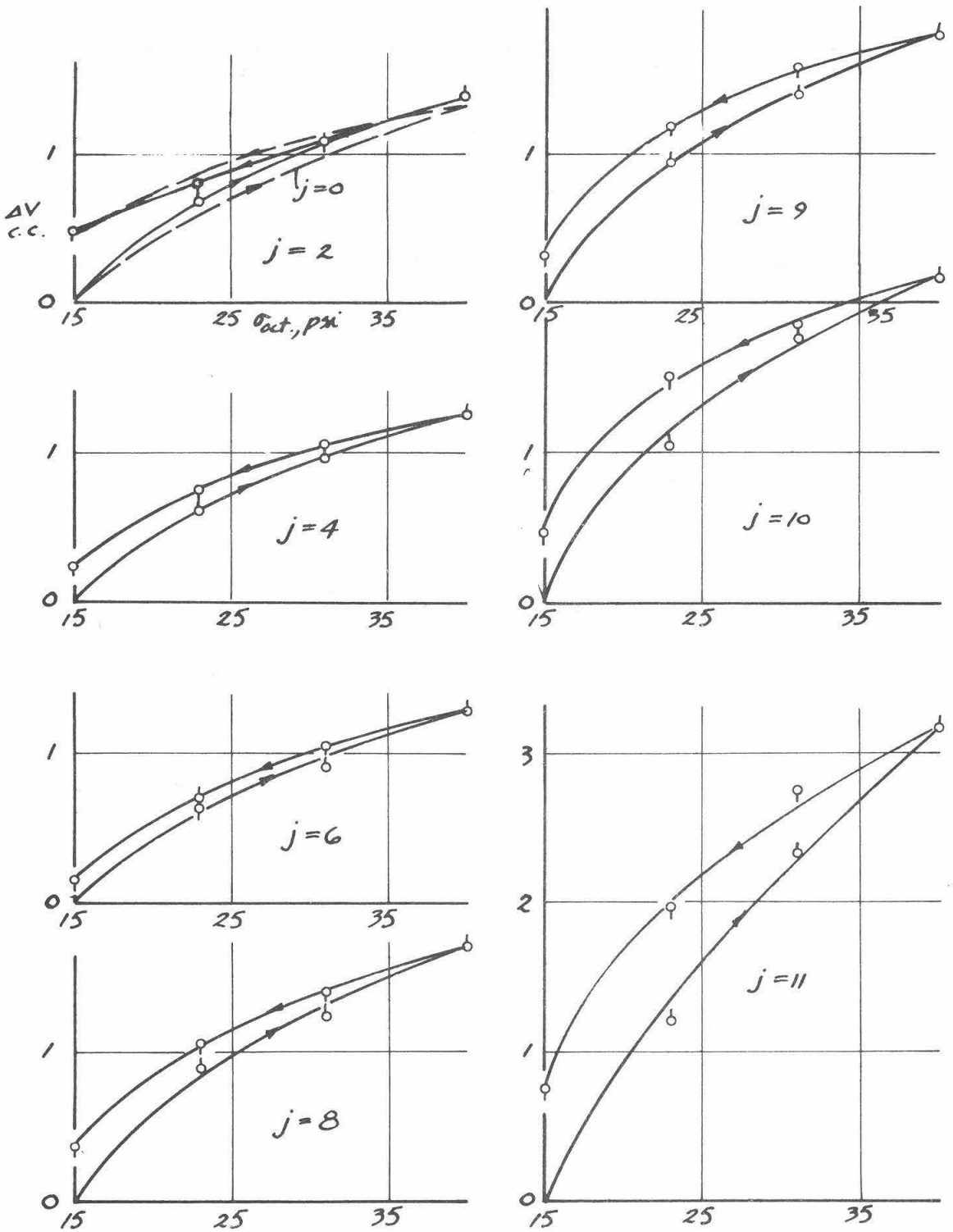

FIG. (VI. 24). (b)

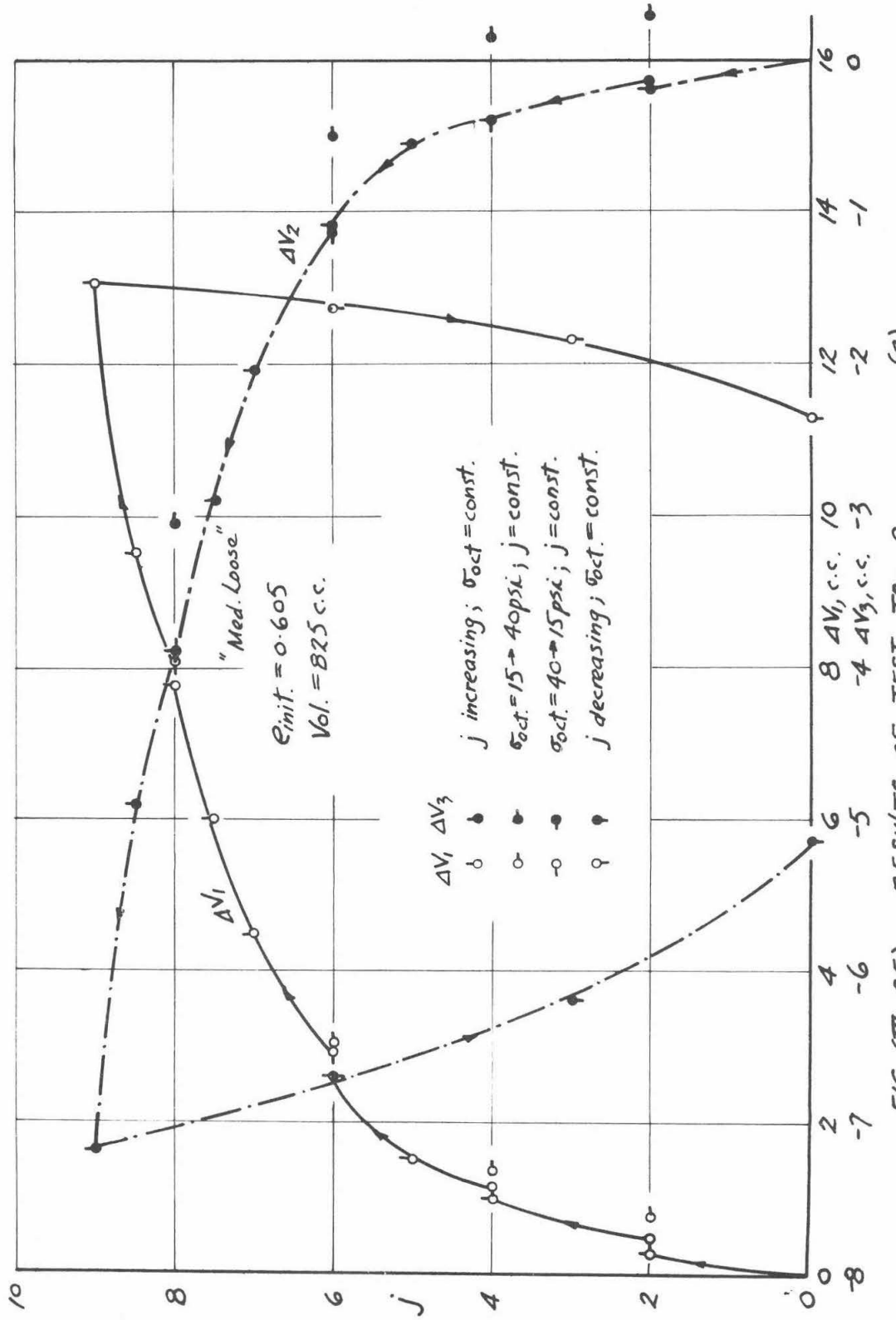

FIG. (VI. 25). RESULTS OF TEST TCe-2

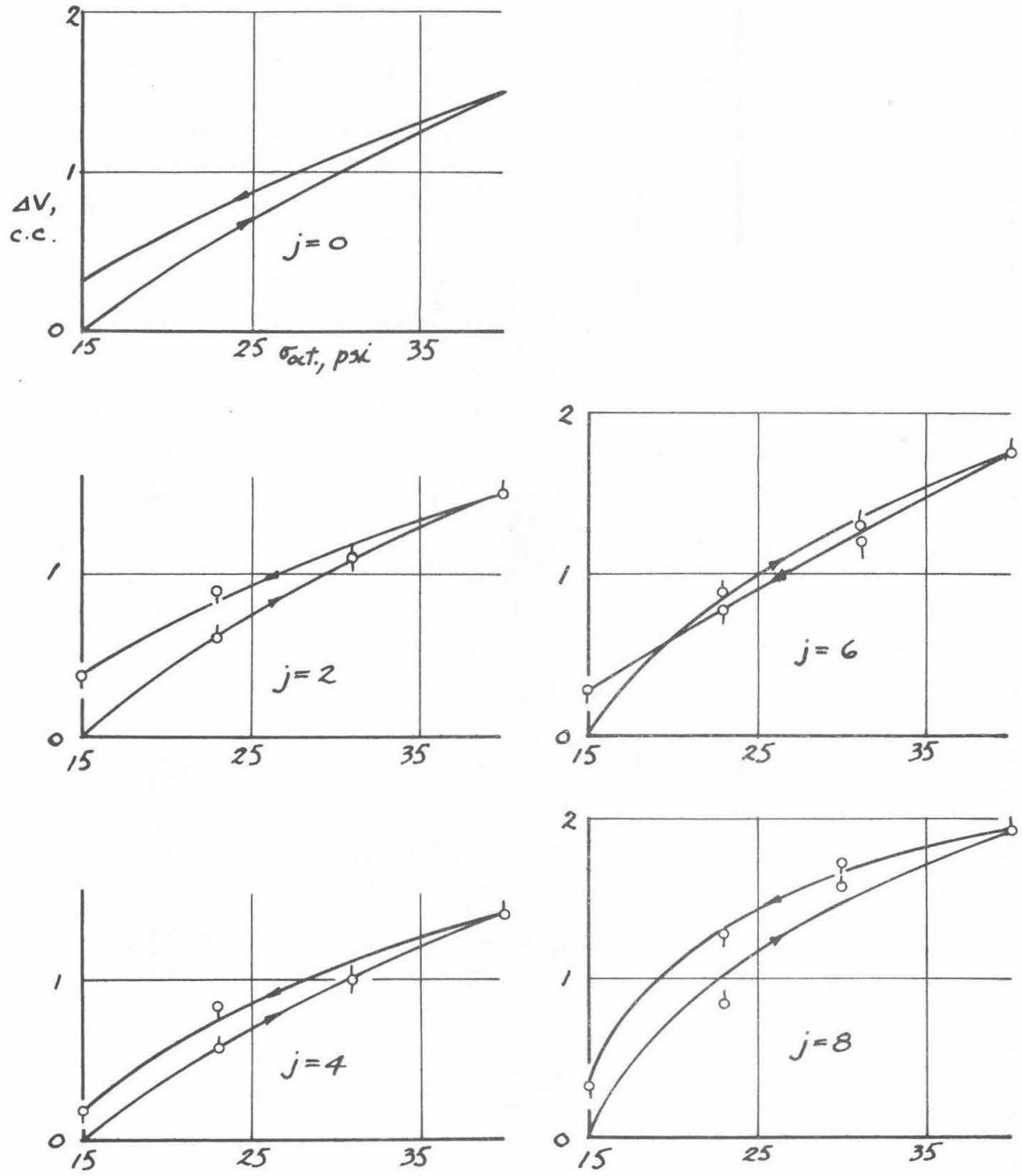

FIG. (VI.25) (b)

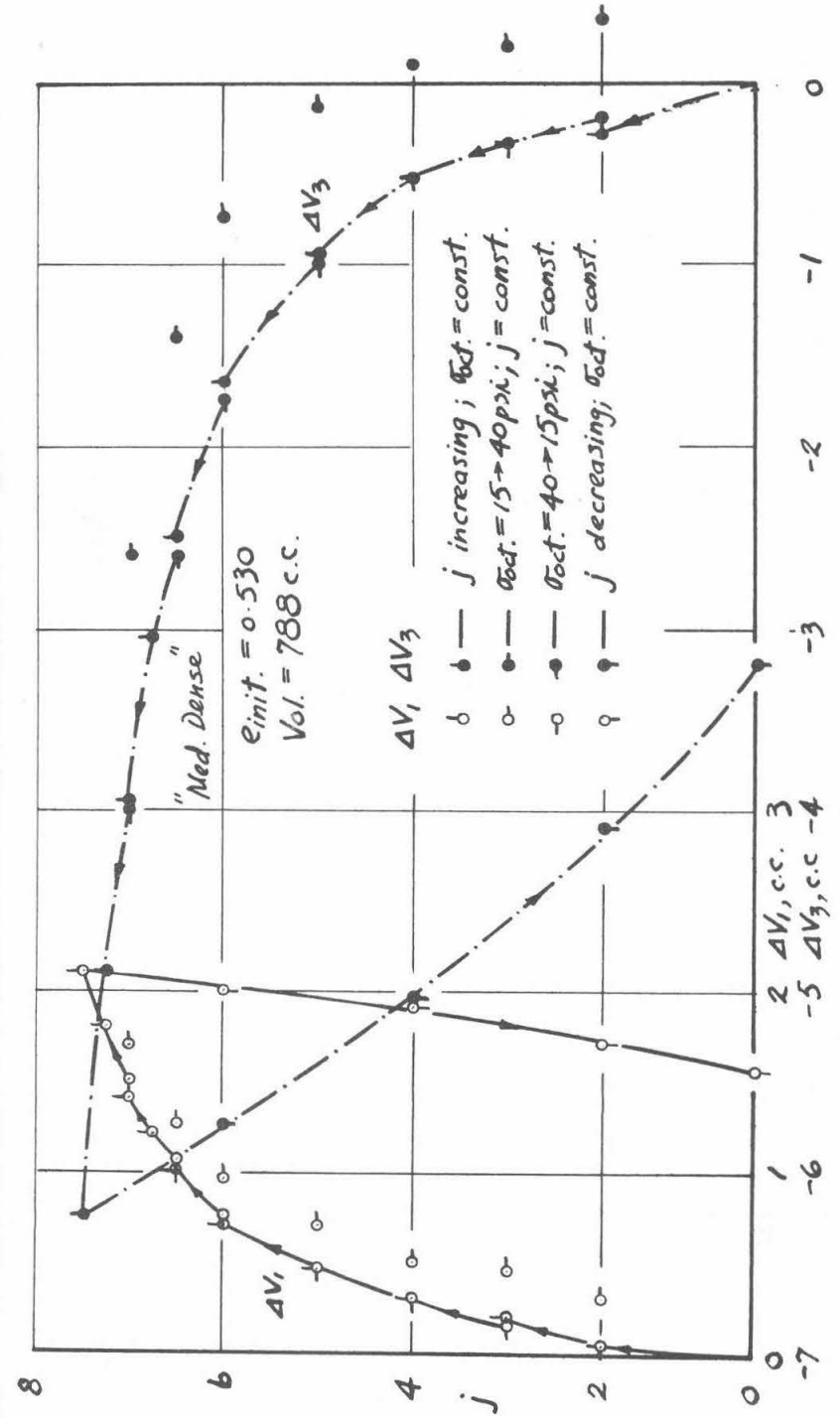

FIG. (VI. 26). RESULTS OF TEST TEe-1

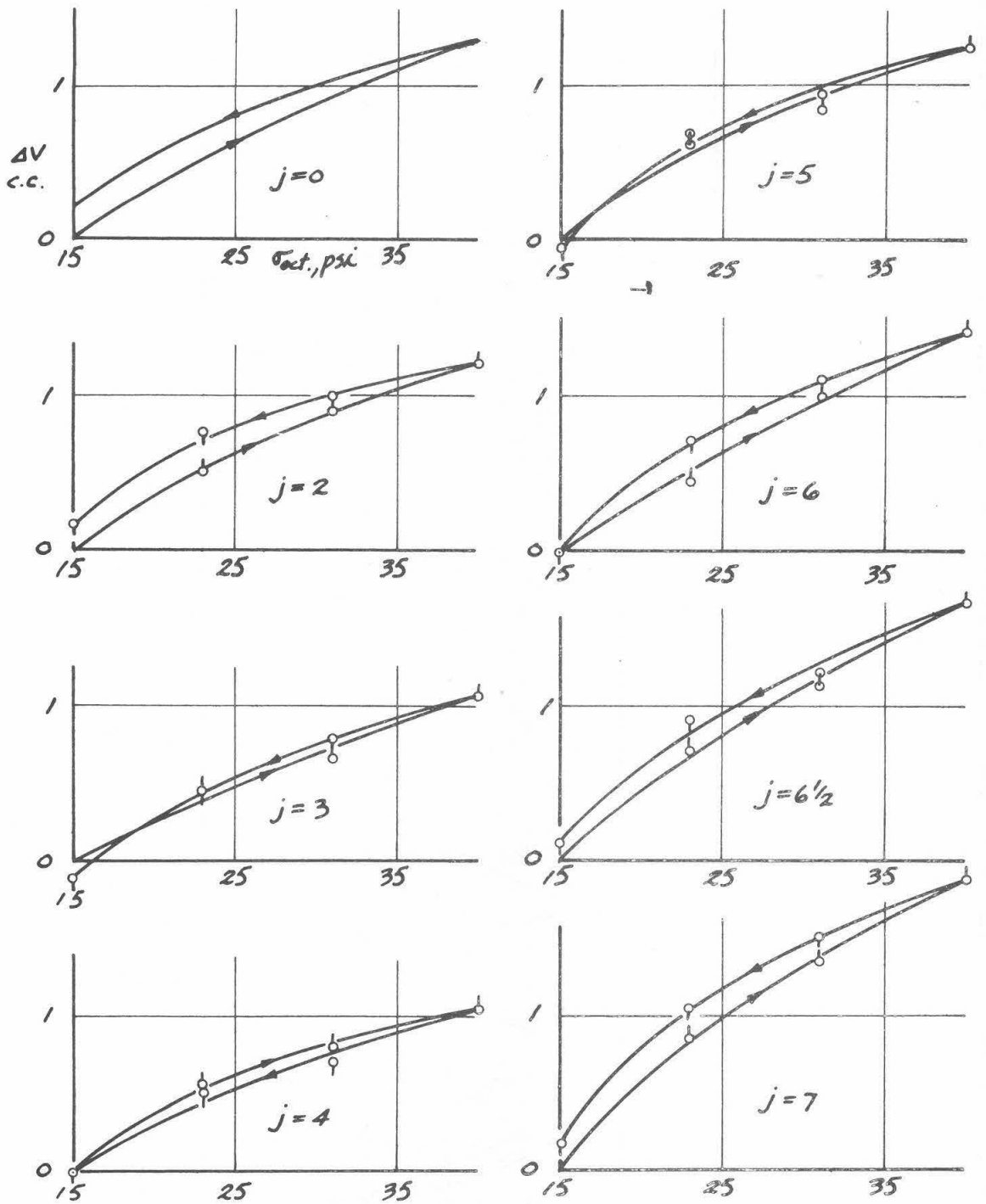

FIG. (VI. 26). (b)

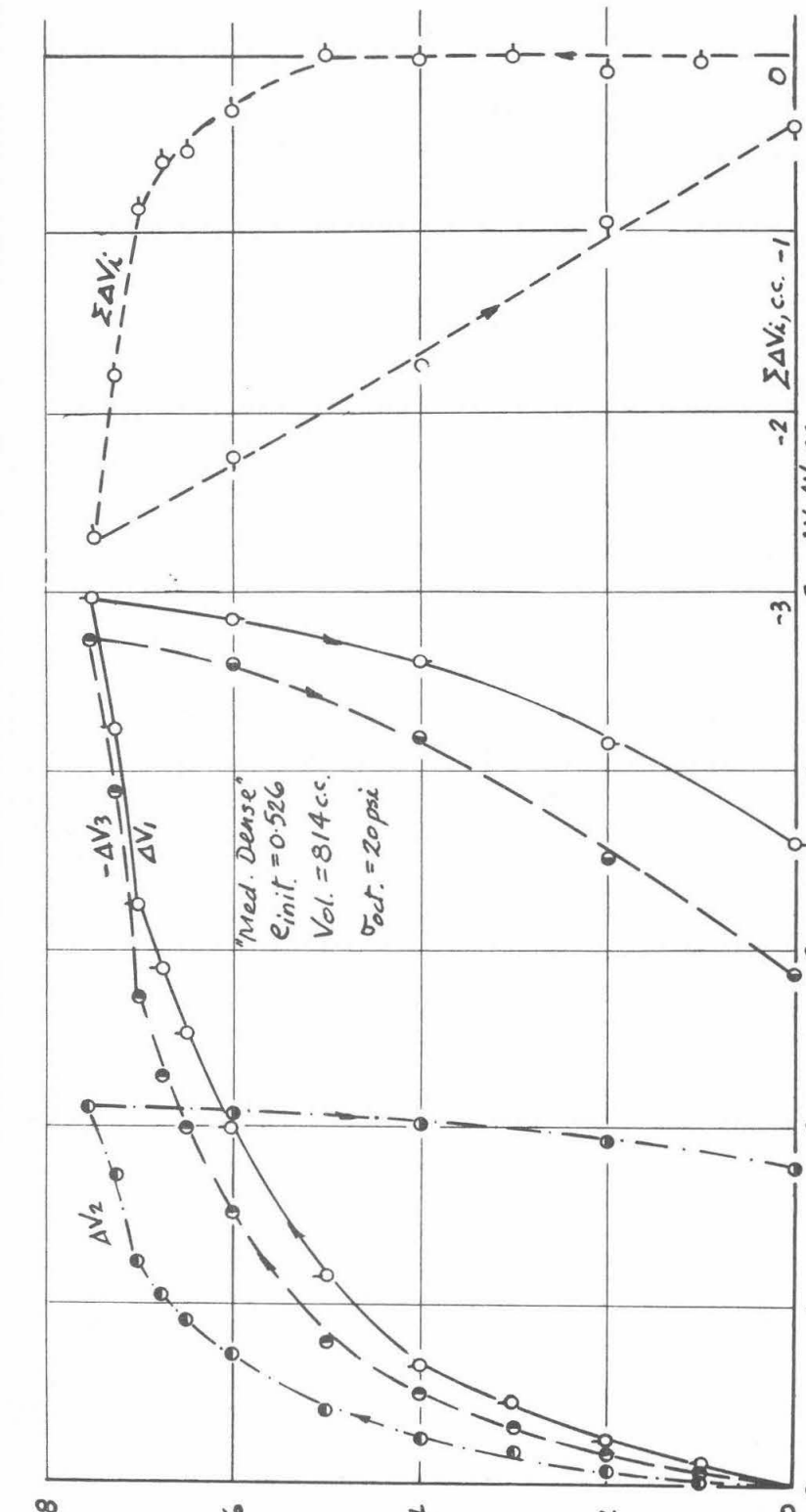

FIG. (VI. 27). RESULTS OF RADIAL SHEAR TEST RS45°-1 (a)

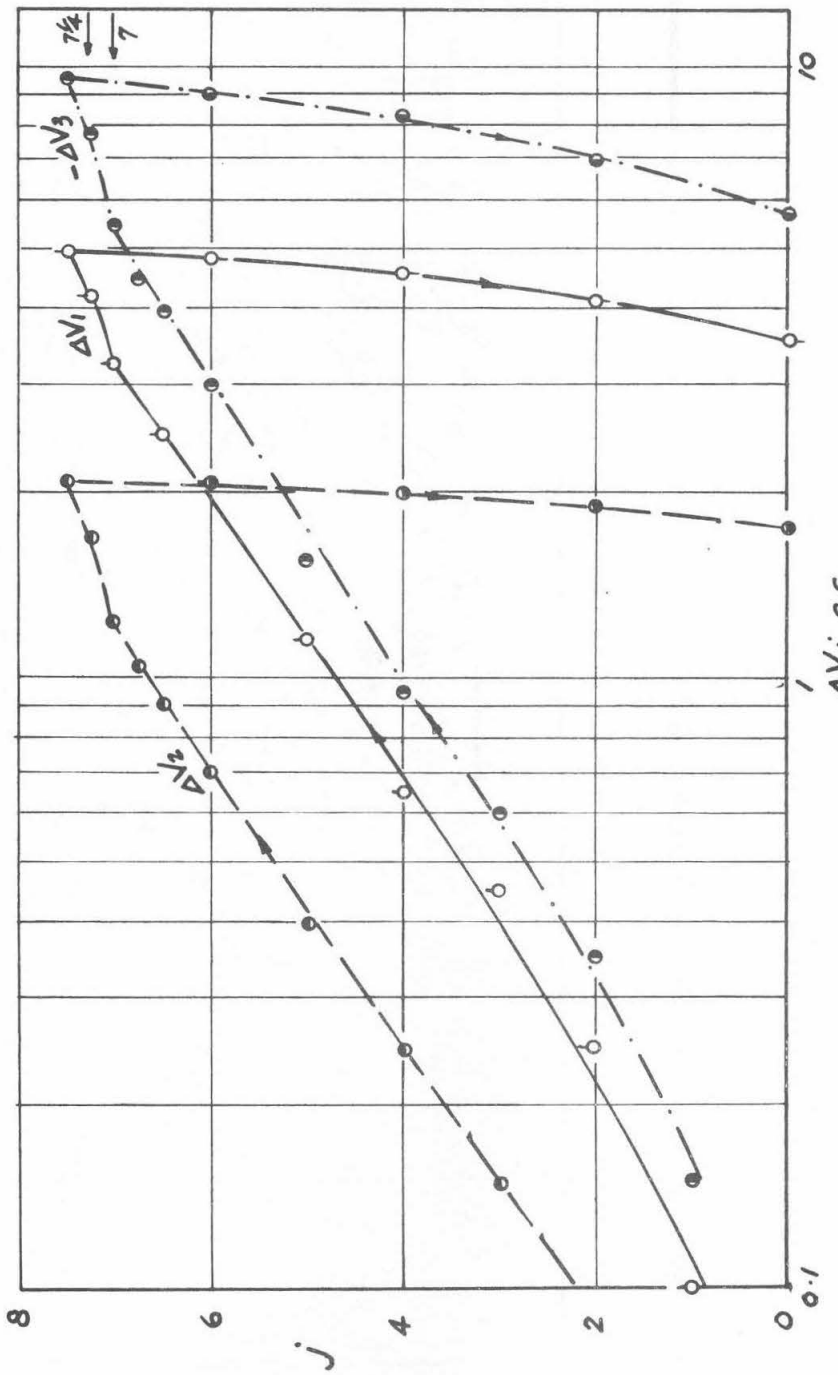

FIG. (VII. 27). (b)

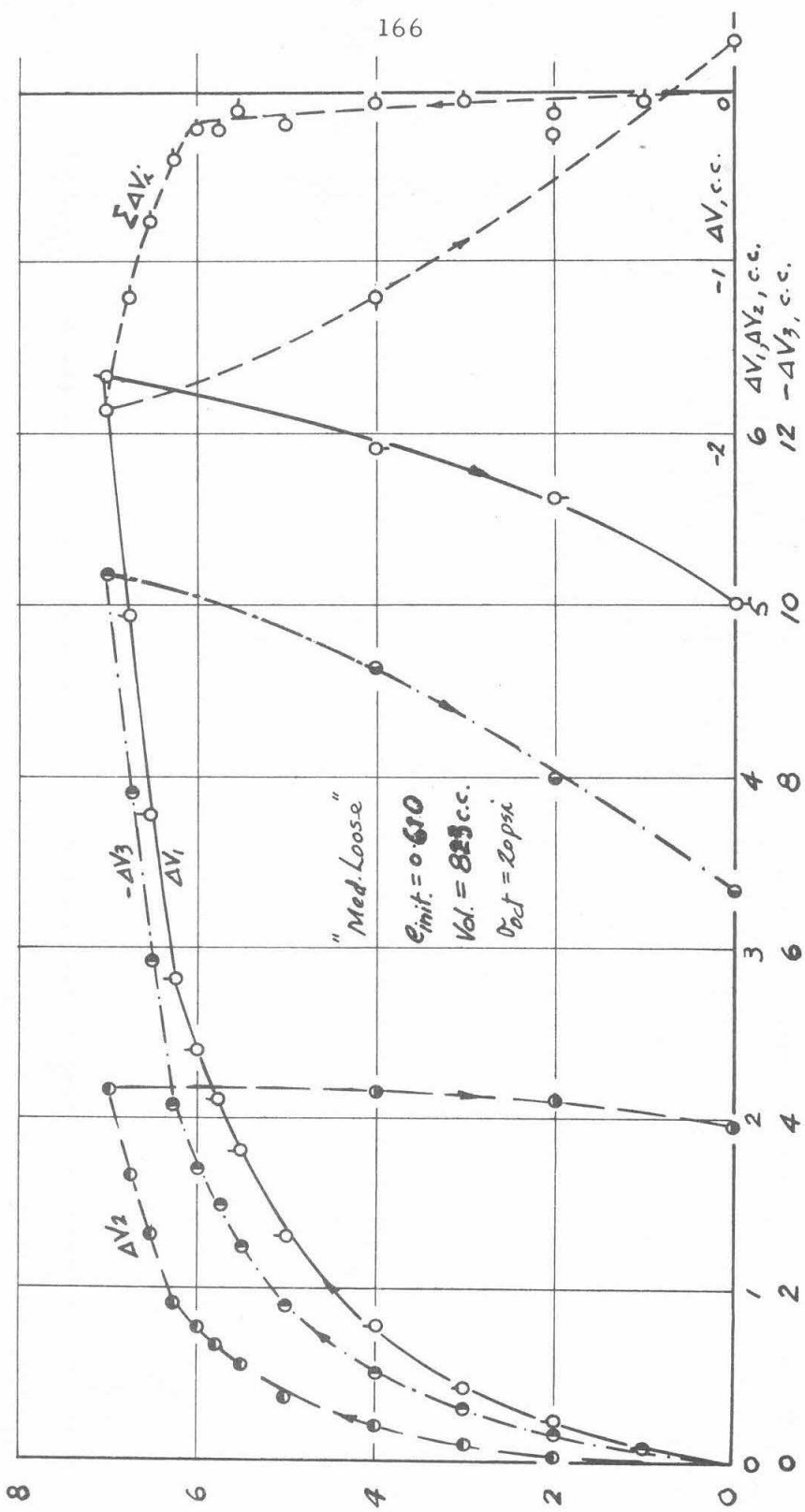

FIG. (III. 28). RESULTS OF RADIAL SHEAR TEST RS45°-2 (a)

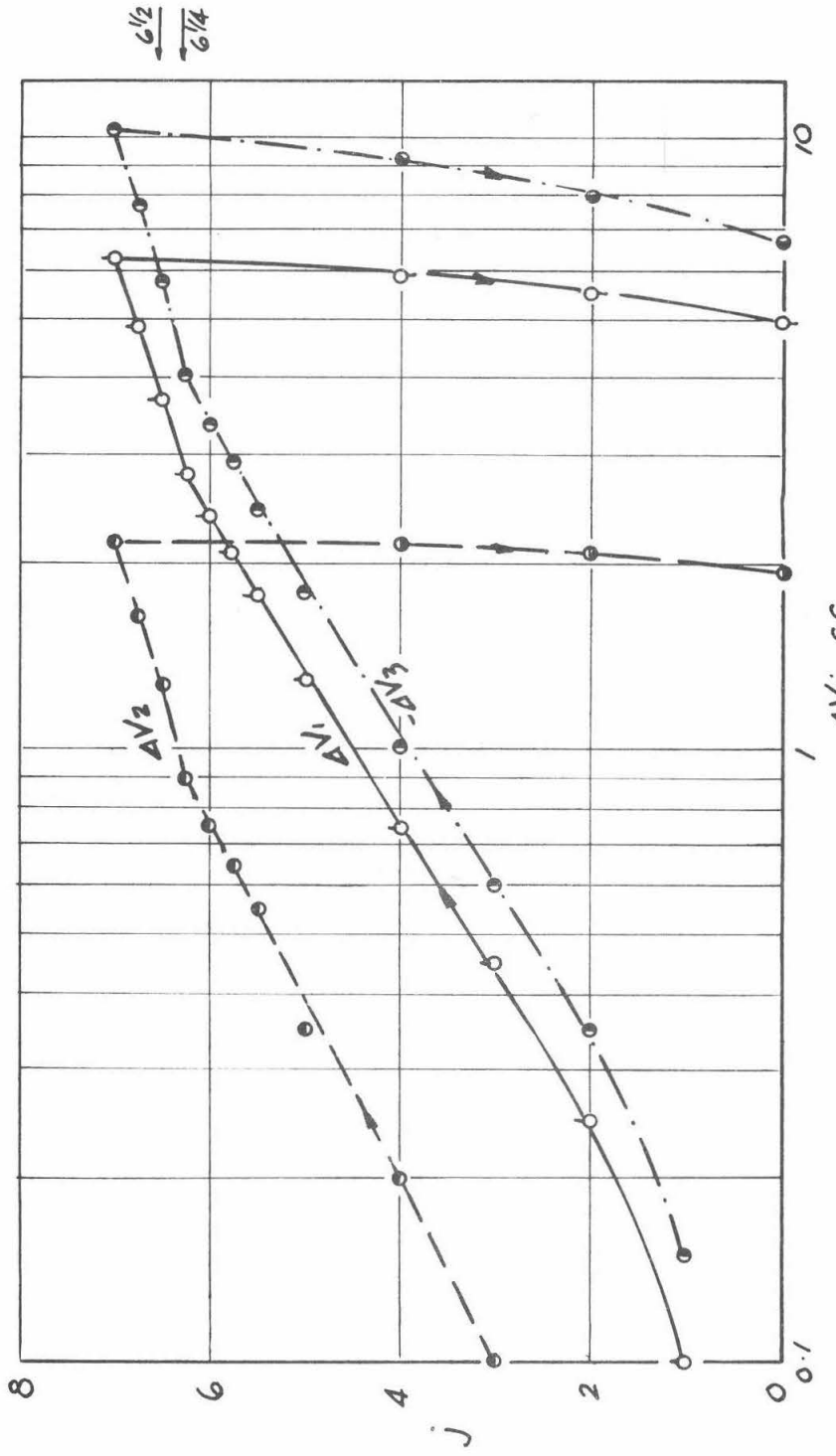

FIG. (XI. 28). (6).

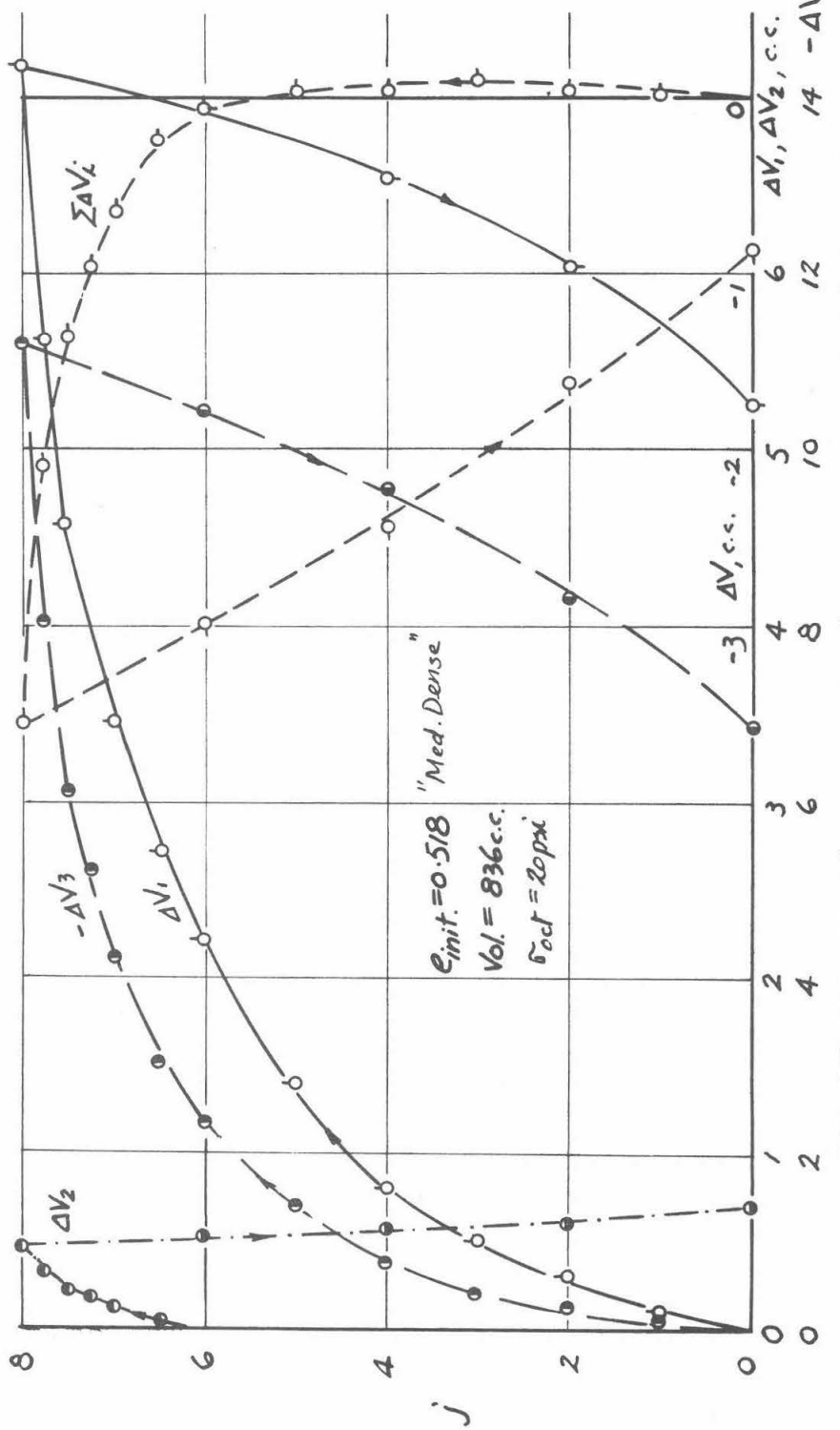

FIG. (III. 29). RESULTS OF RADIAL SHEAR TEST RS60°-1 (a)

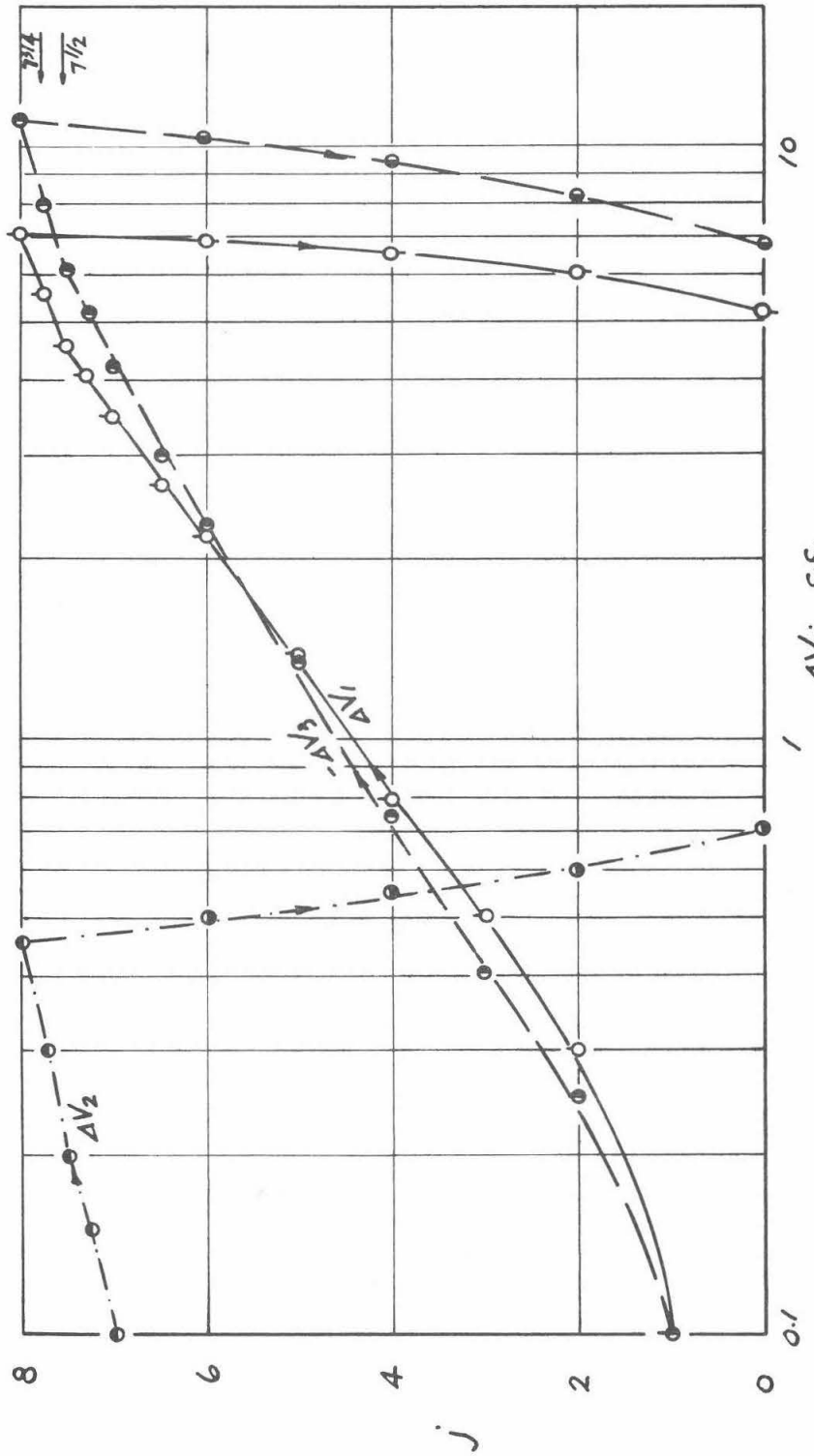

FIG. (XI. 29). (b)

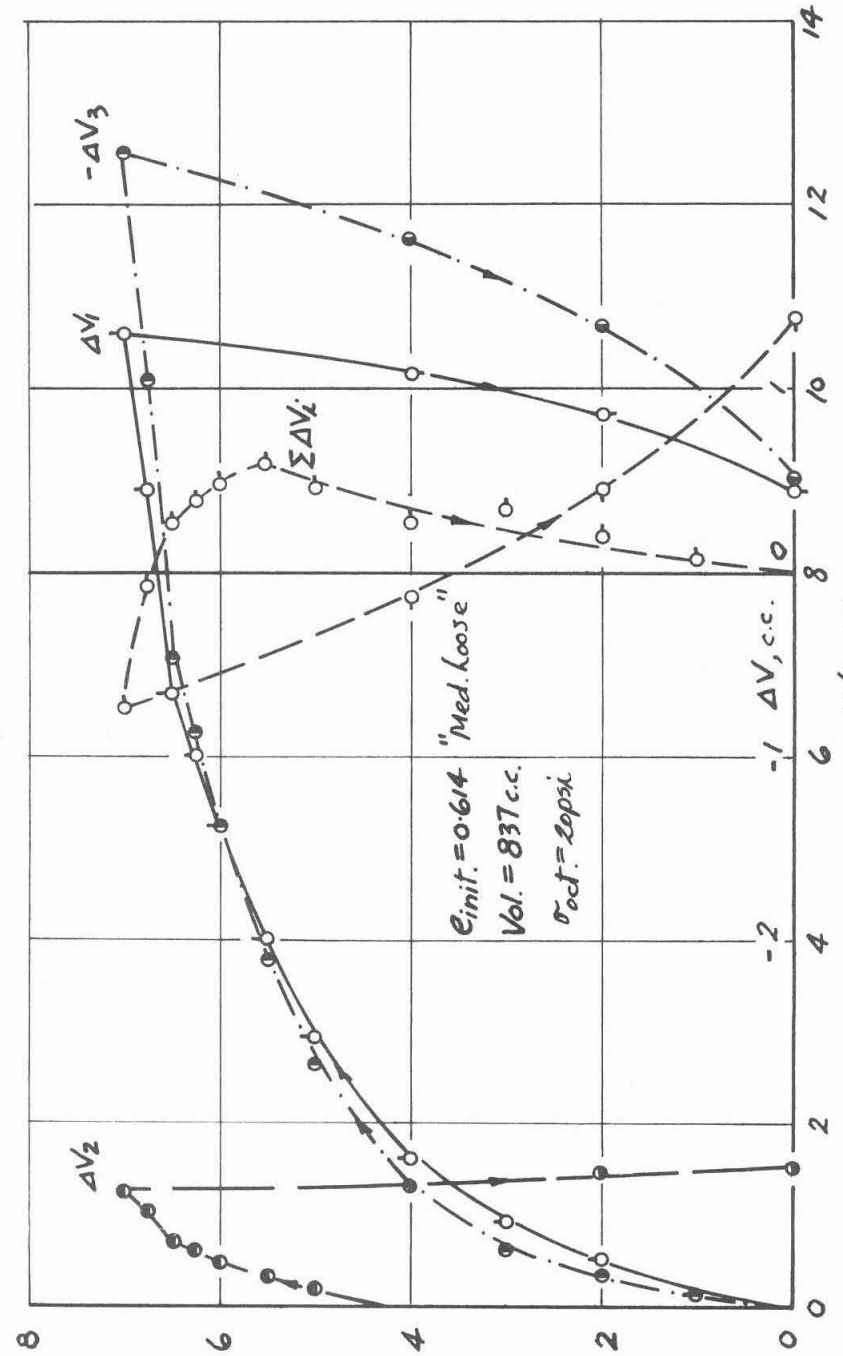

FIG. (III. 30). RESULTS OF RADIAL SHEAR TEST RS60°-2 (a)

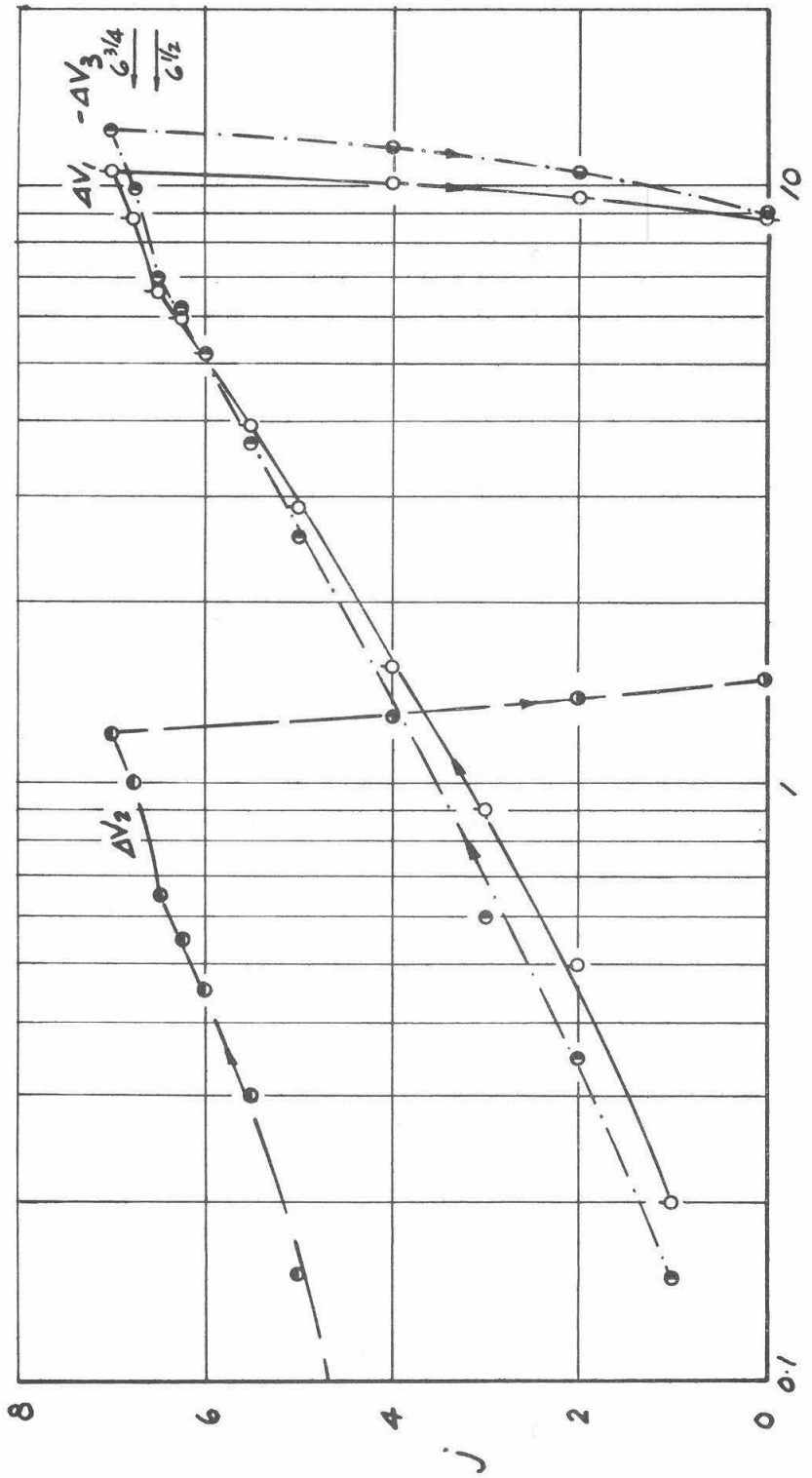

FIG. (III. 30). (b)

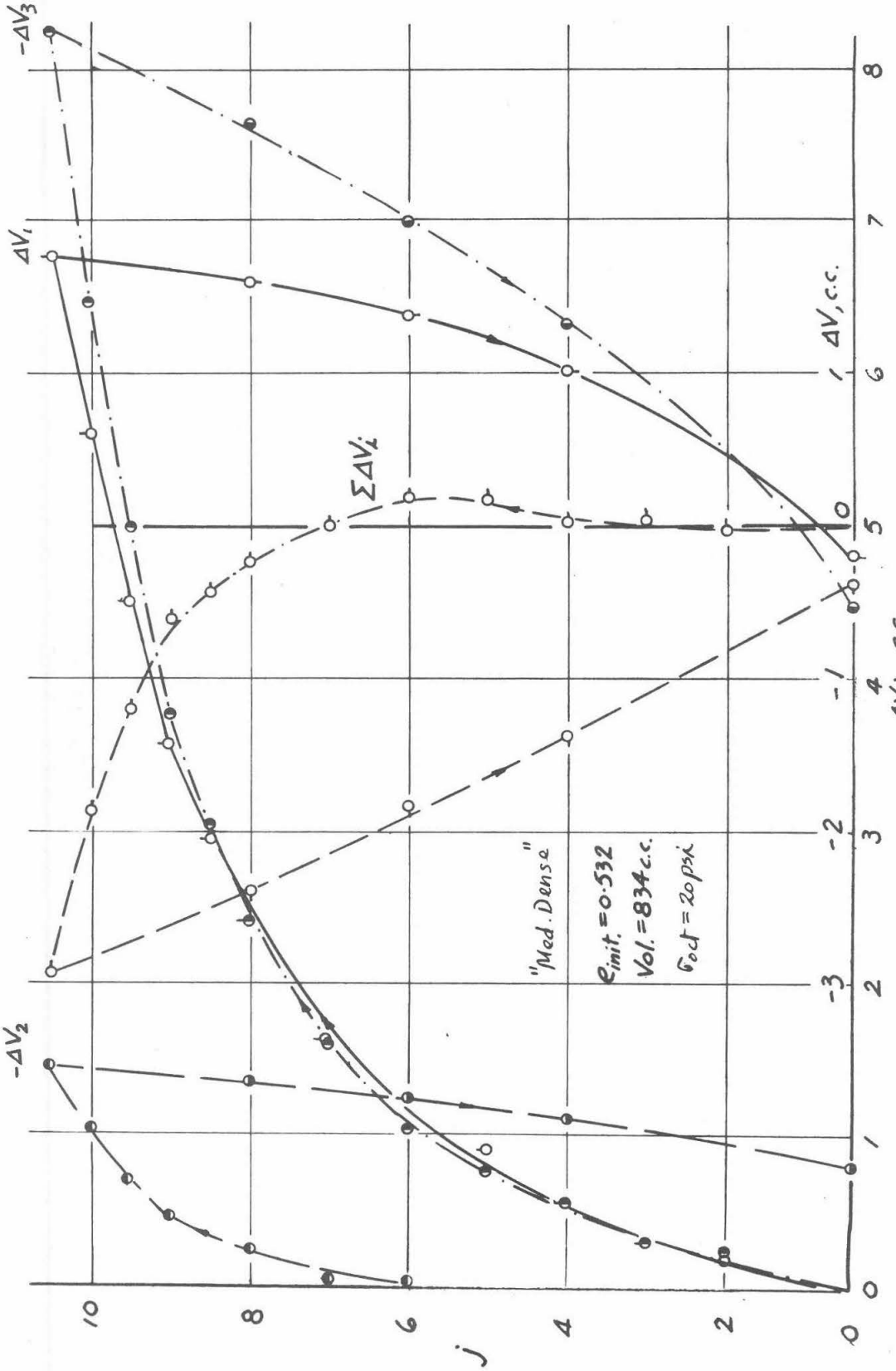

FIG. (VI.31). RESULTS OF RADIAL SHEAR TEST RS75°-1 (a)

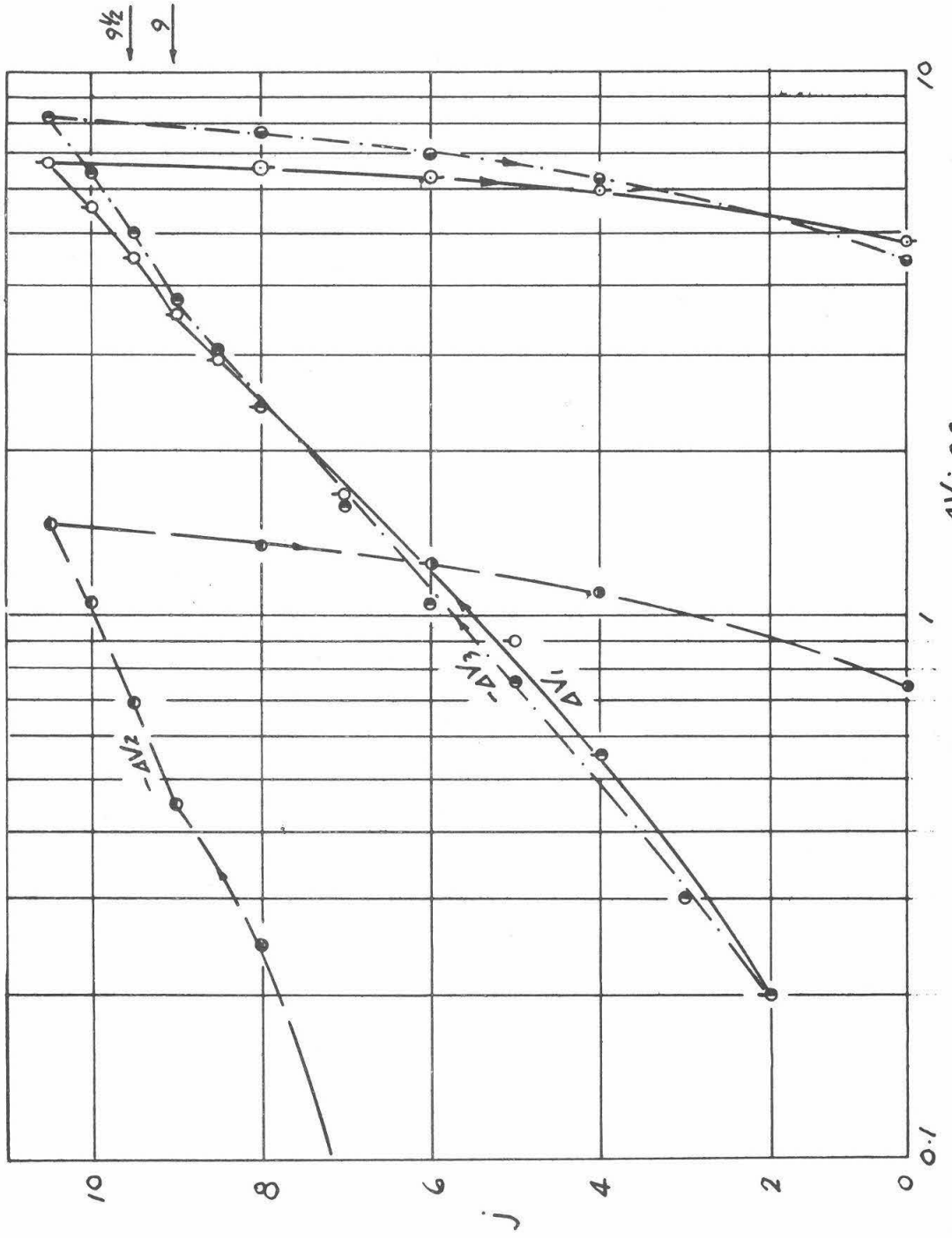

FIG. (III.31). (b)

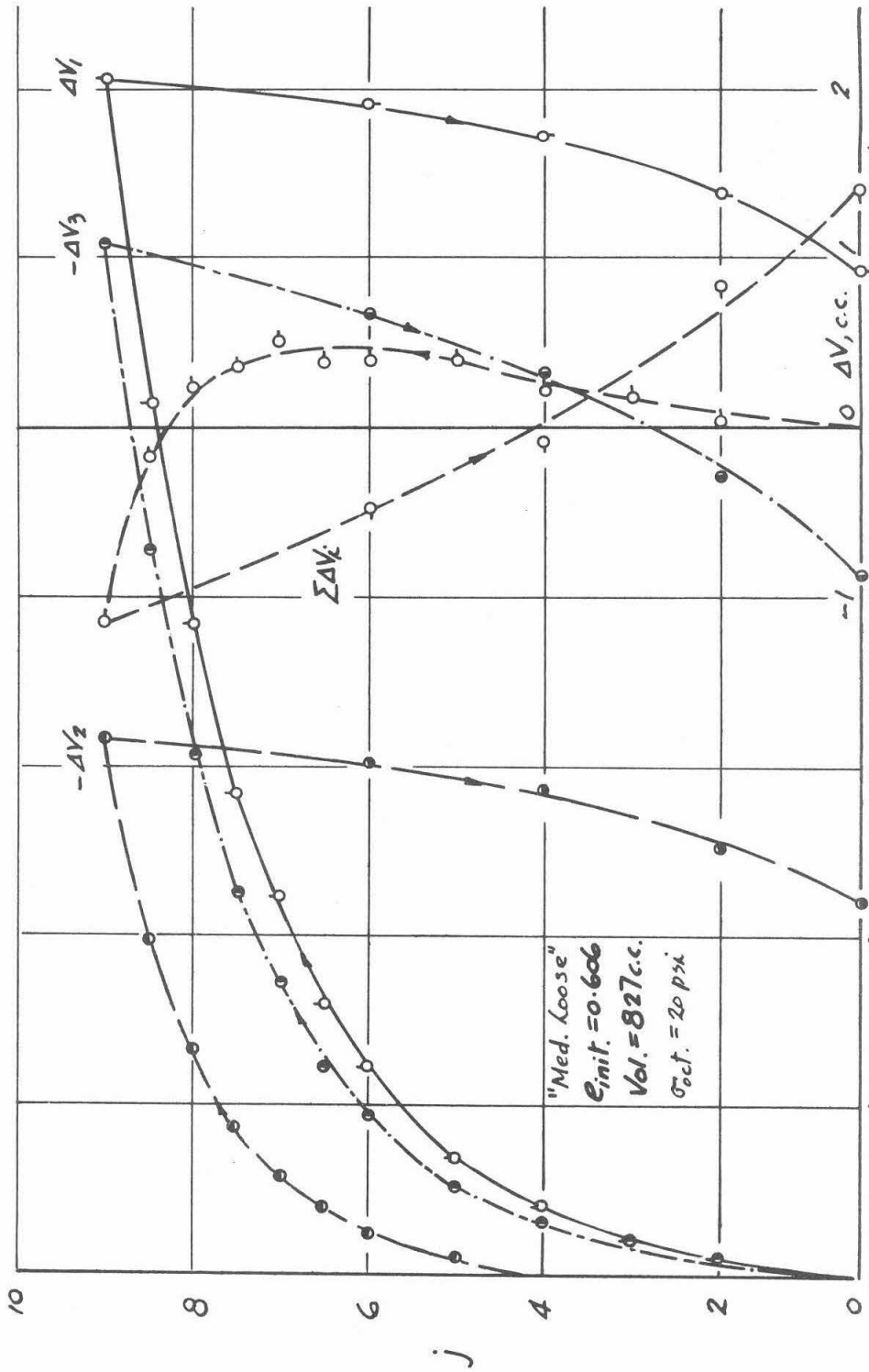

FIG. (II. 32). RESULTS OF RADIAL SHEAR TEST RS75°-2 (a)

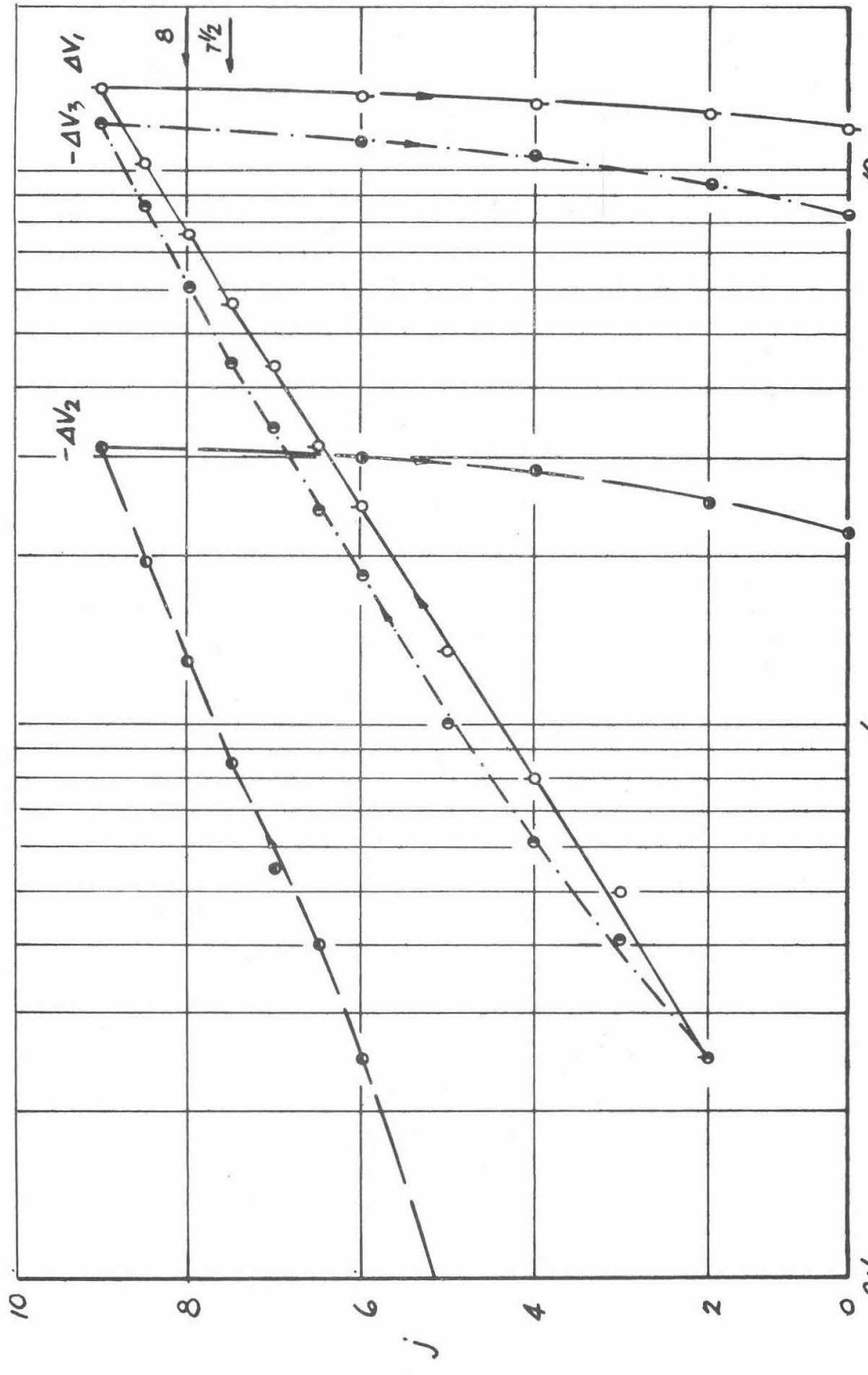

FIG. (XII.32). (b)

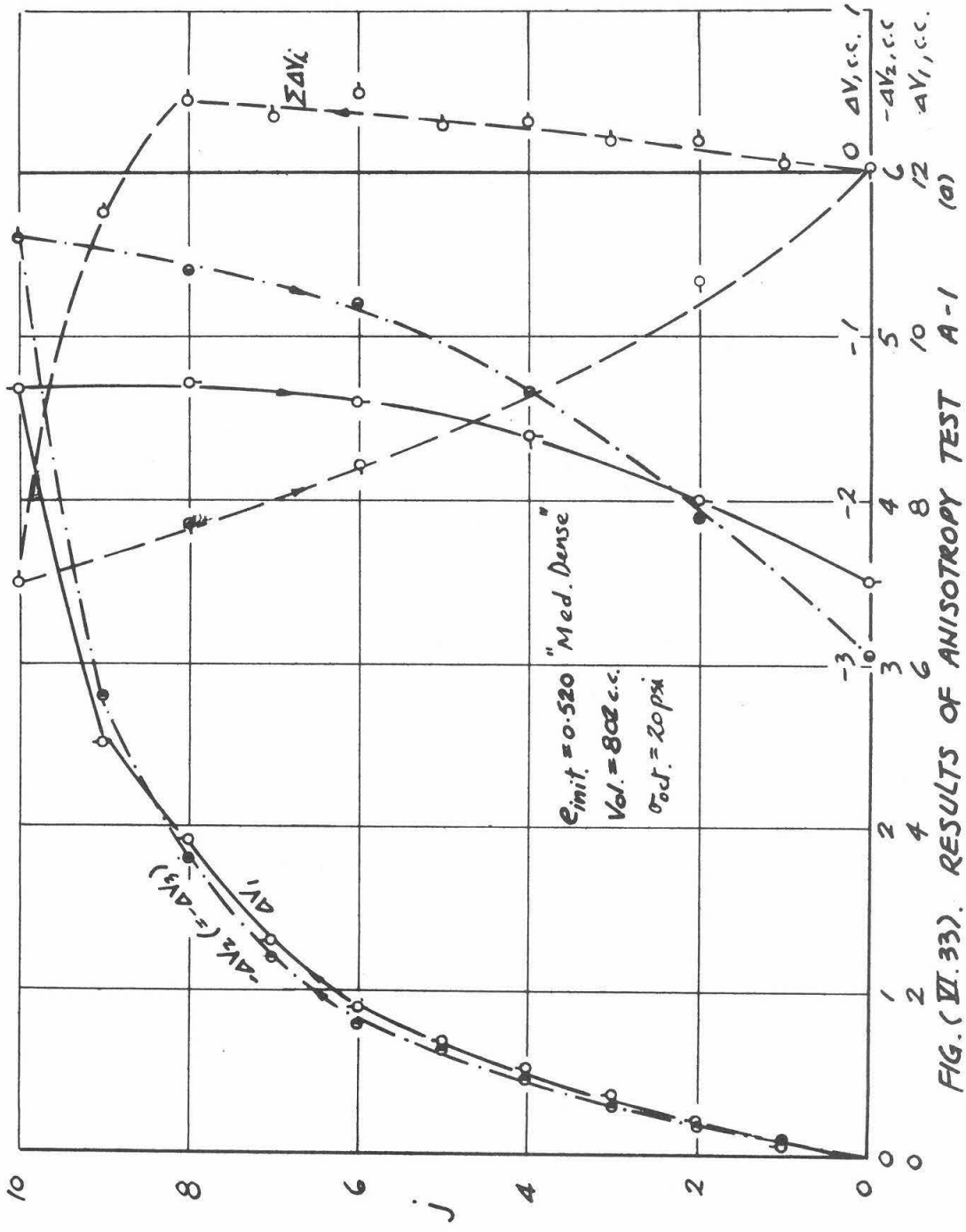

FIG. (VI.33). RESULTS OF ANISOTROPY TEST A-1

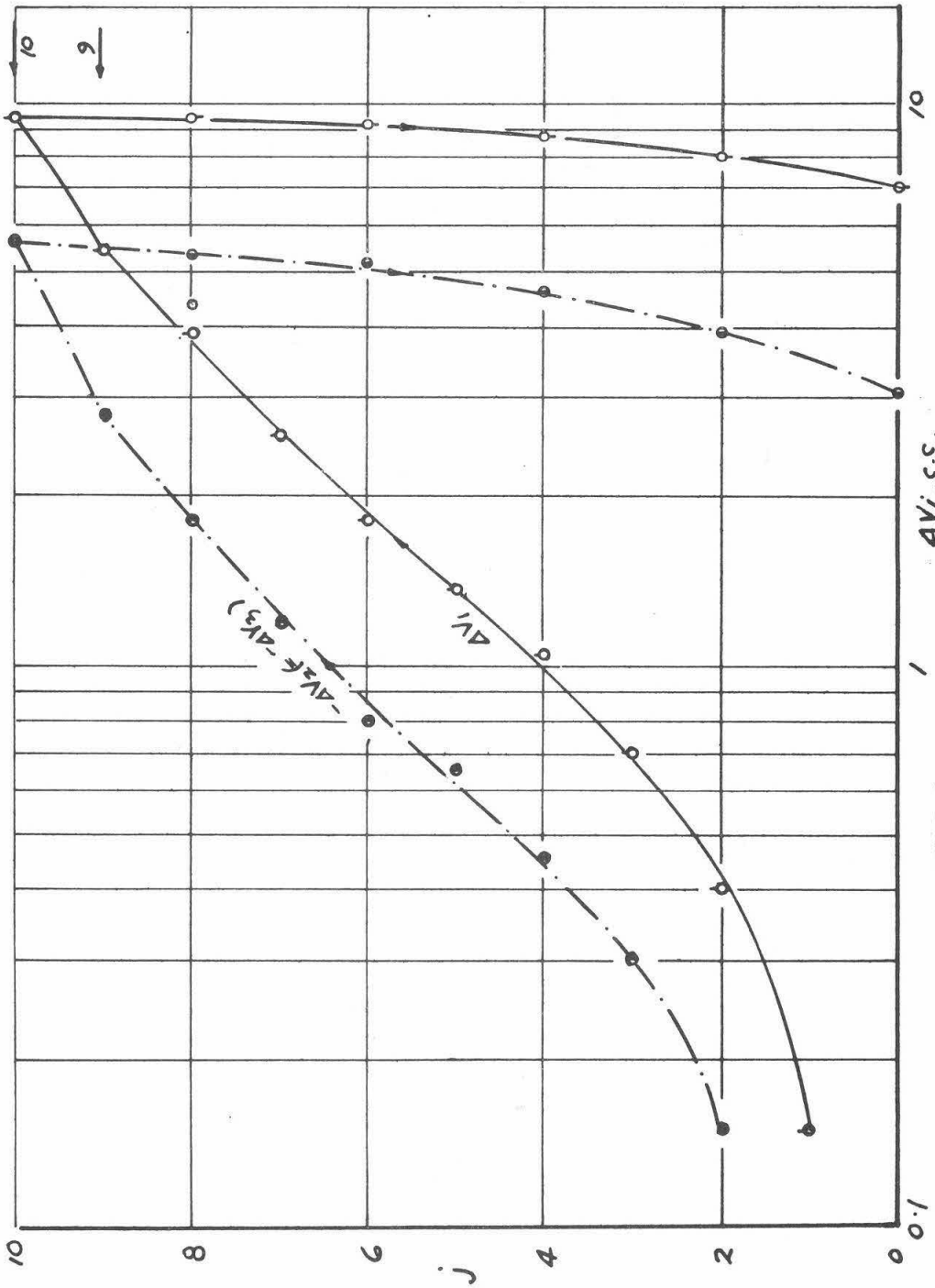

FIG. (VII.33). (b)

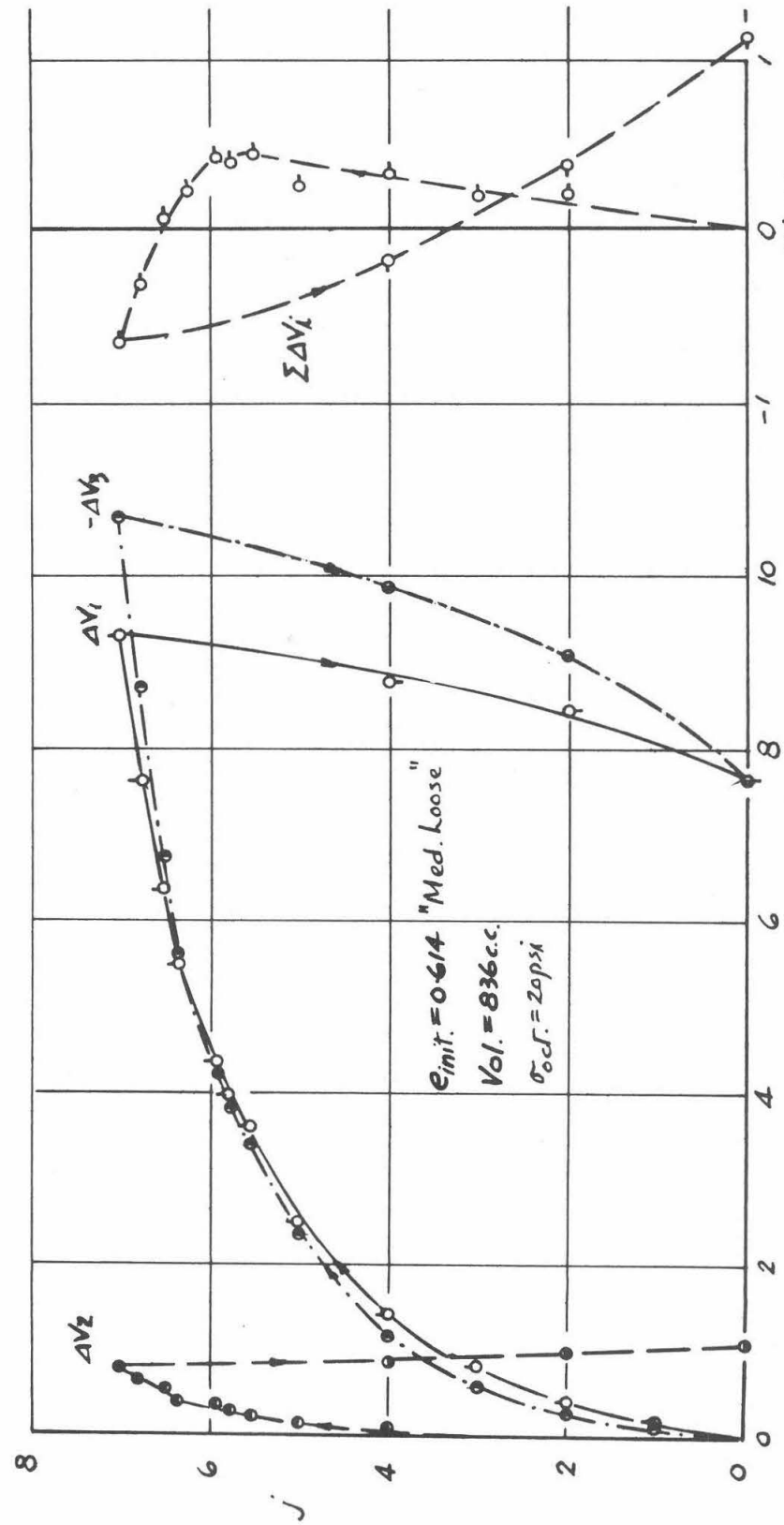

FIG. (III. 34). RESULTS OF ANISOTROPY TEST A-2 (a)

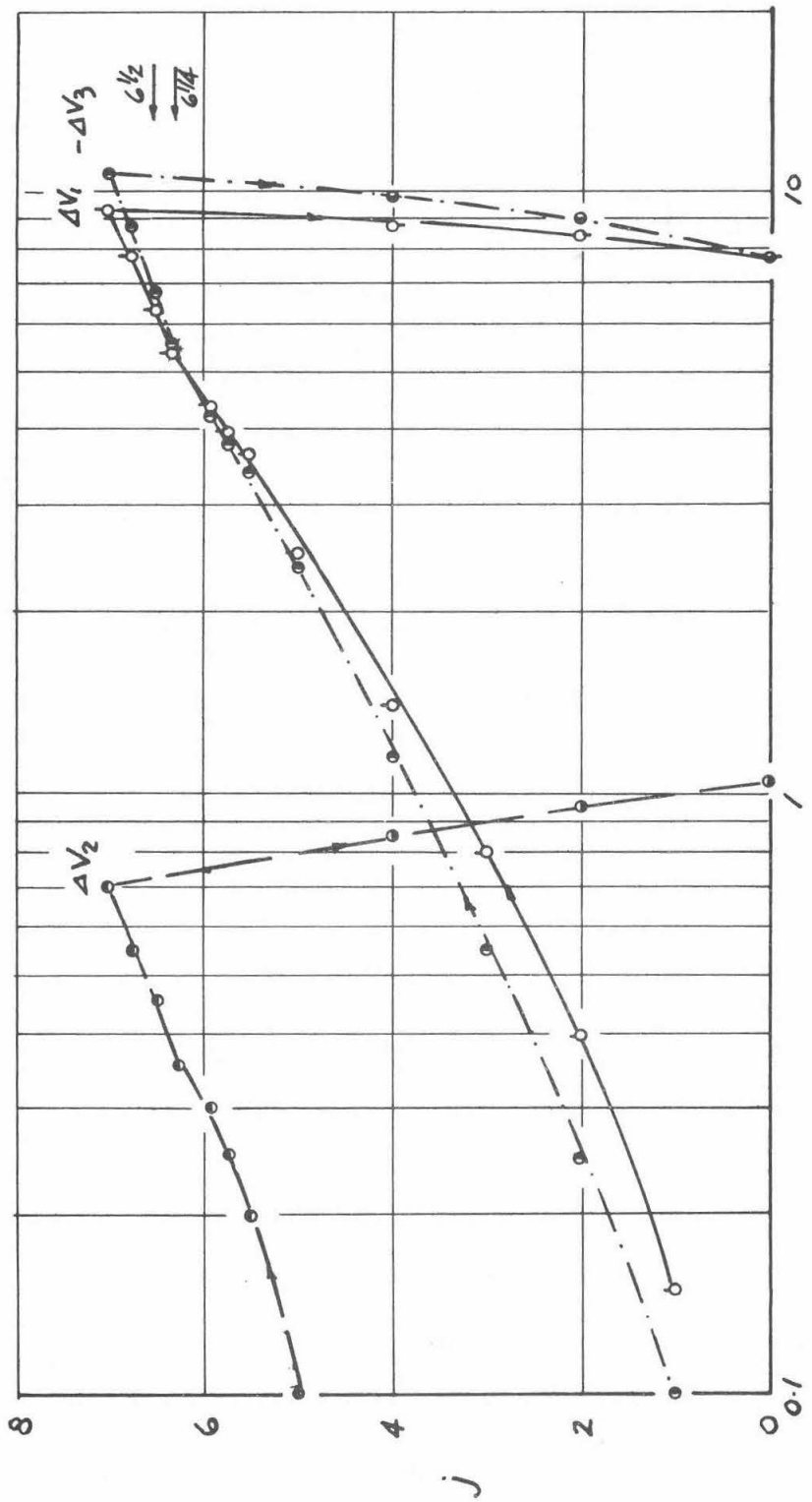

FIG. (III. 34). (b)

CHAPTER VII

DISCUSSION OF TEST RESULTS

Any statement made in this chapter about the behavior of sand applies only to the Ottawa sand tested in this investigation.

(1) Hydrostatic Compression Tests

The results of hydrostatic compression tests HC-1, HC-2 and HC-3 were shown in Figs. (VI.1) to (VI.3). It is seen that the volumetric compression ΔV varied non-linearly as the hydrostatic pressure p and the relationship was a strain-hardening one.

The compressibility of sand was found to depend on the density of the soil, as represented by the void ratio e; the looser the soil, the more compressible it was. During the first cycle of loading and unloading, there was a certain amount of irreversible volumetric compression which was smaller for the denser soil. During the second cycle, the amount of irreversible compression was considerably reduced, especially for the dense soil in HC-1, where all the compression was recoverable at the datum pressure of 4 psi. However, for the two looser samples there was still some irreversible deformation when the hydrostatic pressure was returned to 4 psi.

It is suggested that the irreversible deformation was due to the initially unstable soil grains trying to attain more stable positions when the sample was subjected to hydrostatic stresses. For the magnitude of the maximum pressure employed in these tests (60 psi), grain crushing was undetectable, as supported by comparing the grain size distribution

of a sample after a test to that of the same soil taken before the test. This is not shown, because it is identical to the one shown in Fig. (V.1). The number of initially unstable grains in a dense soil would be less than that in a loose soil. Therefore, it only took one cycle of hydrostatic stress in HC-1 to bring nearly all of these grains into stable positions, and during the second cycle of stress, nearly complete recovery was obtained. For a looser sample, there was still a certain amount of irreversible deformation during the second cycle, Figs. (VI.2) and (VI.3); however, if a few more cycles of stress had been applied, there could have been no irreversible deformation at all. This would be achieved when each grain in the sample had attained a stable position with respect to its surrounding grains.

From the consideration given in Chapter III about the behavior of spheres under combined normal and tangential forces, it seems plausible to assume that the magnitude of tangential forces acting between grains in a random assembly under hydrostatic stress is very small. This is justified because tangential forces would produce "slipping" and "sliding" between grains, both of which involve irreversible movements, whereas experimental evidence showed that the volumetric compression is largely reversible. If this assumption is made, the external stresses are resisted by normal forces between the grains, and the overall volumetric strain results from the elastic compression of grains by the normal forces at the contacts.

Upon this assumption and subsequent reasoning, the theory of holey models presented in Chapter III was based; this theory postulated an increasing number of contacts to be made under increasing hydrostatic

pressure. It is now appropriate to compare the experimental results to the values predicted by the theory of holey models.

Before this comparison is made, we observe that the loading and unloading portions of the hydrostatic compression curves do not coincide even for the dense sample where there was complete recovery at the datum pressure. In other words, there existed a hysteresis loop. It is thought that part of this hysteresis may be due to the uncertainty involved in measuring the correction due to membrane penetration and wall bulging effects. It is quite possible that it is a property of the material itself, but there is no way to predict this from the theory in Chapter III. Therefore, in the following comparison between theory and experiment, only the loading portions of the compressibility curves of the second cycle of the three tests are taken.

These are plotted as volumetric strain ($\frac{\Delta V}{V}$ %) versus $p^{2/3}$ in Fig. (VII.1). In the same figure are shown the theoretical curves for random assemblies of spheres with void ratios as shown, which correspond to those of the samples in the respective tests. It must be remembered that these curves are for an assumed value of the ratio r/R of 1/3 (see Chapter III). It is seen that an excellent correlation is obtained for the medium dense sample of HC-2, while the theory predicts higher values for the dense sample of HC-1 and lower values for the loose sample of HC-3. However, the discrepancies in the last two cases are not great and the curves have roughly the same shapes. Bearing in mind that the total corrections which are applied to the observed volumetric readings to obtain the true deformations were about twice as large as the deformations themselves, we may tentatively conclude that the theory does

predict the behavior of sand under hydrostatic stress. (It must be noted that the volumetric strains are very small and the apparatus is not sensitive for precise measurements at this level. However, when a deviatoric stress is applied, the shearing deformations are much larger and the apparatus has then a greater reliability.)

For the sake of comparison, the compressibility curves obtained by Bell [8], on samples of density comparable to the present tests, were also plotted in Fig. (VI.2) and Fig. (VI.3). It is seen that Bell's results show a much sharper rise at the small pressure range and are roughly parallel to those obtained in this investigation for larger pressures. It is the author's opinion that the discrepancy at small values of the hydrostatic pressure is due to the error in the membrane correction used by Bell.

In Fig. (VII.1) are also shown the compressibility curves for a simple cubic and a face-centered cubic packing, as obtained by assuming only a Hertzian behavior at the points of contact. They are straight lines on the $\frac{\Delta V}{V} \sim p^{2/3}$ plot.

Hence it is felt that the experiments tend to confirm the theory of holey models postulating successively increasing numbers of contacts between grains in a random granular assembly under increasing external hydrostatic stress. The volumetric strain does not depend linearly upon the two-thirds power of the external pressure, as was predicted by using only the Hertzian contact theory, but it increases less rapidly than the two-thirds power function due to the increased number of contacts continuously being made. It is possible to express this hydrostatic stress-volumetric strain relationship in a closed form by curve fitting or

numerical methods, which will be useful in the formulation of constitutive equations for this material, but it must be pointed out that, at present, the expression so obtained will just be valid for the material tested (although at various densities) and it is not known whether another soil will behave similarly. For example, a soil with angular grains would certainly exhibit a greater compressibility than the material tested which has more or less rounded particles; a well-graded soil, capable of being packed to a greater density, may not be described by the holey model, because new contacts may be created at a different rate. If a general theory were to be developed for different kinds of soil, these variables would have to be included.

(2) Tests TCa and TEa

These tests were performed by increasing the deviatoric shear stress from zero while the mean stress was kept constant. The three principal displacements were measured in terms of ΔV_i and were plotted versus j, which is a measure of the shear stress, in Figs. (VI.4) to (VI.14). The volumetric deformation ΔV $(= \sum \Delta V_i)$ was also shown.

It can be seen that under both TC and TE stress conditions, the principal displacements were larger for samples which were loose than those for samples which were dense at the same stress levels. That means a loose sample deformed more than a dense one when subjected to the same stresses. This is expected, because in a dense sample there are more contacts between grains per unit volume. The load-resisting structure made up of the grains in contact is then more compact and not so flexible as in a loose soil. Moreover, slipping grains are surrounded by others to a greater extent and are hence not so easily able to slide.

In the plots to an arithmetical scale, Figs. (VI.4a) to (VI.14a), it is seen that the stress deformation relations were non-linear, with the displacements increasing more rapidly with respect to the shear stress. The displacements were also plotted on the logarithmic scale versus j on a linear scale, Figs. (VI.4b) to (VI.14b). It can be seen that, on many of the diagrams, an approximately linear relationship existed between the shear stress ($\sim$ j) and the logarithm of displacements ($\log \Delta V_1$). The slope of the straight line portion increased with density. The deviation from linearity was small in all the tests except TCa-6. The initial portions of the curves (i.e., at small shear stresses) deviated from the straight line, but at these levels of displacements, the measurements of the deformations were not accurate because of the correction factors. It is also the nature of the semi-logarithmic plot, with the origin at minus infinity. Therefore, as a first approximation, we may assume that there is a linear relationship between the shear stress and the logarithm of the principal displacements in both triaxial compression and triaxial extension stress states.

Tests TCa-6 and TEa-5 were different from the others in that the value of σ_{OCT} in these tests was 15 psi, while it was 20 psi in the others. Comparing Tests TCa-6 to TCa-2 and TEa-5 to TEa-2 (both members in each pair had nearly equal densities), it is seen that the displacements were larger where σ_{OCT} was smaller. Since only one test of each kind was performed with σ_{OCT} = 15 psi, it is impossible to draw any general conclusion about the dependence of the displacements upon σ_{OCT}.

On the stress-deformation plots, when the shear stress was increased to a certain point, there was a sudden increase in the displace-

ments for further shear stress increments, and subsequently a discontinuity could be found on the curves. This discontinuity is more readily identified on the semi-logarithmic plots, which were made mainly for this purpose. As explained in Chapter III, this discontinuity is herein defined to be "failure." Actually, since the shear stress was applied in increments, we can only locate the failure point within an interval. For example, in Fig. (VI.4b), although the discontinuity of the curves was drawn at $j = 10\frac{1}{2}$, failure actually occurred between $j = 10\frac{1}{2}$ and the next stress level, which in this case was $j = 11$.

Such a discontinuity and the interval defining the failure point were marked on the semi-logarithmic plot in each of Figs. (VI.4) to (VI.14). It is observed that in general this discontinuity was more obvious for a dense soil and became obscured for a loose soil. This is in agreement with the reasoning given in Chapter III, based on the consideration of energy stored and work done. However, this has to depend partly on the magnitude of the stress increments near the failure point. Had we been able to apply very small increments near the failure point, we may not be able to detect any discontinuity at all.

Failure occurred at different levels of shear stress for samples of different densities. In Fig. (VII.2), the value of Coulomb φ at failure of each sample is plotted versus the void ratio of the sample for both the triaxial compression and triaxial extension stress paths. It should be noted that the end points of the failure interval corresponds to the values of φ before and after failure. The two shaded bands in this figure define the failure zones for the sand tested under the two stress conditions. The value of φ increases with the density (or

decreases with e). Observe that Test TCa-6 (with σ_{OCT} = 15 psi) gave the same failure interval as TCa-2 (σ_{OCT} = 20 psi), while TEa-5 (σ_{OCT} = 15 psi) had a lower failure interval than TEa-2 (σ_{OCT} = 20 psi). Based on the limited information thus gathered, it is suggested that the position of the failure point does not depend on the value of σ_{OCT}.

In most cases, shearing was continued after the soil had failed. From the semi-logarithmic plots, with the limited information available, it is seen that another straight line could be roughly drawn for the stress-deformation relation after failure. This straight line has a flatter slope than the one before failure. Therefore, the informations obtained from Tests TCa and TEa indicate a bilinear shear stress-log (principal displacements) relationship for sand stressed once to failure and beyond.

The total volume change ΔV, calculated by direct summation of the three principal deformations ΔV_i, was also shown in Figs. (VI.4) to (VI.14). For loose soils, ΔV was positive (compression) in the beginning and then became negative (expansion) when failure was approached. When the density of the sample increased, the amount of initial compression decreased until for a dense sample (TEa-1 and TEa-2) ΔV was negative right from the beginning, and then decreased at a faster rate when failure was approached. At failure, samples of all densities were expanding. The magnitude of ΔV (positive or negative) was rather small at the initial stages of shearing but failure was always preceded by an increased rate of expansion.

In TCa-1 and TCa-2 where the samples were considered dense, a contraction was observed at the beginning, in contrast to what happened

in TEa-1 and TEa-2 where samples of the same density expanded. This leads to a tentative conclusion that the stress conditions may also affect the way a soil dilates.

That a soil would always expand as it fails was explained in Chapter III. It was pointed out that this is in agreement with the mathematical analysis of Drucker and Prager [39]. The concept of critical void ratio is not applicable here, because the deformations obtained in these tests were still small (< 2% strain) and the sample had not reached the ultimate condition.

In all but two (TCa-6 and TEa-2) of these tests, the sample was unloaded to the hydrostatic stress state. The amount of recoverable principal deformations, as measured during unloading, was small (~ 20%) compared to the total deformations immediately before unloading, although strictly speaking the latter included the plastic deformations occurring after the soil had failed. In view of this last fact, the proportion of elastic and plastic deformations will be discussed in connection with tests TCb and TEb in which unloading was performed below the failure stress level.

For the purpose of comparison, the results of a conventional triaxial compression test, taken from Bell [8] are reproduced in Fig. (VII.3), where the results of Test TCa-1 are also shown. It can be seen that the behaviors in these two tests were quite different. Although the initial behaviors of the soils in the two tests were quite similar, they began to deviate from one another as the tests proceeded, with the sample in the conventional test deforming considerably more than the present one. It was pointed out in Chapter II that the development of

failure planes in the presence of the rigid end plates in the conventional test was an indication of non-uniform deformation. During the early stages of the test, failure planes had not formed to any extent, and end friction was relatively unimportant; hence the behavior of the sample was about the same as that observed in the present test, in which the stress conditions were considered to be uniform throughout a test because of the flexible membranes. However, when the strains became bigger, the formation of failure planes in the cylindrical sample produced results which were only representative of the regions where the failure planes were formed. Relatively large movements took place on these planes, thus accounting for the large overall deformations observed, whereas in the present test the soil may have been free from such planes and it deformed uniformly.

An attempt has also been made to plot the results of the triaxial compression tests of this investigation in the stress-dilatancy plot as used by Rowe [24]. Whereas Rowe obtained straight line relationships from results of conventional triaxial compression tests, such relationships are not obtained here.

(3) Tests TCb and TEb

These tests were carried out by applying cycles of shear stress to the sample, while the mean stress was kept constant (15 psi). In each succeeding cycle, the octahedral shear stress was brought to a new high value and then reduced back to zero. The proportion of elastic and plastic deformations can be studied from the results of these tests.

The stress-deformation relations of TCb-1, TCb-2 and TEb-1 are shown in Figs. (VI.15), (VI.16) and (VI.17) respectively. Test TCb-1 should be compared with Test TCa-6, for they had the same value of σ_{OCT} (15 psi) and both samples had the same void ratio (0.535). Similarly, Test TEb-1 should be compared with Test TEb-5. However, since no TCa test was performed on a medium loose soil with σ_{OCT} = 15 psi, Test TCb-2 could only be compared with Test TCa-3 which had σ_{OCT} = 20 psi. In the semi-logarithmic plots of Fig. (VI.15) to (VI.17) are plotted the deformations in the samples when the shear stress was increased to a new high value.

From the arithmetical plots, it can be seen that these deformations were nearly the same as those when the shear stress had been reduced to zero and then increased back to this previous high value. Hence it is possible to draw an envelope to the stress-displacement curve through those points representing the displacements at the maximum values of the shear stress. This envelope was shown on the semi-logarithmic plot. By comparing these envelopes of Tests TCb-1 and TEb-1 to the stress-displacement curves in Tests TCa-6 and TEa-5, it is seen that the envelopes did not differ very much from the stress-displacement curves. This leads to the preliminary conclusion that the displacements in the soil do not depend on the stress history on the soil, provided that this stress history consisted only of loading and unloading along the same radial path on the octahedral plane, and that the soil has not been subjected to shear stress of magnitude greater than the present one. This observation is made based on the results of the two tests on a medium dense sand and with different stress paths (TC and TE).

If we compare the results of Test TCb-2 with those of Test TCa-3 (both were on medium loose sample), bearing in mind the difference in the values of the mean stress in these tests we may tentatively conclude that the observation made in the last paragraph is also valid here. We expect this observation to hold even in situations where we have a real three dimensional stress state, because, even though the stress conditions in these tests were TC and TE, the actual state of stress in the sample was quite homogeneous. Therefore, we reach the conclusion that for granular soils of all densities and under any stress state, the deformations before failure only depend on the existing shear stress, provided that previous loading and unloading occurred along the same radial path on the octahedral plane and that the soil has not been "prestressed" with a larger shear stress. The coincidence of the envelope and the virgin stress-deformation curve was also obtained on the plot of the total volume change ΔV $(= \sum \Delta V_i)$.

In these three tests, failure was observed to take place within the stress interval indicated on the plots. If we compare these intervals with those in the corresponding tests where no unloading was carried out on the sample (specifically j=9½ to 10 in TCb-1 to j=9 to 10 in TCa-6; j=6 3/4 to 7 in TEb-1 to j=6½ to 7 in TEa-5), we can conclude that the failure stress level of the soil in a medium dense state was not affected by previous loading and unloading along the same stress path. However, for a medium loose soil, such a conclusion cannot be drawn, partly because the value of σ_{OCT} used in TCb-2 was different from that in TCa-3. The sample in TCb-2 failed at a stress level lower than that in TCa-3. Maybe a loose soil is less stable than a dense one and is more easily

affected by the stress history. This point will be elaborated on later.

In these tests, as in the regular TCa and TEa tests, the sample always expanded when it began to fail, even though it might have contracted during the unloading cycles.

The unloading and reloading portions of the stress-principal displacement curves in these tests were fairly straight and the area of the hysteresis loop formed by them was quite small, except when the unloading was performed after the sample had failed, as in TEb-1 when unloading from and reloading to j=7 were carried out. As a first approximation, we can assume that unloading and reloading in shear in granular soils take place along the same straight line on the stress-displacement plot. Unloading after the sample had failed produced displacements which were far from linearly related to the stress, especially in the region of low shear stress. For unloading from stress levels below failure and the subsequent reloading, the approximate straight line stress-deformation relationships have slopes which decrease only slightly with the stress level from which unloading started. When this stress level was about midway to the failure state, we can assume that the slope was constant. From the plot of ΔV $(=\sum \Delta V_i)$ it can be seen that unloading was accompanied by a volume contraction in the sample, irrespective of whether the sample had expanded or contracted before unloading started. This means that the soil became stronger during the unloading process.

Since it had been concluded previously that unloading and reloading did not affect the virgin stress-deformation curve, we can treat the deformation recovered by unloading as the elastic portion of the total

deformation. This recoverable deformation is shown in Fig. (VII.4) as a percentage of the total deformation before unloading. It can be seen that the deformations were not all recoverable even at the lowest level of shear stress from which unloading was carried out. Due to the insensitivity of the apparatus and measuring devices, it was impossible to judge whether this was true at very small shear stress (e.g., $j=\frac{1}{2}$). However, it would appear from extrapolating the results shown in Fig. (VII.4) that the irrecoverable portion of the deformation at small shear stress would be quite small. While the ratio of elastic to total deformation was between 60 to 80% at the first shear stress level ($j=2$), this ratio decreased as the shear stress increased and was between 15 to 40% at failure. The elastic portion of the major principal deformation was always less than that of the minor principal deformation, and this comparatively large recoverable portion of the minor principal deformation probably accounted for the contraction of the sample during unloading.

We note also from Fig. (VII.4) that the proportion of elastic deformation was larger in a dense soil than in a loose one. This was anticipated from the consideration of the behavior of particles. Therefore, since a loose soil would undergo largely plastic deformations, from the failure point of view it was more sensitive than a dense one.

In Fig. (VII.4) are also shown the ratios of elastic to total principal deformations calculated for Tests TCa and TEa at the unloading cycle after failure has been passed. It is seen that for ΔV_1 this ratio has an average value of about 15% and for ΔV_3 it is about 30%.

In the following, loading and unloading tests in general (i.e., not TC or TE) are examined from an energy point of view in terms of the

energy supplies by the external stresses and the energy stored in the material.

In Figs. (VIII.5), the three principal stresses are plotted versus their respective principal strains. They are for a test in which $\sigma_1 + \sigma_2 + \sigma_3$ = constant, and σ_1, $\sigma_2 \geqslant \sigma_{OCT}$ and $\sigma_3 \leqslant \sigma_{OCT}$. The total energy input in the shearing portion of the test can be calculated as

$$E = \int_{\epsilon_o}^{\epsilon_1} \sigma_1 \, d\epsilon_1 + \int_{\epsilon_o}^{\epsilon_1} \sigma_2 \, d\epsilon_2 + \int_{\epsilon_o}^{\epsilon_3} \sigma_3 \, d\epsilon_3$$

$$= \int (a_1 j + \sigma_{OCT}) \, d\epsilon_1 + \int (a_2 j + \sigma_{OCT}) \, d\epsilon_2 + \int (a_3 j + \sigma_{OCT}) \, d\epsilon_3$$

$$= a_1 \int j d\epsilon_1 + a_2 \int j d\epsilon_2 + a_3 \int j d\epsilon_3 + \sigma_{OCT} \int (d\epsilon_1 + d\epsilon_2 + d\epsilon_3)$$

$$= a_1 A_1' + a_2 A_2' + a_3 A_3' + (A_1'' + A_2'' + A_3'')$$

$$= E_1 + E_2 + E_3 + E_4 \, . \qquad \text{(VII.1)}$$

Since $1/3 \, (\sigma_1 + \sigma_2 + \sigma_3) = \sigma_{OCT}$ = constant,

$$a_1 + a_2 + a_3 = 0 \, .$$

$$\epsilon_1 = \frac{(\Delta V_i / A)}{L} = \frac{\Delta V_i}{V} \, , \qquad i = 1, 2, 3 \, .$$

$$\therefore \; E_i = \frac{a_i}{V} \int_{\Delta V_o}^{\Delta V_i} j \, d(\Delta V_i), \qquad \text{(VII.2)}$$

assuming that V is constant, which is approximately true $\left(\frac{\Delta V}{V} < 1\% \right)$.

And
$$E_4 = \frac{\sigma_{OCT}}{V} \int d(\Delta V) \qquad \text{(VII.3)}$$

The integral in Eq. (VII.2) is the area under the arithmetic stress-principal deformation curves as plotted in Chapter VI. Therefore the E_i (i = 1, 2, 3) are the contribution from the shearing of the material. The integral in Eq. (VII.3) is the total volumetric change of the sample and hence E_4 is the contribution from the dilation of the material. It would appear at first sight that the presence of E_4 is rather surprising, and it may be neglected. However it must be remembered that granular soil is a dilatant material and it turns out that since $\frac{a_i}{\sigma_{OCT}}$, whose value can be calculated from Appendix A, is rather small (e.g., for a TC stress path, $a_1 = 0.115$, and $a_2 = a_3 = -0.057$), the contribution from E_4 is rather significant with respect to the other items.

Hence to calculate the energy input during loading, we just need to compute the area under each of the stress-deformation curves in the three principal directions, together with the summation of the volumetric change. Similarly, to calculate the energy release during unloading, we compute the corresponding areas under the unloading portions of the curves.

This indicated procedure has been carried out on the results of Tests TCb1, TCb-2 and TEb-1. Due to the limited number of unloading cycles in each test, it is only possible to draw the following conclusion: the amount of recoverable energy is only a small portion of the total energy input, about 20% for unloading from a medium value of j and

less than 5% for loading from a large value of j (say, after failure). For unloading from a small value of j, the contribution from the dilational effects is very pronounced, which, in view of the uncertainty involved in the membrane correction factors, makes the energy calculations doubtful for small values of the shear stress.

(4) Tests TCc and TEc

These tests were identical with Tests TCb and TEb, except when the shear stress was zero at the end of the unloading cycle, the hydrostatic stress on the sample was increased from 15 psi to 40 psi and then back to 15 psi. This cycle of hydrostatic stress was carried out with the main purpose of determining the effect of previous shear stress history on the hydrostatic compression of the material.

The volumetric compression of the sample during this cycle of hydrostatic stress is plotted in Fig. (VI.18c) for TCc-1, Fig. (VI.19c) for TCc-2 and Fig. (VI.20b) for TEc-1, for each value of j from which shear unloading commenced. The value of ΔV was calculated by direct summation of the three principal displacements ΔV_i, which, although not shown, were nearly equal when the previous maximum shear stress was small and became slightly unequal (with ΔV_3 showing more compression than ΔV_1) as this maximum shear stress increased, until failure was reached. That they were equal meant that the compression was isotropic. This leads to the conclusion that shear stress history in which the failure stress state has not been exceeded does not greatly affect the isotropy of the sample as far as can be determined by the apparatus employed in this investigation. The sample became increasingly anisotropic when

failure was approached. When the sample failed, the grains underwent large movements in a preferred direction, which produced a strong anisotropy in the sample.

By examining the compressibility curves of these tests, and comparing them to those where the soil had not been subjected to any shear stress at all (i.e., j=0), it is seen that the compressibility of the sample in all tests remained approximately unchanged by the shear stress history until failure was approached, and the volumetric compression was almost completely elastic. Near or after failure, the soil became more compressible, but this deformation was then less elastic. However, the recoverable portion was the same as before. In fact, the unloading portion of the compressibility curve was the same in all the hydrostatic cycles, irrespective of the maximum shear stress.

This can be explained from the results of previous tests. It has been found that the sample always expanded when it was near to failure, no matter in what density state it was, and that part of this expansion was irreversible when the shear stress was removed. Now when the soil was subjected to a hydrostatic stress increment, it was allowed to recover some of this expansion in addition to the real hydrostatic compression of the soil under hydrostatic stress. Since the expansion arose mainly from the contribution of ΔV_3, the hydrostatic stress increment now produced more compression in the ΔV_3 than in the ΔV_1 direction. When this hydrostatic stress increment was removed, only the real elastic hydrostatic isotropic compression could be recovered, leaving the recompression as an irrecoverable deformation. Since the elastic hydrostatic compression of sand depends only upon its density

(or void ratio), and because the density of the sample was only changed very slightly during shearing $\left(\frac{\Delta V}{V} \leq 0.05\% \right)$, it could be expected that the unloading portion of all the hydrostatic cycles following shear unloading to be the same. The recompression by hydrostatic stress following shear unloading was small when the maximum shear stress was small compared to the failure shear stress. Hence, we reach the conclusion that the hydrostatic compression of this sand is elastic and isotropic and remains unchanged by stress history which consists only of shearing in a radial line on the octahedral plane without producing failure.

By comparing these TCc and TEc tests with the last series (TCb and TEb), it can be seen from the stress-deformation plots that, except in Tests TCc-1 and TCb-1, there was a very good agreement between the virgin curves (i.e., the envelopes of the stress-deformation curves) in the other two pairs of tests in the series. It is the opinion of the author that the results of tests TCc-1 were unreliable, because, if the hydrostatic stress cycle on the sample after each shear loading produced only elastic, isotropic compression, the behavior of the sample upon reloading, especially when the shear stress returned to the virgin region, should not be affected. Hence, basing on the results of the other two tests in this group (i.e., TCc-2 and TEc-2), we may conclude that the shearing behavior of the soil does not depend upon any shear unloading interrupted by a hydrostatic stress history at zero shear stress.

The virgin stress-deformation curves of these three tests were also shown on a semi-logarithmic plot. It can be seen that failure occurred in the samples within the intervals shown. Again by comparison with TCb and TEb tests, we find that these intervals were the same in

both series, except in TCc-2. However, in TCc-2, the sample was a medium loose one, and the discontinuity was not obvious, perhaps due to the large stress increments near to failure. The difference between this and the corresponding TCb-2 was not large. Hence, the author tends to conclude that the failure strength was not affected by the hydrostatic stress cycle applied when the shear stress was unloaded to zero.

(5) Tests TCd and TEd

These tests were carried out by increasing σ_{OCT} when the sample was under a shear stress. The ratio of $\frac{\tau_{OCT}}{\sigma_{OCT}}$ (or $\frac{\sigma_1}{\sigma_3}$) was kept constant and τ_{OCT} increased proportionately with σ_{OCT}. They were carried out with the purpose of determining the effect of τ_{OCT} and σ_{OCT} on the deformations. The results are given in Figs. (VI.21), (VI.22) and (VI.23), where the principal deformations caused by σ_{OCT} increasing from 15 to 25 psi and decreasing to 15 psi are shown. The volumetric compression ΔV, calculated by direct summation of ΔV_i, is also plotted versus σ_{OCT} for different values of j.

It was thought that, as far as the stress path was concerned, the shearing deformations in the soil would depend on three factors: the magnitude of the shear stress τ_{OCT}, the magnitude of the mean stress σ_{OCT} and the ratio of these two. In these tests, the last quantity, represented by j, was held constant. Therefore, the deformation ΔV_i could be decomposed into two parts $(\Delta V_i)_\sigma$ and $(\Delta V_i)_\tau$. From the tests TCd and TEd, the interrelation of these two components could be determined with special reference to the elastic and plastic portions of each. It had been found in previous tests that the deformations due to an in-

crease in σ_{OCT} in a sample under a hydrostatic stress state were elastic and isotropic, and that the deformations caused by a shear stress τ_{OCT} confined on the octahedral plane were partly plastic and partly elastic. We hoped to find out whether the effect of a change in stress σ_{OCT} under the conditions in the present tests was elastic or not.

Referring to Figs. (VII.6), which illustrate the different deformation situations in the tests, points A represent the deformations in the sample when j increased to a new value with σ_{OCT} constant; points B represent the deformations when σ_{OCT} increased from 15 to 25 psi, with j constant; and points C represent the deformations when σ_{OCT} decreased from 25 to 15 psi, with j constant. The difference between A and B then represents the total deformation caused by $\Delta\sigma_{OCT}$ and $\Delta\tau_{OCT}$, which can be split into the elastic portion $(\Delta V_i)^e$ and the plastic portion $(\Delta V_i)^p$, i.e.,

$$(\Delta V_i)_A^B = (\Delta V_i)^e + (\Delta V_i)^p = (\Delta V_i)_\sigma + (\Delta V_i)_\tau$$

$$= \left[(\Delta V_i)_\sigma^e + (\Delta V_i)_\sigma^p\right] + \left[(\Delta V_i)_\tau^e + (\Delta V_i)_\tau^p\right]. \qquad \text{(VII.4)}$$

The elastic components in this deformation $(\Delta V_i)_\sigma^e$ and $(\Delta V_i)_\tau^e$, were recovered when σ_{OCT} decreased from 25 to 15 psi and their sum was equal to the difference between B and C, i.e.,

$$(\Delta V_i)_C^B = (\Delta V_i)^e = (\Delta V_i)_\sigma^e + (\Delta V_i)_\tau^e \; . \qquad \text{(VII.5)}$$

By subtraction, the difference between A and C represents the irrecoverable components of the deformation, i.e.,

$$(\Delta V_i)_A^C = (\Delta V_i)^p = (\Delta V_i)_\sigma^p + (\Delta V_i)_\tau^p \ . \qquad \text{(VII.6)}$$

At small vaues of j, $(\Delta V_i)_\sigma$ and $(\Delta V_i)_\tau$ were of comparable magnitude. While $(\Delta V_1)_\sigma$ and $(\Delta V_1)_\tau$ were both of the same sign (positive, representing a compression), $(\Delta V_3)_\sigma$ and $(\Delta V_3)_\tau$ were of different sign, with $(\Delta V_3)_\tau$ being an expansion. Therefore $(\Delta V_3)_A^B$ was composed of two quantities which tended to cancel each other. Thus, $(\Delta V_3)_A^B$ was observed to be smaller than $(\Delta V_1)_A^B$. Moreover, it was found in previous tests that both $(\Delta V_1)_\tau^p$ and $(\Delta V_3)_\tau^p$ were around 30% of ΔV_1 and ΔV_3 respectively for small values of j (see Figs. VII.4). If $(\Delta V_i)_\sigma$ was almost completely elastic (i.e., $(\Delta V_i)_\sigma^p \doteqdot 0$), then $(\Delta V_i)^p$ in Eq. (VII.6) would be equal to $(\Delta V_i)_\tau^p$. In other words, the irrecoverable portion of the deformation between A and B would be completely due to $(\Delta V_i)_\tau$.

i.e., $$(\Delta V_i)_A^C = (\Delta V_i)^p \doteqdot (\Delta V_i)_\tau^p \ , \qquad \text{(VII.7)}$$

and $$(\Delta V_i)_C^B = (\Delta V_i)^e = (\Delta V_i)_\sigma^e + (\Delta V_i)_\tau^e \ . \qquad \text{(VII.5)}$$

Or, $$(\Delta V_1)_C^B = (\Delta V_1)^e = (\Delta V_1)_\sigma^e + (\Delta V_1)_\tau^e \ , \qquad \text{(VII.5a)}$$

and $$(\Delta V_3)_C^B = (\Delta V_3)^e = (\Delta V_3)_\sigma^e + (\Delta V_3)_\tau^e \ . \qquad \text{(VII.5b)}$$

In Eq. (VII.5a), both $(\Delta V_1)_\sigma^e$ and $(\Delta V_1)_\tau^e$ are positive (compression). For small values of j, $(\Delta V_1)_\tau^e$ did not change rapidly with

respect to j. Indeed, if we postulate that $(\Delta V_1)_\sigma^e$ was constant with respect to j, then the sum of $(\Delta V_1)_\sigma^e$ and $(\Delta V_1)_\tau^e$ at j=2 should not differ appreciably from the sum of the same quantities at j=4 for example. It was indeed observed in the tests that $(\Delta V_1)_C^B$ was about constant for the first few values of j at which the value of σ_{OCT} was varied. At larger values of j, the deformation due to $\Delta \tau_{OCT}$ (i.e. $(\Delta V_1)_\tau$) became larger exponentially with j (remember the straight line on the semi-logarithmic plot of j versus deformation). However, the proportion of elastic deformation became smaller, around 30%. Therefore, $(\Delta V_1)_\tau^e$ was also increasing but rather slowly. By examining Figs. (VI.21a) to (VI.23a), it is found that indeed $(\Delta V_1)_C^B$ increased with respect to j. (Had the shearing deformation been completely plastic, $(\Delta V_1)_C^B$ would be constant at all values of j). By the same reasons, we expect $(\Delta V_1)^p \doteqdot (\Delta V_1)_\tau^p$ to increase rapidly with respect to j since both $(\Delta V_1)_\tau$ and the ratio of $(\Delta V_1)_\tau^p/(\Delta V_1)_\tau^e$ increased with j. This was indeed the case with the tests.

The same argument can be applied to ΔV_3, but here it is a little more complicated, because of the difference in directions of $(\Delta V_3)_\sigma$ and $(\Delta V_3)_\tau$. Depending on the relative magnitudes of these two quantities which in turn depended on j, we can have one of the two situations shown in Figs. (VII.6c) and (VII.6d). In Fig. (VII.6c) for small j, point B was to the right of point A, indicating that the compression of $(\Delta V_3)_\sigma$ was bigger than the expansion of $(\Delta V_3)_\tau$. Upon unloading of σ_{OCT}, $(\Delta V_3)_\sigma$ was completely recovered, but $(\Delta V_3)_\tau$ was about 60% recoverable. This brought us back to point C, with AC representing the 40% of $(\Delta V_3)_\tau$ which was irreversible. For a larger value of j, for example in Fig.

(VII.6d), the expansion of $(\Delta V_3)_\tau$ was larger than the compression of $(\Delta V_3)_\sigma$, thus point B was to the left of point A, indicating a net expansion. When $\Delta \sigma_{OCT}$ was removed, $(\Delta V_3)_\sigma^e$ and $(\Delta V_3)_\tau^e$ (which was about 30% of $(\Delta V_3)_\tau$) were recovered, bringing us to point C, with AC representing the irreversible portion of $(\Delta V_3)_\tau$.

The same reasons as used in the case of ΔV_1 now indicate that a slight decrease in the distance BC for ΔV_3, which represents the recoverable portion of ΔV_3, and a much faster increase in the distance AC which represents the irrecoverable portion of ΔV_3 should take place. Examination of Figs. (VI.21a) to (VI.23a) reveals that this is in agreement with the tests results.

In the above discussion, the assumption was made that $(\Delta V_i)_\sigma$ was completely elastic. This assumption was partly substantiated by the agreement of the experimental results with the conclusion reached from the reasoning above. This can be further shown to be a valid assumption by plotting ΔV $(= \Sigma \Delta V_i)$ versus σ_{OCT}. Writing Eqs. (VII.4) and (VII.6) in terms of ΔV instead of ΔV_i, we have

$$(\Delta V)_A^B = (\Delta V)^e + (\Delta V)^p \qquad \text{(VII.8)}$$

$$(\Delta V)_C^B = (\Delta V)^e = (\Delta V)_\sigma^e + (\Delta V)_\tau^e \qquad \text{(VII.9)}$$

$$(\Delta V)_A^C = (\Delta V)^p = (\Delta V)_\sigma^p + (\Delta V)_\tau^p \qquad \text{(VII.10)}$$

The loading portion of the $\Delta V \sim \sigma_{OCT}$ plots represents $(\Delta V)_A^B$, and the unloading portion represents $(\Delta V)_C^B$. It was found in previous tests that for shear stresses not near to failure, $(\Delta V)_\tau$ was small. Hence Eq. (VII.9) becomes

$$(\Delta V)_c^B = (\Delta V)^e = (\Delta V)_\sigma^e \qquad \text{(VII.9a)}$$

From Figs. (VI.21b) to (VI.23b), it can be seen that the unloading portion of each curve was the same in each test, for all values of j including j=0. This then proves the validity of the assumption that the compressibility by the increase in onctahedral stress with constant τ_{OCT}/σ_{OCT} was elastic.

The loading portions of the $\Delta V \sim \sigma_{OCT}$ curves represented both the plastic and elastic portions contributed by $\Delta \sigma_{OCT}$ and $\Delta \tau_{OCT}$. The contribution from $\Delta \tau_{OCT}$ was rather small and almost elastic except when failure was approached; it was then an expansion which was not completely recoverable. Hence for values of j near to and especially after failure, the loading portion of the curves would show an expansion, as for j=10 and 11 in Fig. (VI.21b) and for j=7 and $7\frac{1}{2}$ in Fig. (VI.23b).

We therefore reach the conclusion that the compression of a granular soil by a hydrostatic stress with a proportionate increase in the shear stress τ_{OCT} so that the ratio τ_{OCT}/σ_{OCT} remains constant can be decomposed into two parts, one from the contribution of $\Delta \sigma_{OCT}$ and the other from $\Delta \tau_{OCT}$. Each can be estimated separately from the results of the hydrostatic compression test HC and the tests TCb and TEb. In this sense, an uncoupling is achieved. Actually, the effects of τ_{OCT} and σ_{OCT} are still coupled because of the dilation of the material.

No attempt was made to draw an envelope for the stress-deformation curves in these tests, because such an envelope is difficult to define and depends on the increment in j after each cycle of σ_{OCT}.

Moreover the stress path did not lie completely on an octahedral plane. For the same reasons, failure was difficult to define for these tests. However, from Figs. (VI.21) to (VI.23), it appears that failure occurred between j=10 and 11 in Tests TCd-1, between j=8 and $8\frac{1}{2}$ in Tests TCd-2, and between 7 and $7\frac{1}{2}$ for Test TEd-1. The judgment was made by observing the shear displacements caused by $\Delta\ \sigma_{OCT}$, and by observing the relative positions of points similar to points A, Figs. (VII.6). If these failure intervals are taken to be correct, then they represent a higher stress level in all three cases than the corresponding Tests TCa-6, TCb-2 and TEa-5, where the sample was sheared directly to failure, (except in TCb-2 which is used for comparison because no TCa test was available near this void ratio with σ_{OCT} = 15 psi). However, the difference is quite small in these, and since this method of determining failure is not reliable, depending on the magnitude of the stress increments, it is suggested that not too big reliance should be put on these failure intervals.

(6) Tests TCe and TEe

These tests consisted of superimposing a hydrostatic stress state on top of the deviatoric stress state in the soil sample. The magnitude of the shear stress τ_{OCT} did not change during the application and removal of the hydrostatic stress, but the mean stress σ_{OCT} changed by an amount equal to the hydrostatic stress applied. At the same time, the ratio τ_{OCT}/σ_{OCT} decreased. Therefore, of the three factors (τ_{OCT}, σ_{OCT}, and τ_{OCT}/σ_{OCT}) which were thought to influence the deformation in the soil, only two were varied in these tests, and by the loading and unloading of the hydrostatic stress, we hoped to distinguish the effects of each

of these two factors. The results of these tests are shown in Figs. (VI.24) to (VI.26).

In the Test Series TCd and TEd, results of previous, simpler, tests were used to predict the behavior of those tests, and it was found that good agreement was obtained between the predictions and the experimental observations. The same procedure will be attempted here.

Referring to Figs. (VII.7), which illustrates the different deformation situations in the present tests, points A represent the deformations in the sample after j had been increased to a new value with σ_{OCT} constant; points B represent the deformations in the stage, when σ_{OCT} was increased from 15 to 40 psi, with j constant (however, it was explained in Section 3 of Chapter VI that j actually decreased and then increased back to its original value during the cycle of hydrostatic stress; but for convenience of plotting, it was treated as constant; actually it was τ_{OCT} that was constant); points C represent the deformations when σ_{OCT} was decreased from 40 to 15 psi, with j constant. The difference between A and B then represents the total deformation caused by $\Delta\,\sigma_{OCT}$ and $\Delta\left(\frac{\tau_{OCT}}{\sigma_{OCT}}\right)$, which can be split into the elastic portion $(\Delta\,V_i)^e$ and the plastic portion $(\Delta\,V_i)^p$ as follows:

$$(\Delta\,V_i)_A^B = (\Delta\,V_i)^e + (\Delta\,V_i)^p = (\Delta\,V_i)_\sigma + (\Delta\,V_i)_{\tau/\sigma}$$
$$= \left[(\Delta\,V_i)_\sigma^e + (\Delta\,V_i)_\sigma^p\right] + \left[(\Delta\,V_i)_{\tau/\sigma}^e + (\Delta\,V_i)_{\tau/\sigma}^p\right]. \qquad \text{(VII.11)}$$

The elastic components in this deformation, $(\Delta\,V_i)_\sigma^e$ and $(\Delta\,V_i)_{\tau/\sigma}^e$, were recovered when σ_{OCT} decreased from 40 to 15 psi and their sum was equal to the difference between B and C, i.e.,

$$(\Delta V_i)_C^B = (\Delta V_i)^e = (\Delta V_i)_\sigma^e + (\Delta V_i)_{\tau/\sigma}^e \qquad \text{(VII.12)}$$

By subtraction, the difference between A and C then represents the irrecoverable components of the deformation, i.e.,

$$(\Delta V_i)_A^C = (\Delta V_i)^p = (\Delta V_i)_\sigma^p + (\Delta V_i)_{\tau/\sigma}^p \qquad \text{(VII.13)}$$

As in the last Section, we make the assumption that $(\Delta V_i)_\sigma$ was completely elastic, i.e., $(\Delta V_i)_\sigma^p = 0$. The effect of τ_{OCT}/σ_{OCT} is more complicated, and we have to go back to Tests TCa and TEa and TCb and TEb in order to find out this effect. In the first set of tests, τ_{OCT} was increased monotonically until the soil failed. During this shearing, the ratio τ_{OCT}/σ_{OCT} also increased. But in the present tests, τ_{OCT}/σ_{OCT} decreased from a maximum value at A to a minimum value at B. At the next cycle of hydrostatic stress, τ_{OCT}/σ_{OCT} decreased from a new maximum value at A. Therefore, as far as the value of τ_{OCT}/σ_{OCT} was concerned, the stress conditions between A and B were similar to unloading from the virgin curve which had τ_{OCT}/σ_{OCT} as its ordinate, and the conditions between B and C were similar to reloading along the same stress path. Now if we consider that the unloading and reloading cycles of TCb and TEb were performed with τ_{OCT}/σ_{OCT} as the variable instead of τ_{OCT} (σ_{OCT} was constant), we can employ the results of those tests in connection with the present context.

From the results of TCb and TEb, we found that the unloading of τ/σ produced deformations which were relatively small and varied linearly with j. The reloading of τ/σ produced deformations which in general were approximately linear and the hysteresis loop between the

unloading and reloading portions of the curve was small. The deformation during unloading would, in the present tests, be represented by $(\Delta V_i)_{\tau/\sigma}$ and that during reloading by $(\Delta V_i)^e_{\tau/\sigma}$. Had there been no hysteresis loop, these two quantities would be equal, i.e., $(\Delta V_i)^p_{\tau/\sigma}=0$. But the presence of the small hysteresis loop meant that $(\Delta V_i)^p_{\tau/\sigma}$ was not zero but a small quantity.

This, together with the assumption that $(\Delta V_i)^p_\sigma=0$, indicates that Eq. (VII.13) will become

$$(\Delta V_i)_A{}^C = (\Delta V_i)^p = (\Delta V_i)^p_{\tau/\sigma} = \text{small}. \qquad \text{(VII.13a)}$$

In Eq. (VII.11), written for ΔV_1, the contribution of $(\Delta V_1)_\sigma$ was a compression and that of $(\Delta V_1)_{\tau/\sigma}$ was an expansion, since τ/σ was unloading. These two tended to balance each other and, therefore, the net result, $(\Delta V_1)_A{}^B$ would be comparatively small. However, for ΔV_3, both contributions from $(\Delta V_3)_\sigma$ and $(\Delta V_3)_{\tau/\sigma}$ were compression and they produced the same effects. For small values of j from which τ/σ began to unload, $(\Delta V_i)_{\tau/\sigma}$ would be small, but it increased with the value of j. Therefore at small j, the compression of $(\Delta V_1)_\sigma$ predominated the expansion of $(\Delta V_1)_{\tau/\sigma}$ and hence $(\Delta V_1)_A{}^B$ should show a net compression. At this value of j, the hysteresis loop was almost negligible; hence $(\Delta V_1)_A{}^C = (\Delta V_i)^p$ was very small as in Fig. (VII.7). At the next value of j from which unloading of τ/σ began, $(\Delta V_1)_{\tau/\sigma}$ increased slightly over the last cycle, and the net change $(\Delta V_1)_A{}^B$ would now be smaller than before. At the same time, the hysteresis loop was more noticeable now, and hence $(\Delta V_1)_A{}^C$ became larger. As the value of j increased, we might reach a situation as shown in Fig. (VII.7b), in which the expansion

of $(\Delta V_3)_{\tau/\sigma}$ was greater than the compression of $(\Delta V_1)_\sigma$ and then the reloading of τ/σ did not recover $(\Delta V_1)_{\tau/\sigma}$ completely, leaving point C to the right of point B. Examination of the test results shows that these behaviors actually occurred.

The same reasoning can be applied to ΔV_3. Here both $(\Delta V_3)_\sigma$ and $(\Delta V_3)_{\tau/\sigma}$ were compression. We expect $(\Delta V_3)_\sigma$ to remain constant while $(\Delta V_3)_{\tau/\sigma}$ to increase with j, resulting in an increase in $(\Delta V_3)_A^B$. We also expect that $(\Delta V_3)^p_{\tau/\sigma}$ to increase with j, as the hysteresis loop became bigger, thus $(\Delta V_3)_A^C$ would be small at first (in Fig. (VII.7c)) and would become larger as j increased (as in Fig. (VII.7d)). Examination of the test results reveals that these observations were borne out by experiment.

In the above, the assumption was made that the $(\Delta V_i)_\sigma$ remained the same at all values of j from which unloading of τ/σ took place and was elastic. That the conclusions reached from the above arguments were in agreement with the test results substantiated this assumption which can also be shown to be valid in the following where ΔV $(=\Sigma \Delta V_i)$ was plotted versus σ_{OCT}. Writing Eqs. (VII.11) to (VII.13) in terms of ΔV, we have

$$(\Delta V)_A^B = (\Delta V)^e + (\Delta V)^p \qquad \text{(VII.14)}$$

$$(\Delta V)_C^B = (\Delta V)_\sigma^e + (\Delta V)^e_{\tau/\sigma} \qquad \text{(VII.15)}$$

$$(\Delta V)_A^C = (\Delta V)_\sigma^p + (\Delta V)^p_{\tau/\sigma} \qquad \text{(VII.16)}$$

The loading portion of the $\Delta V \sim \sigma_{OCT}$ plots represents $(\Delta V)_A^B$, while the unloading portion represents $(\Delta V)_C^B$. Since the hysteresis

loops in the $\Delta V \sim j$ plots of tests TCb and TEb were qualitatively the same as those in the $\Delta V_i \sim j$ plots, we can use the same reasoning as before and reach the conclusion that $(\Delta V)^p_{\tau/\sigma}$ was negligible for small values of j and increased slightly with j. Hence $(\Delta V)_A^C$, which is the irreversible component at the end of the cycles in the $\Delta V \sim \sigma_{OCT}$ plots of Figs. (VI.24b) to (VI.26b), would increase with j. This was indeed the case in those plots. That, at small values of j, we have almost complete recovery meant that $(\Delta V)_\sigma$ was indeed elastic.

The loading portions of these $\Delta V \sim \sigma_{OCT}$ plots consisted of contributions from $(\Delta V)_\sigma$ and $(\Delta V)_{\tau/\sigma}$. Since τ/σ was unloading, $(\Delta V)_{\tau/\sigma}$ would be a compression, as deduced from the $\Delta V \sim j$ plots of Tests TCb and TEb. As the value of j, from which τ/σ unloading took place, increased towards failure, it was found before that the sample was in the process of expanding. Now the τ/σ unloading would recover part of this expansion and hence at large values of j, we find a noticeably larger compression. However, as τ/σ reloaded, this compression was largely recovered and an expansion resulted. Therefore the compressibility of the sample under σ_{OCT} became larger and yet it was still largely reversible. At the small values of j, the compression due to the unloading of τ/σ was small; the compression was thus mainly from the contribution of $(\Delta V)_\sigma$. It was found that at the first value of j, the compressibility was indeed the same as for a soil compressed by a purely hydrostatic stress. We can therefore conclude that the compression of this granular soil by a hydrostatic stress superimposed upon a deviatoric stress is made up of two parts: the first is a contribution from the increase in σ_{OCT} and has the same characteristics (i.e., elastic, isotropic)

as if the same $\Delta \sigma_{OCT}$ were applied on top of a hydrostatic stress state; the second is a contribution from the decrease in τ_{OCT}/σ_{OCT}, which is largely elastic. The contribution from each component can be predicted from the hydrostatic compression test (HC) and from the loading and unloading tests (TCb and TEb). There is an uncoupling between the effects of σ_{OCT} and τ_{OCT}, in the sense that the above components can be estimated separately and then superimposed. But actually a coupling exists because of the dilational effect of the material, (i.e., ΔV caused by τ_{OCT}) and because of the fact that increasing σ_{OCT} creates shearing deformation through the effect of τ_{OCT}/σ_{OCT}.

For the same reasons as given in the last Section for tests TCd and TEd, no attempt was made to define an envelope for the stress-deformation curves. However, if we try to define failure by observing the relative positions of the points similar to points A, Fig. (VII.7), we can roughly define the failure intervals to be j = 9-10 for TCe-1, j=7-7$\frac{1}{2}$ for TCe-2 and j=6-6$\frac{1}{2}$ for TEe-1. These intervals are all lower than those in the corresponding Tests TCa-6, TCb-2, and TEa-5. However, the difference is small and for practical purposes, we may treat them as equal. When we compare some of the stress-deformation curves with those in the regular tests (e.g., ΔV_1 in TCe-1 and TCa-6) we find that they are nearly identical. This and the observation on the small difference in the failure intervals are consequences of the elastic deformations along the stress path in the present tests.

(7) Radial Shear Tests

These tests were similar to Tests TCa and TEa in that the sample was sheared from a hydrostatic stress state by monotonically increasing the octahedral shear stress, while the mean stress was kept constant. (TCa and TEa are equivalent to RS90° and RS30° respectively.) But in these tests, the stress condition was no longer a triaxial one, and hence they were truly three-dimensional tests. These tests were each carried out on a medium dense and a medium loose sample and the results were shown in Figs. (VI.27) to (VI.32) by plotting the three principal displacements and the total volume change versus the shear stress ($\sim j$) linearly and semi-logarithmically.

It is interesting to note that the intermediate principal displacements were comparatively small with respect to the major and the minor displacements. For RS45°, in which the intermediate principal stress was increasing on loading, ΔV_2 was a compression (positive). Upon unloading, ΔV_2 expanded. For RS75°, in which the intermediate principal stress was decreasing, ΔV_2 was an expansion (negative) and during unloading, ΔV_2 was a compression. For RS60° in which the intermediate principal stress remained constant, ΔV_2 was negligibly small until the shear stress was fairly large and then it was a compression in both the dense and the loose samples. Upon unloading in both samples, ΔV_2 continued to be a compression.

In these tests, the intermediate principal stress was different from both the major and the minor principal stresses. According to Scott [4], who reached the following conclusions by analyzing regular packings, the soil developed a preferred plane of shearing under these

conditions, which was parallel to the direction in which σ_2 acted. Shearing, therefore, took place mainly by the movement of the sample normal to the σ_2-direction. This would explain why the observed displacement in the σ_2-direction was small compared to those in the σ_1 and σ_3 directions.

On the semi-logarithmic plots of displacements versus shear stress, it is seen that once again, as in Tests TCa and TEa, there was a roughly linear relationship between the octahedral shear stress and the logarithm of principal displacements with the slope of the straight line increasing with density of the material. That such observations had been made in various tests in which shearing was accomplished by keeping the mean stress constant and increasing the shear stress from zero along a straight line in different directions on the octahedral plane is useful for the purpose of formulating constitutive relationships.

Again, as for Tests TCa and TEa, the data showed an increase in the rate of deformation with respect to the shear stress and a discontinuity could be drawn in the curve joining them. Hence we determine the interval within which failure occurred in the soil. These discontinuities were more obvious than those in Tests TCa and TEa, especially on the semi-logarithmic plots. Whether this was due to the fact that the soil had a preferred direction of shearing is not known.

The failure intervals for a medium dense ($e \doteqdot 0.52$) and a medium loose soil ($e \doteqdot 0.61$) under stress conditions of TC, TE, RS45°, RS60° and RS75° are shown in Fig. (VII.8), where the results are plotted on an octahedral plane. The interval for $e \doteqdot 0.52$ under TC is obtained by

interpolation in Fig. (VII.2), while other intervals are obtained from tests on medium dense samples under the corresponding test conditions. The intervals could be plotted by measuring from the origin O at a distance proportional to j along the respective radial paths, or by calculating the value of the equivalent Coulomb angle φ. A shaded band was drawn for each soil, indicating the region where the failure point must lie for soil sheared to failure along a radial path.

For the purpose of comparison, lines are drawn in Fig. (VII.8) to represent the different values of the equivalent Coulomb φ. These are straight lines joining the points on the TC and TE lines, where φ has a real meaning. It is seen that the value of the equivalent Coulomb φ obtained by experiment is smallest in TC and largest in TE, and is monotonically increasing in between. That φ has to take on a larger value under stress conditions where there is no axial symmetry than in the TC condition was explained by Scott [4], who attributed it to the fact that the soil has to exact a penalty for the presence of a preferred direction of shearing by requiring a higher value of φ at failure. He analyzed the failure by slipping on hexagonal planes of a face-centered packing under triaxial compression conditions, whereby sphere B, Fig. (VII.9a), moves over the valley between the spheres E and F which are on a lower hexagonal plane, and obtained the following relationship for φ in terms of the coefficient of friction μ,

$$\tan \varphi = \frac{\sqrt{3} + 4\sqrt{2}\,\mu}{2(\sqrt{6} - \mu)} \qquad \text{(VII.17)}$$

If we assume failure under triaxial extension stress state to occur by sphere B moving over G, and perform the same calculation as Scott, we obtain the following relationship for φ ,

$$\tan \varphi = \frac{1 + \sqrt{2}\,\mu}{\sqrt{2} - \mu} \qquad \text{(VII.18)}$$

Eqs. (VII.17) and (VII.18) are plotted in Fig. (VII.9b) and it can be seen that for the values of μ shown, φ in TE is always greater than φ in TC. This calculation is not meant to correlate the values of φ obtained experimentally on the real soil to those obtained from the analysis of regular packings, but is presented merely for the purpose of illustrating why there can be a difference in φ in the two stress conditions.

In the same figure, the "yield" envelope obtained by Bell [8] for the same Ottawa sand as used in this investigation at a void ratio of $e \doteqdot 0.52$ was presented for comparison. (Bell used $\sigma_{OCT} = 18$ psi.) It is seen that Bell's value of φ in TC was 38°, 4-6° lower than that obtained here and the value of φ in TE was 52°, which was 4° higher than that obtained here. Whereas the difference between φ_{TC} and φ_{TE} was 14° in Bell's work, it is only 4-6° here. Results of conventional triaxial compression and extension tests show that φ_{TC} and φ_{TE} are about the same [10,11]. Remembering the stress inhomogeneity in these conventional tests and the homogeneity in the present tests, we conclude that inhomogeneity tends to reduce the difference in φ_{TC} and φ_{TE}. Bell's tests were also inhomogenous, yet he obtained a bigger difference in φ_{TC} and φ_{TE} than here. This may be due to anisotropy in his samples, which must have the opposite effect as stress inhomogeneity. From this

we conclude that the degree of anisotropy in Bell's tests was quite large, and that the failure envelopes determined in this investigation are a better representation of the actual failure state of the material.

In Figs. (VI.27) to (VI.32), it is seen that although most of the samples (except in RS45° -1 and RS45° -2) contracted at the initiation of shearing, they all expanded when the failure state was approached, confirming the observations made in connection with Tests TCa and TEa. Hence we can conclude that granular soils must expand when they are sheared near failure.

The stress path RS60° was of special interest in that the intermediate principal stress σ_2 remained constant along this path. From the results of RS60° -1 on a medium dense soil and RS60° -2 on a medium loose soil, we see that the displacements in the σ_2-direction were not zero but consisted of a compression. The question arises as to where on the octahedral plane the stress path corresponding to the plane strain conditions lies. Under plane strain conditions, there is no strain in one of the principal directions. Observing that ΔV_2 was positive in RS60° and negative in RS75°, we see that the stress path which would give rise to plane strain shearing must lie between the RS60° and RS75° radial paths, being closer to the former than to the latter. However, it must be emphasized that such a path is not necessarily a straight line.

On the basis of the limited amount of data on the deformation of the samples after failure had been reached, the bilinear relationship of shear stress ~ log (principal displacements) seems to hold approximately for three-dimensional shearing as well as in triaxial shearing.

This is only tentative, because the present investigation was mainly concerned with the pre-failure behavior of the material.

(8) Anisotropy Tests

These were tests performed by rotating the axes of the stress system on the sample, with the purpose of determining any anisotropy in the sample caused by the method of preparation. Test A-1 should be compared with Test TCa-2, and A-2 with RS60° -2, as both members in each pair had nearly the same density and the same stress path. Results of Tests A-1 and A-2 were shown in Figs. (VI.33) and (VI.34) respectively.

By comparing Fig. (VI.33) to Fig. (VI.5) and Fig. (VI.34) to Fig. (VI.30), it is seen that the general behavior of the soil was not affected by the rotation of the axes of the stress system. A remarkable correspondence in the magnitude of the three principal displacements in the two tests A-2 and RS60° -2 (with medium loose samples) was evident, whereas there was a not very big difference in the results of Tests A-1 and TCa-2. In the latter pair of tests, both samples failed between the same stress interval (j=9 and 10) and both samples started to expand at the same stress level (j=8). In the former pair of tests, both samples started to expand at $j=5\frac{1}{2}$, but the sample of A-2 failed between $j=6\frac{1}{2}$ and $6\frac{3}{4}$, whereas that of RS60° -2 failed between $j=6\frac{1}{4}$ and $6\frac{1}{2}$. However, the last discrepancy was not great.

Although complete agreement was not obtained from these anisotropy tests with the respective regular tests, it is felt that the degree of anisotropy in the sample induced by the method of preparation

was not great. (This does not include the stress-induced anisotropy, which is inherent in the shearing of granular material.) It is, therefore, proposed to treat the samples tested in this investigation as isotropic. This assumption is desirable because the analysis of the test results would have been very difficult had the samples been treated as anisotropic.

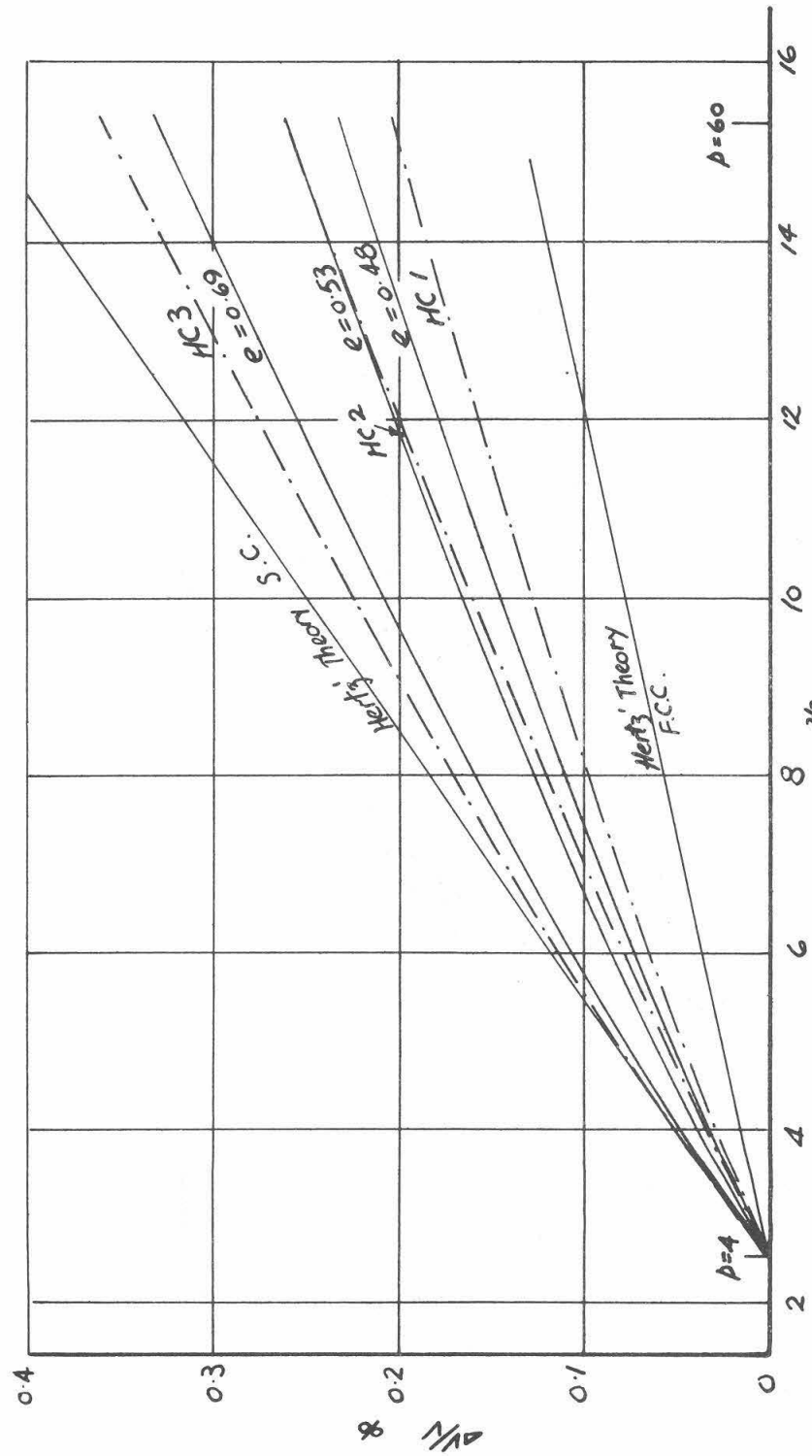

FIG. (VIII.1). HYDROSTATIC TESTS – COMPARISION WITH THEORY

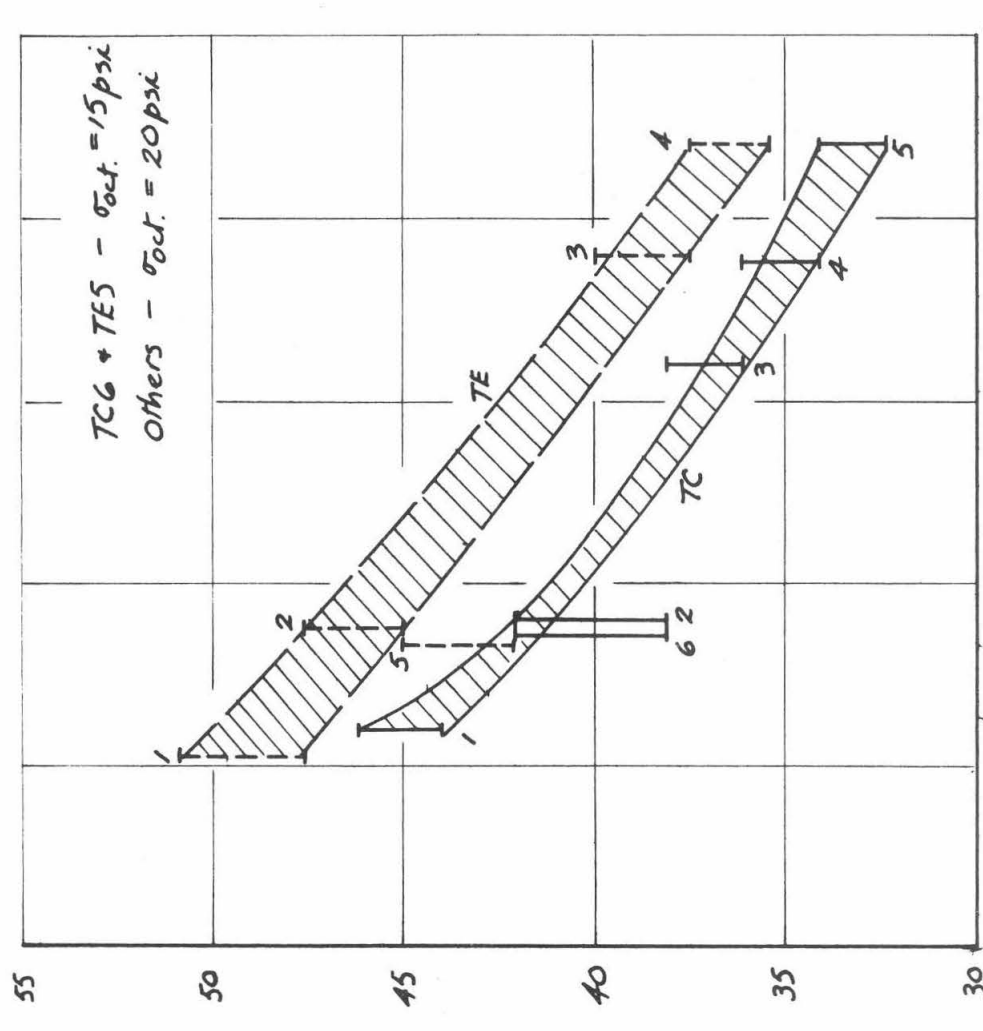

FIG. (VIII.2). φ VERSUS e IN TC AND TE

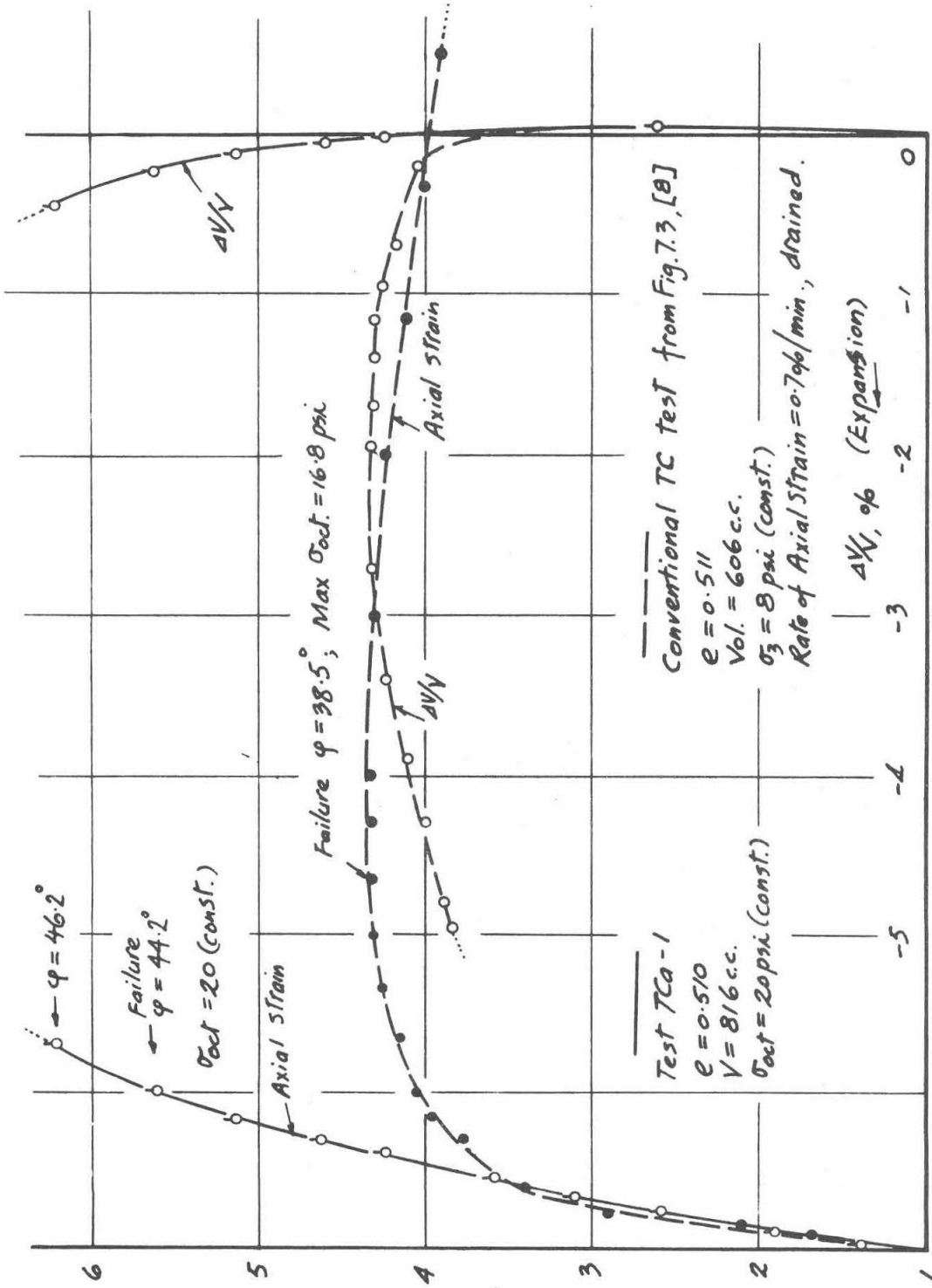

FIG. (VII.3). RESULTS OF CONVENTIONAL TC TEST AND TEST TCa-1

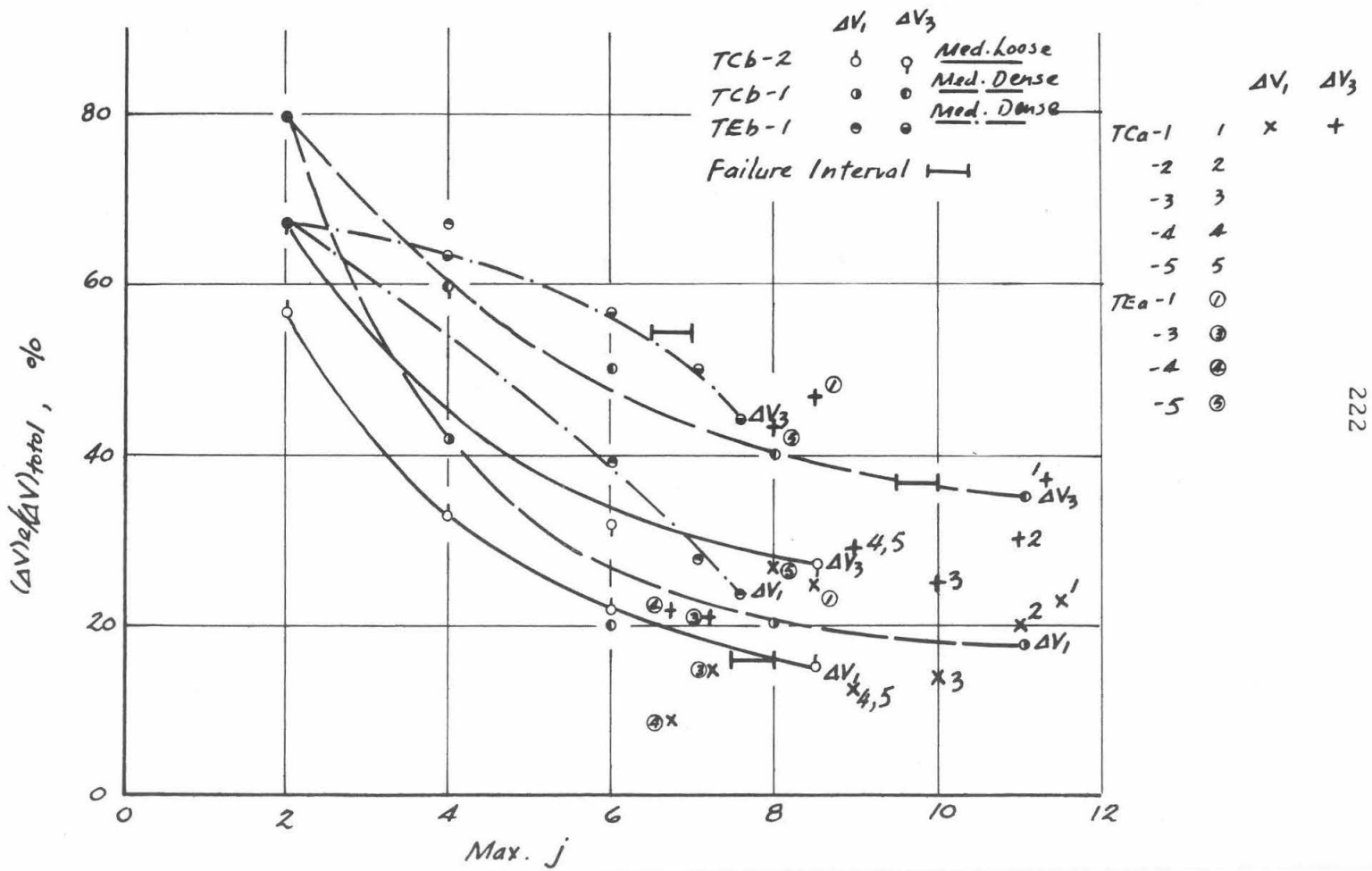

FIG. (VII.4). RATIOS OF ELASTIC TO TOTAL DEFORMATIONS

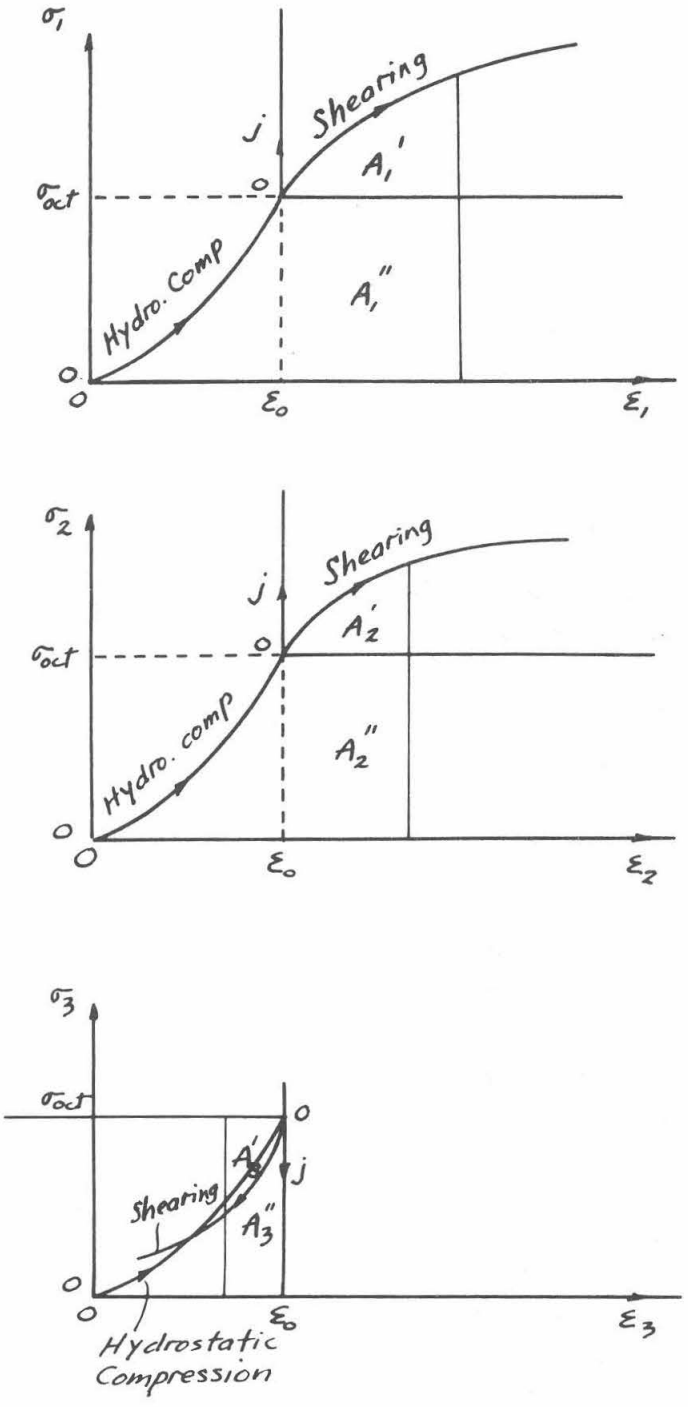

FIG. (VII.5). ENERGY SUPPLY IN SHEAR TESTS.

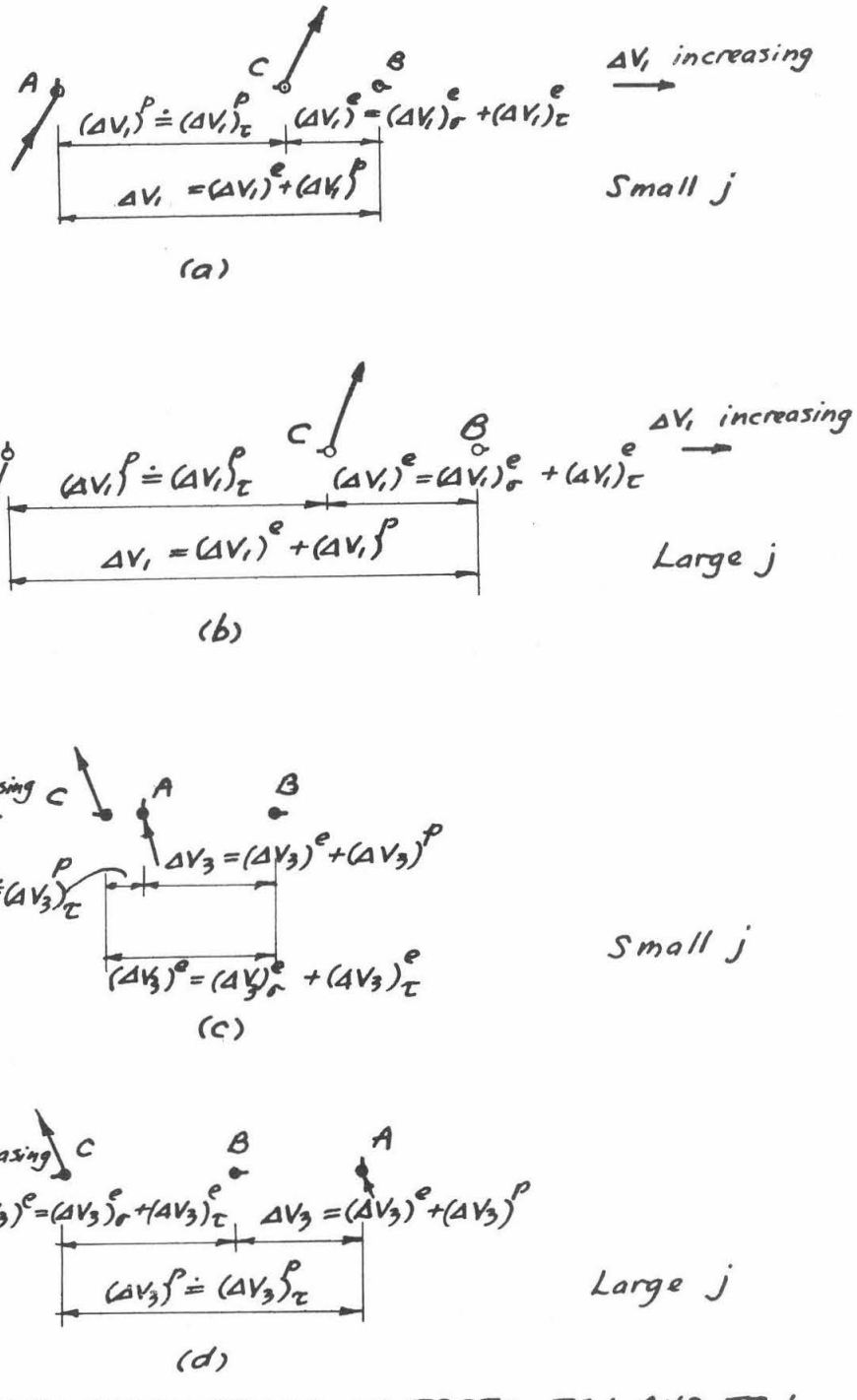

FIG. (VII.6) DEFORMATIONS IN TESTS TCd AND TEd.

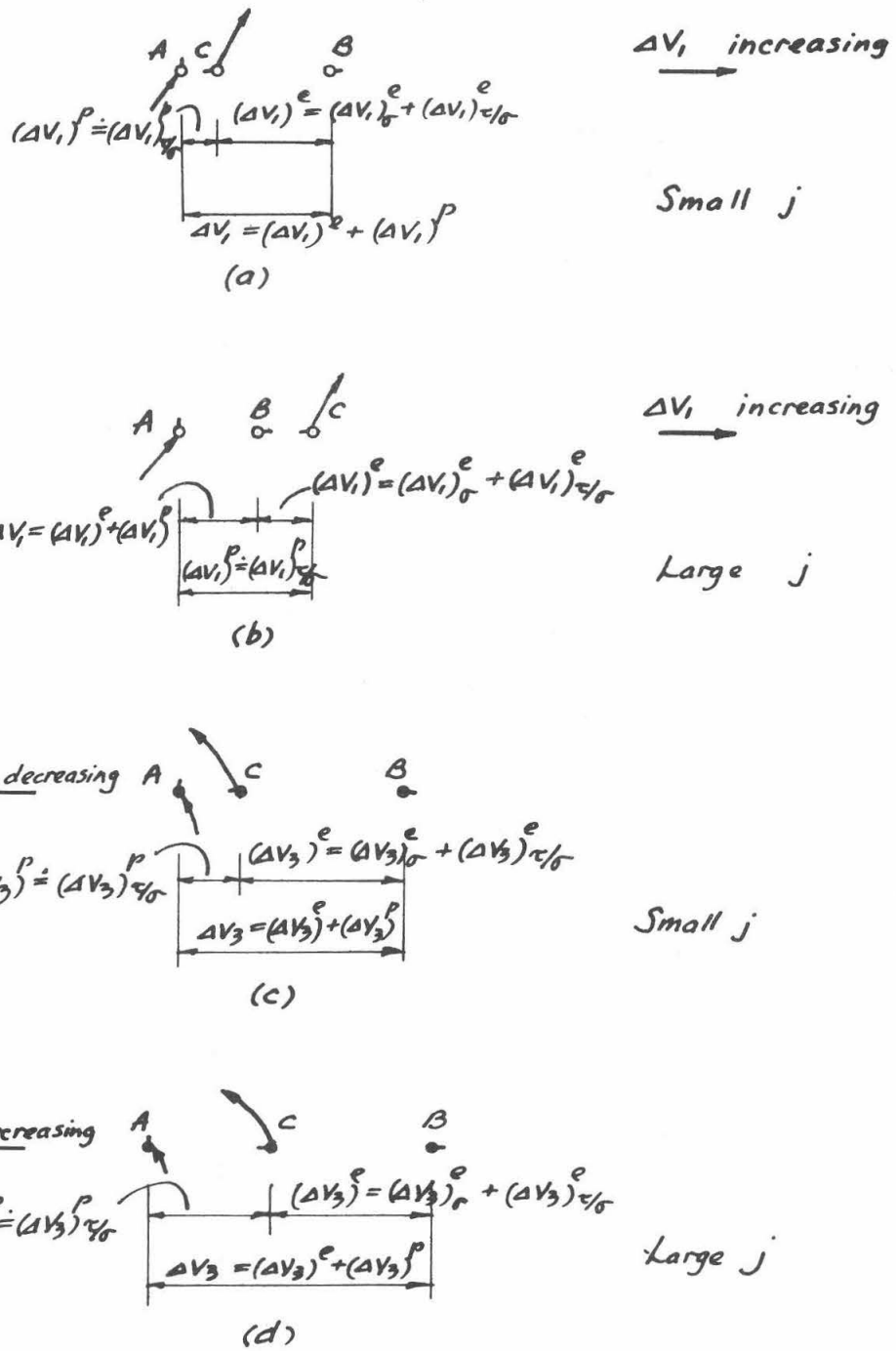

FIG. (VII.7). DEFORMATIONS IN TESTS TCd AND TEe

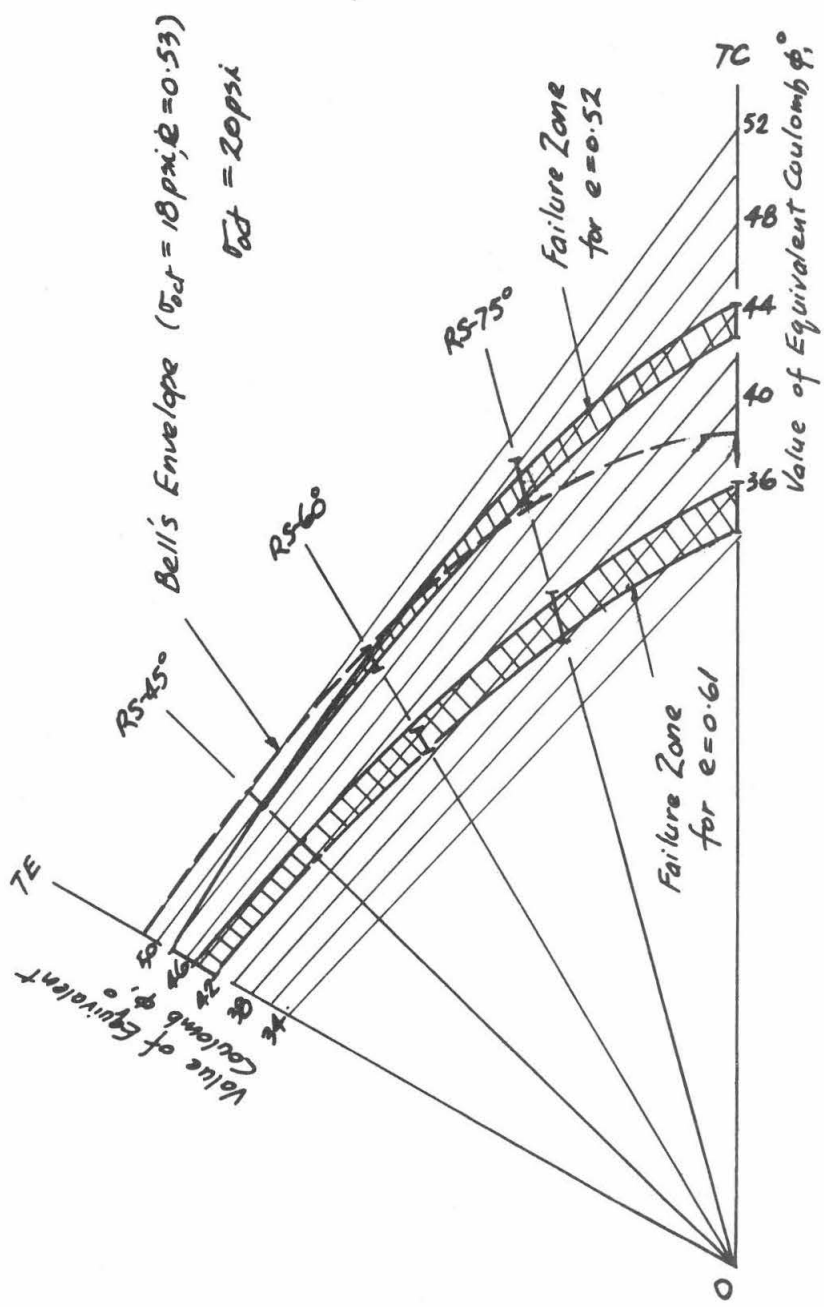

FIG. (VII. 8). FAILURE ENVELOPES FOR OTTAWA SAND

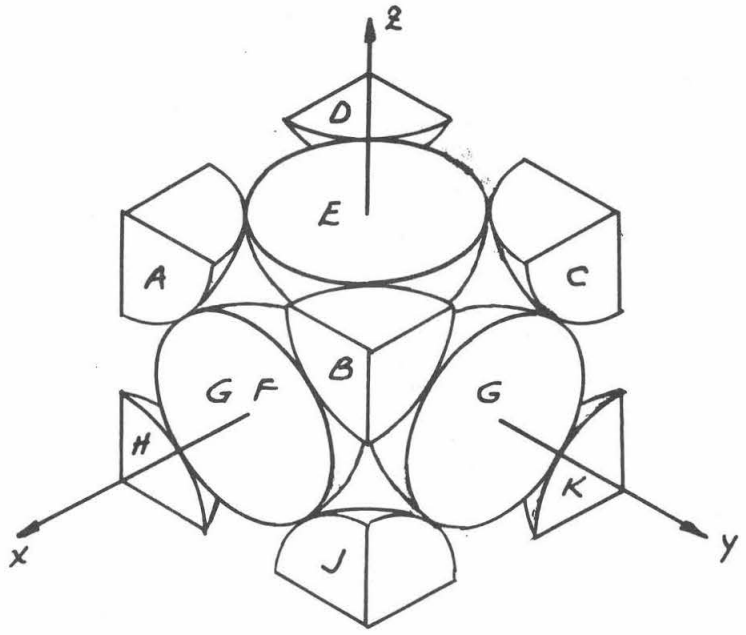

(a)

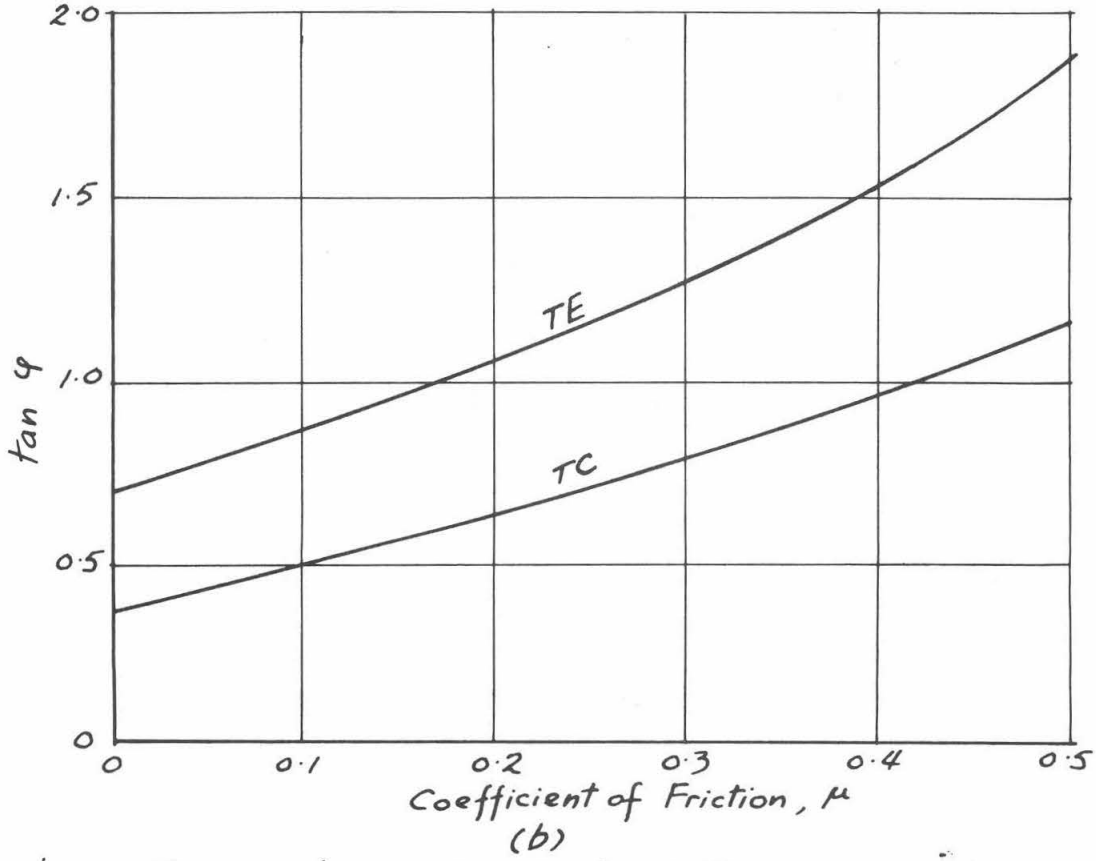

(b)

FIG. (VII.9). VALUES OF TAN ϕ IN TC AND TE FOR F.C.C. PACKING, AS FUNCTIONS OF μ.

CHAPTER VIII

SUMMARY, CONCLUSIONS AND RECOMMENDATIONS FOR FUTURE WORK

(1) Summary

The following is a summary of the results of the theoretical considerations and experimental investigation described earlier in this thesis. It is assumed and substantiated by test studies that the soil samples tested were homogeneous and initially isotropic and that a homogeneous stress state was applied to the sample by rubber membranes. It is also assumed that the stress control device varied the stresses on the sample in a continuous manner and the stresses indeed traced the stress path desired.

A theoretical "holey" model for the compressional behavior of sand under hydrostatic stresses was postulated in Chapter III, the analysis of which showed that the compression of sand by a hydrostatic stress is isotropic and completely elastic. Although the Hertzian contact theory was postulated to hold at each contact where only normal forces were assumed to exist, the presence of potential contacts which were made by successively larger external pressures resulted in a stress-strain relationship in which the volumetric strain does not vary as the two-thirds power of the hydrostatic stress (as predicted by the Hertzian theory), but increases less rapidly than the two-thirds power, showing a strain hardening effect due to the increased number of contacts which form the load-resisting structure.

An almost complete recovery of the volumetric strain was obtained for samples of different densities, indicating that, under external hydrostatic pressure, the tangential forces acting at the contacts between grains were indeed small, and the grains compressed and rebounded elastically under normal forces. The close correlation between the compressibility predicted by the theory of holey models and that obtained experimentally shows that the concept of potential contacts being closed by successively larger pressure may represent a correct picture of the behavior.

In the theory of holey models, the grain size distribution of the soil does not appear and the controlling parameter is the density of the soil (expressed in terms of n or e). Although the angularity is partially taken care of by the radius of curvature of the grains at points of contact, it remains to be proved that this theory would still hold for soils other than the Ottawa sand tested which is fairly uniformly graded and whose grains are rounded. However, the concepts of successive contacts being made will presumably hold for all kinds of granular soil, and it is thought that, after a few cycles of hydrostatic stress to stabilize the critically unstable grains, the hydrostatic compression of all granular soils may well be elastic.

The qualitative behavior of sand under a shear stress was examined at the particulate level and some simple loading and unloading tests involving combinations of hydrostatic and deviatoric stress states were performed to verify the intuitive concepts of the shearing behavior of sand. This was necessitated by the lack of information from the results of other research work in this field. It was thought that these

experiments might help our intuition in the formulation of the general stress-strain relationships.

From the consideration of the material at the grain level, it was found that, even at very small shear stresses, the material would undergo some macroscopic irreversible deformation, irreversible in the sense that when the applied loads are removed, a permanent set would remain. This is due to the fact that a tangential force between two grains in contact produces "slipping" on part of the contact area which is not completely reversible, no matter how small the tangential force may be. While this irreversible deformation is inherent in the deformation of granular material, so is the elastic portion of it, being due to the elastic energy stored in the grains under the action of tangential forces. When the external shear stress is removed, this elastic energy is released, causing a rebound at the grain contacts resulting in a partial recovery of the total deformation macroscopically. When the granular material is subject to a shear stress, at some of the grain contacts the ratio of tangential force to normal force, T/N, may exceed the coefficient of friction μ and "sliding" occurs between the grains. This further contributes to the irreversible deformation due to the slipping of the contacts. During slipping and sliding, part of the energy supplied by the applied stresses is dissipated by friction and is therefore irrecoverable. Since slipping would occur at all contacts and sliding at some contacts at all shear stress levels, "yield," with a meaning as used in plasticity theory, is not a sharply defined point along the stress-deformation curve of the material. However, as shearing goes on, there comes a point on the curve at which the material is

unable to store any more elastic energy and the deformation increases at a faster rate. This point was defined as "failure."

Failure was identified in the experiments by a discontinuity in the shear stress - log(principal displacement) curves, and was located within an interval of the shear stress. The failure envelope was investigated three dimensionally for the sand in a medium dense and a medium loose state, by performing tests in which the mean stress was held constant and the octahedral shear stress was increased monotonically along a radial straight line on the octahedral plane. Five such straight lines were employed, including the triaxial compression and the triaxial extension stress paths. The failure envelopes obtained were shown in Fig. (VII.7). For both states of the sand, the value of equivalent Coulomb φ is least in triaxial compression and increased towards triaxial extension where it is 4°-10° higher. The reason for this increase was briefly discussed and was attributed to the penalty the soil has to exact due to the presence of a preferred direction of shearing dominated by the intermediate principal stress.

Shearing with constant mean stress was also performed on samples of all density states in both triaxial compression and triaxial extension (TCa and TEa). The value of equivalent Coulomb φ was shown as a function of the initial void ratio in Fig. (VII.2) and it can be seen that a difference of about 12° exists between the value of φ for dense and loose soils in these stress states.

From the shearing of samples of different densities under any shearing stress path, it was found (a) that a dense soil would expand at all shearing stress levels away from the hydrostatic state and, when

failure was approached, would expand at a faster rate, and (b) that a loose soil would contract at low shearing stresses and then expand when failure was approached. This is contrary to the observation with the conventional triaxial apparatus and triaxial test stress path, where all soils contract at the beginning. Remembering that the conventional triaxial test does not keep the mean stress constant, the contraction of a dense soil can be due to the increase in the mean stress. The observations in the present experiments were intuitively explained in Chapter III. That samples of all densities expanded during failure is in agreement with the conclusions reached by Drucker and Prager [39] from a mathematical point of view. Since the maximum deformations in the samples were only about 1-2% strain in these experiments, it is not possible to achieve the critical void ratio, because it would take a much larger deformation (~ 10% strain) to reach the ultimate state in the samples.

The results of the tests, in which the shear stress was increased directly to failure, show that an approximately linear relationship existed between the octahedral shear stress and the logarithm of the principal displacements. The displacements were larger for a loose soil and increased as the mean stress (σ_{OCT}) increased. From the limited amount of information on the behavior of the material after failure, it seems that another linear relationship existed between the same two quantities. This bilinear relationship would be useful in the formulation of a general stress-strain law for the material.

Unloading, followed by reloading, of the octahedral shear stress was carried out in Tests TCb and TEb from different levels of the shear

stress before and after failure. The results show that the envelope of the shear stress-principal displacement curves was not greatly affected by this stress history of unloading and reloading along the same radial line on the octahedral plane, indicating that only the maximum shear stress is sufficient to determine the deformations on the virgin curve. The same kind of stress history did not affect the failure point. The same bilinear relationship existed between shear stress and log (principal displacement). Before failure, unloading and reloading were roughly along the same straight line on the linear scale, with the slope of the straight line decreasing only slightly with the level of the shear stress from which unloading commenced. The small hysteresis loop before failure indicated that only small amount of energy was dissipated during the cycle of unloading and reloading. After failure, the unloading curve became more non-linear and the hysteresis loop larger, indicating a greater energy dissipation.

In Tests TCc and TEc, at the end of each cycle of shear unloading, a hydrostatic stress cycle was applied. It was found that the response of the sample was the same as if the soil had not been subjected to any shear stress, i.e., the compression by the hydrostatic stress cycle was isotropic and almost elastic. When the shear unloading was begun at a stress level above failure, the soil showed some degree of anisotropy by compressing more in the direction in which the previous minor principal stress acted. This indicated that the anisotropy developed in the sample was small before failure and became noticeable after failure had been reached. As in Tests TCb and TEb, the envelope of the stress-deformation curve seemed to be unchanged by the stress

history which in this case consisted of unloading, followed by a hydrostatic stress cycle and then reloading. The linear relationships therefore still holds between the shear stress and log(principal displacement).

The stress paths in Tests TCd and TEd consisted of excursions in which σ_{OCT} and τ_{OCT} increased proportionately but the ratio τ_{OCT}/σ_{OCT} remained constant. It was found that the results of these tests could be predicted from those of previous tests, by separating the principal deformations into two parts, one due to the change of σ_{OCT} and the other to that of τ_{OCT}. The first was isotropic and elastic and had the same value as if $\Delta\,\sigma_{OCT}$ were applied along the hydrostatic axis; the second was partly elastic and partly plastic, with the latter becoming dominant as the magnitude of τ_{OCT}/σ_{OCT} increased. The volume change could also be decomposed into two parts: the contribution from $\Delta\,\sigma_{OCT}$ which was completely elastic and the contribution of $\Delta\,\tau_{OCT}$ (the dilation effect). The expansion of the soil when failure was approached was also reflected in the volume change.

Tests TCe and TEe consisted of superposition of hydrostatic stress state on an existing deviatoric stress state in the sample. τ_{OCT} was constant, but σ_{OCT} increased and the ratio τ_{OCT}/σ_{OCT} decreased, representing an unloading. It was found that the results of these tests could again be predicted from those of previous tests, by separating the deformations into two parts, one due to the change of σ_{OCT} and the other to the unloading of τ_{OCT}/σ_{OCT}. The first was isotropic and elastic and had the same value as if $\Delta\,\sigma_{OCT}$ were applied along the hydrostatic axis; the second deformation was also almost elastic in the sense that during

the reloading of τ_{OCT}/σ_{OCT}, it was recoverable to a large extent. The volume change could also be calculated in two parts, one from the contribution of $\Delta\ \sigma_{OCT}$ which was completely elastic and the other from the contribution of $\Delta\ (\tau_{OCT}/\sigma_{OCT})$ which was also largely elastic. Since the soil would expand as τ/σ was increased toward failure, unloading of τ/σ produced compression which was superimposed upon the compression due to $\Delta\ \sigma_{OCT}$.

Therefore, if we postulate the shearing deformations of a granular material being due to three factors, $\Delta\ \sigma_{OCT}$, $\Delta\ \tau_{OCT}$ and $\Delta\ (\tau_{OCT}/\sigma_{OCT})$ along a general stress path on the triaxial plane, we can predict these deformations from the results of simple tests like the hydrostatic compression test and the triaxial compression or extension tests, and then superimpose the contribution from each factor. Although these tests were performed with triaxial stress paths, presumably the qualitative results will also be true for a truly three-dimensional situation in which all three principal stresses are unequal. Stress paths on which the axes of the principal stress rotate are more complicated and, since the behavior of granular soils is highly non-linear, the effect of the rotation may be great. The equipment employed in this investigation are not capable of investigating such effects.

(2) Conclusions

The following conclusions are based on the theoretical considerations and experimental investigation described in previous chapters of this thesis, and apply only to the Ottawa sand tested in this investigation.

(i) The soil test box is capable of applying any homogeneous state of stress to a cubic soil sample and is simple to operate.

(ii) The stress control device is an analog of an octahedral plane of the principal stress space and affords simple control and variations of the three principal stresses along any stress path with no rotation of the principal stress axes.

(iii) The hydrostatic compression of sand is isotropic and almost completely elastic and can be predicted from the theory of holey models. It does not vary as the two-thirds power of the hydrostatic pressure but increases less rapidly due to the increased number of grain contacts at higher pressures. It does not depend upon any shear stress history below failure.

(iv) Shearing of sand with a constant mean stress produces deformations in the directions of the principal stresses, which increase exponentially with the octahedral shear stress.

(v) Dense soils expand and loose soils contract in the initial stages of shearing with a constant mean stress, but failure, as defined in this work, occurs in all granular soils with an expansion in volume.

(vi) Shear unloading and reloading produce deformations which vary linearly with the shear stress, and hysteresis is small on repeated loadings. Deformations in the present

granular soil sheared with a constant mean stress depend only upon the maximum shear stress on the soil. Loading and unloading do not affect the deformation at a higher shear stress.

(vii) The deformations in a granular soil under general stress conditions in which the principal axes do not rotate can be separated into three parts, due to $\Delta \sigma_{OCT}$, $\Delta \tau_{OCT}$ and $\Delta (\tau_{OCT}/\sigma_{OCT})$ respectively, and each can be calculated from simple tests like the hydrostatic compression test and the radial shear tests and then superimposed.

(3) Recommendations for Future Work

One obvious extension of this investigation is to perform the experiments described in this thesis on other granular soils, to find out whether the same qualitative behaviors occur as in the Ottawa sand used in this investigation. If so, we may proceed to formulate constitutive relationships for granular soils under simple stress paths, using density, grain size distribution and angularity of grains as parameters in these relationships.

Formulation of the general constitutive relationships may require more experiments in which the stresses are varied in a more general manner, e.g., with rotation of the principal stress axes, which will require new apparatus being designed. However, the soil test box and the stress control device can still be employed, for instance, in the investigation of the effect of a complicated stress history on the behavior of the material. Tests may be required in which a circular stress path

on an octahedral plane is employed with constant τ_{OCT} and σ_{OCT}. This is easily achieved in the apparatus used here.

On the analytical side, further work can be done in postulating a model for granular soils under shear stress. Since a granular soil is a random assembly of particles, a statistical approach seems attractive, with the number of contacts and the angle of their inclination as the statistical parameters. Having extracted the characteristic behavior of the material, constitutive relationships can be formulated which can then be used to solve practical problems. Solution of such problems can be compared to the results of carefully performed model tests. A close correlation then means a triumph in the mechanics of granular soils.

APPENDIX A

ANALOGY BETWEEN STRESS CONTROL DEVICE AND DEVIATORIC PLANE AND DETERMINATION OF STRESSES FOR VARIOUS STRESS PATHS

The analogy between the triangular plate of the stress control device and the deviatoric plane in the principal stress space is shown as follows.

In Fig. (A.1), a weightless plate is represented by the equilateral triangle ABC, and is supported at the corners A, B, and C by upward forces F_1, F_2 and F_3 normal to its plane. At the centroid O of the triangle is set up a cartesian coordinate system (x,y).

A force F, representing the load applied by the top cylinder, acts downwards at point P with coordinates (x,y). The forces F_i can be determined from equilibrium as follows:

$$F_1 + F_2 + F_3 = F \ . \qquad (A.1)$$

Taking moments about BC,

$$F\ (\ell/\sqrt{3} + y) = F_1 \sqrt{3}\ \ell \ ;$$

$$\text{i.e.,} \quad F_1 = F\ (1/3 + y/\sqrt{3}\ \ell) \ , \qquad (A.2)$$

where $2\ \ell$ = length of one side of triangle ABC.

Rotate the coordinates clockwise through 30° to Ox' and Oy'. P now has new coordinates x' and y', and taking moments about AC, we find that

$$F_2 = F\ (1/3 + x'/\sqrt{3}\ \ell) \ .$$

But, $\quad x' = x \cos 30° - y \sin 30° = \frac{\sqrt{3}\, x}{2} - \frac{1}{2}\, y.$

$$\therefore F_2 = F\left(1/3 + \frac{x}{2\ell} - \frac{y}{2\sqrt{3}\,\ell} \right). \tag{A.3}$$

Rewriting Eqs. (A.2) and (A.3) in the dimensionless quantities

$$\bar{x} = x/\ell \quad \text{and} \quad \bar{y} = y/\ell \ ,$$

we have

$$\left.\begin{aligned} F_1 &= F\ (1/3 + \bar{y}/\sqrt{3}) && \text{(A.2)}', \\ F_2 &= F\left(1/3 + \bar{x}/2 - \frac{\bar{y}}{2\sqrt{3}\,\ell} \right) && \text{(A.3)}', \\ \text{and}\quad F_1 + F_2 + F_3 &= F && \text{(A.1)}\ . \end{aligned}\right\} \text{(a)}$$

From Eqs. (a), we can find the coordinates of the point P, given F_1, F_2, and F_3. Therefore

$$\bar{y} = (3F_1 - F)/\ /3\ F = (2F_1 - F_2 - F_3)/3\ F. \tag{A.4}$$

$$\tfrac{1}{2}\,\bar{x} = F_2/F + \bar{y}/2\sqrt{3} - \frac{1}{3} = (2F_1 - F_2 - F_3)/6\ F - (F-3F_2)/3\ F.$$

$$\text{Or,}\quad \bar{x} = \frac{F_2 - F_3}{F}\ . \tag{A.5}$$

In Fig. (A.2) are shown the principal stress space and the deviatoric plane.

The coordinates of the point P' on the deviatoric plane (x,y), are found as follows:

$$\overrightarrow{OP'} = \sigma_1\vec{i} + \sigma_2\vec{j} + \sigma_3\vec{k}\ ,$$

where $\vec{i}$, $\vec{j}$ and $\vec{k}$ are the unit vectors in the σ_1, σ_2 and σ_3 directions respectively.

$$\overrightarrow{OA} = 1/3\ (\sigma_1 + \sigma_2 + \sigma_3)\ (\vec{i} + \vec{j} + \vec{k})\ .$$

$$\therefore\ \overrightarrow{AP'} = \overrightarrow{OP'} - \overrightarrow{OA} = 1/3\Big\{ (2\sigma_1 - \sigma_2 - \sigma_3)\ \vec{i} + (2\sigma_2 - \sigma_3 - \sigma_1)\ \vec{j} + (2\sigma_3 - \sigma_1 - \sigma_2)\ \vec{k}\Big\}\ .$$

But, $$\overrightarrow{Oy} = \frac{1}{\sqrt{6}}\ (2\vec{i} - \vec{j} - \vec{k})\ .$$

$$\therefore\quad y = \overrightarrow{AP'} \cdot \overrightarrow{Oy} = \frac{1}{3\sqrt{6}}\Big\{2(2\sigma_1 - \sigma_2 - \sigma_3) - (2\sigma_2 - \sigma_3 - \sigma_1) - (2\sigma_3 - \sigma_1 - \sigma_2)\Big\}$$

$$= \frac{1}{\sqrt{6}}\ [2\sigma_1 - \sigma_2 - \sigma_3]\ . \qquad \text{(A.6)}$$

$$\text{i.e.,}\ \overrightarrow{AB'} = 1/6\ [2\sigma_1 - \sigma_2 - \sigma_3][2\vec{i} - \vec{j} - \vec{k}]\ .$$

$$\therefore\ \overrightarrow{AB''} = \overrightarrow{AP'} - \overrightarrow{AB'} = 1/6\Big\{ [4\sigma_1 - 2\sigma_2 - 2\sigma_3 - (4\sigma_1 - 2\sigma_2 - 2\sigma_3)]\ \vec{i} + [4\sigma_2 - 2\sigma_3 - 2\sigma_1 + (2\sigma_1 - \sigma_2 - \sigma_3)]\ \vec{j} + [4\sigma_3 - 2\sigma_1 - 2\sigma_2 + (2\sigma_1 - \sigma_2 - \sigma_3)]\ \vec{k}\Big\}$$

$$= 3(\sigma_2 - \sigma_3)\ \vec{j} + 3(\sigma_3 - \sigma_2)\ \vec{k}$$

$$= \frac{(\sigma_2 - \sigma_3)}{2}\ (\vec{j} - \vec{k})\ ,$$

$$\text{and,}\quad x = \|\overrightarrow{AB''}\| = \tfrac{1}{2}\ (\sigma_2 - \sigma_3)\ \sqrt{2}$$

$$= \frac{\sigma_2 - \sigma_3}{\sqrt{2}} \qquad \text{(A.7)}$$

Comparing Eqs. (A.4) and (A.5) to Eqs. (A.6) and (A.7), it is seen that there is indeed a geometric analogy between the triangular plate and the deviatoric plane. A point represented by P $(\bar{x},\bar{y})$ on the plate has the coordinates (x,y) on the deviatoric plane, and we have the following analogous quantities:

On the plate	In the stress space
F_1, F_2, F_3	$\sigma_1/3$, $\sigma_2/3$, $\sigma_3/3$
$F = F_1 + F_2 + F_3$	$\sigma_{OCT} = 1/3\ (\sigma_1+\sigma_2+\sigma_3)$
$\bar{x} \cdot F$	$\sqrt{2}\ x$
$\bar{y} \cdot F$	$\sqrt{2}\ y$

In using the stress control device, it is more convenient to find the stresses for a given position of P. For this purpose, we make the following reduction. From Eqs. (a), we have

$$F_1 = \sigma_1 A = F\ (1/3 + \bar{y}/\sqrt{3}) = pA\ (1/3 + y/\sqrt{3}) = \sigma_{OCT} A\ (1 + \sqrt{3}\ \bar{y})\ ,$$

where A = cross sectional area of cylinders,

and p = pressure in top cylinder.

$$\therefore\ \sigma_1 = \sigma_{OCT}\ (1 + \sqrt{3}\ \bar{y})\ , \tag{A.8}$$

$$\sigma_2 = \sigma_{OCT}\ (1 + 3/2\ \bar{x} - \sqrt{3}/2\ \bar{y})\ , \tag{A.9}$$

$$\text{and}\quad \sigma_3 = \sigma_{OCT}\ (1 - 3/2\ \bar{x} - \sqrt{3}/2\ \bar{y})\ , \tag{A.10}$$

$$\text{where } \sigma_{OCT} = 1/3\ p. \tag{A.11}$$

Now τ_{OCT} is related to the length, $\bar{r}$, of the radius vector from the centroid of the plate and the relationship is found to be

$$\tau_{OCT} = \sqrt{3}/2 \; \sigma_{OCT} \cdot \bar{r} \; . \tag{A.12}$$

In Eqs. (A.8) - (A.12), $\bar{x}$, $\bar{y}$, and $\bar{r}$ are all dimensionless quantities, the length of one side of the triangular plate being made equal to 2 units.

In Fig. (A.3) is shown the triaxial compression stress path, $\bar{x} = 0$, $\bar{y} \geq 0$. The sides of the plate are of length $2\ell = 15"$, and steps are made at 1/2" intervals along the path and numbered j, with j = 0 at the centroid. Hence in terms of j, the three principal stresses are given below:

$$\left.\begin{aligned} \sigma_1 &= \sigma_{OCT}\,(1 + j/5\sqrt{3}), \\ \sigma_2 = \sigma_3 &= \sigma_{OCT}\,(1 - j/10\sqrt{3}), \\ \tau_{OCT} &= \sigma_{OCT} \cdot j/5\sqrt{6} \; . \end{aligned}\right\} \quad \begin{array}{c} j \geq 0 \\ \text{triaxial} \\ \text{compression.} \end{array} \tag{A.13}$$

The quantities $\frac{\sigma_1}{\sigma_{OCT}}$, $\frac{\sigma_3}{\sigma_{OCT}}$, $\varphi \left(= \sin^{-1} \frac{\sigma_1/\sigma_3 - 1}{\sigma_1/\sigma_3 + 1} \right)$ and $\alpha \left(= \tan^{-1} \frac{\tau_{OCT}}{\sigma_{OCT}} \right)$ are plotted as functions of j in Fig. (A.3).

In Fig. (A.4) is shown the triaxial extension stress path, $\bar{y} = \bar{x} \tan 30°$, $\bar{x}$, $\bar{y} \geq 0$. Steps are made at 1/2" intervals along this path, but due to a miscalculation during construction, the first step is only 3/10". The stresses are obtained as follows:

$$\left.\begin{aligned} \sigma_3 &= \sigma_{OCT}\left[1 - (j - 2/5)/5\sqrt{3}\right], \\ \sigma_1 = \sigma_2 &= \sigma_{OCT}\left[1 + (k - 2/5)/10\sqrt{3}\right], \\ \tau_{OCT} &= \sigma_{OCT} \cdot \frac{(j - 2/5)}{5\sqrt{6}} . \end{aligned}\right\} \begin{array}{l} j \geq 1 \\ \text{triaxial} \\ \text{extension} \\ [1\underline{st} \text{ step} = 3/10"]. \end{array} \qquad (A.14)$$

In Fig. (A.4) the quantities $\frac{\sigma_1}{\sigma_{OCT}}$, $\frac{\sigma_3}{\sigma_{OCT}}$, φ and α are plotted as functions of j.

Three other stress paths have also been studied and they are shown in Figs. (A.5) - (A.7). For these stress paths, the following relationships are obtained:

$$\left.\begin{aligned} &(\sigma_1 > \sigma_2 > \sigma_3) \\ \sigma_1 &= \sigma_{OCT}\,(1 + 0.0816j), \\ \sigma_2 &= \sigma_{OCT}\,(1 + 0.0299j), \\ \sigma_3 &= \sigma_{OCT}\,(1 - 0.1115j), \\ \tau_{OCT} &= \sigma_{OCT}\,\frac{j}{5\sqrt{6}} . \end{aligned}\right\} \begin{array}{l} \text{(stress path at } 45^\circ \text{ to} \\ \text{the x-axis) } j \geq 0 . \end{array} \qquad (A.15)$$

$$\left.\begin{aligned} \sigma_1 &= \sigma_{OCT}\,(1 + 0.1j), \\ \sigma_2 &= \sigma_{OCT} = \text{constant}, \\ \sigma_3 &= \sigma_{OCT}\,(1 - 0.1j), \\ \tau_{OCT} &= \sigma_{OCT}\,\frac{j}{5\sqrt{6}} . \end{aligned}\right\} \begin{array}{l} \text{(stress path at } 60^\circ \text{ to} \\ \text{the x-axis) } j \geq 0 . \end{array} \qquad (A.16)$$

$$\left.\begin{aligned}
\sigma_1 &= \sigma_{OCT}\,[1 + 0.1116\,(j - 2/5)]\,, \\
\sigma_2 &= \sigma_{OCT}\,[1 + 0.0299\,(j - 2/5)]\,, \\
\sigma_3 &= \sigma_{OCT}\,[1 - 0.0817\,(j - 2/5)]\,, \\
\tau_{OCT} &= \sigma_{OCT}\,\frac{(j - 2/5)}{5\sqrt{6}}\,.
\end{aligned}\right\}\ \text{(stress path at } 75^\circ \text{ to the } \bar{x}\text{-axis) } j \geq 1\,. \qquad \text{(A.17)}$$

In Figs. (A.5) - (A.7), $\frac{\sigma_1}{\sigma_{OCT}}$, $\frac{\sigma_2}{\sigma_{OCT}}$, $\frac{\sigma_3}{\sigma_{OCT}}$, φ and α are plotted against j for these stress paths.

An estimate was made of the errors induced in the stresses due to an inaccuracy in the position of the top cylinder along the triaxial stress path. Suppose an error of 0.05" was involved in the position of the top cylinder, then, for a triaxial compression test, the maximum error in the major principal stress occurs at $j = 0$ and is 1.2%, whereas the error in the minor principal stresses increases as j increases and at $j = 8$, this error is 1.1%. For a triaxial extension test, the maximum error in the major principal stresses occurs at $j = 0$ and is 1.6% and that in the minor principal stress increases as j increases and at $j = 6$. This error is 3.8%.

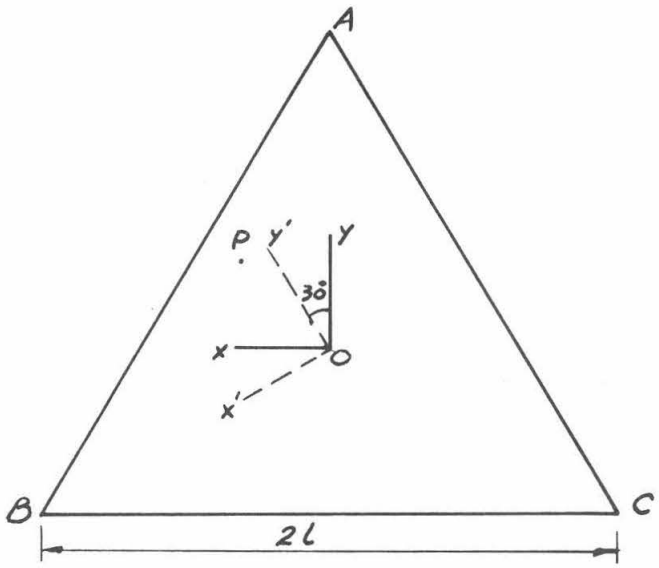

FIG. (A.1)
THE WEIGHTLESS PLATE OF THE STRESS CONTROL DEVICE

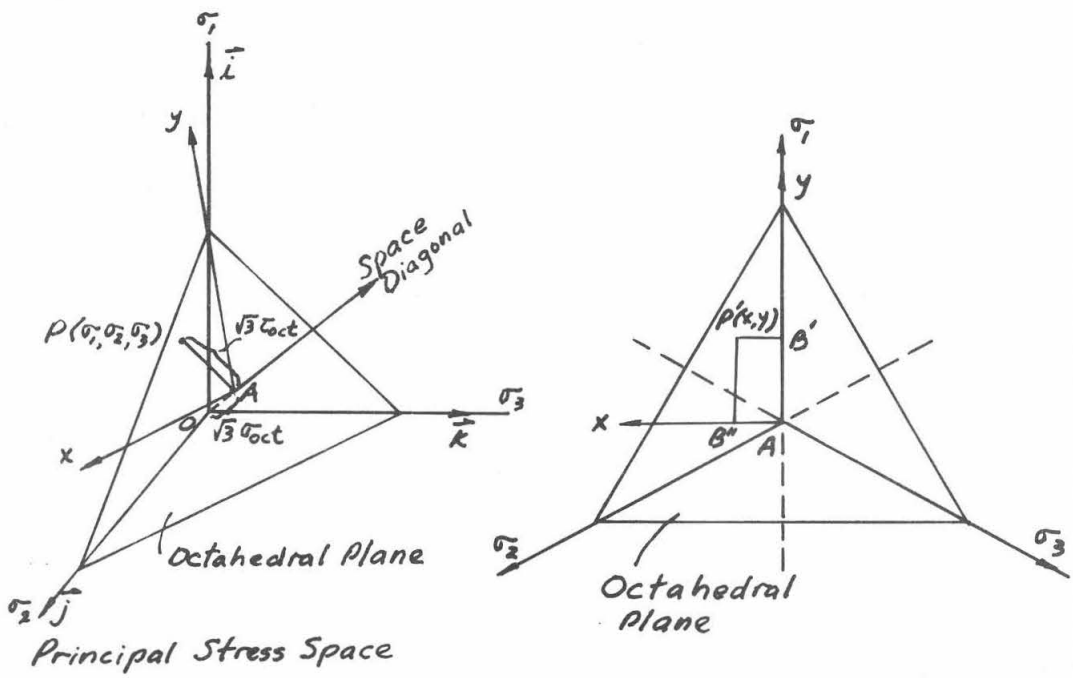

FIG. (A.2)
PRINCIPAL STRESS SPACE AND OCTAHEDRAL PLANE

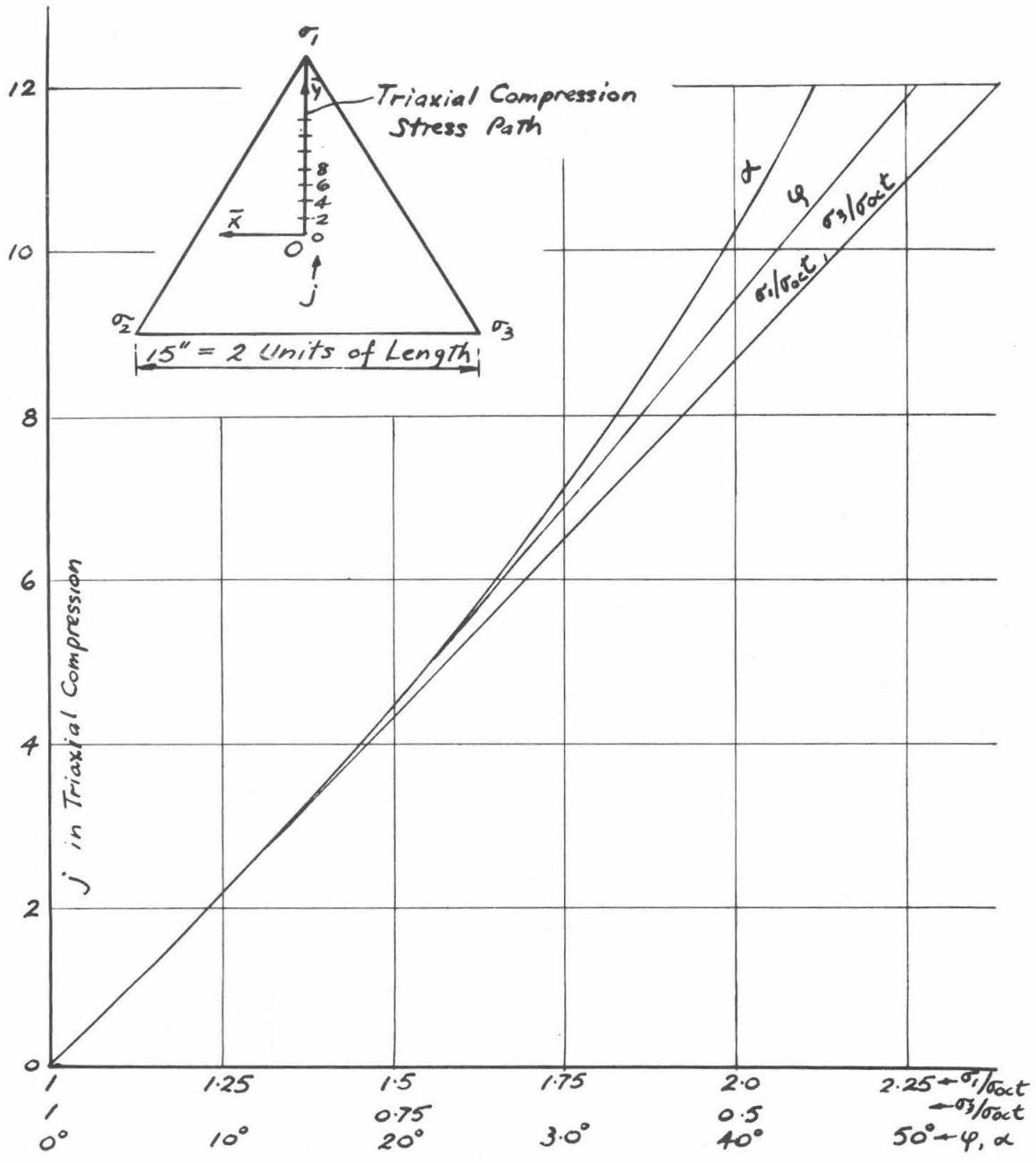

FIG. (A.3)
STRESSES FOR TC STRESS PATH

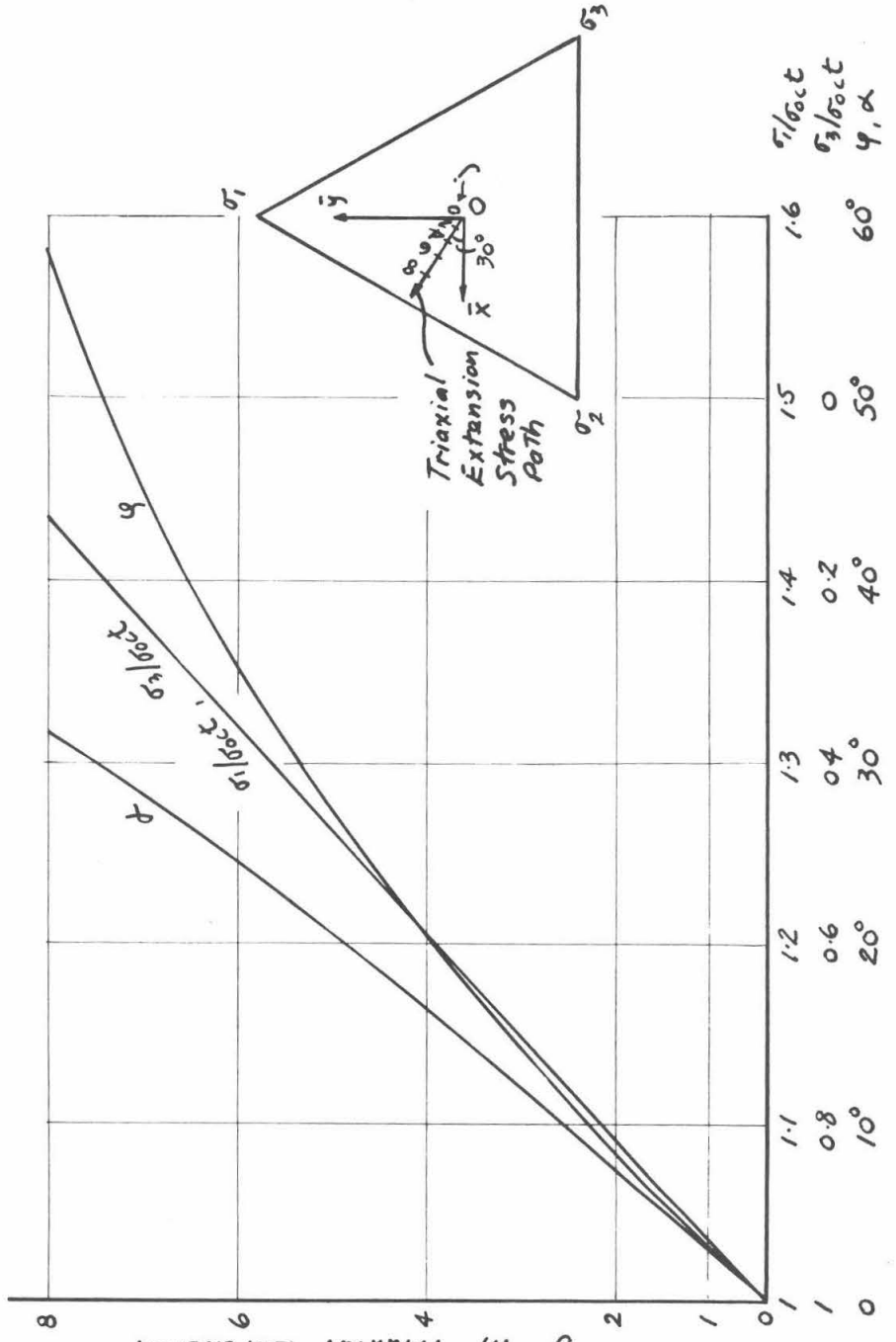

FIG. (A.4)
STRESSES FOR TE STRESS PATH

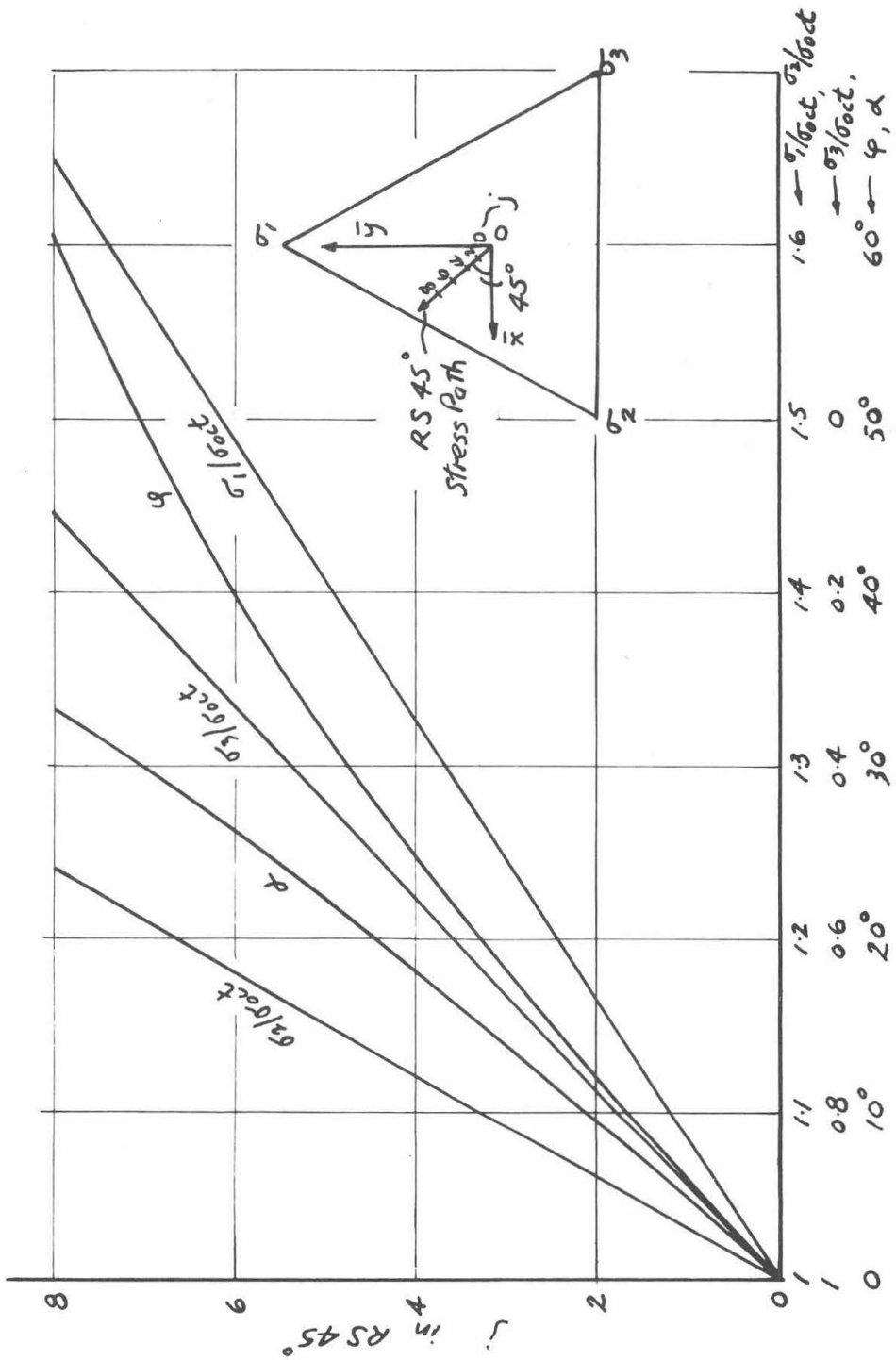

FIG. (A.5)
STRESSES FOR RS45° STRESS PATH

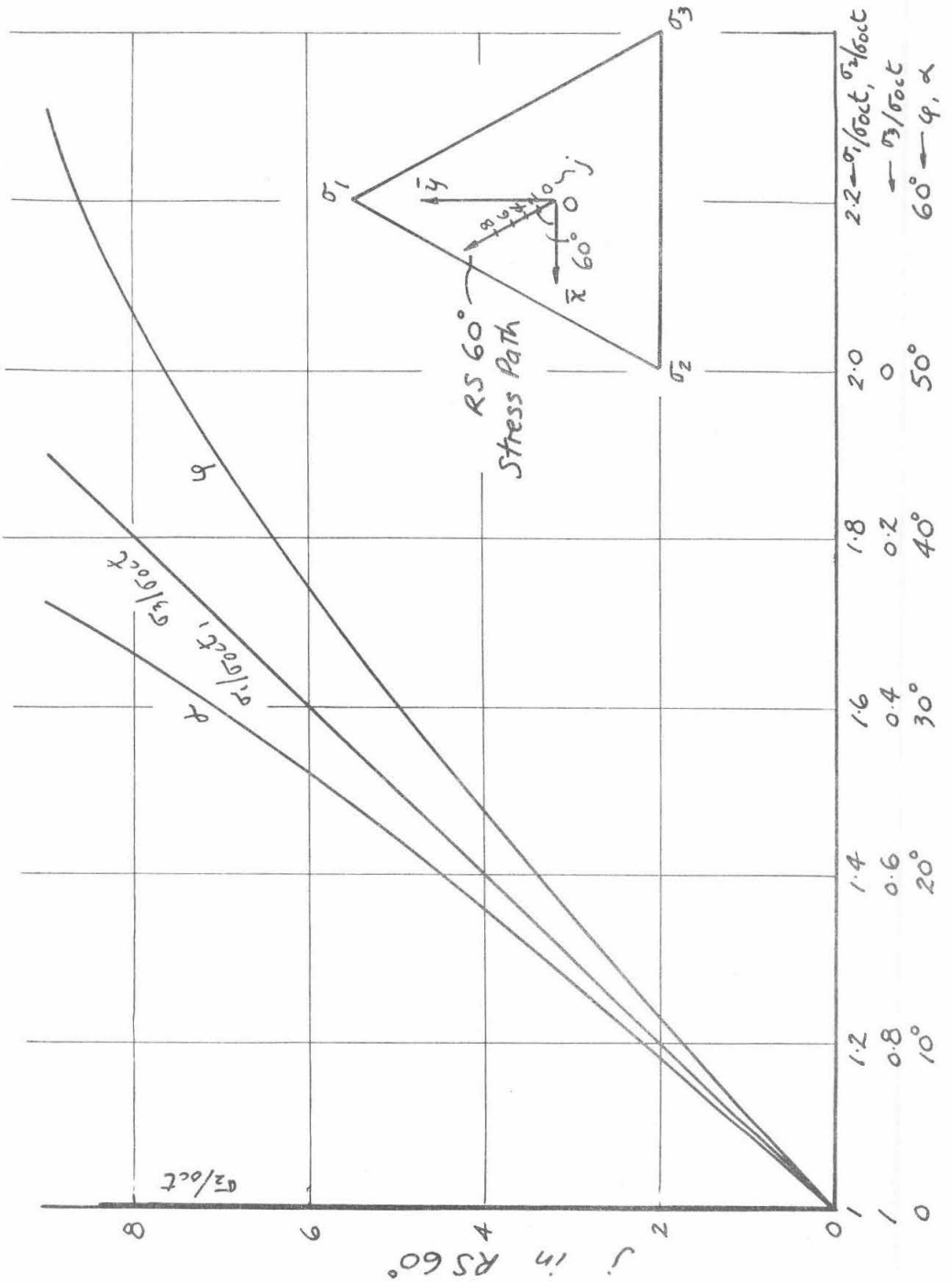

FIG. (A.6)

STRESSES FOR RS60° STRESS PATH

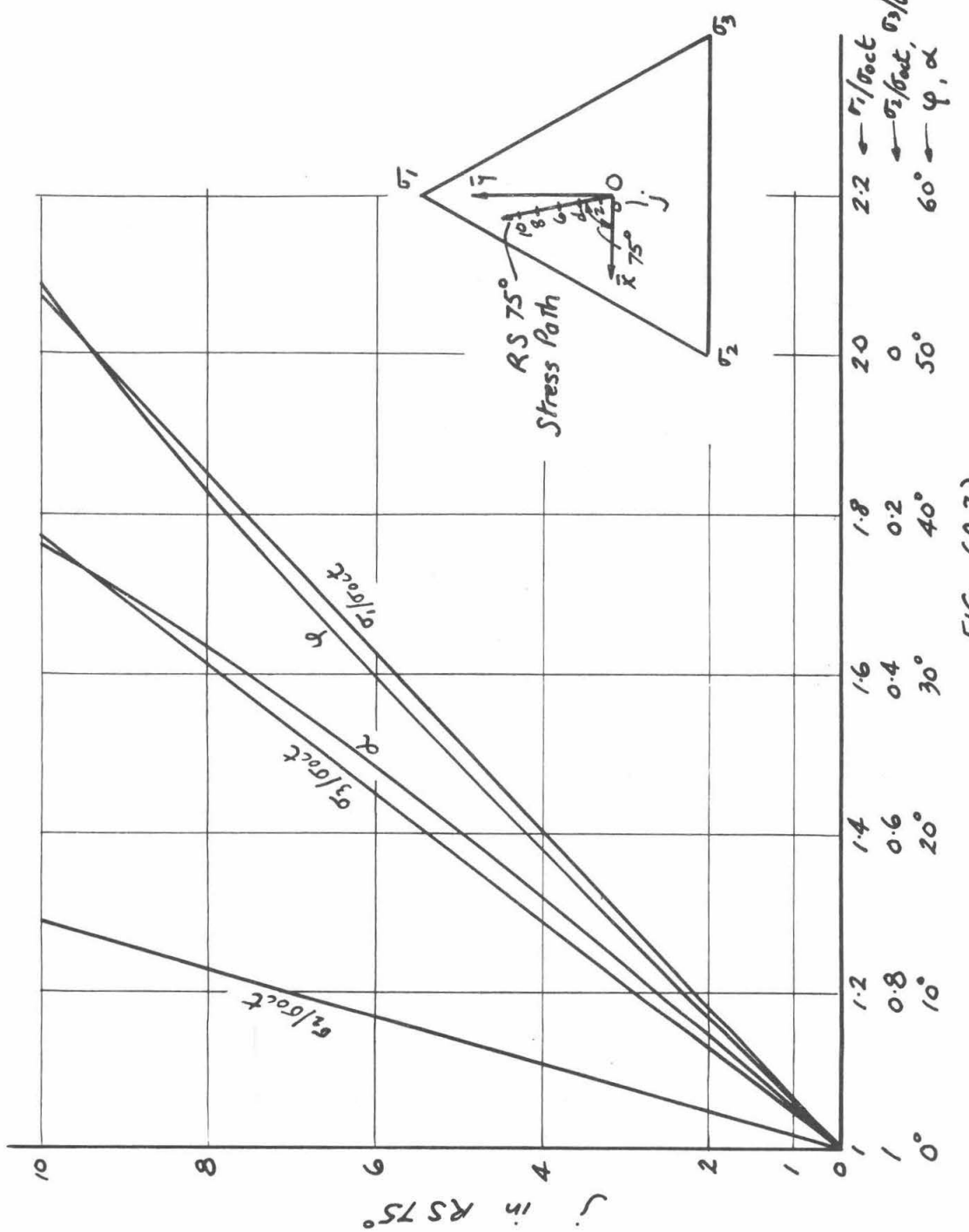

FIG. (A.7)

STRESSES FOR RS75° STRESS PATH

APPENDIX B

(1) Calibration of Bellofram Cylinder

A Bellofram cylinder, set up as shown in Fig. (IV.14), was filled with hydraulic oil and placed on a bathroom scale, as in Fig. (B.1), and the oil was connected to a Statham pressure transducer. The output of the transducer was recorded by an auto-recording potentiometer, and the transducer-recorder set-up was previously calibrated by air pressures. The bathroom scale is assumed to be true.

The plunger A of the scale was screwed downwards to produce an axial load of P lbs. in the piston of the cylinder, as recorded by the scale. The pressure p generated in the cylinder was recorded by the potentiometer in terms of the voltage output of the transducer, which was readily converted to p. The cylinder was loaded in this way in steps to 67 psi and then unloaded. The $P \sim p$ relation was plotted in Fig. (B.1). It is seen that a linear relationship exists between these two quantities and there is very little hysteresis in the cylinder, since the loading and the unloading portions of the curve are almost identical. The fact that the straight lines do not pass through the origin is due to the zero error of the scale.

The slope of the straight line represents the effective area of the hydraulic cylinder and was calculated to be 2.24 sq. in. This can be compared to the value of 2.26 sq. in. listed in the manufacturer's catalog. This difference and the slight hysteresis could be due to the bathroom scale.

(2) Calibration of the Stress Control Device

A calibration test was carried out to determine the principal stresses generated in the hydraulic cylinders A supporting the triangular plate of the stress control device as a function of the position of the top cylinder B.

A Statham pressure transducer was connected to a manifold which had connections for each of the three cylinders A. An auto-recording potentiometer was used to record the voltage output of the transducer. The transducer and recorder set-up had been previously calibrated by air pressures.

For each position of the top cylinder B along the selected triaxial compression stress path with a constant σ_{OCT}, starting at the hydrostatic position, the transducer was first switched to one of the three cylinders A. The potentiometer recorded the pressure generated in the cylinder. It only took a few seconds for the pressure to build up to its new steady value. After this steady value had been attained, the transducer was switched to another cylinder until the pressures in all three cylinders had been recorded. The top cylinder was then moved to a new position with the pressure in it being kept constant.

The steady values of the three principal stresses are shown in Fig. (B.2), where they are compared to the values calculated from Eq. (A.13). It can be seen that a close correspondence exists between the two sets of values, and the maximum error was about 0.2 psi. Hence it can be assumed that the stress control device does produce the correct principal stresses along a stress path.

Tests were not carried out along other stress paths.

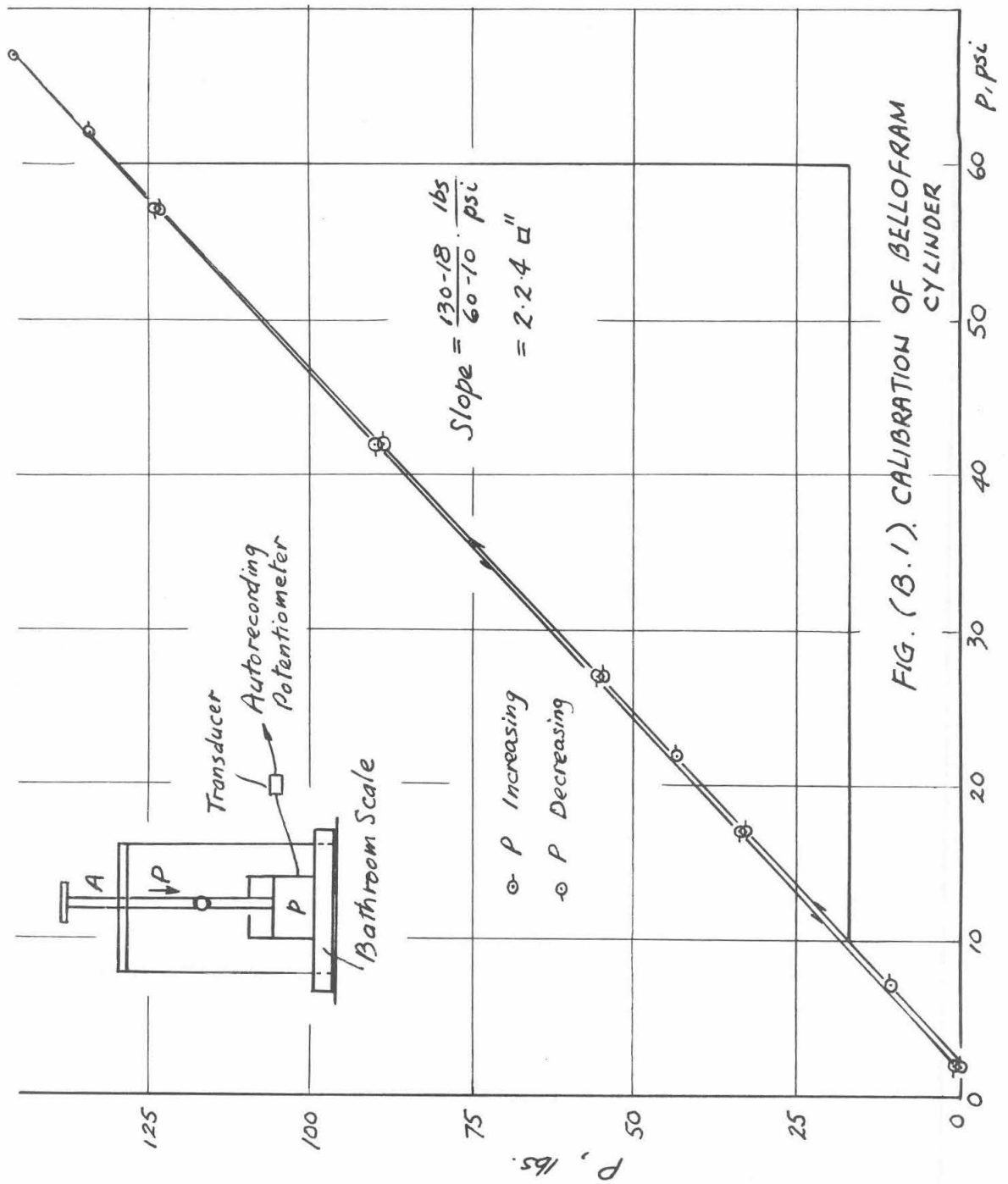

FIG. (B.1). CALIBRATION OF BELLOFRAM CYLINDER

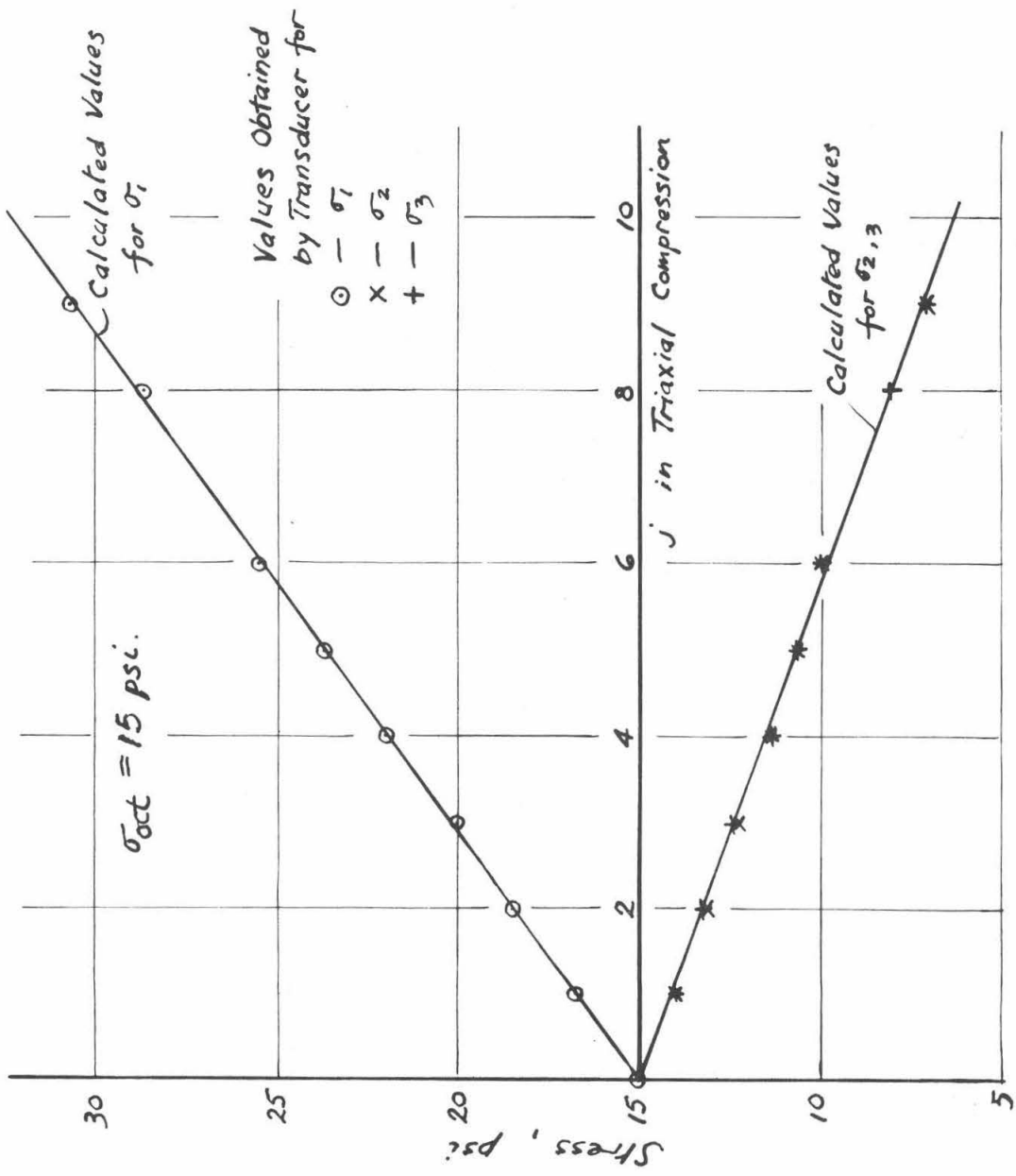

FIG. (B.2). CALIBRATION OF STRESS CONTROL DEVICE

TEST: TCa-1

Volume of Sample = 816 c.c.
Void Ratio of Sample = 0.510

NOTES: Dense Sample; σ_{oct} = 20 psi
Temp. = 23°C.

DATE: 8/31/65
PAGE: 1 of 3

Time hr. m.	P psi	P' psi	σ_{oct} psi	j	σ_1	σ_2	$\sigma_3 = \sigma_2$	ΔV_3 (0.1 c.c.) Rdg.	ΔV_3	Correction	Corr. ΔV_3	ΔV_2 (0.1 c.c.) Rdg.	ΔV_2	Correction	Corr. ΔV_2	ΔV_1 (0.1 c.c.) Rdg.	ΔV_1	Correction	Corr. ΔV_1	$\Delta V = \sum \Delta V_n$ (0.1 c.c.)	$\Delta V_{int.}$ Rdg.	$\Delta V_{int.}$ (0.1 c.c.)
10:39.0	60	0	20	0	20	20	20	265	0	0	0	265	0	0	0	140	0	0	0	0	257	0
39.5	↓	↓	↓	2	24.6	17.7	17.7	/				/				/					/	
40.6				"	"	"	"	262				262				145+					257+	
41.9				"	"	"	"	"	-3	+2+	-2+	"	-3	-2+	-2+	146	6	2+	3+	0+	"	0+
42.4				4	29.2	15.4	15.4	/				/				/					/	
43.6				"	"	"	"	258+				258+				153+					258	
44.9				"	"	"	"	"	-7+	-3	-4+	"	-7+	-3	-4+	"	13+	4+	9	2	"	1
45.4				6	33.9	13.1	13.1	/				/				/					/	
46.2				"	"	"	"	252+				253				165					257+	
47.8				"	"	"	"	"	-13+	-5+	-8	"	-12	-5+	-8+	165+	25+	6+	19	3+	"	0
48.0				7	36.2	11.9	11.9	/				/				/					/	
49.0				"	"	"	"	248				249				172+					256+	
50.0				"	"	"	"	"	17	-6+	-12+	248+	-17+	-6+	-11	173	33	7+	25+	3	"	0-
50.3				8	38.5	10.8	10.8	/				/				/					/	
51.3				"	"	"	"	241+				242+				183+					255	
52.3				"	"	"	"	"	-24+	-7+	-17	242	-23	-7+	-17+	184	44	8	36	2+	"	-2
52.6				9	40.8	9.6	9.6	/				/				/					/	
53.5				"	"	"	"	232				233				198					251	
54.7				"	"	"	"	"	-33	-7	-26	"	-32	-7	-25	198+	58+	9	49+	-2+	"	-6
54.9				9½	41.9	9.1	9.1	/				/				/					/	
56.3				"	"	"	"	227+				228				205					248	
57.5				"	"	"	"	227	-38	-8+	-31+	"	-37	-8+	-30+	"	65	9+	55+	-5+	"	-9

APPENDIX C

TEST: TCa-1 (cont'd)

Volume of Sample =

Void Ratio of Sample =

NOTES:

DATE: 8/31/65

PAGE: 2 of 3

Time hr. m.	P psi	P' psi	σ_{oct} psi	j	σ_1	σ_2	σ_3	ΔV_3 (0.1 c.c.) Rdg.	ΔV_3	Correction	Corr. ΔV_3		ΔV_2 (0.1 c.c.) Rdg.	ΔV_2	Correction	Corr. ΔV_2		ΔV_1 (0.1 c.c.) Rdg.	ΔV_1	Correction	Corr. ΔV_1		ΔV = $\Sigma \Delta V_i$ (0.1 c.c.)	$\Delta V_{int.}$ Rdg.	$\Delta V_{int.}$ (0.1 c.c.)
10:57.7	60	0	20	10	43.1	8.5	8.5	/					/					/						/	
58.6	↓	↓	↓	"	"	"	"	217					217+					218						243	
11:0.0				"	"	"	"	"	-48	-8	-40		"	-48+	-8	-40+		218+	78+	10	68+		-11	"	-15
0.2				10½	44.2	7.9	7.9	/					/					/						/	
1.4				"	"	"	"	207+					207					230+						235	
3.0				"	"	"	"	206+					205+					232+						234	
4.1				"	"	"	"	"	-59+	-9+	-50		"	-60+	-9+	-51		233	93	10+	82+		-19+	"	-23
4.4				11	45.4	7.3	7.3	/					/					/						/	
5.5				"	"	"	"	188					184					256						219	
6.9				"	"	"	"	187					182+					257+						218	
8.2				"	"	"	"	"	-78	-9	-69		182	-83	-9	-74		258	118	11	108		-35	"	-39
8.4				11½	46.6	6.7	6.7	/					/					/						/	
9.9				"	"	"	"	170+					164					276+						204	
11.0				"	"	"	"	169					162+					278						202+	
12.5				"	"	"	"	168+	-97+	-10+	-87		161+	-104+	-10+	-94		279	+139	11+	127+		-54+	202	-55
13.0				8	38.5	10.7	10.7	/					/					/						/	
14.0				"	"	"	"	175					169					274						209	
15.0				"	"	"	"	"	-90	-6	-84		"	-96	-6	-90		"	134	8	126		-48	209+	-48+
15.3				5	31.6	14.2	14.2	/					/					/						/	
16.2				"	"	"	"	183					177					266						217	
17.4				"	"	"	"	"	-82	-4+	-79+		177+	-88+	-4+	-84		"	126	5	121		-42+	"	-40
17.6				2	24.6	17.7	17.7	/					/					/						/	

TEST: TCa-1 (Cont'd)

NOTES:

DATE: 8/31/65

PAGE: 3 of 3

Volume of Sample =

Void Ratio of Sample =

Time hr. m.	p psi	p' psi	σ_{oct} psi	j	σ_1	σ_2	σ_3	ΔV_3 (0.1 c.c.) Rdg.	ΔV_3	Corr-ection	Corr. ΔV_3	ΔV_2 (0.1 c.c.) Rdg.	ΔV_2	Corr-ection	Corr. ΔV_2	ΔV_1 (0.1 c.c.) Rdg.	ΔV_1	Corr-ection	Corr. ΔV_1	ΔV $= \Sigma \Delta V$ (0.1 c.c.)	$\Delta V_{int.}$ Rdg.	$\Delta V_{int.}$ (0.1 c.c.)
11:18.7	60	0	20	2	24.6	17.7	17.7	195+				191				254					230	
19.4	↓	↓	↓	"	"	"	"	196	-69	-1	-68	191+	-74+	-1	-73+	"	114	2+	111+	-29	"	-27
19.8				0	20	20	20	/				/				/					/	
20.4				"	"	"	"	209				206				239					242	
21.5				"	"	"	"	209+	-56+	0	-56+	"	-59	0	-59	"	99	1	98	-17+	242+	-15+

LIST OF SYMBOLS

Symbols	Meanings
a	r/R
a_i	$(\sigma_i - \sigma_{OCT})/j$, $i = 1,2,3$
C	constant
e	void ratio
E	Young's modulus of elasticity
E_i	Contribution of σ_i to the total energy input, $i = 1,2,3$
E_4	Contribution of dilation to the total energy input
F.C.C.	Face-centered Cubic
j	Number of steps from the centroid along a straight stress path in the stress control device
n	Porosity
N	Normal force at point of contact of grains
N_1	Normal force between two large spheres in the holey models
N_2	Normal force between a large and a small sphere in the holey models
N_α	Proportion of potential contacts with initial gap width α
p	Hydrostatic pressure
p_i	Hydrostatic pressure at which the gaps in the holey models are closed
p_m	Maximum hydrostatic pressure at which all potential contacts have been made
r	Radius of curvature of grain at point of contact
R	Radius of grain
S.C.	Simple Cubic
T	Tangential force at point of contact of grains

u_i Principal displacement in σ_i directions ($i = 1,2,3$)

V Volume of sample

ΔV Total volume change in sample ($= \sum_i \Delta V_i$)

ΔV_i Deformation in σ_i direction ($i = 1,2,3$)

ΔV_{int} Internal volume change measured by hypodermic needle

x Volumetric fraction of F.C.C. grains in a random assembly

α $\tan^{-1} \dfrac{\tau_{OCT}}{\sigma_{OCT}}$

α Relative approach of the centers of two spheres in contact under a normal force

δ Tangential displacement of two spheres under a tangential force

ϵ_i Principal strains in σ_i direction ($i = 1,2,3$), $\epsilon_i = \dfrac{\Delta V_i}{V}$

μ Coefficient of friction

ν Poisson's ratio

σ_1, σ_2, σ_3 Major, intermediate and minor principal stresses

σ_{OCT} Octahedral normal stress or mean stress

τ_{OCT} Octahedral shear stress

φ Equivalent Coulomb angle of friction $\left(= \sin^{-1} \dfrac{\frac{\sigma_1}{\sigma_3} - 1}{\frac{\sigma_1}{\sigma_3} + 1} \right)$

ω $\dfrac{3}{4} \dfrac{(1 - \nu^2)}{E}$

REFERENCES

1. Timoshenko, S., and Goodier, J. N., Theory of Elasticity, McGraw Hill, New York, 1951.

2. Haigh, B. P., "The Strain Energy Function and the Elastic Limit," Engineering, vol. 109, p. 158, 1920.

3. Westergaard, H. M., "On the Resistance of Ductile Materials to Combined Stresses," J. Franklin Inst., p. 627, May, 1920.

4. Scott, R. F., Principles of Soil Mechanics, Addison-Wesley, Reading, Mass., 1963.

5. Coulomb, C. A., "Essai sur une application des règles des maximis et minimis à quelques problemes de statique relatifs à l'architecture," Mem. Acad. Roy. Pres. divers Sav., vol. 5, p. 7, Paris, 1776.

6. Whitman, R. V., and Miller, E. T., "Yielding and Locking of Confined Sand," Jour. Soil Mech. and Found. Div., Proc. ASCE, SM.4, vol. 90, p. 57, July, 1964.

7. Reynolds, O., "On the Dilatancy of Media Composed of Rigid Particles in Contact," Phil. Mag., Series 5, vol. 20, p. 469, 1885.

8. Bell, J. M., "Stress-Strain Characteristics of Cohesionless Granular Materials Subjected to Statically Applied Homogeneous Loads in an Open System," Ph.D. Thesis, California Institute of Technology, 1965.

9. Kjellman, W., "Report on an Apparatus for Consummate Investigation of the Mechanical Properties of Soils," Proc. Int. Conf. Soil Mech., vol. 2, p. 16, 1936.

10. Bishop, A. W., and Eldin, A. K. G., "The Effect of Stress History on the Relation Between ϕ and Porosity in Sand," Proc. 3rd Int. Conf. Soil Mech. and Found. Eng., vol. 1, p. 100, 1953.

11. Kirkpatrick, W. M., "The Condition of Failure of Sands," Proc. 4th Int. Conf. Soil Mech. and Found. Eng., vol. 1, p. 172, 1957.

12. Chaplin, T. K., "Compressibility of Sands and Settlements of Model Footings and Piles in Sand," Proc. 5th Int. Conf. Soil Mech. and Found. Eng., vol. 2, p. 33, 1961.

13. Haythornthwaite, R. M., "Mechanics of the Triaxial Test for Soils," Jour. Soil Mech. and Found. Div., Proc. ASCE, SM5, vol. 86, p. 35, October, 1960.

14. Balla, A., "Stress Conditions in Triaxial Compression," Jour. Soil Mech. and Found. Div., Proc. ASCE, vol. 86, p. 57, December, 1960.

15. Roscoe, K. H., "An Apparatus for the Application of Simple Shear to Soil Samples," Proc. 3rd Int. Conf. Soil Mech., vol. I, p. 186, 1953.

16. Kondner, R. L., "Hyperbolic Stress-Strain Response," Jour. Soil Mech. and Found. Div., Proc. ASCE, SM1, vol. 89, p. 115, February, 1963.

17. Roscoe, K. H., Schofield, A. N., and Wroth, C. P., "On the Yielding of Soils," Géotechnique, vol. 8, p. 22, 1958.

18. Deresiewicz, H., "Mechanics of Granular Matter," Adv. App. Mech., vol. 5, p. 233, 1958.

19. Brandt, H., "A Study of the Speed of Sound in Porous Granular Media," Jour. of App. Mech., Proc. ASME, vol. 77, p. 479, 1955.

20. Fatt, I., "Compressibility of a Sphere Pack--Comparison of Theory and Experiment," Jour. of App. Mech., Proc. ASME, vol. 79, p. 148, 1957.

21. Dantu, P., "Mechanical Study of a Closely Packed Assembly of Spheres with Identical Elastic Properties," Proc. 5th Int. Conf. Soil Mech. and Found. Eng., vol. 1, p. 61, 1961.

22. Rennie, B. C., "On the Strength of Sand," Jour. Aust. Math. Soc., vol. 1, p. 71, 1959.

23. Parkin, A. K., "The Application of Discrete Unit Models to Studies of the Shear Strength of Granular Materials," Ph.D. Thesis, University of Melbourne, Australia, January, 1965.

24. Rowe, P. W., "The Stress-Dilatancy Relation for Static Equilibrium of an Assembly of Particles in Contact," Proc. Royal Soc. (London) Series A, No. 269, p. 174, 1959.

25. Rowe, P. W., "Stress-Dilatancy, Earth Pressures and Slopes," Jour. Soil Mech. and Found. Div., Proc. ASCE, SM3, vol. 89, p. 37, May, 1963.

26. Discussions to Ref. 25, Jour. Soil Mech. and Found. Div., Proc. ASCE, SM6, p. 127, November, 1963; SM1, p. 133, January, 1964; SM4, p. 145, July, 1964.

27. Horne, M. R., "The Behavior of an Assembly of Rotund, Rigid, Cohesionless Particles, Pts. I and II," Proc. Royal Soc. (London), Series A, vol. 286, p. 62, 79, 25 May, 1965.

28. Litwiniszyn, L., "New Theoretical and Experimental Research in the Mechanics of Loose Bodies Treated as Media Characterized by Stochastic Equations," Rev. Mech. Appl., vol. 6, p. 255, 1961.

29. Sweet, A. L., and Bogdanoff, J. L., "Stochastic Model for Predicting Subsidence," Jour. Eng. Mech., Proc. ASCE, EM2, vol. 91, p. 21, April, 1965.

30. Mindlin, R. D., "Compliance of Elastic Bodies in Contact," Jour. Appl. Mech., Trans. ASME, vol. 16, p. 259, 1949.

31. Terzaghi, K., and Peck, R. E., Soil Mechanics in Engineering Practice, Wiley, New York, 1948.

32. Smith, W. O., Foote, P. D., and Busang, P. F., "Packing of Homogeneous Spheres," Phys. Rev., vol. 34, p. 1271, 1929.

33. Mantell, C. L., Engineering Materials Handbook, p. 27-6, McGraw-Hill, New York, 1958.

34. Duff, J., and Mindlin, R. D., "Stress Strain Relations and Vibrations of a Granular Medium," Jour. App. Mech., Trans. ASME, vol. 24, p. 585, 1957.

35. Thurston, C. W., and Deresiewicz, H., "Analysis of a Compression Test of a Face-Centered Cubic Array of Elastic Spheres," Jour. App. Mech., Trans. ASME, vol. 26, p. 251, 1959.

36. Deresiewicz, H., "Stress-Strain Relations for a Simple Model of a Granular Medium," Jour. App. Mech., Trans. ASME, vol. 25, p. 402, 1958.

37. Vold, M. J., "The Sediment Volume in Dilute Dispersions of Spherical Particles," Jour. Phys. Chem., vol. 64, p. 1616, 1960.

38. McCormick, C. W., "Plane Stress Analysis," Jour. Struct. Div., Proc. ASCE, vol. 89, p. 37, August, 1963.

39. Drucker, D. C., and Prager, W., "Soil Mechanics and Plastic Analysis on Limit Design," Quart. App. Math., vol. 10, p. 157, 1952.

40. Rowe, P. W., and Barden, L., "Importance of Free Ends in Triaxial Testing," Jour. Soil Mech. and Found. Div., Proc. ASCE, SM1, vol. 90, p. 1, 1964.

41. Lee, K. L., and Seed, H. B., Discussion of Ref. 40, Jour. Soil Mech. and Found. Div., Proc. ASCE, SM6, vol. 90, p. 173, 1964.

42. Bishop, A. W., and Green, G. E., "The Influence of End Restraint on the Compression Strength of a Cohesionless Soil," Géotechnique, vol. 15, p. 243, 1965.